Role of cellular ion channels in the BK polyomavirus life cycle

Margarita-Maria Panou

Submitted in accordance with the requirements for the degree of Doctor of Philosophy

The University of Leeds

School of Molecular and Cellular Biology

August, 2018

The candidate confirms that the work submitted is her own and that appropriate credit has been given where reference has been made to the work of others.

Acknowledgement

I would like to thank my two supervisors Dr Andrew Macdonald and Dr Jamel Mankouri for the opportunity to study for a PhD and for their invaluable support and guidance throughout this project.

I would also like to thank all past and present members of the Macdonald and Mankouri labs for their helpful discussions. In particular, thank you to Dr Emma Prescott for the advice and the time spent training me up in the lab and Dr Christopher Wasson for invaluable support throughout my studies. Thank you to Ethan Morgan, David Kealy, Gemma Swinscoe and Dan Hurdiss for your advice and interesting perspectives.

I would also like to thank Kidney Research UK for funding my PhD.

Δεν θα μπορούσα να παραλείψω την ανεκτίμητη βοήθεια και στήριξη της Μικαέλλας Αντώνη, διδακτορικής φοιτήτριας στην ομάδα του Dr Andrew Macdonald. Εκτός από στήριγμα στο εργαστήριο, ήταν και θα είναι εξαιρετική φίλη.

Θα ήθελα επίσης να ευχαριστήσω τους γονείς μου τόσο για την ψυχολογική αλλά και την υλική υποστήριξη κατά τη διάρκεια των σπουδών μου.

Ένα μεγάλο ευχαριστώ σε όλους τους ανθρώπους του στενού μου περιβάλλοντος που με στήριξαν στις δύσκολες στιγμές μου και χάρηκαν με τις επιτυχίες μου.

Abstract

BK polyomavirus (BKPyV) is a human pathogen that infects the majority of the population, worldwide, establishing a lifelong infection. Immunocompromised patients following renal transplantation, are likely to suffer from severe clinical complications, including polyomavirus-associated nephropathy (PVAN), which can ultimately lead to kidney graft failure. Currently, there are no direct acting anti-viral compounds targeting BKPyV and the number of renal transplants is increasing significantly. Therefore, there is an urgent need to understand the viral life cycle in order to identify potential targets that can be exploited for therapeutic development.

Ion channels play a critical role in kidney physiology by controlling several processes, implicating them as candidate proteins required for BKPyV infection. A pharmacological analysis was performed in which human primary renal epithelial cells were treated with a range of pharmacological modulators of host ion channels and the effect on BKPyV production assayed using a fluorescence-based technique. From this approach, it was identified that the clinically available drug, Glibenclamide is a potent inhibitor of BKPyV infection. Biochemical analysis and molecular-based techniques revealed that the cystic fibrosis transmembrane conductance regulator (CFTR) was the target of Glibenclamide and time-of-addition experiments indicated that CFTR might be required during the entry and trafficking of BKPyV through the cytoplasm. These studies provide the first reported requirement for host ion channels in the BKPyV life cycle.

Studies on other related polyomaviruses, including JCPyV, SV40 and Merkel cell polyomavirus determined a cell type-dependent requirement of CFTR in the viruses' life cycle, highlighting the importance of understanding the role of host ion channels in polyomaviruses' life cycle. Ion channels are an emerging target for many medical conditions and such compounds that target these may represent a novel strategy for developing therapeutics to treat PVAN and/or other polyomavirus-associated clinical complications.

Table of Contents

List of Tables

List of illustrative materials

Abbreviations

α-	anti-
Å	Angstrom
^{o}C	Degrees Celsius
µ	Micro
µg	Microgram
µl	Microliter
3’	Three prime
5’	Five prime
5-HT_{1A}R	Serotonin receptor
A	Adenine
aa	Amino acid
ADP	Adenosine diphosphate
Akt	AK strain transforming
Ala	Alanine
ALTO	Alternative tumour antigen
APS	Ammonium persulphate
Arg	Arginine
ATP	Adenosine triphosphate
BKPyV	BK polyomavirus
bp	Base pairs
C	Cytosine
Ca^{2+}	Calcium ion
CD4	Cluster of differentiation 4
cAMP	Cyclic adenosine monophosphate
CD8	Cluster of differentiation 8

CFTR	Cystic fibrosis transmembrane conductance regulator
Cl^-	Chloride ion
cDNA	Complementary deoxyribonucleic acid
CMV	Cytomegalovirus
C-terminus	Carboxyl-terminus
Cys	Cysteine
CV-1	African green monkey kidney cells (*Cercopithecus aethiops*)
ddH_2O	Double-distilled water
DMEM	Dulbecco's modified Eagle's medium
DMSO	Dimethyl sulphoxide
DNA	Deoxyribonucleic acid
EDTA	Ethylenediaminetetraacetic acid
EGF	Epidermal growth factor
EGFR	Epidermal growth factor receptor
EM	Electron microscopy
ER	Endoplasmic reticulum
ERK1/2	Extracellular signal-regulated kinase 1/2
g	Gram
GAPDH	Glyceraldehyde 3-phosphate dehydrogenase
GFP	Green fluorescent protein
Golgi	Golgi apparatus
Grp170	Glucose-regulated protein 170
h	Hour
hpi	Hour post-infection
hpt	Hour post-transfection

H^+	Proton
HA	Haemagglutinin
HCV	Hepatitis C virus
HEK293TT	Human embryonic kidney 293 TT antigen cells
HEPES	N-2-hydroxyethylpiperazine-N'-2-ethanesulfonic acid
HIV	Human immunodeficiency virus
HLA	Human leukocyte antigen
HPV	Human papillomavirus
HPyV6	Human polyomavirus 6
HPyV7	Human polyomavirus 7
HPyV9	Human polyomavirus 9
HPyV12	Human polyomavirus 12
Hsp	Heat shock protein
IFN	Interferon
IgG	Immunoglobulin G
IL-2	Interleukin 2
Ile	Isoleucine
JCPyV	JC polyomavirus
k	Kilo
K^+	Potassium ion
kbp	Kilo base pairs
kDa	Kilo dalton
KIPyV	Karolinska Institute polyomavirus
Leu	Leucine

Lys	Lysine
M	Molar concentration
m	Milli
m	Metre
MAP	Mitogen-activated protein
MCPyV	Merkel cell polyomavirus
mg	Milligram
Mg	Magnesium
MHC	Major histocompatibility complex
miRNA	microRNA
MMF	Mycophenolate mofetil
MOI	Multiplicity of infection
mRNA	Messenger ribonucleic acid
MTAg	Middle tumour antigen
mTOR	Mammalian target of rapamycin
MWPyV	MW polyomavirus
mV	milliVolt
NS	Not significant
Na^+	Sodium ion
NBD	Nucleotide binding domain
NCCR	Non-coding control region
NES	Nuclear export signal
NF-κB	Nuclear factor of kappa light polypeptide gene enhancer in B-cells
ng	Nanogram

NIH 3T3	Murine fibroblast cell line
NJPyV	New Jersey polyomavirus
NLS	Nuclear localization signal
nm	Nanometer
N-terminus	Amino-terminus
o/n	Overnight
OD_{600}	Optical density measured at 600 nm
ORF	Open reading frame
ori	Origin of replication
p	Probability
PBS	Phosphate buffered saline
PCR	Polymerase chain reaction
pH	-log10 concentration of hydrogen ions
Phe	Phenylalanine
PML	Progressive multifocal leukoencephalopathy
pRB	Retinoblastoma-associated protein
PV	Papillomavirus
PVAN	Polyomavirus-associated nephropathy
qPCR	Quantitative polymerase chain reaction
Rab18	Ras-related protein
Ref	Reference
rpm	Revolutions per minute
RPTE	Renal proximal tubular epithelial
RNA	Ribonucleic acid

ROMK	Renal outer medullary potassium channel
SA12	Simian agent 12
SDS	Sodium dodecyl sulphate
SDS-PAGE	Sodium dodecyl sulphate polyacrylamide gel electrophoresis
Ser	Serine
siRNA	Small interfering RNA
STLPyV	Saint Luis polyomavirus
SV40	Simian vacuolating virus 40
Tac	Tacrolimus
TAg	Large tumour antigen
tAg	Small tumour antigen
TBS	Tris buffered saline
TBS/T	Tris buffered saline containing Tween-20
$TCID_{50}$	Tissue culture infective dose
TEMED	Tetramethylethylenediamine
Thr	Threonine
TM	Trans-membrane
TMD	Trans-membrane domain
TPC	Two-pore channel
truncTAg	Truncated tumour antigen
t-SNARE	Target soluble N-ethylmaleimide-sensitive facto attachment protein receptor
TSPyV	Trichodysplasia spinulosa polyomavirus
UV	Ultraviolet
V	Volts

VLP	Virus-like particle
VP	Viral protein
v-SNARE	Vesicle soluble N-ethylmaleimide-sensitive facto attachment protein receptor
w/v	Weight per volume
WHO	World health organization
WUPyV	Washington University polyomavirus
x g	Times gravitational force

1 Introduction

1.1 Taxonomy, Classification and Characteristics of Polyomaviridae

Polyomaviruses are double-stranded DNA viruses and their classification has undergone several revisions due to discovery of new family members. Formerly, papillomaviruses and polyomaviruses were classified in the same family, named as *Papovaviridae*. The name of the family derived from three abbreviations; Pa for *Papillomavirus*, Po for *Polyomavirus* and Va for "vacuolating". Family members shared many structural features although, they had very different genome organization (IARC Working Group on the Evaluation of Carcinogenic Risks to Humans, 2014).

A more recent update in 2010, the *Polyomaviridae* was divided into three genera. These were the *Orthopolyomavirus* and *Wukipolyomavirus* genera, which include polyomaviruses that infect mammalian species and the *Avipolyomavirus* that contains avian infecting species of virus. The criteria utilized in new viruses' classification include the genetic background, the identity of DNA sequence throughout the genome and the host range of the virus (Johne et al., 2011).

Currently, following another reclassification, the International Committee on Taxonomy of Viruses now recognizes four distinct genera, *Alphapolyomavirus*, *Betapolyomavirus*, *Gammapolyomavirus* and *Deltapolyomavirus* based on the amino acid sequence of Large Tumour Antigen (TAg) viral protein (Calvignac-Spencer et al., 2016). Phylogenetic relationships among polyomaviruses are shown in Figure 1.1 (Moens et al., 2017). Studies have identified that viruses belonging to these genera can infect both birds and mammals and most recently, polyomavirus infection was detected in fish (Peretti et al., 2015). It is also established that some members of the *Polyomaviridae* are closely associated with cancer and severe clinical complications. However, clinical symptoms are observed mainly in immunosuppressed individuals (Moens et al., 2017). Members of *Alphapolyomavirus* genus can infect humans and other mammals. Raccoon polyomavirus and Merkel cell polyomavirus are members

of this genus and are closely associated with cancer within their host. *Betapolyomavirus* genus includes members that infect mammals with BKPyV and JCPyV being characteristic members of this genus. Members of *Gammapolyomavirus* genus infect birds. Finally, human polyomavirus 6, 7, 10 and 11 belong to *Deltapolyomavirus* genus (Calvignac-Spencer et al., 2016).

Polyomaviruses are approximately 40-45 nm in diameter and the major capsid protein, VP1, represents the 75% of the total virion protein content (Moens et al., 2017). Two other structural proteins, VP2 and VP3, are detected in most mammalian polyomaviruses, whereas an additional viral protein called VP4 has been detected in bird polyomaviruses and Simian Virus 40 (SV40) (Shen et al., 2011; Raghava et al., 2011). The mature virions are non-enveloped with icosahedral symmetry and consisted of 72 pentameric capsomers. VP1 is the component of each of these pentameres. Furthermore, it has been identified that capsomers are linked by the C-terminal arm of VP1 and each capsomer is stabilized by disulphide bonds and calcium ions (Hurdiss et al., 2016; Hurdiss et al., 2018). A single molecule of the minor capsid proteins, VP2 or VP3, is linked to the internal face of each VP1 pentamer. The circular double-stranded viral genome is contained in each mature virion and is organized as a minichromosome, whereas, histone proteins such as H2A, H2B, H3 and H4 facilitate the packaging of viral genome (Pagano, 1984). Polyomavirus minichromosome lacks histone H1 (Fang et al., 2010), which is required for chromatin compaction (Thoma et al., 1979). This suggests that the minichrosome is not highly compacted within the virus particle (Hurdiss et al., 2016). Recent studies have shown that VP1 is bound to the viral genomic DNA, although both minor capsid proteins, VP2 and VP3 can also be linked with the genomic DNA (Hurdiss et al., 2016).

Most polyomaviruses contain a genome of approximately 5,000 bp, although the size of the genome may vary in some species. For example, the black sea bass-associated polyomavirus 1 contains a single circular genomic DNA of 7,369 bp (Calvignac-Spencer et al., 2016). On the other hand, the smallest polyomavirus genome (3,962 bp) has been identified in an unclassified polyomavirus, which is linked with the giant guitarfish (Calvignac-Spencer et al., 2016). Small variations are also observed in human polyomaviruses, such as Merkel cell polyomavirus and Saint Louis polyomavirus. The former contains the largest genome of 5,387 bp and the latter has the smallest genome identified of 4,776 bp (Calvignac-Spencer et al., 2016).

Most of the polyomaviruses encode for 5 distinct proteins, 2 regulatory and 3 other structural proteins. The 2 regulatory proteins, TAg and tAg, are expressed before the initiation of genome replication and the 3 structural proteins VP1, VP2 and VP3, are expressed following genome replication. However, it is established that several polyomaviruses express additional proteins as well. A number of studies describe an additional open reading frame, which encodes for a protein called alternative tumour antigen (ALTO) or a second exon of middle tumour antigen (MTAg) in some polyomaviruses, such as Merkel cell polyomavirus and Trichodysplasia Spinulosa polyomavirus (Carter et al., 2013; Lauber et al., 2015; van der Meijden et al., 2015). Studies have reported that another late protein, VP4, has been expressed in some polyomaviruses and its function is still controversial (Raghava et al., 2011; Raghava et al., 2013; Giorda et al., 2012; Henriksen et al., 2016). VP4 open reading frames have been detected in SV40, BKPyV, JCPyV and in some non-human primate polyomaviruses (Ehlers and Moens, 2014). It is also identified that another auxiliary protein, which is named agnoprotein, is expressed by BKPyV, JCPyV and SV40 (Saribas et al. 2016). Studies have demonstrated that agnoprotein is involved in several processes including virus transcription, maturation and egress (Saribas et al., 2016). A gene detected in avian polyomaviruses in a similar genomic position, was originally annotated as an agnogene, although there is no detectable sequence similarity to the mammalian examples. The protein product generated by this gene, is implicated in capsid formation and genome packaging, resulting to its reclassification as VP4 to show its role as a structural protein. However, it is still often referred to as avian agnoprotein 1a (Shen et al., 2011; Gerits and Moens, 2012; Müller and Johne, 2001).

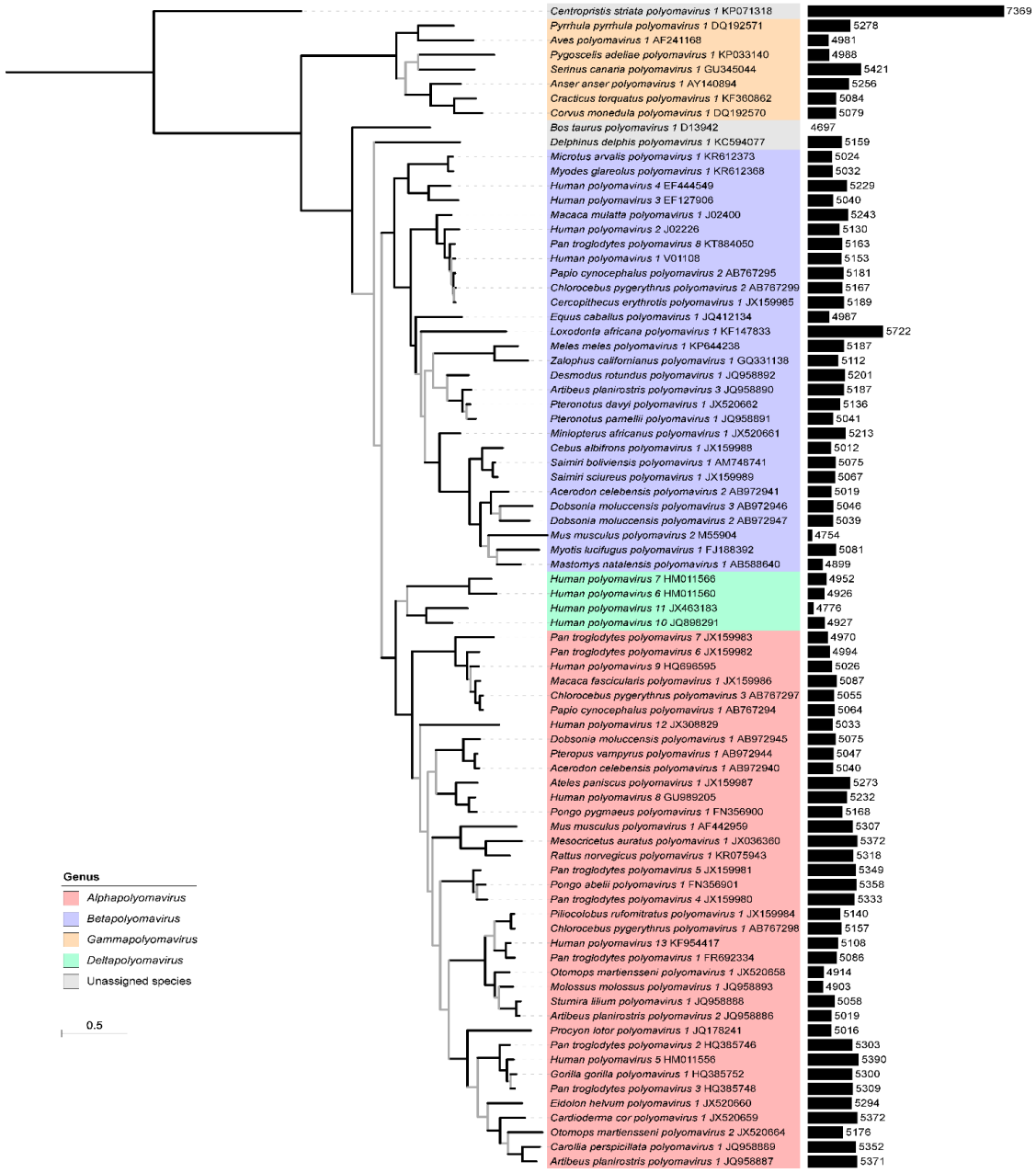

Figure 1. 1 A maximum likelihood rooted phylogenetic tree of polyomaviruses based on conserved TAg coding sequence. Polyomaviruses, Genbank accession numbers and genome sizes are represented. Polyomaviruses are shown into genera by different colouring. Scale bar represents the number of substitution per site (Moens *et al*., 2017).

1.2 Human polyomaviruses

In 1971, the first human polyomaviruses were identified, BK (BKPyV) polyomavirus and JC (JCPyV) polyomavirus are named after the initials of the index case patients (Gardner et al., 1971; Padgett et al., 1971). BKPyV causes severe clinical complications in certain immunocompromised individuals, although primary infections in immunocompetent individuals is usually asymptomatic or may be associated with signs of a mild respiratory infection (Mazalrey et al., 2015). Serological studies have shown that primary BKPyV infection usually occurs at a young age and virus establishes a lifelong infection into the hosts (Kean et al., 2009; Stolt et al., 2003; Knowles, 2006). Following virus reactivation, under conditions of immunosuppression, BKPyV is strongly correlated with two severe diseases, polyomavirus-associated nephropathy (PVAN) and hemorrhagic cystitis in patients who have undergone renal and bone marrow transplantation, respectively (Kuypers, 2012). Studies have identified that JCPyV is a neurotropic virus and is characterized as the main causative agent of a lethal clinical complication of the central nervous system, progressive multifocal leukoencephalopathy (PML), which is usually diagnosed in patients with HIV/AIDS (Ferenczy et al., 2012).

Since 2007, many more human polyomaviruses have been identified and categorized. Some of these new polyomaviruses were named after the institution in which they were discovered such as Washington University polyomavirus (WUPyV) and Karolinska Institute polyomavirus (KIPyV) (Allander et al., 2007; Gaynor et al., 2007). Malawi polyomavirus (MWPyV), Saint Louis polyomavirus (STLPyV) and New Jersey polyomavirus (NJPyV) were named after the geographical source of detected virus (Siebrasse et al., 2012; Lim et al., 2013; Mishra et al., 2014). Two more polyomaviruses are named after their disease association; Merkel cell polyomavirus (MCPyV) and Trichodysplasia spinulosa-associated polyomavirus (TSPyV) (Haycox et al., 1999; van der Meijden et al., 2015; Feng et al., 2008). Furthermore, polyomavirus 6, 7, 9 and 12 (HPyV6, HPyV7, HPyV9 and HPyV12) were named after the chronological order of first detection (Schowalter et al., 2010; Scuda et al., 2011; Korup et al., 2013). The table (Table 1.1) below shows a list of human polyomaviruses as are listed by Calvignac-Spencer et al., (2016). A very recent study described the isolation of a new human polyomavirus in human skin. Lyon IARC polyomavirus

(LIPyV) is related to the raccoon polyomavirus based on phylogenetic analyses (Gheit et al., 2017).

Phylogenetic analyses of human polyomaviruses have suggested that there are distinct clades of polyomaviruses. DeCaprio and Garcea (2013) represented a phylogenetic tree of human polyomaviruses describing the relationship between human and primate polyomaviruses based on TAg and VP1 conserved amino acid sequences (Figure 1.2). It was identified that polyomaviruses isolated from same tissue or sample types were grouped together. In particular, WUPyV and KIPyV are grouped together, also HPyV6 with HPyV7 and MWPyV with STLPyV are seen paired as they were isolated from nasopharyngeal, skin and stool, respectively. This might indicate a potential tissue tropism between closely related polyomaviruses (Rozenblatt-Rosen et al., 2012). BKPyV and JCPyV are also closely related to SV40 and simian agent 12 (SA12). The authors also proposed that HPyV9 is paired with African green monkey polyomavirus (AGMPyV) and MCPyV is grouped with Gorilla gorilla gorilla polyomavirus 1. Furthermore, TSPyV is very similar to Bornean orangutan polyomavirus (DeCaprio and Garcea, 2013).

Table 1. 1 Human polyomaviruses. A list of 13 members of polyomaviruses that infect humans. Species, virus name, abbreviation, year of discovery and clinical complications are represented. Adapted from (Calvignac-Spencer *et al*., 2016)

Species	Virus name	Abbreviation	Year of discovery	Clinical correlate
Human polyomavirus 1	BK polyomavirus	BKPyV	1971	Polyomavirus-associated nephropathy and hemorrhagic cystitis (DeCaprio and Garcea, 2013)
Human polyomavirus 2	JC polyomavirus	JCPyV	1971	Progressive multifocal leukoencephalopathy (DeCaprio and Garcea, 2013)
Human polyomavirus 3	KI polyomavirus	KIPyV	2007	Not known (Allander et al., 2007)
Human polyomavirus 4	WU polyomavirus	WUPyV	2007	Not known (Gaynor et al., 2007)
Human polyomavirus 5	Merkel cell polyomavirus	MCPyV	2008	Merkel cell carcinoma (DeCaprio and Garcea, 2013)
Human polyomavirus 6	Human polyomavirus 6	HPyV6	2010	HPyV6-associated pruritic and dyskeratotic dermatosis (Nguyen et al., 2017)
Human polyomavirus 7	Human polyomavirus 7	HPyV7	2010	HPyV7-related epithelial hyperplasia (Nguyen et al., 2017)

Species	Virus name	Abbreviation	Year of discovery	Clinical correlate
Human polyomavirus 8	Trichodysplasia spinulosa polyomavirus	TSPyV	2010	Trichodysplasia spinulosa (DeCaprio and Garcea, 2013)
Human polyomavirus 9	Human polyomavirus 9	HPyV9	2011	Not known (Scuda et al., 2011)
Human polyomavirus 10	MW polyomavirus	MWPyV	2012	Not known (Siebrasse et al., 2012)
Human polyomavirus 11	STL polyomavirus	STLPyV	2013	Not known (Lim et al., 2013)
Human polyomavirus 12	Human polyomavirus 12	HPyV12	2013	Not known (Korup et al., 2013)
Human polyomavirus 13	New Jersey polyomavirus	NJPyV	2014	Not known (Mishra et al., 2014)
Human polyomavirus 14	Lyon IARC polyomavirus	LIPyV	2017	Not known (Gheit et al., 2017)

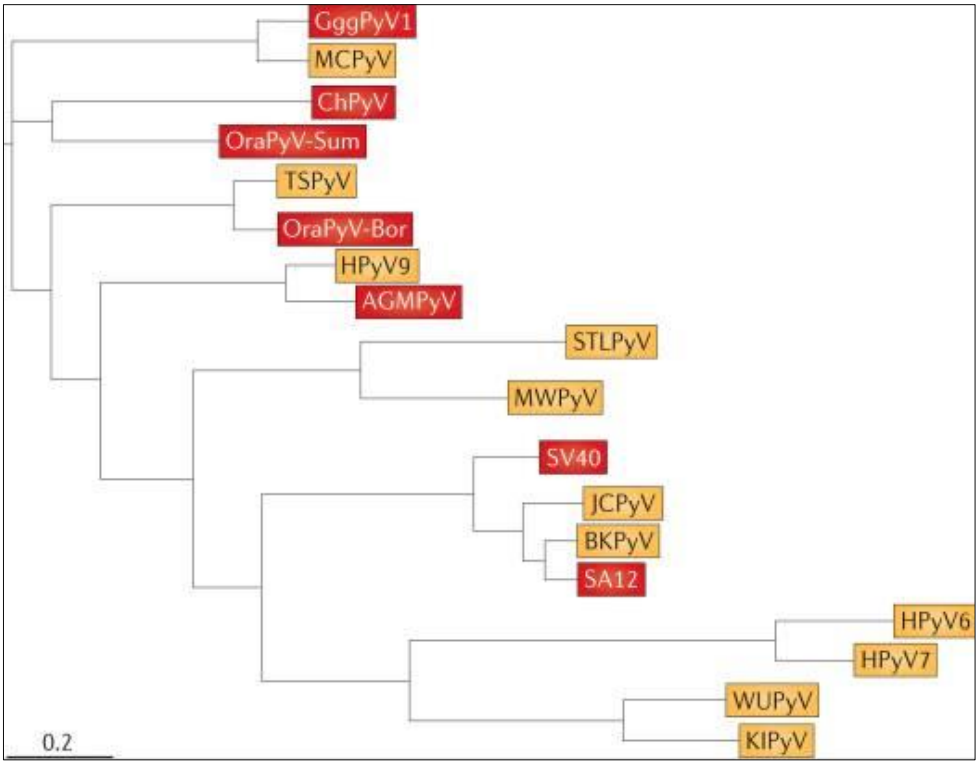

Figure 1. 2 Phylogenetic tree of human and primate polyomaviruses. Human polyomaviruses are represented in yellow and primate polyomaviruses are shown in red. Amino acid sequences from TAg and VP1 proteins from 19 different isolates were used to construct this simplified rooted phylogenetic tree. Scale bar represents the number of substitution per site (DeCaprio and Garcea., 2013).

1.3 Polyomavirus-associated nephropathy (PVAN)

1.3.1 History and background of the disease

Polyomavirus-associated nephropathy (PVAN) is the most common viral clinical complication in kidney transplant recipients, causing transplant dysfunction and graft loss. An increasing prevalence rate of PVAN from 1% to 10% has been reported since 1995 (Hirsch et al., 2006). This increase might occur due to usage of new-generation and stronger immunomodulatory drugs and/or the decrease in acute transplant rejection rates. Studies have shown that PVAN causes renal graft rejection in between 10%-100% of the diagnosed cases, with patients undergoing to haemodialysis within 6 to 60 months, therefore decreasing the kidney allograft survival (Costa and Cavallo, 2012).

The main causative viral agent of PVAN is the human BK polyomavirus (BKPyV) in most of the reported cases. In 1978, 4 distinct features of nephropathy after kidney transplantation were first described by Mackenzie et al., (1978). The authors stated that urinary decoy cells and viral inclusion bodies in uroepithelial cells were detected in renal graft biopsies. They also highlighted the difficulties in the diagnosis with acute renal rejection and the critical role of immunosuppressive drugs in the development of this nephropathy. In 1995, the first clinical case of PVAN was described and recognized as a defined clinical complication strongly associated with BKPyV (Purighalla et al., 1995). JCPyV alone has been also associated with PVAN, but in less than 3% of all the cases (Kazory et al., 2003; Wen et al., 2004) or in conjunction with BKPyV (Cavallo et al., 2007). Li et al., (2002) suggested that there might be a potential implication of SV40 in PVAN. It is demonstrated that co-infection of BKPyV and SV40 has been identified in renal transplant individuals diagnosed with PVAN (Li et al., 2002).

The pathogenesis of PVAN is still only partially understood, however multiple risk factors coincide to the development of PVAN including the source of the BKPyV infection, host immunity to BKPyV, the immunosuppression and HLA matching (Scadden et al., 2017). It is known that primary BKPyV infection from the renal graft itself or BKPyV reactivation in the transplant recipient's native urinary tract may lead to development of PVAN (Scadden et al., 2017). Studies have indicated that patients

who are transplanted with an allograft from seropositive donors may show increased rate of BKPyV infection within the renal graft, therefore highlighting the importance of donor-derived BKPyV infection (Andrews et al., 1988). This was also supported by another study stating that BKPyV infection was observed in 46% of renal recipients from seropositive donors compared with only 15% of recipients from seronegative donors. They also reported that BK viruria was developed faster and lasted longer in individuals receiving graft from seropositive donors (Bohl et al., 2005).

Host innate immunity is implicated with pathogenesis of PVAN and both CD8+ and CD4+ T cells are involved in the recognition and clearance of BKPyV (Scadden et al., 2017). The lack of IgG specific against BKPyV may be crucial for the development of PVAN (Chand et al., 2016). Patients being seronegative for BKPyV at the time of transplantation have a greater risk of developing BKPyV infection as they do not have pre-existing BKPyV-specific antibodies, although individuals exposed to BKPyV may not develop BKPyV infection following transplantation (Beimler et al., 2007). Patients that have produced antibodies against BKPyV are still at risk of PVAN as host cellular immunity plays a pivotal role in BKPyV control (Comoli et al., 2013). Studies have reported that less secreted interferon-γ (IFN-γ) was detected in patients diagnosed with PVAN, as they contain fewer BKPyV-specific lymphocytes. This level of secretion was around 10 times less than the observed levels during infection with other viruses associated with transplantation, such as Epstein-Barr virus (EBV). These data suggest that BKPyV immunity is decreased, which following could lead to increased rate of developing PVAN (Comoli et al., 2004).

Immunosuppressive drugs are required following a transplantation to prevent allograft rejection by the host immune system. To date, strong immunomodulatory drugs such as tacrolimus (Tac) and mycophenolate mofetil (MMF) are administered and the reduced rate of renal graft rejection has been inversely correlated with increased incidence of BKPyV reactivation and infection (Scadden et al., 2017). Tac is a calcineurin inhibitor, which interferes with T cell activation, whereas MMF is an anti-proliferative agent that interferes with T cell proliferation, downstream of the interleukin-2-receptor activation (Ginevri et al., 2007; Brennan et al., 2005; Halloran, 2004). Most of the reported cases received immunosuppressive combinations containing Tac or MMF. However, studies have shown that there is an increased rate of developing PVAN using a combination of Tac-MMF-corticosteroids or cyclosporin

(Brennan et al., 2005). Hence, no specific immunosuppressive drug can be exclusively related to PVAN.

Furthermore, HLA matching is being considered as another critical risk factor of developing PVAN. Studies have identified that there is ineffective clearance of BKPyV due to MHC mismatching using a mouse model (Scadden et al., 2017). Other clinical studies have also supported that increased HLA mismatch may lead to PVAN (Hirsch et al., 2002; Masutani et al., 2013; Awadalla et al., 2004). There are also several other risk factors that might increase the risk of developing PVAN, such as male gender, age older than 50 years, white ethnicity, diabetes mellitus or whether the organ was sourced from a deceased donor (Mengel et al., 2003; Dharnidharka et al., 2009; Dharnidharka et al., 2009; Vasudev et al., 2005).

1.3.2 Clinical manifestation of PVAN

The median time for PVAN diagnosis is within the first-year post-transplantation (Nickeleit et al., 2000; Drachenberg et al., 1999), however approximately 25% of the reported clinical cases have been diagnosed at later stages (Costa and Cavallo, 2012). Varying degrees of renal dysfunction and stages of PVAN might be identified, whereas even normal serum creatinine levels might be detected in early stages (Krishna and Prasad, 2011). The stereotypical progression of PVAN is thoroughly characterized and is as follows (Ramos et al., 2009). Most of the cases are initially asymptomatic with a persistent and significant viruria, as indicated by detectable urine viral load > 10^5 BKPyV copies/ml or by urine cytology. Viremia usually follows BKPyV viruria within the next few weeks (Ramos et al., 2009). The significant and sustained BKPyV viremia indicates the uncontrolled viral replication in patients, which potentially results in parenchymal injury. Progression of PVAN ultimately leads to deterioration of renal graft function and kidney failure (Ramos et al., 2009). Interstitial nephritis and ureteric stenosis with ureteric obstruction, hydronephrosis and urinary tract infections may be developed during PVAN as well (Hariharan, 2006).

There are several histologic features which are observed in patients diagnosed with PVAN, including viral inclusion bodies which are detected in epithelial cells of the urothelium. The virus is usually detected by immunohistochemical staining with an

antibody that detects the SV40 TAg, and effectively cross-reacts with BKPyV TAg (Nickeleit et al., 1999; Costa and Cavallo, 2012). There are three distinct histological patterns of PVAN. In pattern A, which includes the early stage of the disease, cytopathic alterations with little to no inflammation sign or tubular atrophy are observed. Cytopathic changes with inflammation, tubular atrophy and fibrosis indicate pattern B of PVAN. Finally, extensive tubular atrophy, interstitial nephritis and chronic inflammatory infiltrate are present in the end-stage of PVAN, which is described as pattern C. Thus, the degree of damage reflects the degree of renal graft dysfunction and outcome (Scadden et al., 2017; Costa and Cavallo, 2012; Drachenberg et al., 2004).

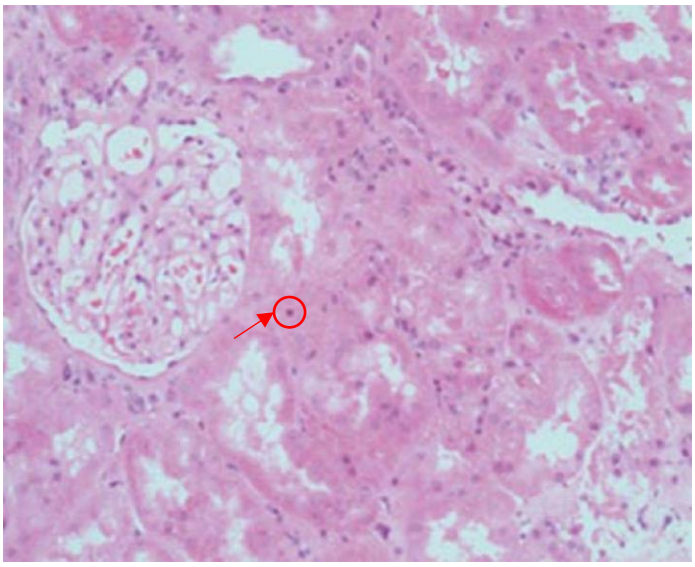

Figure 1. 3 Renal biopsy sample. Renal biopsy with preserved tubular morphology, without significant damage or inflammation. PVAN confirmed by positive SV40 staining which is shown in dark purple colour. Adapted from Scadden *et al*., (2017).

1.3.3 Diagnosis of PVAN

BKPyV is first detected in the urine after its reactivation, and then follows viremia several weeks later. However, there are some rare cases reported, which identify patients with viremia without developing viruria. Studies have shown that screening for BKPyV has higher positive predictive rates for PVAN (50-60%) compared with BKPyV viruria, therefore specific screening for BKPyV is more preferred (Bechert et al., 2010). Table 1.2 presents the different screening methods that are currently used (Sawinski and Goral, 2015).

Real-time PCR can be used to diagnose PVAN in individuals by detecting BKPyV in plasma. Studies have shown that this screening method is very specific and sensitive reaching 90% and 100%, respectively. Positive predictive values for PVAN is approximately 50%, whereas negative predictive rate is 100% (Hirsch et al., 2002; Viscount et al., 2007). Currently, this is the most preferred screening test and a suggested BKPyV viral load more than 4log copies/ml is strongly correlated with diagnosis of PVAN on renal biopsy (Hirsch et al., 2005; Scadden et al., 2017).

BKPyV can also be detected in the urine of approximately 30% of kidney transplant recipients (Wiseman, 2009). There are two distinct methods for screening urine samples: BKPyV detection by cytology and quantification of BKPyV DNA by real-time PCR reaction. “Decoy cells” are infected tubular epithelial cells with BKPyV and can be detected in urine samples. These cells have a characteristic morphology and are easily recognizable as they have a basophilic nucleus containing viral inclusion bodies (Wiseman, 2009). Although, studies have highlighted that screening methods for urine BKPyV based on PCR reaction are more sensitive compared to urine cytology for diagnosis of PVAN. The detection of decoy cells shows only 25% sensitivity and approximately 84% specificity for PVAN in comparison with urine BKPyV PCR which reaches 100% sensitivity and 78% specificity, respectively (Viscount et al., 2007; Costa and Cavallo, 2012).

Icosahedral BKPyV viral aggregates (“Haufen”) were first investigated by Singh et al., (2009) in urine samples of renal transplant recipients diagnosed with PVAN using negative staining electron microscopy. These aggregates are originated from lysed BKPyV infected renal cells. It was reported that 21 renal transplant recipients

diagnosed with PVAN by biopsy were also positive for Haufen aggregates in their urine, suggesting that Haufen are highly related with PVAN. These findings suggest that detection of Haufen might serve as a noninvasive screening method for diagnosis of PVAN in the future (Kuypers, 2012; Sawinski and Goral, 2015).

Another biomarker for native renal disease is urine mRNA profiles. Studies have proposed that BKPyV VP1 mRNA molecules derived from urinary cells can be used for PVAN diagnosis (Singh et al., 2009). An approximate $6.5x\ 10^5$ VP1 mRNA/ng RNA is the threshold value indicating PVAN, as it was suggested by Dadhania et al., (2010) by studying patients diagnosed with PVAN by renal biopsy. A very recent study revealed that BKPyV miRNA molecules are highly abundant in urinary exosomes of patients diagnosed with PVAN and can be quantified using standard PCR methods. The diagnostic power of BKPyV miRNA is comparable to those of plasma and urine BKPyV viral load, suggesting that urinary exosomal miRNA could be used as a biomarker for the diagnosis of PVAN (Kim et al., 2017).

Renal biopsy remains the gold standard for PVAN diagnosis and is obligatory in transplant recipients with a level of BKPyV viral load over than 4log copies/ml regardless of levels of serum creatinine (Sawinski and Goral, 2015). Renal biopsy as a screening method is challenging due to the fact that a negative renal biopsy cannot eliminate PVAN at early stages with 100% certainty. Although, the level of renal fibrosis and tubular atrophy appears to be the most predictive of renal graft clinical outcome (Masutani et al., 2012). Importantly, tubular cytopathic alterations and interstitial nephritis that are developed during PVAN can be focal or isolated solely to the medulla and missed on one third of renal biopsies if only a single core is tested (Drachenberg et al., 2004; Sawinski and Goral, 2015). Therefore, at least two cores including medulla should be extensively examined. In some reported cases, there is high suspicion of PVAN, although there are no cytopathic alterations on renal histology. For that reason, immunohistochemistry against BKPyV or cross-reacting SV40 TAg is suggested (Howell et al., 1999).

Table 1. 2 Screening methods for PVAN diagnosis. Four distinct methods that are currently used for PVAN diagnosis are represented and positive/negative predictive values, sensitivity and specificity of each method are also summarized. Adapted from Sawinski and Goral, (2015).

Screening method	Positive predictive value (%)	Negative predictive value (%)	Sensitivity (%)	Specificity (%)
Decoy cells (Hirsch et al., 2002)	29	100	25	84
Haufen aggregates (Singh et al., 2009)	97	100	100	99
BKPyV urine PCR (Hirsch et al., 2002; Nickeleit et al., 2000; Kuppachi et al., 2013)	40	100	100	78
BKPyV serum PCR (Hirsch et al., 2002; Nickeleit et al., 2000; Kuppachi et al., 2013)	50-60	100	100	88
BKPyV miRNA (urinary exosome) (Kim et al., 2017)	-	-	100	98.5

1.3.4 Therapeutic interventions for PVAN

There are more than 100,000 patients in the USA in the waiting list for renal transplantation and in 2014 there were only 17,000 donor kidneys available for transplantation. Today there are approximately 5,000 people in the UK, waiting for a renal transplantation and around 3,000 donor kidneys are reported each year. Currently, there is no specific anti-viral therapy to treat PVAN and knowing that the level of immunosuppression is the main risk factor for the development of PVAN, the management of BKPyV infections is currently relied on reduction of immunosuppressive treatments (Mazalrey et al., 2015). Although, this may lead to acute allograft rejection (Johnston et al., 2010). Reduction of immunosuppressive drugs is applied in patients diagnosed with PVAN, histologically, as a curative treatment. It can also be applied in patients who are positive for BKPyV viremia, but not diagnosed with PVAN yet, as a pre-emptive treatment. Studies have proposed that pre-emptive treatment can be applied in patients with BKPyV plasma viral load higher than 10^4 DNA copies/ml (Hirsch et al., 2013). These therapeutic approaches include reduction or discontinuation of corticotherapy and the dose of other immunosuppressive drugs are reduced by 50% or switching to less potent drugs including Azathioprine, Sirolimus or Leflunomide and Cyclosporine A (Mazalrey et al., 2015; Hirsch et al., 2013; Alméras et al., 2008; Saad et al., 2008; Trofe et al., 2004). Despite the lack of specific clinical treatment against BKPyV, there are some additional treatments which are used as adjuvant therapies alongside the immunosuppressive drugs and are based on their anti-viral activity *in vitro* (Lamarche et al., 2016; Ambalathingal et al., 2017).

The acyclic deoxycytidine monophosphate analogue Cidofovir was first described for its anti-viral activity against cytomegalovirus (CMV), which impairs virus DNA replication (Mazalrey et al., 2015). Previous studies have reported that inhibition of BKPyV replication was observed *in vitro* upon Cidofovir treatment, although the drug shows significant cytotoxic effects (Bernhoff et al., 2008). Importantly, side effects of Cidofovir are observed in *in vivo* studies revealing significant nephrotoxicity (Kuypers et al., 2008). Brincidofovir (CMX001), is a lipid-conjugated derivative of Cidofovir and is internalized by cells similar to lysophosphatidylcholine. Following, cellular internalization Cidofovir is liberated from Brinicidofovir and become active after its phosphorylation. It is highlighted that Brincidofovir shows a greater anti-viral function

compared to Cidofovir in urothelial and human primary kidney epithelial cells and has a lower incidence of nephrotoxicity (Rinaldo et al., 2010; Marty et al., 2013; Tylden et al., 2015).

The immunosuppressive drug Leflunomide is used as a treatment for rheumatoid arthritis (Mazalrey et al., 2015). This drug acts by blocking protein kinase activity and the synthesis of pyrimidines (Elder et al., 1997). Recent studies have established that Leflunomide can also be administered in renal transplant recipients to prevent chronic graft rejection and due to its low nephrotoxicity. It impedes BKPyV replication *in vitro* and reduces TAg expression (Bernhoff et al., 2010). Encouraging results have been seen in *in vivo* studies (Williams et al., 2005), although further validation by clinical studies is required (Mazalrey et al., 2015).

Fluoroquinolones are antibiotics that target bacterial topoisomerases, however they can also have an activity against polyomaviruses (Sharma et al., 2011). It is known that Quinolones inhibit BKPyV replication in human renal proximal epithelial cells, due to the blockade of TAg as helicase as well as DNA topoisomerase (Sharma et al., 2011). Studies have also identified that Fluoroquinolones impair SV40 replication in monkey kidney cells (Josephson et al., 2006). Initial non-randomized studies show encouraging reductions in BKPyV viral load of patients diagnosed with PVAN upon a combination treatment of Ciprofloxacin and Leflunomide (Zaman et al., 2014). Whereas, two more recent randomized controlled studies reported that Levofloxacin was not effective as either a curative (Knoll et al., 2014) or pre-emptive (Lee et al., 2014) PVAN therapy.

The mTOR inhibitor, Sirolimus, is used as an immunosuppressive drug due to its ability to impede IL-2 dependent T cell proliferation and its impact on TReg generation and T cell metabolic programming (Lo et al., 2014). However, Sirolimus can also decrease BKPyV TAg expression but not DNA replication in *in vitro* studies (Liacini et al., 2010a).

Intravenous immunoglobulins have also been used as an adjuvant therapy for PVAN. Previous studies have proposed that immunoglobulins are capable of blocking BKPyV replication in human primary kidney cells (Randhawa et al., 2010; Randhawa et al., 2015). Although, due to the high levels of existing and specific antibodies against

BKPyV in patients diagnosed with PVAN, intravenous immunoglobulins are not sufficient to control BKPyV replication. Furthermore, the efficacy of immunoglobulins is not fully understood as they are administered in combination with immunosuppressive drugs; therefore, further investigation by clinical trials is required (Mazalrey et al., 2015).

Clinical trials are currently performed including treatments with BD03 from SL VAXIGEN. BD03 is a DNA vaccine that consists of 3 plasmid DNA molecules encoding for CMV and BKPyV antigens. It is expected to express antigen specific T-cell immune response, and ultimately prevent activation of both viruses. Kidney transplant patients are receiving BD03 intramuscularly by electroporator three times on 6 weeks and 2 weeks prior to renal transplantation and up to 4 weeks after. The study completion date is eastimated in July 2019 (Clinicaltrials.gov, 2018).

1.4 BK Polyomavirus (BKPyV)

1.4.1 Epidemiology and transmission of BKPyV

Epidemiology studies have reported that primary BKPyV infection occurs during childhood at a median age of 4-5 years (Shah et al., 1973; Knowles, 2001). It is identified that seroprevalence is lowest at the early age of 6 months after the loss of maternal antibodies and reaches to approximately 75% among adults (range 46-94%), worldwide (Ambalathingal et al., 2017; Knowles, 2001). The natural route of virus transmission might be a respiratory route as viral DNA is present in tonsillar tissue (Goudsmit et al., 1982; Knowles, 2006). Additionally, there are other routes of transmission, including blood transfusion, urino-oral, fecal-oral and transplacental (Abend, et al., 2009).

It is established that BKPyV persists for a lifelong infection and disseminates to the urinary tract (Heritage et al., 1981). Studies have shown that BKPyV DNA has been detected not only in the ureter, bladder and renal epithelial cells, but also in peripheral blood mononuclear cells, proposing that BKPyV might hijack host cell immune system to spread from the primary site of infection to its site of persistence (Chatterjee et al., 2000). However, it is still poorly understood whether BKPyV enters a true state of viral

latency or maintain a minimal level of replication (Bennett et al., 2012). Doerries (2006) reported that BKPyV may be re-activated and detected in the urine of healthy individuals, periodically, which supports the evidence of an urino-oral infectious transmission route.

Moreover, there are four distinct BKPyV genotypes: I, II, III and IV which present sequence variation in VP1 protein and correspond to specific serotypes, as well (Jin et al., 1993; Pastrana et al., 2013). Hemagglutination inhibition assays revealed that genotypes I, II, III and IV correspond to BK, SB, AS and IV serotypes, respectively (Knowles et al., 1989). Epidemiological studies have identified a correlation between geographical areas and BKPyV genotypes and subgroups within genotypes. BKPyV genotype I is the predominant and within this genotype, subgroup I/b-2 is mainly detected in European and American populations, although subgroup I/c-2 is primarily observed in Asian populations (Zhong et al., 2009). It still remains unclear whether there is any correlation between genotypes and clinical disease (Bennett et al., 2012).

1.4.2 Cellular tropism of BKPyV

Several different cell lines can be productively infected, *in vitro*, by BKPyV including simian and human kidney epithelial cells, endothelial cells, foetal neuronal cell lines, human fibroblasts and epithelial cells from salivary glands (Jeffers et al., 2009). Furthermore, BKPyV genomic DNA has been isolated, *in vivo*, from many different tissues such as salivary glands, the urothelium and renal epithelia, however kidney epithelial cells appear as the main reservoir of BKPyV persistent infection (Mazalrey et al., 2015). In addition, previous studies have identified the presence of BKPyV DNA in lymphocytes of both healthy and unhealthy individuals (Dolei et al., 2000; Azzi et al., 1996), supporting the evidences which show BKPyV receptors on the surface of lymphocytes (Possati et al., 1983). It is established that JCPyV can enter B-lymphocytes so as to be transmitted to glial cells and not in order to be actively replicated. These findings proposed a model for JCPyV transportation across the blood-brain barrier of the human host (Chapagain and Nerurkar, 2010). Even though, the role of lymphocytes in a successful BKPyV infection has not been fully identified, a similar mechanism of transmigration in human hosts might occur in the case of

BKPyV. BKPyV might enter B-lymphocytes to transport from the initial site of infection to distant target tissues including renal epithelial cells and the urothelium. However, there is no experimental evidence indicating that BKPyV actively replicates in lymphocytes or that a cell-to-cell transmigration including lymphocytes has been identified (Mazalrey et al., 2015).

1.5 Molecular Virology of BK Polyomavirus (BKPyV)

1.5.1 Structure and Genome Organization

BKPyV is a non-enveloped virus containing a double-stranded DNA genome, which is super-coiled with the host cell histone proteins H2A, H2B, H3 and H4 generating a minichromosome (Mazalrey et al., 2015; Fang et al., 2010; Wright and Di Mayorca, 1975). It is established that infectious BKPyV particles have a diameter of approximately 45 nm and a density of 1.34 g/ml (Hurdiss et al., 2016; Seehafer et al., 1975; Wright and Di Mayorca, 1975).

Current resolutions of cryo-electron microscopy (EM) BKPyV virion structures range from 8 to 25 Å (Hurdiss et al., 2016; Li et al., 2003; Nilsson et al., 2005; Shen et al., 2011; Li et al., 2015). A recent study solved the solution structures of native BKPyV virions and virus-like particles (VLPs) using single particle cryo-EM with a direct electron-detecting camera (Hurdiss et al., 2016). BKPyV virions and VLPs were detected at a resolution of 7.6 Å and 9.1 Å, respectively (Figure 1.4A). A more recent study determined the structure of BKPyV at a resolution of 3.8 Å (Figure 1.4B), using high-resolution cryo-EM and presenting the highest-resolution EM structure solved for any other human polyomaviruses to date (Hurdiss et al., 2018). These high-resolution structures allowed the visualization of secondary structural motifs, including β sheets and α helices (Hurdiss et al., 2016). Moreover, differences between human pathogens and those that infect murine and simian hosts, including differences in how both disulphide bonds and C-terminal arms stabilize the capsid can be highlighted (Hurdiss et al., 2018).

Previous studies of SV40 (Stehle et al., 1996) and murine polyomavirus (MPyV) (Stehle and Harrison, 1996) proved that both native virions and VLPs are isometric

particles. A more recent study reported that BKPyV virions and VLPs are isometric particles as well (Hurdiss et al., 2016). It is known that BKPyV capsids are composed of 360 molecules of VP1 forming 72 pentamers arranged in a T = 7d icosahedral symmetry stabilized by intra- and inter-pentameric disulphide bonds and Ca^{2+} cations (Nilsson et al., 2005). Furthermore, studies have demonstrated that there are six distinct conformations of VP1 in the BKPyV shell (Figure 1.4C) (Hurdiss et al., 2016; Hurdiss et al., 2018). The pentamers are tied together using C-terminal arms, with each pentamer of VP1 interacting with five such arms to and from adjacent pentamers (Hurdiss et al., 2016). In addition to these pentamers found in the outer surface of BKPyV capsid, VP2 and VP3, the two other structural proteins, reside in the inner part of BKPyV virions (Hurdiss et al., 2016). Electron microscopy studies have also reported that there are bridges between VP2/VP3 proteins and the encapsidated double-stranded genomic DNA with packaged histone proteins (Figure 1.4D) (Hurdiss et al., 2016). Moreover, it is identified that there are bridges between the VP1 capsid and encapsidated double-stranded DNA situated beneath the N-termini of each of the six VP1 quasi-equivalent conformers (Hurdiss et al., 2016).

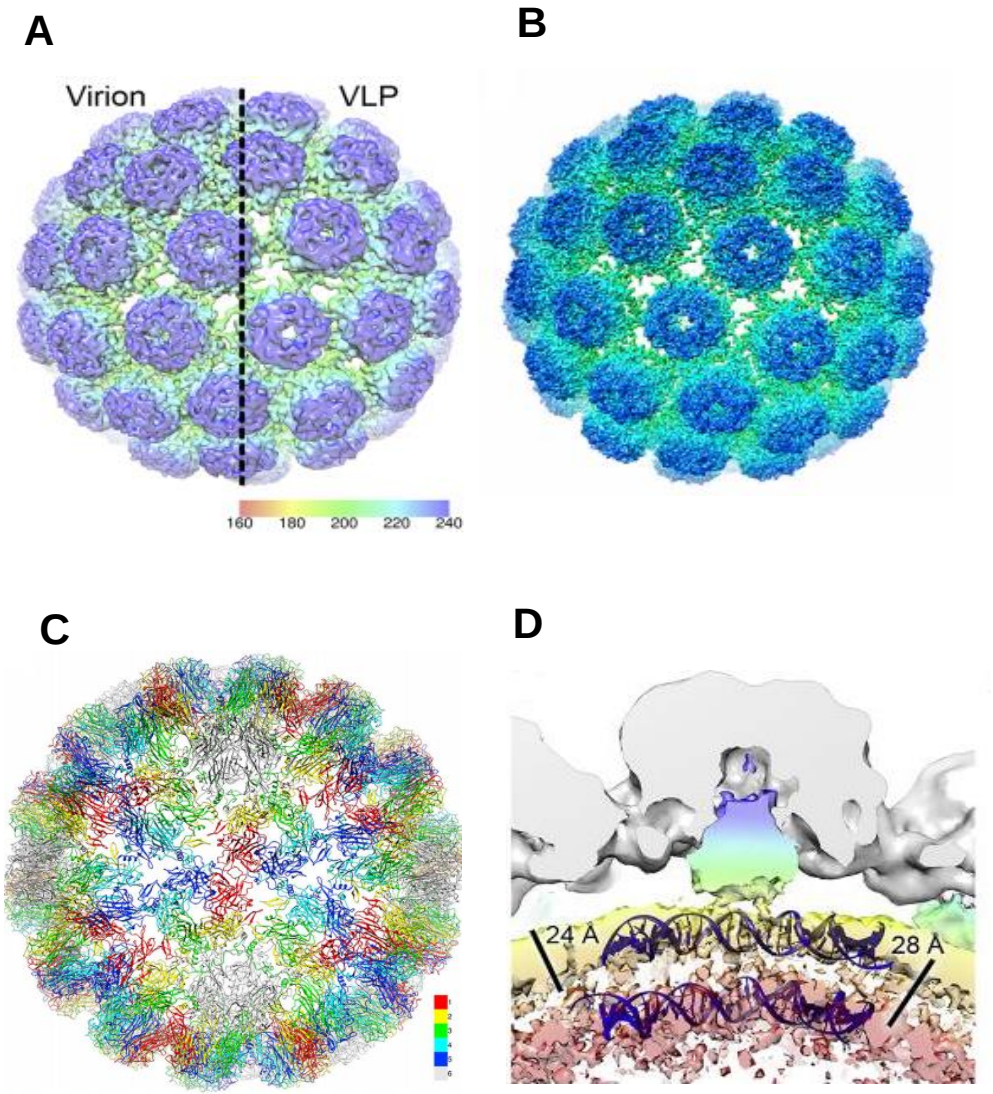

Figure 1. 4 Cryo-electron microscopy structures of native BKPyV virions and VLPs. A. External view of BKPyV native virion (left) (7.6 Å) and VLP (right) (9.1 Å) is presented at contour levels of 0.022 and 0.009, respectively (Hurdiss *et al*., 2016). B. Isosurface representation of the 3.8 Å structure of BKPyV (Hurdiss *et al*., 2018). C. The architecture of a polyomavirus capsid showing how the T = 7d capsid is consisted of 72 pentamers of VP1, and an identical VP1 polypeptide is identified in six distinct quasi-equivalent conformations in the capsid shell (1, red; 2, yellow; 3, green; 4, cyan; 5, blue and 6, gray) (Hurdiss *et al*., 2018). D. Enlarged view of a pyramidal density below each single VP1 penton. Strands of double-stranded DNA wrapped around a human histone octamer are represented. The density within 6 Å of the fitted co-ordinates for SV40 VP1 is coloured grey. Density for VP2 and VP3 is coloured blue/green and for packaged double stranded DNA yellow/pink. Scales bars shown (Hurdiss *et al*., 2016).

The BKPyV genome is approximately 5,000 bp in size and replicates bidirectionally from a unique origin. It is composed of two regions, that are highly conserved, and coding for early and late proteins, located adjacent a non-coding control region (NCCR) of approximately 400 bp (Figure 1.5) (Helle et al., 2017). Large tumour antigen (TAg), small tumour antigen (tAg) and the truncated TAg (truncTAg) are encoded by the early genes and expressed by alternative splicing soon after infection of host cells and prior to genome replication. The late structural proteins VP1, VP2 and VP3 and the non-structural protein, agnoprotein, are encoded by the late genes and expressed after the initiation of genome replication (Helle et al., 2017).

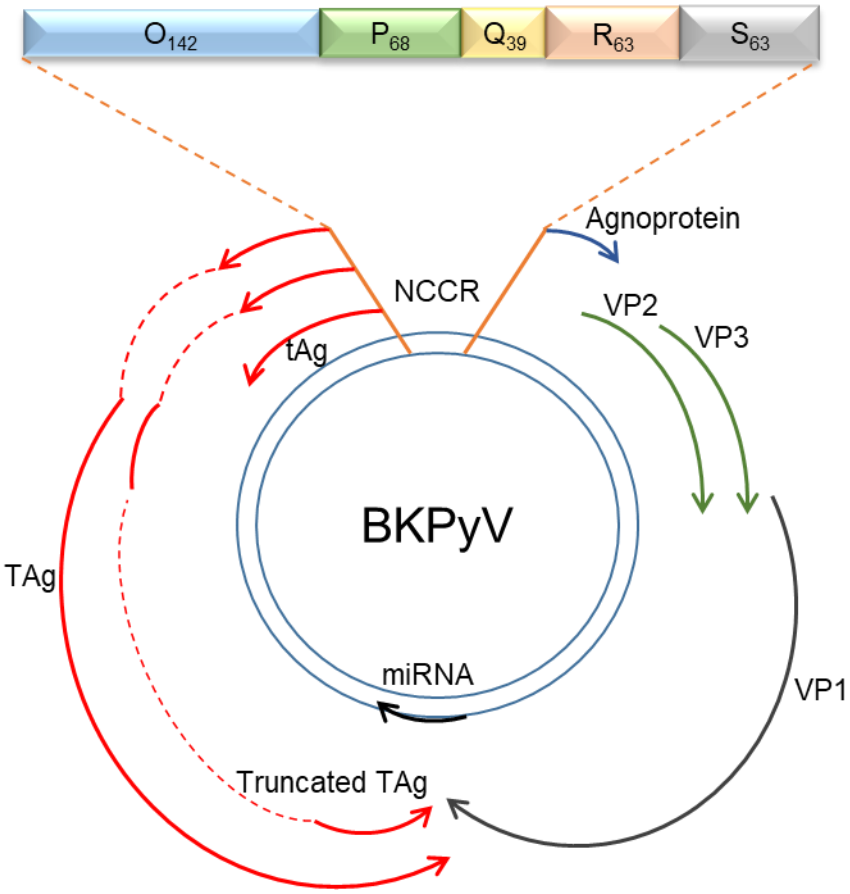

Figure 1. 5 Schematic representation of the BK Polyomavirus (BKPyV) genome. BKPyV genome is a double-stranded DNA molecule of approximately 5,000 bp and is organized in three main regions: the early region (on the left) encodes for the tumour antigens (TAg, tAg, trucTAg), the late region (on the right) expresses structural (VP1, VP2 and VP3) and non-structural (agnoprotein) proteins and the non-coding control region (NCCR). Transcription of both early and late genes occurs in opposing directions. Solid arrows represent exons and dashed lines represent introns. The viral miRNA is transcribed from the late transcript. The archetype form of the NCCR (WW strain) is shown as a sequence of blocks (OPQRS) with the number of base pairs in each domain. Adapted from Mazalrey *et al*., (2015).

1.5.2 Non-coding control region (NCCR)

The archetypal strains of BKPyV are predominately found in the urine of human individuals and are thought to be the transmissible form of the virus (Rubinstein et al., 1987; Yogo et al., 2008). The NCCR of BKPyV archetypes consists of five distinct sequence regions starting from the O domain which is 142 bp in length and includes the origin of BKPyV genome replication and TATA-box. Then follows the P block of 68 bp, the Q block which is 39 bp in length, the R block of 63 bp and the S block of 63 bp in length is the last block. TATA-like elements and other regulatory regions that facilitate both early and late genes expression are contained in the PQRS blocks (Cubitt, 2006; Bethge et al., 2015; Bethge et al., 2016). *In silico* studies have reported approximately 30 different transcription factor binding sites, which might be contained in the NCCR (Bethge et al., 2015; Moens et al., 1995; Johnsen et al., 1995). There is evidence that Sp1 play a major role in regulation of early and late gene expression (Bethge et al., 2015; Bethge et al., 2016). It is identified that the number of binding sites, the strand orientation and the affinity of Sp1 transcription factor is critical for the bidirectional balance of early and late genes expression. Other studies have also highlighted the importance of NF-κB, NF1 and Ets-1 (Bethge et al., 2015; Gorrill and Khalili, 2005). Additionally, oestrogen-responsive elements, phorbol ester-, glucocorticoid/progesterone-, and cAMP can also control BKPyV transcription and replication (Moens et al., 1990; Moens et al., 1994).

The NCCR varies considerably amongst different BKPyV isolates, even though protein coding sequences are highly conserved in most BKPyV strains. Therefore, the NCCR variety isolated from human kidneys is often associated with clinical complications (Cubitt, 2006). Duplications or triplications of P block are the most common re-arrangement of NCCRs observed, although variations of the neighboring O and Q blocks have been identified as well. Moreover, other variations such as deletions can occur within the P, Q, R and S blocks, however part or even the whole R block might be deleted in some cases. Studies have shown that most known variants tend to retain P and S blocks, suggesting the importance of these sequences (Moens and Van Ghelue, 2005). Nonetheless, all these important variations in the NCCR sequence lead to the creation or deletion of transcription factor binding sites (Bethge et al., 2015; Markowitz et al., 1990). Previous studies have established that a relatively weak early gene expression and a strong late gene expression are

benefited by the archetypal NCCR sequence, although the opposite phenomenon is observed in re-arranged NCCR forms regardless of deletions or insertions (Markowitz et al., 1990; Gosert et al., 2008).

The architecture of NCCR might indicate the oncogenic potential and the cell tropism of BKPyV, *in vitro* (Johnsen et al., 1995). The ability amongst polyomaviruses to adapt to different environments might be reflected by the NCCR architecture. Additionally, a progressive number of re-arrangements of the BKPyV NCCR might be observed with the disease progression (Helle et al., 2017). It is determined that an increased BKPyV replication and cytopathology were detected in renal transplant recipients positive for BKPyV with a re-arranged NCCR form (Gosert et al., 2008). BKPyV with both archetypal or re-arranged form of NCCR can be isolated from patients who suffer from PVAN, whereas archetypal BKPyV is often detected in the urine for an unknown reason. Contrary, re-arranged forms of BKPyV are often isolated from plasma samples and are correlated with higher values of plasma viral loads (Gosert et al., 2008). Moreover, it is identified that both the archetype and the re-arranged NCCR form of BKPyV have been detected not only in PVAN sufferers, but also in cerebrospinal fluid from neurological patients with suspected JCPyV infection (Barcena-Panero et al., 2012).

The archetypal form of BKPyV replicates poorly in cell culture systems compared with the re-arranged strains (Helle et al., 2017). As such, these re-arrangements of the NCCR sequence might be critical for the virus adaptation which in turn are important for efficient growth in various cell types in cell culture (Moens and Van Ghelue, 2005). Other studies have also supported this hypothesis indicating that the NCCR sequence has a major impact on virus replication *in vitro* (Broekema et al., 2010). Furthermore, NCCR sequencing following viral amplification *in vitro* reveals duplications and/or deletions, that are not observed in NCCR sequences directly extracted from human urine samples (Rubinstein et al., 1987; Markowitz et al., 1990). A weak TAg protein expression from the archetypal BKPyV might be a limiting factor for the virus propagation as TAg overexpression is able to rescue genome replication (Broekema and Imperiale, 2012).

1.5.3 BKPyV proteins

1.5.3.1 Early proteins

TAg, tAg and truncTAg are expressed by the early region of the BKPyV genome through alternative splicing. After the removal of the first intron, the first and the second exons generate the TAg, which is a protein of approximately 80 kDa. Alternatively, retention of the first intron reveals the presence of a stop codon, allowing generation of tAg, which is translated into a protein of around 20 kDa. Therefore, TAg and tAg share the same first 82 amino acids but have unique carboxyl regions (Helle et al., 2017). Studies have also identified the expression of a third translation product, the truncTAg protein of approximately 17 kDa (Abend et al., 2009). truncTAg is generated from alternative splicing and the removal of a second intron from the mRNA product encoding for TAg. Therefore, truncTAg and TAg share the first 133 amino acids, but the additional slice leads to translation from a different reading frame, adding three new amino acids before reaching a stop codon (Abend et al., 2009).

A nuclear localization signal (NLS) is contained in both TAg and truncTAg and as a result both proteins are detected in the nucleus (Helle et al., 2017). Studies have shown that both proteins contain a J domain in their N-terminus which exhibits high homology with members of the DnaJ family, the molecular chaperone proteins, which interacts with the heat shock cognate 70 co-chaperone (Hsc70) and plays a critical role in viral replication (Kelley and Georgopoulos, 1997; An et al., 2012; DeCaprio and Garcea, 2013). Another conserved LXCXE motif is contained in both TAg and truncTAg and this facilitates their interaction with pRb and the p107 and p130 family members (Harris et al., 1996; Harris et al., 1998). This interaction displaces pRb from the E2F transcription factor, transactivating genes associated with the S phase progression and DNA synthesis resulting in cell cycle progression and viral genome replication (Harris et al., 1996; Harris et al., 1998; An et al., 2012; DeCaprio and Garcea, 2013).

The region of TAg that is unique compared to truncTAg, contains a Zinc-binding domain, an ATPase domain and a DNA-binding domain (DBD) providing a DNA helicase activity to TAg, which is critical for BKPyV genome replication (An et al., 2012; DeCaprio and Garcea, 2013). The sequence GRGGC is present in the origin

of replication within the NCCR and is recognized specifically by the DBD of TAg. In addition, the interaction between DBD and the Replication Protein A (RPA) is critical for efficient viral amplification. The active helicase consists of TAg hexamers, formed by the Zinc-binding domain, and the energy that is required for helicase function is provided through the ATPase domain. Studies have also reported that the helicase domain can bind to the p53 tumour suppressor to block cell cycle arrest and apoptosis (An et al., 2012; DeCaprio and Garcea, 2013; Harris et al., 1996; Nakshatri et al., 1988).

In contrast to TAg, tAg can localize to both the cytoplasm and the nucleus. In additional to the N-terminal J domain, tAg contains a unique C-terminal region containing two zinc-fingers. Through this region, tAg inactivates proteins phosphatase 2A and this supports cell cycle progression (An et al., 2012; DeCaprio and Garcea, 2013). All these functions of both TAg and tAg implicating them in cell cycle events are primarily responsible for the potential cell transformation by BKPyV. There is evidence identifying BKPyV as a potential co-factor involved in human prostate cancers (Tognon and Provenzano, 2015). Furthermore, a recent study highlighted that BKPyV integrated into the human chromosomal DNA in a kidney graft tumour, showing strong TAg protein expression, interference of late genes expression and blockade of genome amplification (Kenan et al., 2015). Although, BKPyV is still characterized as potential carcinogenic to humans due to inadequate evidence (Helle et al., 2017).

1.5.3.2 Structural late proteins

The BKPyV structural proteins VP1, VP2 and VP3 are essential during the viral life cycle as they form the virus capsid necessary for virus entry and egress (Helle et al., 2017). VP1 is the major capsid protein composed of 362 amino acids and approximately 42 kDa in mass. It is divided into five distinct loops, BC, DE, EF, GH and HI that bridge the strands of the protein (Teunissen et al., 2013). Pentamers of VP1 are located at the exterior of the capsid and it is demonstrated that VP1 loops play critical roles in capsid assembly (Dugan et al., 2007). BKPyV capsid has a quasi-symmetry and is formed by 72 pentons of VP1 (Hurdiss et al., 2018). It is highlighted

that VP1 pentamers are composed of five β-barrel-shaped VP1 monomers that form a ring and are tightly linked through loops that interact with the frameworks of β-strands (Hurdiss et al., 2016; Hurdiss et al., 2018). Moreover, it is identified that the N-terminal of VP1 protein is located in the interior of the virion and binds to the encapsidated viral DNA genome (Hurdiss et al., 2016). The C-termini of each VP1 undergoing exchange with neighboring pentons to stabilize the capsid shell, adopting six distinct conformations that allow a single VP1 sequence to adopt all of the positions in a T = 7d lattice (Hurdiss et al., 2016; Hurdiss et al., 2018) (Figure 1.4). This is also supported by evidences stating that VP1 monomers lacking C-terminal region cannot form stable virus-like particles even though capsomers are formed (Teunissen et al., 2013).

Studies have also shown that VP1 plays an essential role in viral attachment to host cell receptors of target cells. Site directed mutagenesis analysis revealed that there are key residues of VP1 protein sequence that are essential for several processes during the BKPyV life cycle including viral infectivity, binding to host cell receptor, entry, and assembly (Dugan et al., 2007; Neu et al., 2013). Studies have also reported that phosphorylation of Ser-80 of VP1 has been determined crucial for BKPyV propagation (Chen et al., 2011). Moreover, a shallow groove between BC and HI loops of BKPyV VP1 protein is predicted to be the receptor-binding site (Figure 1.6) (Jin et al., 1993; Dugan et al., 2007). Also, the epitopes which are responsible for the variation of the different BKPyV serotypes are located on BC loop (Jin et al., 1993). The VP1 subtyping region is located between amino acids 61 and 83 and is used as a tool to distinguish the different serotypes (Jin et al., 1993). A recent study by Morel et al., (2017) generated an algorithm to facilitate the recognition and confirmation of the 12 different BKPyV subtypes/subgroups based on a 100 bp-region located on VP1 sequence and called the BKPyV typing and grouping region.

VP2 and VP3 are the minor capsid proteins and are approximately 38 kDa and 27 kDa in mass, respectively. The same late mRNA transcript expresses both VP2 and VP3 protein and as a result, the C-terminal region of both proteins is common. The initiating AUG codon of VP3 is in-frame with the downstream initiating VP2 AUG codon, therefore VP3 is an N-truncated isoform of VP2 (Figure 1.5) (Schowalter and Buck, 2013). In related polyomaviruses such as SV40 and JCPyV, the VP2 N-terminus is modified by the addition of myristic acid. Whilst BKPyV VP2 shares the

consensus myristoylation sequence including the critical glycine at residue 2, mass spectrometry studies have thus far failed to detect this modification (Fang et al., 2010). Three important features reside in the common C-terminal region shared by VP2 and VP3 including a DNA-binding region, an NLS and the VP1-binding region (Henriksen et al., 2016). A single copy of either protein interacts with each VP1 pentamer through hydrophobic interactions (Hurdiss et al., 2016). In addition, viral assembly or virion stability are not affected by the absence of both minor capsid proteins (Hurdiss et al., 2016; Teunissen et al., 2013). Stable VLPs consisted of VP1 only, were able to transduce cell lines suggesting that the absence of either VP2 or VP3 did not impact on BKPyV capsid formation (Hurdiss et al., 2016). Contrary mutations in one amino acid of BKPyV VP2 (amino acid 229) and/or VP3 (amino acid 110) negatively affect the viral replication cycle at a stage prior to DNA replication, as that impact was not noticed upon DNA transfection in RPTE cells (Henriksen et al., 2016). Moreover, it is demonstrated that mutations of start codons of the BKPyV minor capsid proteins together or alone cause a reduction of infectivity by approximately 99% in comparison with the wild-type (Henriksen et al., 2016). Similar results were also observed in experiments utilizing BKPyV pseudoviruses or mouse polyomavirus and SV40, JCPyV mutants lacking either VP2 or VP3 or both VP2/VP3, although the mechanism by which the minor capsid proteins facilitate virus infection remains controversial (Bagchi et al., 2015; Schowalter et al., 2012; Daniels et al., 2006; Gasparovic et al., 2006; Mannová et al., 2002).

Daniels et al., (2006) suggested that SV40 minor capsid proteins promote the escape of the virus from the endoplasmic reticulum (ER). Other studies suggested that VP3 is critical for ER escape, whereas the VP2 role is to direct transportation of the virus to the ER (Inoue and Tsai, 2011). Contrary, it is proposed that SV40 VP2 and VP3 are critical for the nuclear import of the viral genome, and the virus escape occurs without the benefit of the minor capsid proteins (Nakanishi et al., 2007). In 2008, Merkel cell polyomavirus (MCPyV) was discovered and associated with Merkel cell carcinoma (Feng et al., 2008). MCPyV lacks VP3 protein, although both VP1 and VP2 proteins are expressed (Schowalter and Buck, 2013). Studies utilizing both MCPyV and BKPyV pseudoviruses revealed the importance of minor capsid proteins on pseudovirion transduction (Schowalter and Buck, 2013). It is reported that VP2 is dispensable for MCPyV infectious entry in some cell types including UACC-62 cells

and SK-MEL-2 cells (melanoma cell lines), whereas it is required for the transduction of HEK293TT cells (embryonic kidney cells), NCI/ADR-RES cells (ovarian cancer line) and A549 cells (lung cancer line) (Schowalter and Buck, 2013). However, BKPyV pseudovirions transduction was significantly higher in the presence of all the structural proteins, highlighting the importance of the minor capsid proteins (Schowalter and Buck, 2013).

Post-translational modifications of the structural proteins might be essential for different functions (Fang et al., 2010; Ponder et al., 1977). Key phosphorylated residues of polyomavirus VP1 have been detected at Ser-66, Thr-63 and Thr-156 (Li and Garcea, 1994; Li et al., 1995). Studies have demonstrated that mutations at that positions negatively affect the replication cycle of polyomaviruses (Li and Garcea, 1994; Li et al., 1995). Other studies have stated that specific post-translational modifications of both VP1 and VP2 might be crucial for BKPyV propagation (Chen et al., 2011). BKPyV VP1 is phosphorylated at Ser-80, Ser-133 and Ser-327, BKPyV VP2 at Ser-223 and Ser-254 and BKPyV VP3 at Ser-129, respectively. However, only the phosphorylation of Ser-80 of VP1 and Ser-254 of VP2, respectively, have been reported as crucial for BKPyV propagation since mutations at these specific positions led to inhibition of the replication cycle. Nevertheless, the mechanism of how phosphorylation of structural proteins contributes to regulation of BKPyV replication is still not clear (Chen et al., 2011).

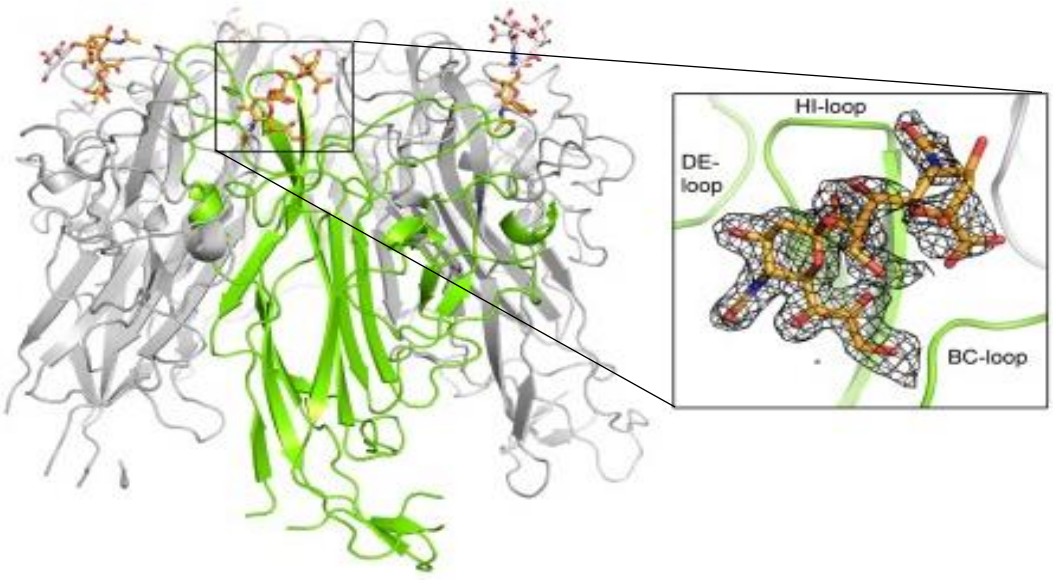

Figure 1. 6 Crystal structure of a BKPyV VP1-GD3 oligosaccharide complex. Structure of a BKPyV VP1 pentamer is shown in complex with GD3 oligosaccharide. One of the five VP1 monomer is represented in green. Monosaccharides are shown in orange and the other monomers in white. Adapted from Neu *et al*., (2013).

1.5.3.3 Non-structural late protein

The agnoprotein is a small non-structural late protein. It possesses a highly basic amino acid composition with dominant Arg (R) and Lys (K) residues, which are detected in the amino and carboxy regions of the protein (Figure 1.7A) and is approximately 8 kDa in mass (Rinaldo et al., 1998; Leuenberger et al., 2007). The subcellular localization of agnoprotein is primarily in the cytoplasm during the later stages of the virus life cycle, although, is also detected in the perinuclear area and a small fraction is located in the nucleus (Rinaldo et al., 1998; Johannessen et al., 2008). The central part of BKPyV agnoprotein contains a stretch of hydrophobic residues, including Ile, Leu and Phe and is predicted to form an α-helix (Figure 1.7A) (Gerits and Moens, 2012). This region is implicated in the formation of stable dimers and oligomers whose function is still not understood (Saribas et al., 2011; Saribas et al., 2016). The agnoproteins of BKPyV, JCPyV and SV40 share a high degree of homology, within the N-terminal region of the peptide (up to 83% identity between BKPyV and JCPyV) (Figure 1.7B) (Royle et al., 2015; Rinaldo et al., 1998). The crystal structure of agnoprotein has not been solved, however Coric et al., (2017) generated a nuclear magnetic resonance structure of JCPyV agnoprotein as Figure 1.7C shows, identifying the a-helical structure at the N-terminal and central regions. It also known that the SV40 Ri257 variant agnoprotein contains a hydrophobic region in the N-terminal region, whilst an additional hydrophobic region is detected in the unique C-terminal region (Gerits and Moens, 2012).

Previous studies have identified that BKPyV and JCPyV agnoproteins undergo post-translational modification such as phosphorylation on multiple serine and threonine residues (Ser-7, Ser-11, Thr-21 and Ser-64) (Figure 1.7A) (Johannessen et al., 2008; Sariyer et al., 2006). Studies have shown that both Ser-7 and Ser-11 are also detected in SV40, SV40 Ri257 variant and SA12 agnoprotein, whereas Thr-21 is conserved in SA12 agnoprotein, but replaced by Ser-21 in SV40 agnoprotein (Gerits and Moens, 2012). Single and/or double replacement of the key phosphorylation residues with Ala in JCPyV agnoprotein resulted to mutant viruses that failed to propagate (Sariyer et al., 2006). Similar results were also observed when Ser-11 replaced with Ala in BKPyV agnoprotein (Johannessen et al., 2008), highlighting the importance of the phosphorylation sites to viral multiplication. Moreover, studies have indicated that phosphorylation not only impacts on viral propagation, but also on the

stability of the protein (Johannessen et al., 2008; Sariyer et al., 2006). Single T21A, double S7A/S11A, and triple S7A/S11A/T21A mutations cause an increase of expression levels of the mutant agnoprotein compared to the wild-type JCPyV agnoprotein, whereas BKPyV S11A agnoprotein was less stable than the wild-type protein (Johannessen et al., 2008; Sariyer et al., 2006). In addition to this, residue-specific phosphorylation might control agnoprotein degradation. Phosphorylation of Ser-7 and Thr-21 may trigger JCPyV degradation (Sariyer et al., 2006). Hunter (2007) stated that phosphorylation can trigger a substrate's ubiquitination and degradation by the proteasome. *In silico* studies have predicted that agnoprotein of different polyomaviruses contains putative lysine residues for ubiquitination, however it is not known whether phosphorylation of agnoprotein results in its subsequent degradation (Lee et al., 2011).

Phosphorylation might also affect the subcellular localization of agnoprotein (Gerits and Moens, 2012). A putative Leu-rich nuclear export signal (NES) and a region of basic amino acids, which may represent a nuclear localization signal (NLS) are contained in BKPyV, JCPyV, SV40 and SA12 agnoproteins (Fu et al., 2011; Lange et al., 2007). Subcellular localization of a protein might be controlled by phosphorylation due to conformational changes that expose NLS or NES (Whitmarsh and Davis, 2000). Studies have identified that JCPyV agnoprotein retained in the nucleus upon treatment with H89, a cAMP-dependent protein kinase/protein kinase A (PKA) (Okada et al., 2001). Other studies have demonstrated that there is a co-localization of BKPyV agnoprotein and lipid droplets and residues at positions 20-42 are required for this co-localization (Unterstab et al., 2010). Lipid droplets are highly dynamic organelles in a donut-like structures, consist of a hydrophobic core formed of neutral lipids (Unterstab et al., 2010), and they can travel along microtubules and interact with cellular organelles (Liu et al., 2007; Zehmer et al., 2009). Studies have identified that mutations within the hydrophobic domain, inhibited the lipid droplets targeting, whereas switching the Ser-11 phosphorylation site to aspartic acid or alanine did not affect the lipid droplets co-localization (Unterstab et al., 2010). At present, the role of agnoprotein in the context of lipid droplets remains speculative.

BKPyV lacking agnoprotein, could infect Vero cells, however reduced propagation was observed compared to the wild-type BKPyV (Johannessen et al., 2008). A recent study in human renal epithelial cells demonstrated that BKPyV without agnoprotein

expression fails to release from host cells and does not propagate in culture to similar levels as wild-type virus. Although, they also proved that agnoprotein does not play a critical role in native virion infectivity or morphogenesis (Panou et al., 2018). Both studies confirmed that agnoprotein plays an important role in BKPyV life cycle. Moreover, BKPyV strains containing a deletion within NCCR and also lacking the 5'-end of the agnoprotein peptide cannot release infectious viral progeny. However, rescue assays with agnoprotein exogenously added showed that production and release of infectious virions were recovered (Myhre et al., 2010). Additionally, there is evidence suggesting that JCPyV agnoprotein destabilizes the nuclear envelope to facilitate native virion nuclear release (Okada et al., 2005). For this, the N-terminal region of JCPyV agnoprotein interacts with Heterochromatin Protein 1α (HP1α) and due to this interaction, the lamin B receptor cannot interact with HP1α (Okada et al., 2005). Interestingly, despite the high homology between JCPyV and BKPyV agnoprotein, BKPyV agnoprotein does not cause gross destabilization of the nuclear membrane in human primary renal epithelial cells. Immunofluorescence microscopy revealed that Lamin B localization was unaffected in both wild-type containing cells and cells lacking agnoprotein (Panou et al., 2018).

Several host cellular proteins interact with agnoprotein to favour BKPyV infection, including p50, p75 and p100 (Rinaldo et al., 1998). Johannessen et al., (2011) demonstrated an interaction between the N-terminal region of BKPyV agnoprotein and the α-soluble N-ethylmaleimide-sensitive fusion attachment protein (α-SNAP) using a yeast two-hybrid assay. α-SNAP (33 kDa in mass) is required for the disassembly of vesicles during secretion (Johannessen et al., 2011). Similar findings were also confirmed recently by Panou et al., (2018). In this study, interaction between α-SNAP and BKPyV agnoprotein was confirmed using glutathione S-transferase pull down assays with recombinant agnoprotein and cell lysates from primary renal epithelial cells. The necessity of α-SNAP for a successful BKPyV egress was also shown in this study (Panou et al., 2018). Moreover, BKPyV DNA amplification is inhibited due to the interaction between the proliferating cell nuclear antigen (PCNA-35 kDa in mass) and agnoprotein (Gerits et al., 2015). Agnoprotein is also involved in DNA repair after DNA damage as it can control the DNA damage-induced cell cycle by binding directly to the DNA repair enzyme Ku70 (Darbinyan et al., 2004). Studies have additionally highlighted that agnoprotein can negatively

control both early and late gene translation (Gosert et al., 2008). These findings agreed with the observation that both late and early proteins expression was increased in cells lacking BKPyV agnoprotein (Johannessen et al., 2008; Panou et al., 2018). Thus, agnoprotein appears to be a multifunctional protein associated with viral transcription, replication, assembly and release, although its role remains enigmatic in many processes.

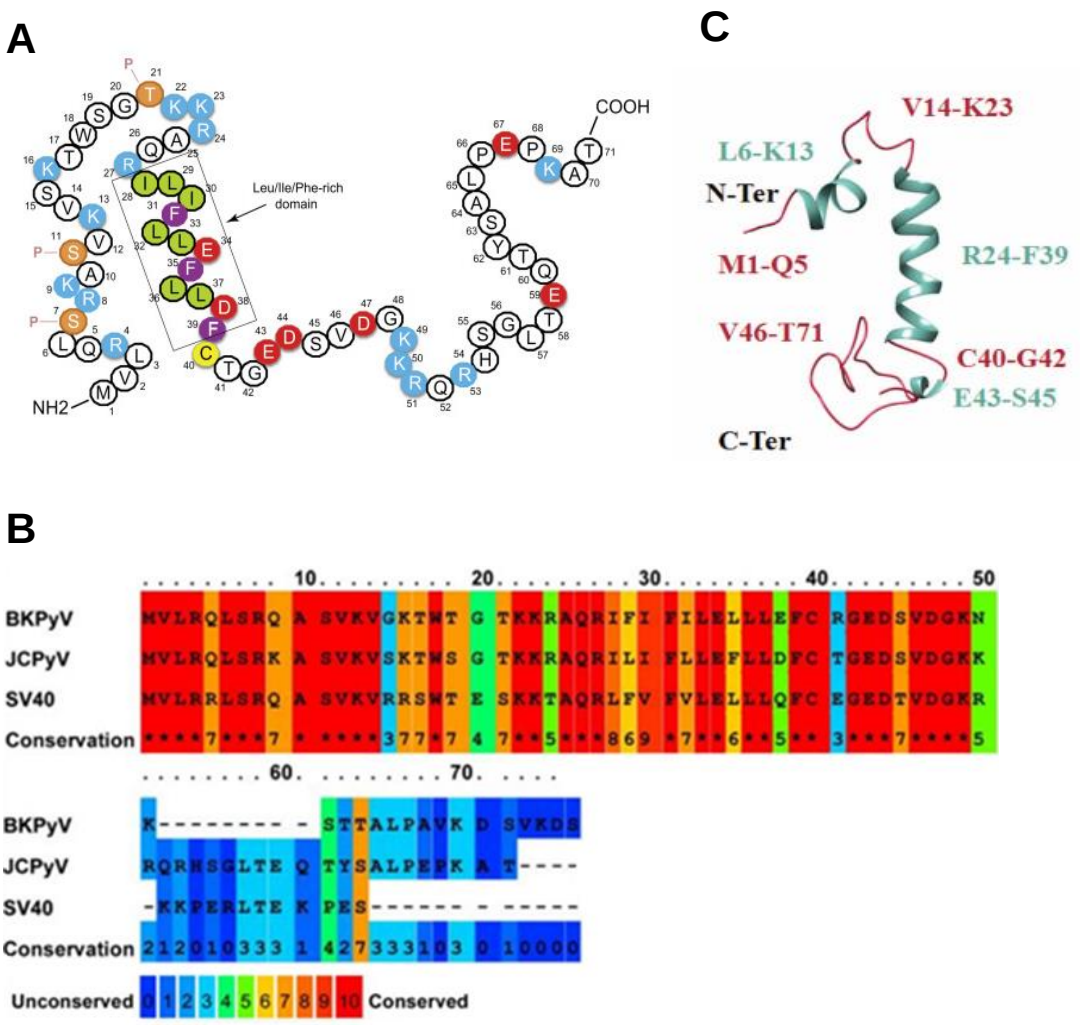

Figure 1. 7 Primary and NMR structure of JCPyV agnoprotein. A. Schematic representation of primary structure of JCPyV agnoprotein. The Leu/Ile/Phe-rich domain is highlighted. Phosphorylation sites at key residues (Ser-7, Ser-11 and Thr-21) are also indicated. P stands for phosphorylation (Saribas *et al*., 2013). B. Conserved sequences of BKPyV, JCPyV and SV40 agnoproteins. Residues are presented using amino acid single letter codes. Conserved residues are displayed in red through to unconserved residues in blue. * represents a residue conserved in all three agnoproteins' sequences (Royle *et al*., 2015). C. NMR structure of JCPyV agnoprotein is shown. Two α-helices were shown between Leu-6 and Lys-13 and from Arg-24 to Phe-39. α-helices are represented in green. Two more unstructured regions were also shown between Val-14 and Lys-23 and from Cys-40 to Thr-71. These two domains are represented in red. In some NMR structures a third α-helix is formed between Glu-43 and Ser-45 (Coric *et al*., 2017).

1.5.3.4 Putative VP4 protein

A very late protein named as VP4 is encoded by SV40 and is generated from a downstream AUG start codon located within the sequence of VP2. Consequently, all VP2, VP3 and VP4 proteins share a common C-terminal sequence (Daniels et al., 2007). It is proposed that VP4 is implicated in SV40-mediated cell lysis and the egress of viral progeny. Interestingly, a corresponding VP4 open reading frame was detected in the BKPyV genome (Daniels et al., 2007). A more recent study confirmed that BKPyV genome contains the putative VP4 and two even smaller proteins, the putative VP5 and VP6 which all share a common C-terminal region (Figure 1.8) (Henriksen et al., 2016). The role of BKPyV VP5 and VP6 is still not identified. However, Henriksen et al., (2016) failed to detect VP4 in BKPyV infected cells by mass spectrometry and in further experiments were unable to demonstrate a role for VP4 in SV40 (Henriksen et al., 2016). Thus, the role of VP4 in SV40 infection is still not clear.

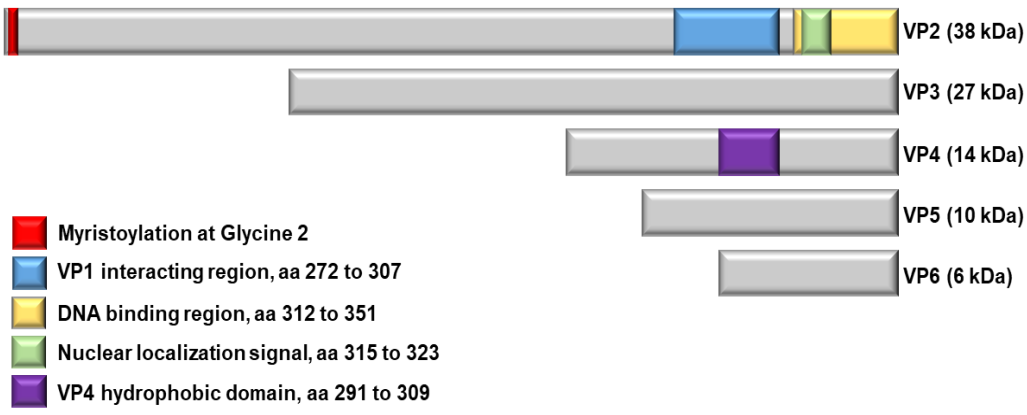

Figure 1. 8 Schematic representation of BKPyV minor capsid proteins. BKPyV VP2 and VP3 and the putative proteins are shown. Highlighted regions and motifs are derived from the UntiProtKB database and the VP4 hydrophobic domain is represented by similarity to SV40 VP4. Adapted from Henriksen *et al*., (2016).

1.5.4 BKPyV microRNA molecules

JCPyV, BKPyV and SV40 genome encode a pre-miRNA hairpin, which can generate two distinct miRNAs, the 3p-miRNA and 5p-miRNA that are complementary to mRNA molecules transcribed from the viral early genes (Seo et al., 2008). Initially, it was suggested that these miRNAs control expression of early genes at later stages of viral infection due to cleavage of the complementary early viral mRNA molecules. That, subsequently, could decrease the sensitivity of SV40 infected cells to cytotoxic T cells (Sullivan et al., 2005). Although, further studies demonstrated that these miRNAs regulate the expression of early mRNA transcripts before genome amplification (Broekema and Imperiale, 2013). The sequences in the NCCR control the miRNA expression in a trend similar to late mRNA transcripts. As a result, early mRNAs in archetype viruses are weakly expressed and targeted for degradation by the robustly translated miRNAs. As a consequence, DNA amplification is limited in archetype viruses. In contrast, high levels of early mRNA transcripts cannot be sufficiently degraded in re-arranged strains as miRNAs are weakly expressed (Helle et al., 2017). The miRNAs can also target cellular genes, in particular the stress-induced ligand ULBP3 is recognized by the killer receptor NKG2D and can be targeted by both BKPyV and JCPyV 3p-miRNA (Bauman et al., 2011). Viral miRNA induced down-regulation of ULBP3 leads to decreased NKG2D-mediated eradication of virus-infected cells by natural killer cells. This might explain a potential mechanism of viral latency and how BKPyV escapes the host immune system. Thus, miRNA molecules might be of great importance for viral persistence (Broekema and Imperiale, 2013).

1.6 BK Polyomavirus (BKPyV) life cycle

An infectious native BKPyV virion needs to attach to the host cell receptor to initiate the virus life cycle. This interaction leads to internalization of the virus into the host cell to exploit the host cell machinery for its favour. BKPyV navigates through the cytoplasm exploiting host cell factors en route the nucleus. Once BKPyV reaches the nucleus transcription of early genes, genome replication and transcription of late genes occur. Finally, infectious viral particles are assembled, and newly generated viral progeny are released from host cells to infect neighboring ones.

1.6.1 BKPyV-host cell receptor attachment

BKPyV infection initiates with the binding of VP1 pentamers to host cell receptor molecules. Polysialylated gangliosides are the candidates host cellular receptors for BKPyV (Sinibaldi et al., 1990; Low et al., 2006). Gangliosides are glycosphingolipids and are abundantly found in host cell membranes. The carbohydrate moiety ceramide is a component of gangliosides, which consists of two arms with one or more sialic acid residues (Groux-Degroote et al., 2017). Gangliosides are also defined as GM, GD and GT describing the mono-, di- and trisialogangliosides, respectively. Sialic acids that are found on gangliosides are usually located in α(2, 3)-binding to galactosyl residues or in α(2, 8)-binding to other sialic acids. The conserved α(2, 8)-disialic acid motif located on the right arm of b-series gangliosides is the critical and minimal binding epitope for BKPyV, with the variable left arm contributing some additional contacts (Neu et al., 2013). GD3, GD2, GD1b and GT1b are b-series gangliosides that interact with BKPyV, whereas a-series gangliosides such as GM1 cannot interact with native BKPyV virions (Neu et al., 2013; Low et al., 2006) (Figure 1.9). A very recent study using high-resolution cryo-EM determined the structure of native BKPyV virions bound to the ganglioside GT1b at a 3.4 Å resolution, which is the highest resolution of a polyomavirus with the host cell receptor bound up to date (Hurdiss et al., 2018) (Figure 1.10). The binding mode of GT1b is similar to GD3, an oligosaccharide that lacks the left arm. This study revealed bridges between Asp-59 and Lys-83 of BKPyV VP1 and the GT1b receptor (Hurdiss et al., 2018), which was previously shown in other studies (Neu et al., 2013). It is also indicated that α(2, 3)-

linked sialic acid is crucial for BKPyV as its enzymatic removal from cells results in blockade of BKPyV infection (Dugan et al., 2005). They also reported that inhibition of N-linked glycosylation reduces BKPyV infection, however that is not observed after inhibition of O-linked glycosylation. Therefore, N-linked glycoprotein consisted of an α(2, 3)-linked sialic acid might be an essential host cellular co-receptor for BKPyV (Dugan et al., 2005).

Genotype BKPyV-Ia uses GT1b or GD1b oligosaccharides as an entry receptor (Low et al., 2006). A study was performed to examine whether all BKPyV genotypes require gangliosides for internalization (Pastrana et al., 2013), utilizing murine GM95 cells which lack gangliosides (Ichikawa et al., 1994). Cells were transduced with pseudovirions of each BKPyV variant in the presence or not of exogenous GT1b ganglioside. It is demonstrated that only BKPyV-Ic, -II and -III variants were highly responsive to ganglioside supplementation. BKPyV-Ib2 show a modest increase of the transduction, while exogenous GT1b supplementation had no impact on BKPyV-IV (IVb1 and IVc2) variant (Pastrana et al., 2013). Therefore, BKPyV-IV transduces the murine GM59 cells through a ganglioside-independent internalization pathway. Similar experiments performed in other cell lines, including A549 and ART (ovarian cancer cell line NCI/ADR-RES stably transfected with SV40 TAg) cells with GM3 synthase knocked down. Knockdown of GM3 synthase cause inhibition of BKPyV-IV transduction, suggesting that gangliosides were required for an infectious entry of BKPyV-IV in A549 and ART cells (Pastrana et al., 2013). Thus, BKPyV-IV follows different entry pathways in different cell lines showing distinct cellular tropisms.

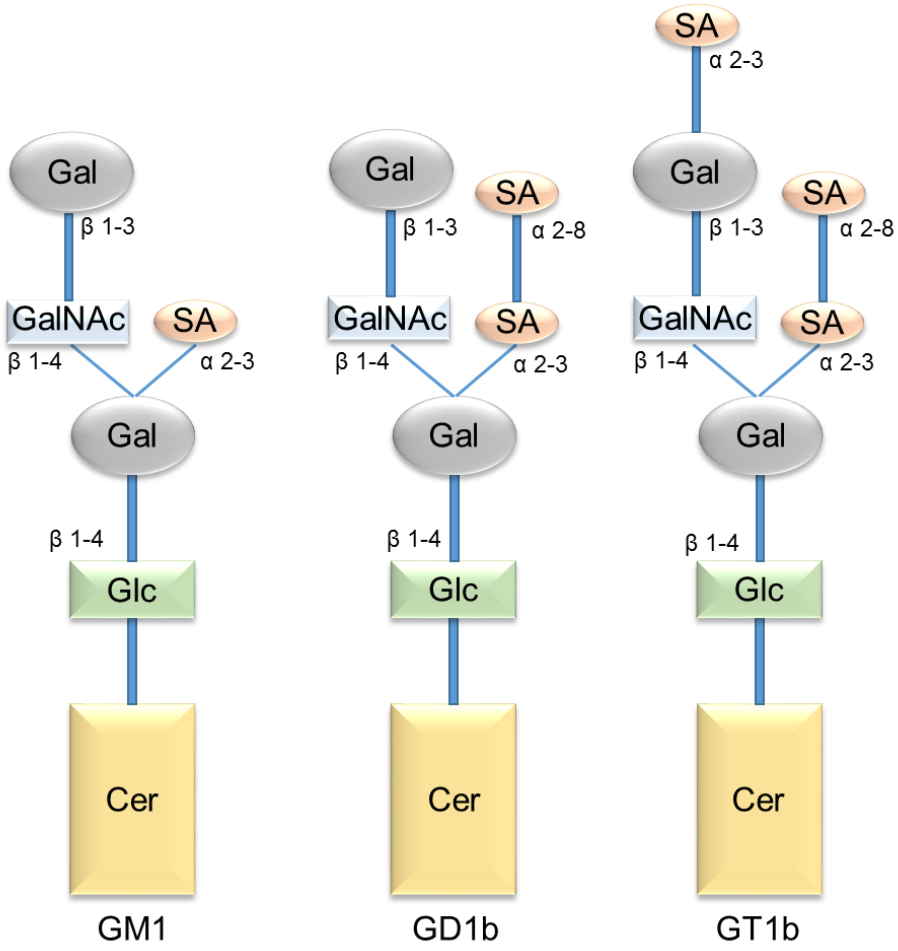

Figure 1. 9 BKPyV binds to GD1b and GT1b. Schematic representation of GM1, GD1b and GT1b gangliosides. Ceramide (Cer) is presented in yellow; Glucose (Glc) in green; Galactose (Gal) in grey; N-acetyl- galactosamine (GalNAc) in blue; Sialic acid (SA) in pink. Adapted from Low *et al*., (2006).

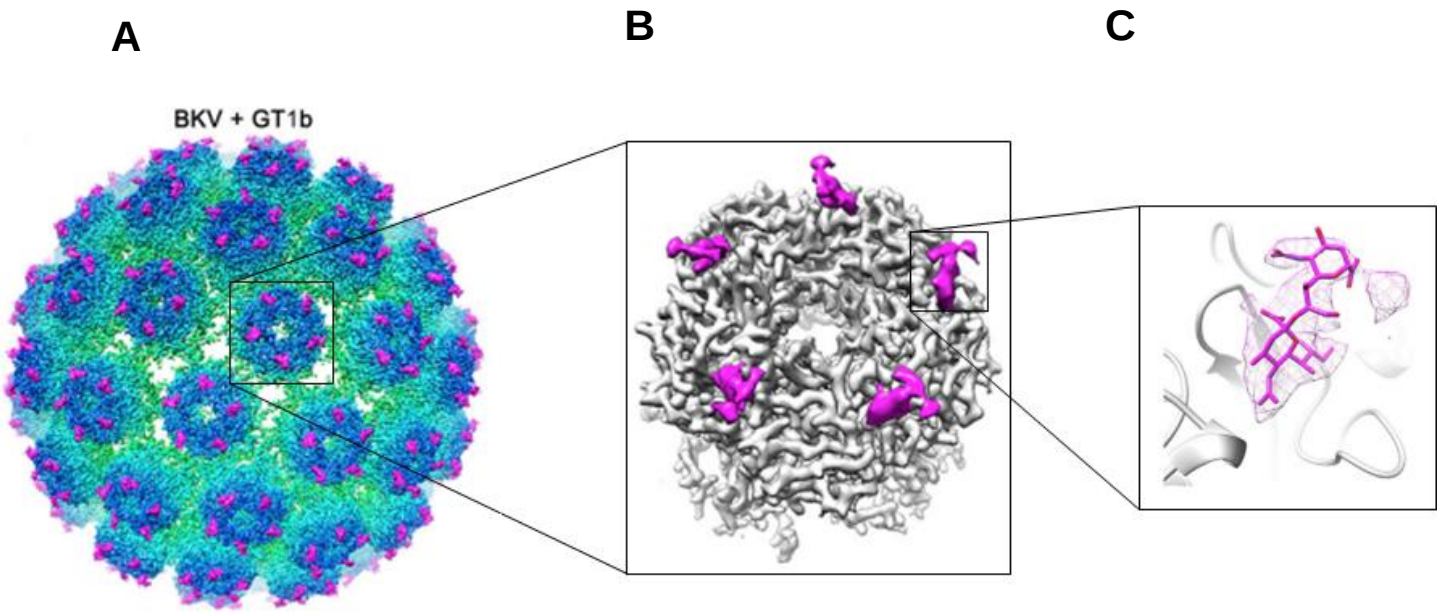

Figure 1. 10 The structure of BKPyV: GT1b host cell receptor molecule. A. Representation of the 3.4 Å structure of BKPyV native virion, in complex with GT1b shown in magenta. B. Representation of a single 5-fold pentamer of the BKPyV: GT1b complex. C. Enlarged view of the GT1b containing the atomic model for the disialic motif of the GT1b right arm. Adapted from Hurdiss *et al*., (2018).

1.6.2 Internalization of BKPyV

BKPyV enters host cells after the initial binding to cellular receptors. BKPyV internalization into Vero cells occurs in a manner independent of clathrin-coated-pit assembly but through a caveolae-mediated endocytosis (Eash et al., 2004). Dominant-negative mutants of caveolin 1 and Eps15 were used to deconstruct caveolin and clathrin-dependent endocytosis, respectively. Similar findings were observed in RPTE cells suggesting that BKPyV is internationalized into the most physiologically relevant cell line by a caveolae-mediated endocytic pathway (Moriyama et al., 2007; Moriyama and Sorokin, 2008). Time-of-addition assays also revealed that infectious BKPyV particles are localized in a neutralizing compartment between 2-4 hours post-infection (Eash et al., 2004) and co-localization of caveolin 1 with BKPyV peaked approximately 4 hours after infection (Moriyama et al., 2007).

Caveolae- and clathrin-mediated endocytosis are two major well-characterized pathways that form small endocytic vesicles, however there are other alternative endocytic pathways that are not dependent on caveolin or clathrin-coated pit (Figure 1.11) (Mayor and Pagano, 2007). Caveolin 1, 2 and 3 belong to a cholesterol binding proteins family with caveolin 1 and 2 abundantly expressed in cells including epithelial cells, and caveolin 3 in muscle cells (Murata et al., 1995). Studies have demonstrated that only caveolin 1 is required for caveolae formation (Drab et al., 2001; Razani et al., 2002). Previous studies have identified that BKPyV, SV40 and murine polyomavirus use caveolae-mediated endocytosis to enter host cells (Pelkmans et al., 2001; Richterova et al., 2001). However, JCPyV internalizes host cells via a clathrin-mediated endocytic pathway (Pho et al., 2000). The clathrin protein complex is composed of three light and three heavy chains (Fotin et al., 2004). Clathrin complexes are not able of interacting with plasma membrane directly, therefore adaptor proteins are essential to recruit clathrin complexes on the membrane. Then, the clathrin coated pit with the help of dynamin forms clathrin-coated vesicles (Hinrichsen et al., 2003).

A recent study re-examined the BKPyV entry process in RPTE cells (Zhao et al., 2016). Silencing of clathrin heavy chain, caveolin 1 and 2 and UDP-Glucose

Ceramide Glucosyltransferase (UGCG) using siRNA molecules revealed that BKPyV requires gangliosides, although enters RPTE cells in a caveolin- and clathrin-independent endocytic pathway (Zhao et al., 2016). There have been identified several caveolin- and clathrin-independent endocytic pathways that could be utilized by BKPyV for an infectious entry implicating RhoA GTPases (Lamaze et al., 2001), a Cdc42-based actin machinery (Chadda et al., 2007), ADP-ribosylation factor (ARF) 6 (Radhakrishna and Donaldson, 1997) and flotillin (Glebov et al., 2006). Taken together that polyomaviruses enter tight fitting vesicles following endocytosis (Damm et al., 2005; Drachenberg et al., 2003) and actin is not essential for a BKPyV infectious entry (Eash and Atwood, 2005), Zhao et al., (2016) suggested that BKPyV is more likely to enter RPTE cells by a yet undefined endocytic pathway, since most of the previously mentioned pathways require actin polymerization.

It is also possible that BKPyV uses a lipid-dependent endocytic pathway in which cholesterol and gangliosides might be required (Zhao et al., 2016). *In vitro* studies have demonstrated that caveolae-like vesicles, named giant unilamellar vesicles, can be formed by artificial liposomes with gangliosides and cholesterol alone (Bacia et al., 2005). Ewers et al., (2010) indicated that SV40 was able to cause invaginations on the surface of these vesicles, highlighting that polyomavirus successful entry might be mediated via a protein-independent pathway. In that case, tight fitting vesicles could be structured by direct interactions between the VP1 major capsid protein and gangliosides, with cholesterol facilitating the stabilization of the vesicle membrane invagination (Zhao et al., 2016). The distinct BKPyV endocytosis process is still controversial, thus further studies are required.

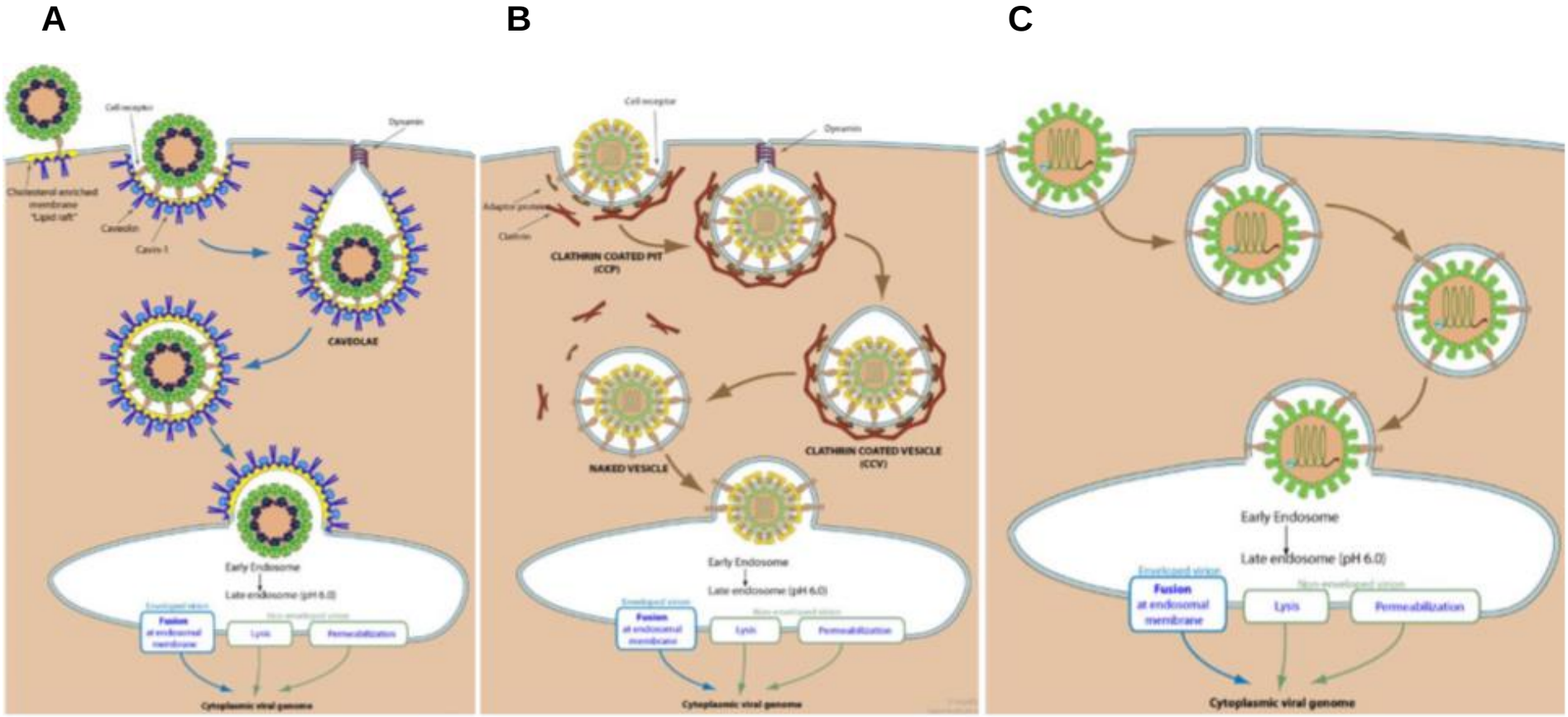

Caveolae-mediated endocytosis

Clathrin-mediated endocytosis

Caveolae-, Clathrin-independent endocytosis

Figure 1. 11 Endocytic pathways followed into host cells. A. Virus internalization by the host cell via caveolae, which are specialized lipid rafts that form flask-shaped invaginations of the plasma membrane. Caveolins form the structural backbone of caveolae. Internalized viruses bound to their host cell receptor are transported to the early endosome. B. Clathrin-mediated endocytosis is triggered by the binding of the virion to host cell receptors. This induces the binding of an adaptor protein to the receptor cytoplasmic tail, which allows clathrin to multimerize to form characteristic invaginations or Clathrin-coated pit (CCP). Membrane scission proteins pinch off the CCP from the host membrane thereby releasing the Clathrin-coated vesicle (CCV). Following the vesicle delivers its viral content to early endosomes. C. Several pathways that do not use a caveolin or clathrin coat are hijacked by viruses to enter host cells. These pathways can be further defined by their dependency to various molecules such as cholesterol, small GTPases and non-caveolar lipid rafts (Gasteiger *et al*., 2003).

1.6.3 Trafficking of BKPyV through the Endoplasmic Reticulum

Following endocytosis, BKPyV might enter the endosomes of host cells (Zhao and Imperiale, 2017). BKPyV native and infectious virions traffic to smooth tubular structures adjacent to rough endoplasmic reticulum (ER) based on findings using transmission electron microscopy (Drachenberg et al., 2003). Pharmacological experiments demonstrated that BKPyV relies on an intact microtubule network and not on an intact actin cytoskeleton in both Vero and RPTE cells (Eash and Atwood, 2005; Moriyama and Sorokin, 2008; Jiang et al., 2009). Microtubules are cytoskeletal filaments composed of α- and β-tubulin dimers and their function is to define intracellular structure for the maintenance of cell shape and motility, intracellular transport of vesicles, molecules and granules between organelles (Moriyama and Sorokin, 2008). Microtubule dynamics consist of growing and shrinking of tubulin dimers at microtubule ends (Moriyama and Sorokin, 2008). Studies have shown that BKPyV can move along the microtubules, but their dynamics are not essential for the virus transportation in Vero cells (Eash et al., 2004; Eash and Atwood, 2005). Studies performed pharmacological analysis using nocodazole and colchicine as microtubule disrupting agents and paclitaxel as microtubule dynamics disrupting agents to identify their requirement on BKPyV transportation in RPTE cells. Findings revealed that BKPyV transportation is relied on intact microtubules and on microtubule dynamics in RPTE cells (Moriyama and Sorokin, 2008). Additionally, studies have identified that BKPyV intracellular transportation is dynein-independent. These discrepancies might be observed as BKPyV transportation was investigated in different cell lines in these studies. Another factor that is associated with intracellular transportation of vesicles is the motor proteins, dynein and kinesin, which facilitate cargo transportation along microtubules (Moriyama and Sorokin, 2008). Dynein is a minus-end microtubule motor protein attached to the microtubule organizing centre (MTOC) and is identified to transport several viruses including adenovirus, herpes simplex virus, rabies virus and vaccinia virus (Greber and Way, 2006; Leopold and Pfister, 2006; Radtke et al., 2006). Studies have demonstrated that there was no correlation between BKPyV transportation and dynein activity (Moriyama and Sorokin, 2008). Similar findings were observed with JCPyV and SV40 (Ashok and Atwood, 2003), indicating that members of *Polyomaviridae* might be transported along microtubules independently of dynein function.

During endocytosis a pH-dependent step occurs at a very early stage of BKPyV life cycle, during the first 2 hours post-infection. This was identified using lysosomotropic agents such as ammonium chloride and chloroquine, indicating that acidification and maturation of endosomes are critical for a successful BKPyV infection in RPTE cells (Eash et al., 2004; Jiang et al., 2009). Following to this, BKPyV co-localizes with caveolin 1 at 4 hours post-infection, suggesting that BKPyV is found in caveosome, a pH-neutral compartment at this stage of the life cycle (Moriyama et al., 2007). Treatments with brefeldin A (BFA) and Retro-2cycl, two agents that inhibit retrograde transport to the ER, showed a decrease of BKPyV protein expression. However, co-localization of BKPyV with markers of the Golgi apparatus was not observed. Taken together these findings proposed that BKPyV traffics through the ER, although bypasses the Golgi apparatus in its natural host cells (Low et al., 2006; Moriyama et al., 2007; Moriyama and Sorokin, 2008; Jiang et al., 2009; Nelson et al., 2013). Co-localization of BKPyV with markers of ER and time-of-addition experiments using brefeldin A showed that BKPyV reaches ER approximately 8-10 hours after infection (Moriyama and Sorokin, 2008; Jiang et al., 2009). Similar findings were observed with other polyomaviruses including SV40 and murine polyomavirus (Bernacchi et al., 2004; Gilbert et al., 2003; Norkin et al., 2002; Tagawa et al., 2005), however the course of BKPyV infection in RPTE cells is relatively slow. Studies have shown that SV40 is co-localized with caveolin 1 at 0.5 hours post-infection and is detected at the perinuclear region approximately 4 hours after infection in CV-1 cells (Pelkmans et al., 2001). Whereas, murine polyomavirus is co-localized with caveolin 1 at 0.5 hours post-infection, is transported along microtubules at 2 to 4 hours and reaches the ER at 4 hours after infection in rat glioma cells (Gilbert and Benjamin, 2004).

A recent study using a whole human genome siRNA screen identified key host cell factors that are associated with BKPyV late-endosome-to-ER transportation in RPTE cells (Zhao and Imperiale, 2017). Rab18, ZW10, RINT1 and syntaxin 18 were identified as critical host factors for a successful BKPyV infection in RPTE cells (Zhao and Imperiale, 2017). Rab18 has been linked in vesicular transportation between the ER and the Golgi apparatus and lipid droplets homeostasis (Dejgaard et al., 2008; Liu and Storrie, 2012). Studies have shown that Rab18 is primarily detected on the membranes of cis-Golgi apparatus and ER (Dejgaard et al., 2008). Moreover, Rab18 can be detected on the surface of other organelles including the endosomes, the

lysosomes and lipid droplets (Zhang et al., 2016; Zhang et al., 2017). Affinity chromatography and mass spectrometry analyses revealed that Rab18 interacts with RINT1, ZW10 and syntaxin 18 (Gillingham et al., 2014). It is also established that RINT1 and ZW10 interact through each other N-terminal region and with NAG protein construct the NRZ complex. Syntaxin 18, a t-SNARE protein, located on the ER membrane binds to the NRZ complex indirectly (Tagaya et al., 2014; Hirose et al., 2004; Çivril et al., 2010). Zhao and Imperiale (2017) identified that silencing of Rab18 cause BKPyV accumulation in the late endosomes, suggesting that Rab18 mediates late-endosome-to-ER transportation of BKPyV and transportation along microtubules together with the virus-containing vesicles. After the NRZ complex located on the ER surface captures and tethers vesicles to the ER surface, a yet-to-be-identified v-SNARE interacts with syntaxin 18 on the vesicles and in turn this complex promotes vesicle fusion to the ER membrane allowing entry of BKPyV into ER (Figure 1.12) (Zhao and Imperiale, 2017). More details of the Rab18-mediated pathway are still not known, thus further studies are required to fully define the BKPyV retrograde endocytic pathway.

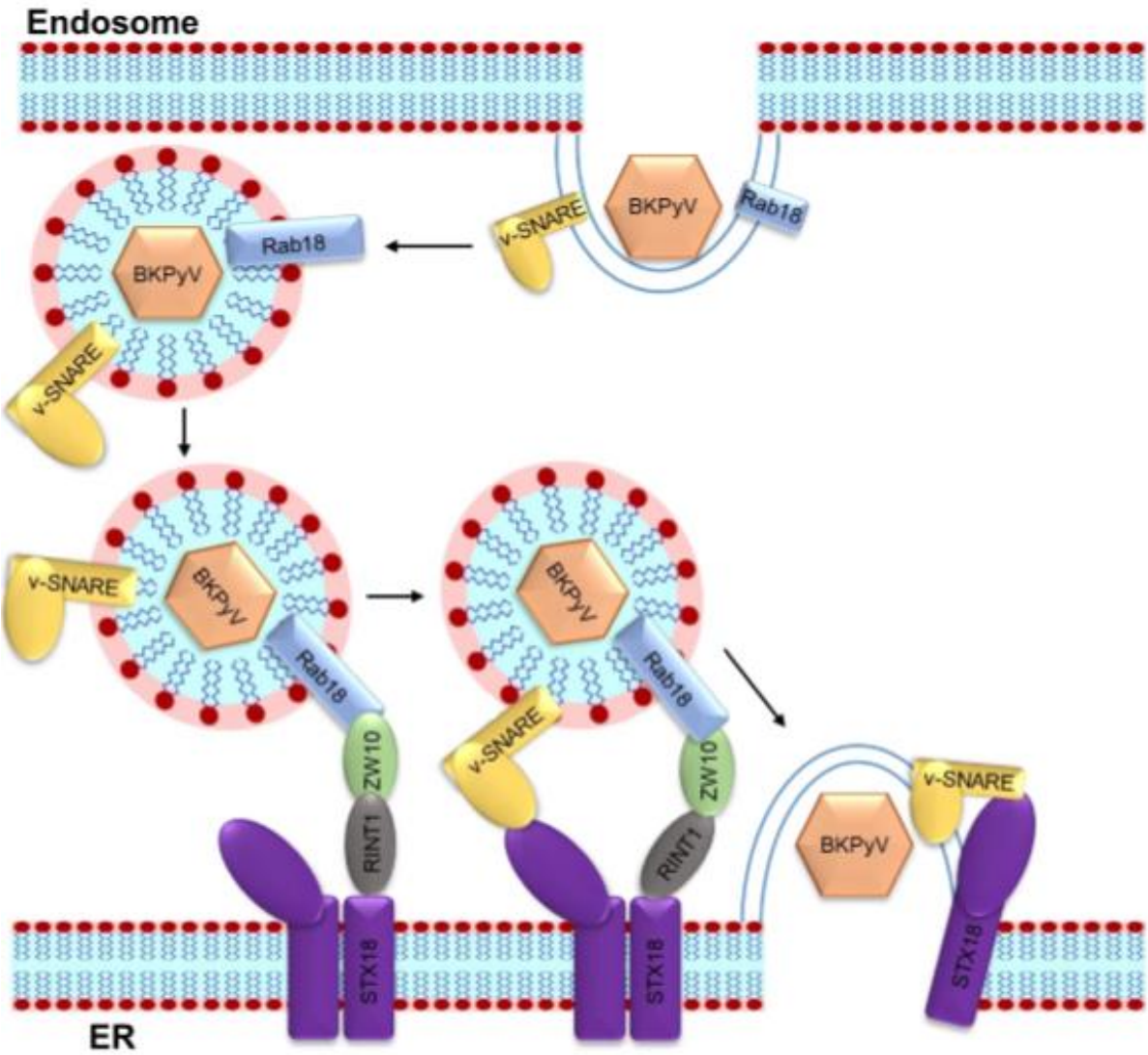

Figure 1. 12 Schematic representation of BKPyV vesicular transportation. BKPyV internalizes a vesicle from the membrane of the endosome. Rab18 located on the membrane of endosomes, interacts with ZW10 kinetochore protein and RAD50 interactor 1 (RINT1), which are members of the NRZ complex, forming a Rab18/NRZ/syntaxin (STX18) complex at the ER surface. STX18 functions as a t-SNARE on the ER membrane, where the NRZ components work as a tether to assist with retrograde vesicle docking. Another yet-to-be-identified v-SNARE protein, located on endosomal membranes, interacts with STX18 to facilitate the vesicle fusion to the ER membrane and the release of BKPyV virions into the ER of infected RPTE cells. Adapted from Zhao and Imperiale (2017).

1.6.4 Release from the ER and nuclear entry

Viruses must penetrate host cell membranes in order to reach the nucleus, where replication and assembly of viral progeny occurs (Inoue et al., 2015). The non-enveloped viruses have a distinct mechanism by which viruses penetrate the host cell membrane. In that case, non-enveloped virus is transported to the site for penetration and undergoes conformational changes mediated by host cell factors and environments including a low-pH microenvironment, reductases, proteases and chaperones (Inoue et al., 2015). These changes might, in turn, expose hydrophobic domains of the native virions or release small lytic peptides that were not exposed before (Chandran et al., 2002; Walczak and Tsai, 2011). Then, this hydrophobic viral intermediate disrupts the integrity of the lipid bilayer facilitating its cross of the membrane, which in some cases is mediated by host cellular machineries (Walczak et al., 2014).

A distinct feature of polyomaviruses is the trafficking through the ER during the entry process. Blockade of BKPyV transportation to the ER impacts on VP1 cleavage and disulphide bond isomerization (Jiang et al., 2009). Studies have shown that an ER reductase, ERdj5, acts synergistically with Protein Disulphide Isomerase (PDI) to decrease the disulphide bonds in SV40 capsids (Inoue et al., 2015). Based on these findings, it is likely that BKPyV exploits the disulphide isomerases, reductases and chaperones localized in the ER for further uncoating of the capsid and viral ER-to-cytosol trafficking (Helle et al., 2017). Studies have also demonstrated that ERdj5 cooperates with PDI to promote structural alterations to SV40, which are required for SV40 to interact with the ER membrane protein BAP31 (Inoue et al., 2015). This interaction in turn promotes SV40 ER-to-cytosol translocation (Inoue et al., 2015). A summarized model describing how ERdj5 and PDI mediate SV40 penetration of the ER membrane is shown in Figure 1.13 (Inoue et al., 2015).

The ER-associated protein degradation (ERAD) pathway and proteasome have been strongly linked with BKPyV trafficking into the cytoplasm from the ER compartment (Dupzyk and Tsai, 2016). Under normal circumstances, the ERAD pathway is required for transportation of misfolded protein out of the ER compartment for degradation by the proteasome. This process implicates several proteins including membrane J-protein, membrane proteins of Derlin families, Hsp70 and Hsp110.

Inhibition of the ERAD machinery and proteasome, using pharmacological compounds impeded BKPyV infection and as a result partially uncoated BKPyV virions with exposed VP2/VP3 proteins accumulated in the ER of infected RPTE cells (Bennett et al., 2013). Time-of-addition experiments using epoxomicin, a potent blocker of the chymotrypsin-like activity of the proteasome (Meng et al., 1999) revealed that BKPyV no longer required proteasome function after approximately 18 hours post-infection. This suggested that BKPyV traffics through the ER between 8 to 16 hours post-infection (Bennett et al., 2013), which is also in agreement with previous studies in the same cell line (Jiang et al., 2009). The role of ERAD pathway was also examined independently from the proteasome function by using Eeyarestatin I (Bennett et al., 2013). Eeyarestatin I inhibits the AAA-ATPase p97, which is upstream of the proteasome as a component of the ERAD pathway and provides the driving energy for extraction of ERAD substrates from the ER (Wang et al., 2008; Wolf and Stolz, 2012). Similar inhibition kinetics were observed with Eeyarestatin I and epoxomicin, suggesting that proteasome acts as part of the ERAD pathway to allow BKPyV to exit from the ER (Bennett et al., 2013). Interestingly, VP1 monomers can enter the cytoplasm from the ER irrespective of the inhibition of ERAD machinery and proteasome function (Bennett et al., 2013). Bennett et al., (2013) proposed that some infectious viral particles might be trapped within the ER when ERAD is blocked, even though VP1 monomers can still enter cytosol. Before membrane penetration, the ER-resident Hsp70 Bip is recruited to maintain the hydrophobic BKPyV intermediate in a soluble state (Inoue and Tsai, 2015; Goodwin et al., 2011). Studies have also identified that Grp170, a Nuclear Exchange Factor (NEF), by converting ADP-BiP to ATP-BiP, the release of ER-localized BKPyV is triggered (Inoue and Tsai, 2015). It is also known that Derlin-1, an ER membrane component interacts with VP1 and is implicated in the ER-to-cytoplasm trafficking, however the exact contribution to the process is not clear (Jiang et al., 2009). Then, a cytosolic complex composed of SGTA proteins and Hsp105 might be recruited for BKPyV translocation to the cytoplasm (Ravindran et al., 2015; Walczak et al., 2014).

There is conflicting evidence for the nuclear entry mechanism of polyomaviruses. Partial uncoating might give the virus a smaller shape enough for active transport through the nuclear pore complex (Panté and Kann, 2002). It is demonstrated that there is direct interaction between the SV40 chromosome and importins α and β in

the cytosol indicating that SV40 uses the canonical nuclear import pathway for its entry (Nakanishi et al., 2002; Nakanishi et al., 2007). The nuclear localization signal (NLS) of a protein is recognized and bound to the adaptor proteins, importins α and β. NLS of SV40 VP2 and VP3, located in their C-terminus interact with the importins showing that SV40 transported through the nuclear pore complex and via the canonical nuclear import machinery (Nakanishi et al., 2002; Nakanishi et al., 2007). However, other studies have reported that SV40 infection cause a breakdown of the nuclear lamina and in turn disruption of the nuclear envelope permitting SV40 to pass from the ER directly into the nucleus (Butin-Israeli et al., 2011).

BKPyV capsid proteins have extensive homology with the SV40 proteins. Bennett et al., (2015) identified that a Lysine located in the C-terminal region of VP2/VP3 is critical for the nuclear localization of the minor capsid proteins. The significance of NLS involves the classical importin α/β 1 pathway for nuclear entry. Inhibition of BKPyV infection was observed after knocking down of importin 1 and in the presence of ivermectin, a nuclear import inhibitor, supporting the hypothesis that BKPyV enters the host nucleus using the NLS of the minor capsids (Bennett et al., 2015). Ivermectin is known to target specifically only the importin α/β 1-mediated pathway and not others importin β- or transportin-mediated pathways (Wagstaff et al., 2012). Importin α recognizes the NLS and then importin β interacts with the NLS-importin α complex to mediate transport through the nuclear pore (Yoneda et al., 1999).

Studies have proposed alternative entry pathways existing along with nuclear import through the nuclear pore. Bennett et al., (2015) demonstrated that mutation in BKPyV VP2/VP3 NLS resulted in attenuated infectivity. Butin-Israeli et al., (2011) proposed that cytosolic viral particle may enter the nucleus during mitosis, when nuclear envelope breaks down. In addition, BKPyV might utilize an alternative NLS from VP2/VP3 NLS. Studies have shown that VP1 contains an NLS, although is considered to be hidden within the partially disassembled particle (Ishii et al., 1996; Moreland and Garcea, 1991). Treatment with ivermectin blocked the wild-type virus to similar level as the mutant, therefore the mutant virus still uses the canonical nuclear import pathway indicating the use of another viral NLS potentially (Bennett et al., 2015). Thus, BKPyV internalizes host nucleus via the nuclear pore complex, but another pathway of entry might exist as well.

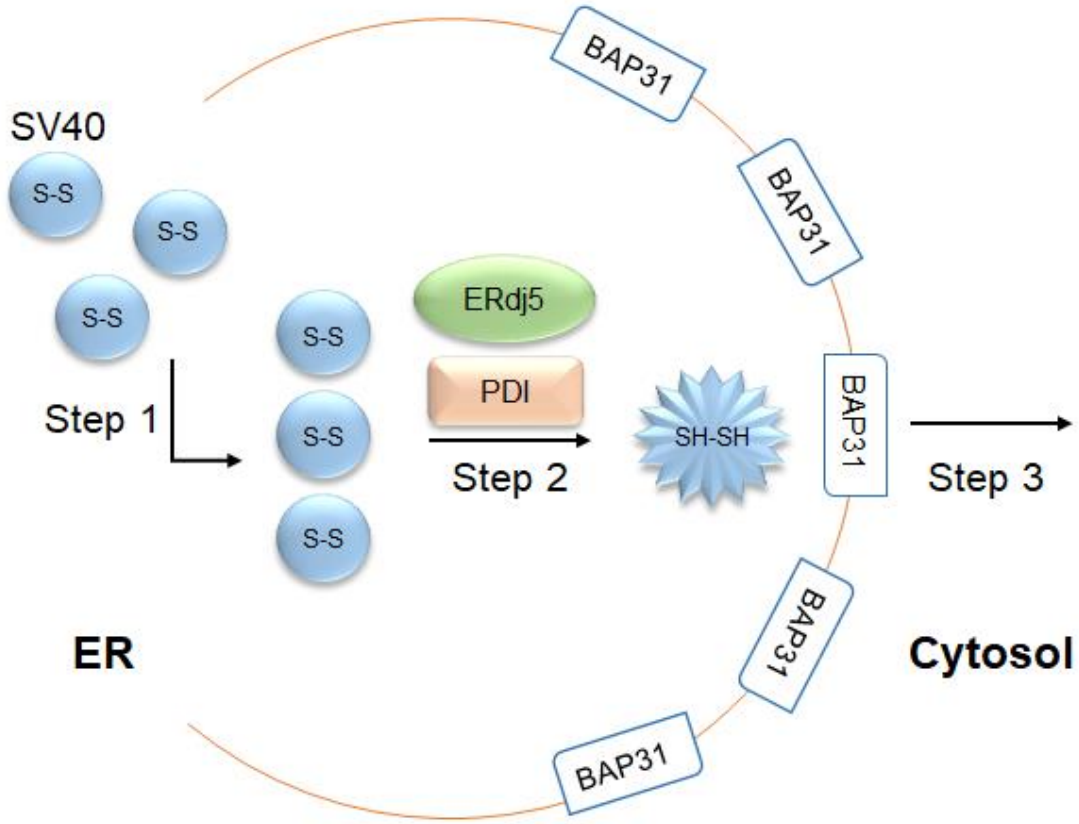

Figure 1. 13 Schematic representation of ERdj5- and PDI-dependent conformational changes of SV40. After reaching the ER, SV40 is delivered to subdomains containing BAP31, called foci (Step 1). ERdj5 decreases disulphide bonds of SV40, while PDI is likely to unfold the viral particle. These two processes mediate conformational changes generating a hydrophobic viral core particle (Step 2). The altered hydrophobic virus binds to BAP31, where positioned to cross the ER membrane to reach the cytosol (Step 3). Adapted from Inoue *et al*., (2015).

1.6.5 BKPyV Gene expression and Genome replication

Polyomavirus replication has been extensively studied in the context of SV40, which is closely related to BKPyV. The BKPyV genome enters the host nucleus, early viral genes generate early mRNA molecules. Following this, early proteins are produced in the cytoplasm and TAg, containing the NLS, traffics into the nucleus. Both SV40 and BKPyV TAg regulate cell cycle progression and halts the process of apoptosis due to its interactions with the pRb and p53 tumour suppressors (Figure 1.14A). This interaction leads to an inability to sequester E2F transcription factors which ultimately results in G1/S-phase transition and activation of the host cell DNA machinery, which is required for BKPyV genome amplification (Helle et al., 2017). The mitogen-activated protein (MAP) kinases are critical in several processes and include the extracellular signal related kinases ERK-1 and ERK-2 (Seamone et al., 2010). Signaling via ERK1/2 is a crucial element that promotes transition to S-phase and cellular proliferation (Liu et al., 2004; Mansour et al., 1994). The activation of ERK1/2 signaling pathway leads to upregulation of cyclin D1, which in turn phosphorylates pRb and triggers G1/S-phase transition (Lavoie et al., 1996). Studies demonstrated that MAP kinase signaling increases BKPyV genome replication *in vitro* (Seamone et al., 2010). It is also identified that BKPyV, did not promote ERK1/2 phosphorylation or cyclin D1 expression *in vitro* (Seamone et al., 2010). However, the inhibition of cyclin D1 function decreased BKPyV genomic replication, suggesting that ERK1/2 signaling pathway acts synergistically with TAg (Seamone et al., 2010). Another signaling pathway that plays an important role in BKPyV replication is the protein kinase Akt (Akt)/mammalian target of rapamycin (mTOR) pathway (Tikhanovich and Nasheuer, 2010). Akt is a serine/threonine kinase, also known as protein kinase B, and is activated by cytokines, mitogens and growth factors (Fayard et al., 2010). The mTOR signaling pathway is downstream of Akt and regulates protein synthesis, cell growth and division. There are two mTOR complexes; mTOR complex 1 (mTORC1), which regulates initiation of translation and mTOR complex 2 (mTORC2), which controls cytoskeletal changes and is also known as a 3'-phoshoinositide-dependent kinase-2 (PDK2) phosphorylating Akt (Bhaskar and Hay, 2007). Tikhanovich and Nasheuer, (2010) identified that BKPyV infection leads to activation of the Akt/mTOR signaling pathway in RPTE cells. Whereas, inhibition of mTORC1 after treatment with Sirolimus led to decrease of BKPyV TAg expression. Moreover, blockade of PKD1

and Akt phosphorylation was observed upon treatment with Leflunomide, which ultimately led to decrease of BKPyV TAg expression and genomic replication (Figure 1.14B).

Moreover, cell cycle progression is also controlled by tAg through the blockade of protein phosphatase 2A enzyme activity. This interaction results in increased cyclins D and A, and downregulation of p27, factors in the control of cell cycle progression into the G1/S-phase (Bennett et al., 2012) (Figure 1.14C). The multifunctional BKPyV TAg is required for viral genome amplification, as a viral DNA polymerase is not encoded. It is known that the host cell supplies all of the other factors that are essential for genome replication (Helle et al., 2017). Viral genome amplification is initiated by TAg due to its ability to bind to GRGGC motifs within the origin of replication, forming two distinct hexamers, which show a helicase function and exhibit an orientation head-to-head. Then, the double-stranded genomic DNA is separated by TAg double hexamer and replication protein A (RPA) is recruited to bind to single-stranded DNA molecules. Topoisomerase I is also present to promote the separation of genomic DNA. Furthermore, DNA polymerase α-primase generated short RNA primers, which are elongated by the enzyme complex of DNA polymerase. RPA, replication factor C, proliferating cell nuclear antigen (PCNA), DNA polymerase α-primase and DNA polymerase δ are then recruited in order to complete the leading and lagging single-strand of genomic DNA (Tikhanovich and Nasheuer, 2010; Tikhanovich et al., 2011).

Studies have also identified that BKPyV disrutps the expression of several host genes (Grinde et al., 2007; Abend et al., 2010). Particularly, BKPyV infected cells are protected from BKPyV-induced host DNA damage response due to activation of the cellular DNA damage response through ataxia telangiectasia mutated (ATM) and Rad3-related (ATR) kinases by viral genome replication (Jiang et al., 2012; Verhalen et al., 2015). Severe DNA damage is observed during BKPyV infection in the absence of ATM and/or ATR kinase. In addition, BKPyV replication causes a dramatic re-structuring of Promyelocytic Leukemia Nuclear Bodies (PML-NBs) as a decrease in PML-NBs number and an increase in size were observed (Jiang et al., 2011). It is of great importance that PML-NBs are localized adjacent to BKPyV DNA foci during later stages of a successful infection and this re-organization might reveal a mechanism of inactivation of PML-NBs intrinsic antiviral activities which is utilized by BKPyV. Late proteins expression occurs following genome replication and is facilitated by the

activation of transcription from the late promoter and controlled by TAg (Helle et al., 2017).

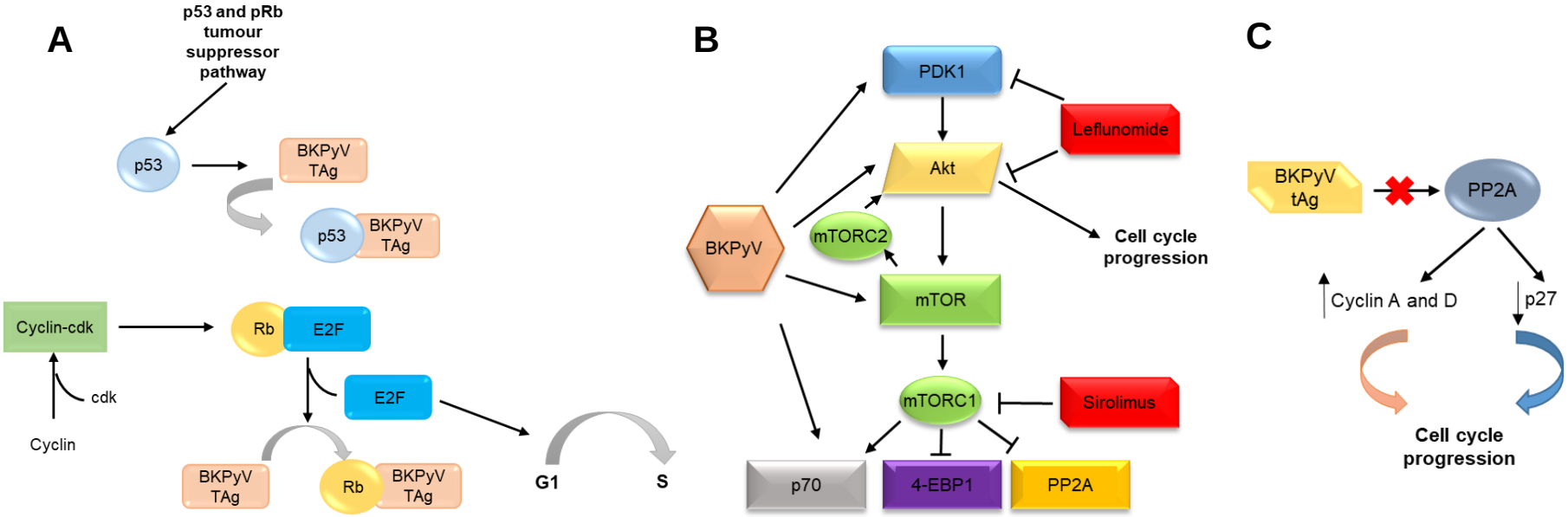

Figure 1. 14 Schematic representation of signaling pathways involved in BKPyV life cycle. A. BKPyV, JCPyV and SV40 TAg interacts with p53 leading to inactivation of p53 and downregulation of p21 that eventually impacts on the release of E2F. E2F is liberated from pRb:E2F by the interaction of TAg with pRb resulting to the transition of G1 to S phase of the cell cycle. Adapted from (Reiss and Khalili, 2003). B. Growth factors and mitogens activate the Akt/mTOR signaling pathway through the PDK1 phosphorylation of Akt. Akt indirectly activates mTOR. mTOR exists in two protein complexes, mTORC1 which phosphorylated p70 and 4-EBP1 to initiate protein translation and mTORC2 which phosphorylates Akt. This in turn activates Akt. mTOR also blocks PP2A. mTORC1 is inhibited by Sirolimus and Leflunomide blocks PDK1 and Akt (Liacini *et al*., 2010). C. BKPyV inactivates the activity of PP2A leading to upregulation of Cyclin A and D and downregulation of p27, which in turn result in cell cycle progression. Adapted from Bennett *et al*., (2012).

1.6.6 BKPyV assembly and progeny release

Following the synthesis of late proteins in the cytoplasm, newly generated proteins are translocated into the nucleus for virion assembly. NLS contained in VP1 is critical for protein import into the nucleus and for VP1-VP2 and VP1-VP3 complexes, respectively (Bennett et al., 2015). Interactions between VP1 and chaperone proteins located in the cytoplasm might inhibit assembly of pre-mature virions. Studies have shown that production of progeny virions can be detected in host RPTE cells' nucleus approximately 2 days after infection (Low et al., 2004). Renal biopsies from patients diagnosed with PVAN contain approximately 6000 BKPyV progeny virions per infected cell (Hirsch and Steiger, 2003).

The mechanism of BKPyV release is not fully understood, although non-enveloped viruses, such as BKPyV, might be released through passive lysis. There is recent evidence for a range of non-enveloped viruses suggesting that passive lysis might not always be the case. It is identified that poliovirus promotes the formation of autophagosome-like vesicles that are associated with viral egress (Taylor et al., 2009). Parvovirus Minute Virus of Mice (MVM) has been shown to be released through late endosomal or lysosomal vesicles (Bär et al., 2008). Interestingly, a recent study suggested that a non-lytic egress of BKPyV from infected RPTE cells occurs (Evans et al., 2015). This route of release is impaired by treatment with 4, 4'–diisothiocyano-2, 2'–stilbenedisulfonic acid (DIDS). DIDS is an anion channel inhibitory agent that impacts on cellular secretion pathways (Evans et al., 2015). Treatment with DIDS traps BKPyV virions in acidic compartments of lysosomal or late endosomal-origin compartments (Evans et al., 2015). Currently, the target of DIDS responsible for virion egress is not clear. However, previous studies have demonstrated that a lytic replication cycle occurs in BKPyV infected RPTE cells (Low et al., 2004). Moreover, cytopathic effects are observed in SV40 infected cells and not in BKPyV infected cells (Henriksen et al., 2016). As it is previously mentioned (Section 1.5.3.3), agnoprotein plays a critical role in viral progeny egress. The mechanism of BKPyV release is controversial and there are conflicting evidences, thus further studies are required to fully define it.

A schematic representation (Figure 1.15) of BKPyV life cycle is shown, below, summarizing the most critical stages as described.

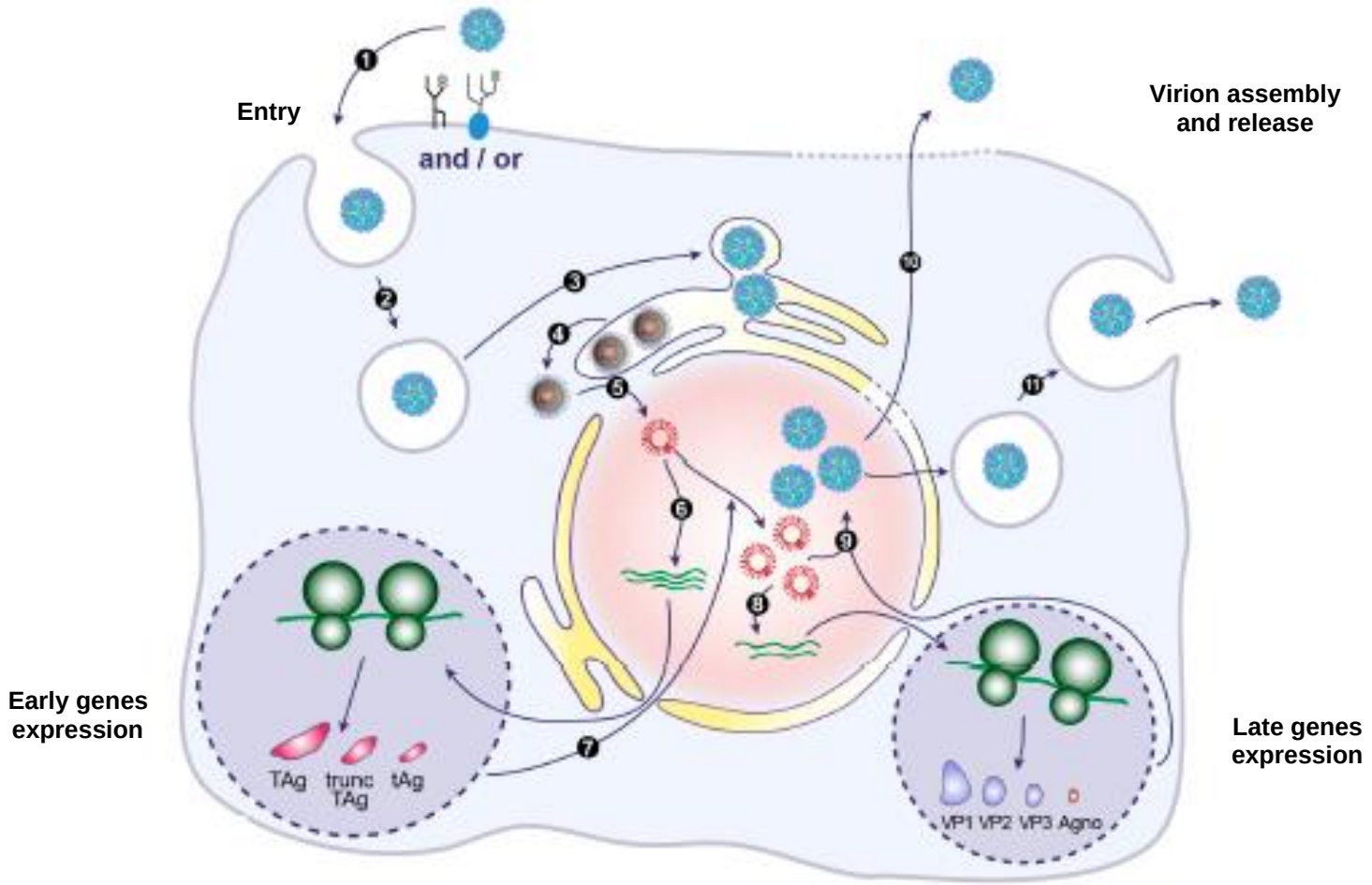
Entry
and / or
Virion assembly
and release
Early genes
expression
Late genes
expression
TAg
trunc
TAg
tAg
VP1 VP2 VP3 Agno

Figure 1. 15 Schematic representation of BKPyV life cycle. (1) BKPyV infectious virions attach to host cell receptor, and especially GD1b, GT1b and/or N-linked glycoprotein with an α-(2, 3)-linked sialic acid. (2) BKPyV is internalized into the host cells during the first 4 hours post-adsorption potentially through a caveolin- or clathrin-indepedent endocytic pathway. (3) Then the virus traffics to the endoplasmic reticulum (ER), where is detected around 10 hours after infection. (4) In the ER, BKPyV is partially uncoated exposing VP2/VP3 proteins from the viral capsid. ER-associated protein degradation (ERAD) machinery is involved in the release of partially uncoated BKPyV. (5) The NLS of VP2/VP3 and the importin α/β1 import pathway are linked with the transportation of BKPyV genome into the nucleus. (6) Early genes expression occurs approximately 24 hours after infection. (7) BKPyV genome replication is initiated after the early proteins translocation into the nucleus to facilitate the process. (8) Late genes are translated. (9) Self-assembly of VP1, VP2 and VP3 proteins into the nucleus occurs to form capsids. Genomic DNA is encapsidated into the newly synthesized capsid. (10) Viral progeny is released mainly by cell lysis or (11) A potential non-lytic egress of virions might occur (Helle *et al*., 2017).

1.7 Renal Ion Channels

Ion channels are transmembrane proteins that create a pore to permit the influx and efflux of ions by passive diffusion. Most ion channels are susceptible to conformational changes when they switch from the closed to open states. Opening of the channel permits the passage of ions across the membrane (Jentsch et al., 2004). Voltage, post-translational modifications like phosphorylation and the binding of specific ligands including neurotransmitters or intracellular Ca^{2+} are all factors that regulate the opening and closing of ion channels. Most ion channels have a function as protein complexes of either homologous or identical subunits that act synergistically to form the pore. These are often involved with other channel-specific subunits that are structurally unrelated and might control the function of ion channels (Jentsch et al., 2004).

Ion channels in renal epithelial cells are associated with the maintenance of cell volume and ion composition not only of the epithelial cells but also of the entire organism. Maintaining the balance of ion composition is dependent on transepithelial ion transportation, a mechanism that implicates ion channels at the basolateral and/or apical cell membranes (Palmer and Sackin, 1988). Potassium (K^+) channels can regulate a broad spectrum of cellular processes, including neurotransmitter release, insulin secretion, cell volume regulation, T-cell stimulation and heart rate. Also, by controlling K^+ secretion and maintaining the right levels of K^+ into cells, several cellular processes can be activated or inhibited (Giebisch, 2001). There have been identified two different broad classes of K^+ channels based on transmembrane topology including: the six-transmembrane-helix voltage-gated (K_v) and the two-transmembrane-helix inward-rectifier (K_{ir}) subgroups (Miller, 2000). Renal epithelial sodium (Na^+) channel (ENaC) regulates the Na^+ reabsorption via the distal nephron in kidneys. Blood volume, blood pressure and Na^+ balance are all controlled by ENaC. In contrast, dysregulation of ENaC leads to essential hypertension, the main cause of cardiovascular mortality and morbidity. ENaC is composed of three partly homologous subunits (Sagnella and Swift, 2006; Warnock and Rossier, 2005). In addition, calcium (Ca^{2+}) channels have significant tubular and vascular effects on renal cells. Renal blood flow, electrolyte excretion and increase of glomerular filtration

rates are included in these renal effects (Chan and Schrier, 1990). Voltage-gated Ca^{2+} channel subtypes, including N-, T-, L- and P/Q-type, can be found in kidneys. Studies have shown that blockade of these channels creates diverse actions on renal microcirculation (Hayashi et al., 2007). Furthermore, several chloride (Cl^-) channels are involved in a various range of renal physiological procedures, including cell volume regulation, transepithelial Cl^- transport, vesicular acidification and regulation of the excitability of neurons (Nilius and Droogmans, 2003). There are several distinct Cl^- subfamilies: the Glycine receptors; the transmitter-gated GABA; the voltage-sensitive ClC subfamily; the Ca^{2+}-activated channels; the high-(maxi) conductance channels; the cystic fibrosis transmembrane conductance regulators (CFTR) and the volume-regulated channels (Verkman and Galietta, 2009). Most of the subfamilies are well defined, although the role of glycine receptors and GABA remains poorly characterized (Devuyst and Guggino, 2002).

1.8 CFTR ion channels

1.8.1 CFTR localization

One of the major roles of mammalian kidneys is to maintain the concentration of extracellular sodium chloride, which in turn controls blood pressure and extracellular fluid volume (Morales et al., 2000). Chloride anions (Cl^-) are re-absorbed along the nephron and are the predominantly glomerular infiltrate. Transportation of Cl^- occurs through several transmembrane proteins, the ion channels (Morales et al., 2000). Many Cl^- channels have been extensively studied and some of them have been directly linked with severe clinical complications (Jentsch, 1994; Lehmann-Horn and Jurkat-Rott, 1999; Sasaki et al., 1994). Cystic fibrosis (CF) is a lethal autosomal recessive genetic disorder, which is caused by mutations within the cystic fibrosis transmembrane conductance regulator (CFTR) gene. The *cftr* gene expresses an integral membrane protein, which is a member of the ABC transporter family and localized in a variety of epithelia such as the renal tubules (Riordan, 1993).

CFTR is abundantly expressed in kidneys of both rats and humans and is greater expressed in renal cortex and outer renal medulla kidney areas in comparison with other areas (Morales et al., 1996). Particularly, CFTR protein was detected at the

apical surface of both distal and proximal tubules of rat kidneys, although there was no expression in the outer medullary collecting ducts (Crawford et al., 1991). In human kidneys, CFTR protein is detectable in several areas, including distal and proximal tubular cells, collecting duct, the thin limbs of Henle's loop and the branching ureteric bud (Crawford et al., 1991; Morales et al., 1996; Devuyst et al., 1996). Studies have demonstrated that despite the fact that CFTR is a plasma membrane ion channel, in proximal tubular cells, CFTR is localized in intracellular organelles along the endocytic and secretory pathways. CFTR might regulate pH by importing Cl^- into endocytic vesicles equilibrating H^+ accumulation (Bradbury, 1999).

1.8.2 CFTR as an intracellular chloride channel

Regulation and maintenance of an acidic environment within intracellular organelles controlled by CFTR ion channels is controversial (Bradbury, 1999; Edwards and Kahl, 2010). It is identified that living cells have developed mechanisms to control the pH inside organelles and within the cytoplasm. Several studies performing biochemical and functional analyses have identified acidic intracellular compartments, such as secretory granules, endosomes, lysosomes and some compartments of the Golgi apparatus (Bradbury, 1999).

Lipophilic weak bases and fluorescent dextrans have been utilized to study and measure vacuolar acidification (Anderson et al., 1991; Maxfield, 1982; Mellman et al., 1986). Internal pH of endosomes has been estimated between 5.0 and 6.0. However, this range might vary as probes such as FITC-dextran is transported from less to more acidified endosomes after initial internalization (Geisow and Evans, 1984; Tycko and Maxfield, 1982; Haggie and Verkman, 2009). Moreover, the lysosomal acidic environment ranges between 4.6-5.0 (Haggie and Verkman, 2009; Tycko and Maxfield, 1982).

Proton pumps (H^+-ATPases) are strongly associated with vesicular acidification as they not only create a ΔpH across the organelle membrane, but also cause a distinct membrane potential $\Delta\Psi$ because of the proton transportation (Bradbury, 1999; Forgac, 2007). H^+-ATPases create a membrane potential and inhibition of further proton transportation and creation of ΔpH occur if the proton permeability of the

subcellular membrane organelle is low. Whereas, the presence of CFTR localized within the membrane of intracellular organelles permits Cl^- transportation into the organelles, functioning to collapse the membrane potential and promote vesicular acidification (Figure 1.16) (Bradbury, 1999; Tamir et al., 1994; Jouret et al., 2007). Lysosomes and endosomes in different cell types may contain K^+ conductance in order to facilitate acidification (Galloway et al., 1983; Harikumar and Reeves, 1983; Hover et al., 2018).

Findings suggested that Cl^- conductance can regulate vesicular pH, although protein kinases have been identified to regulate subcellular Cl^- transportation and consequently acidification process as well (Bradbury, 1999). Endosomal Cl^- channels are regulated in a tissue and organelle-specific manner. Cl^- channels of endosomes contained in renal cells are controlled by protein kinase A and a decrease in endosome acidification was observed upon treatment with phosphatases that counteract the function of PKA (Reenstra et al., 1992).

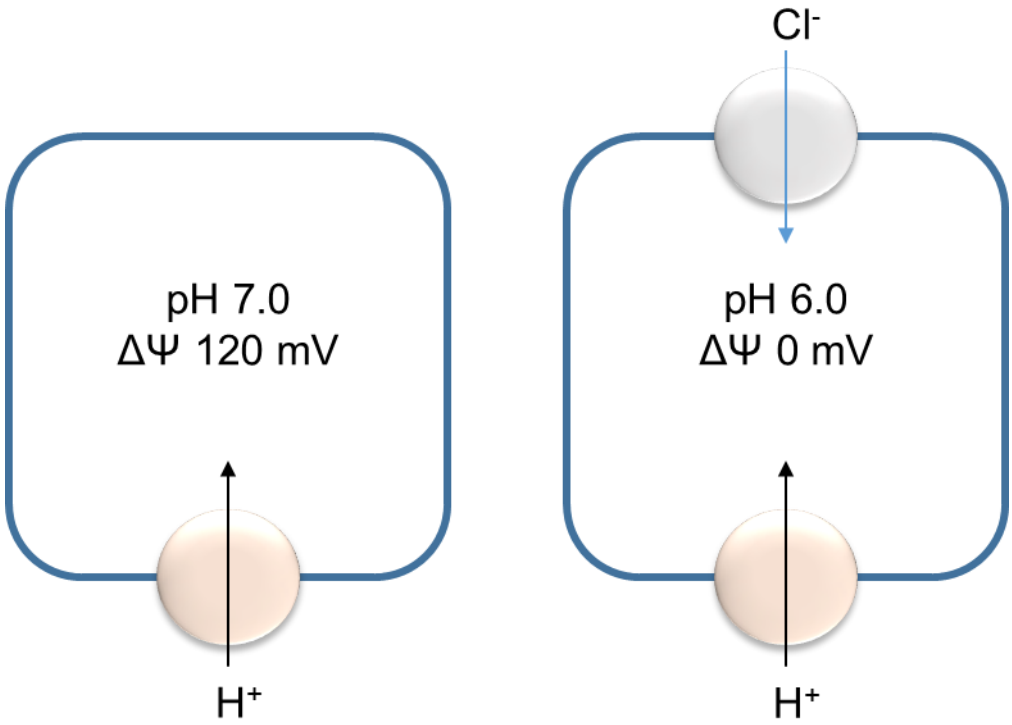

Figure 1. 16 Schematic representation of organelle acidification mechanism. Vesicular proton pumps are localized in the subcellular membrane and generate a membrane potential (ΔΨ) and a pH gradient inhibiting proton transportation and acidification (left). Chloride ion channels, such as CFTR, collapse subcellular membrane potential and permit organelle acidification (right). Adapted from Bradbury, (1999).

1.8.3 Structure and function of the CFTR ion channel

CFTR belongs to the ABC transporter family and works as an ion channel and not as an active transporter like other members of the family (Bear et al., 1992). Sulfonylurea receptor (SUR) is also member of the ABC family and does not function as an active transporter (Souza-Menezes and Morales, 2009).

The human *cftr* gene is localized within chromosome 7 (7q31.2) and encodes for a protein of approximately 1,480 amino acids (Knowlton et al., 1985; Morales et al., 1999). Studies have demonstrated that CFTR consists of an intracellular N-terminal arm, six transmembrane-spanning domains (TMD1), which are linked with a nucleotide-binding domain (NBD1) containing sequences for ATP binding (Morales et al., 1999). NBD1 is followed by a regulatory domain (R), which contains sequences capable of being phosphorylated by PKA and PKC (Chen and Hwang, 2008). This is followed by a second set of six transmembrane-spanning domains (TMD2) and a nucleotide-binding domain (NBD2) (Figure 1.17) (Souza-Menezes and Morales, 2009). A recent study revealed the molecular structure of the human CFTR ion channel (Figure 1.18) (Liu et al., 2017).

The main trigger for CFTR activity *in vivo* is its phosphorylation by PKA and PKC (Sheppard and Welsh, 1999). Studies have reported that CFTR opening rate is increased by the addition of PKA in the presence of MgATP and burst duration is also increased under phosphorylating conditions, suggesting that phosphorylation sites control CFTR channel closing (Mathews et al., 1998; Wang et al., 2000). Five distinct Ser (Ser-700, Ser-737, Ser-768, Ser-795 and Ser-813) residues are phosphorylated by PKA in the R domain *in vivo* (Hegedűs et al., 2009) and specifically Ser-737 and Ser-768 are argued to be inhibitory on the basis of the observation that their disruption increases CFTR channel activity (King et al., 2009). In contrast, unphosphorylated R domain blocks CFTR channel opening (Hwang and Kirk, 2013), although the mechanism of how phosphorylation impacts on this inhibition is still unclear.

Similar to other ABC transporters, the NBDs of CFTR are able to form a dimmer (Vergani et al., 2005). Moreover, there are two distinct binding pockets for ATP (ABP). ABP1 contains the Walker A and B consensus sequences of NBD1 and the signature sequence of NBD2, whereas ABP2 consists of the signature sequence of NBD1 and

Walker A and B motifs contained within NBD2 (Chen and Hwang, 2008). Binding of ATP to NBDs causes the close interaction of the two NBDs and the locking of two ATPs in the NBD1 and NBD2 interface (Gadsby et al., 2006). Due to this interaction, the signal transmission occurs through cytoplasmic-linking domains, and the channel gate opens (Gadsby et al., 2006). The channel remains open until hydrolysis of one of the ATPs, which results in the separation of NBD1 and NBD2 interface (Gadsby et al., 2006). Closure of the ion channel gate abolishes Cl^- flux until binding of ATP to the NBDs of CFTR occurs again (Gadsby et al., 2006) (Figure 1.19).

CFTR is critical not only for Cl^- transportation but also for regulation of other transporters, which might be crucial for epithelia and strongly associated with transportation of several ions. Stimulation of an outward rectifying Cl^- channel, ORCC, and blockade of the epithelial Na^+ channels, ENaC, occur due to CFTR function (Fulmer et al., 1995; Schwiebert et al., 1998; Kunzelmann et al., 2001).

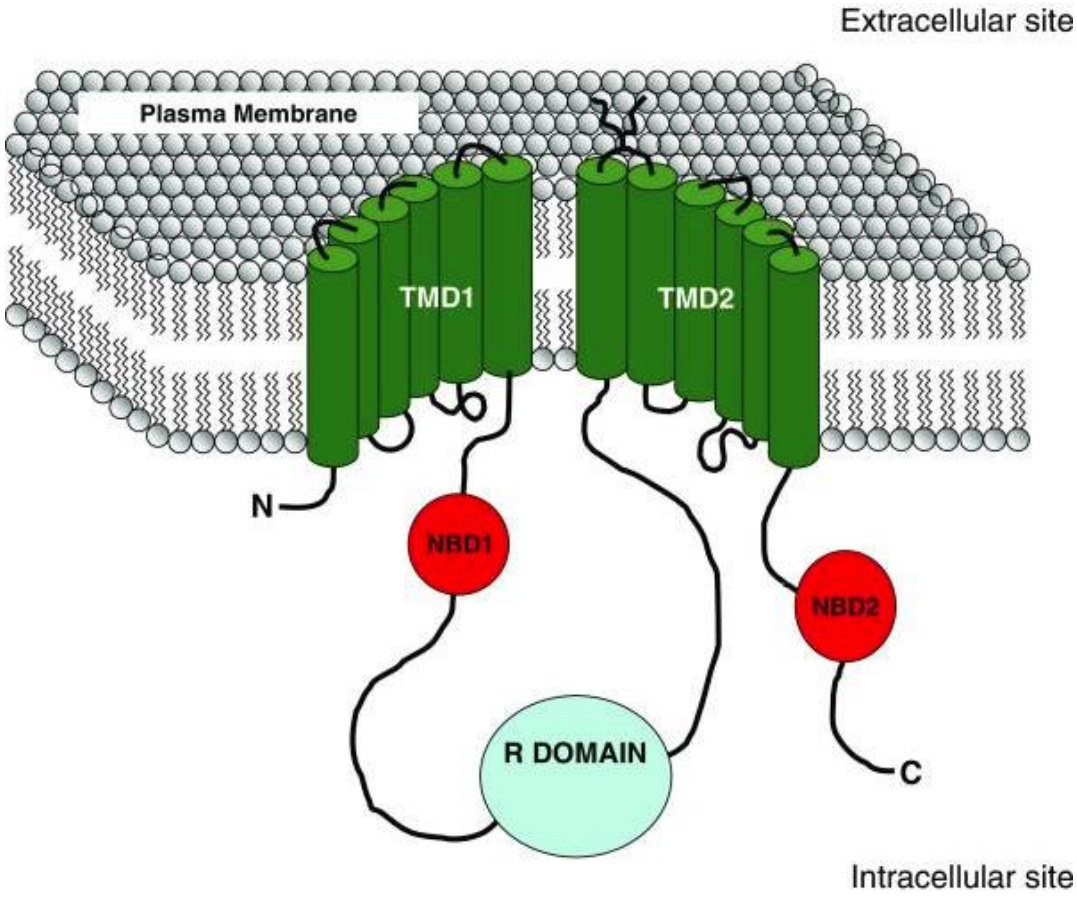

Figure 1. 17 Schematic representation of CFTR ion channel located in the plasma membrane. CFTR consists of two distinct sets of transmembrane-spanning domains, TMD1 and TMD2; two distinct nucleotide-binding domains, NBD1 and NBD2; a regulatory domain, R; a N-terminal domain, N and a carboxy-terminal domain, C (Souza-Menezes and Morales, 2009).

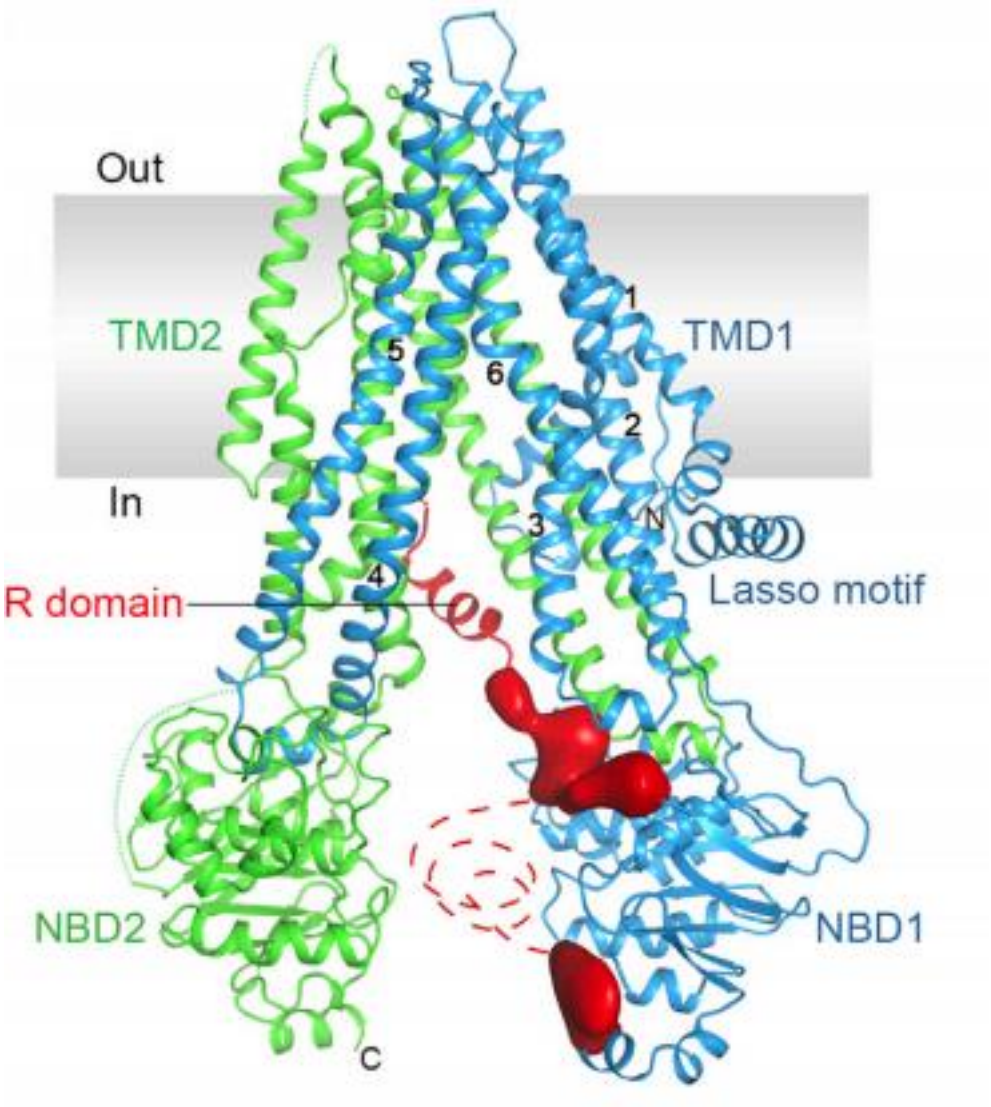

Figure 1. 18 Structure of human CFTR ion channel in a dephosphorylated and ATP-free confirmation state. Electron microscopy structure of human CFTR are represented with the EM densities shown in red corresponding to unstructured areas within the R domain or the R insertion of NBD1. Dashed lines represent unresolved structures (Liu *et al*., 2017).

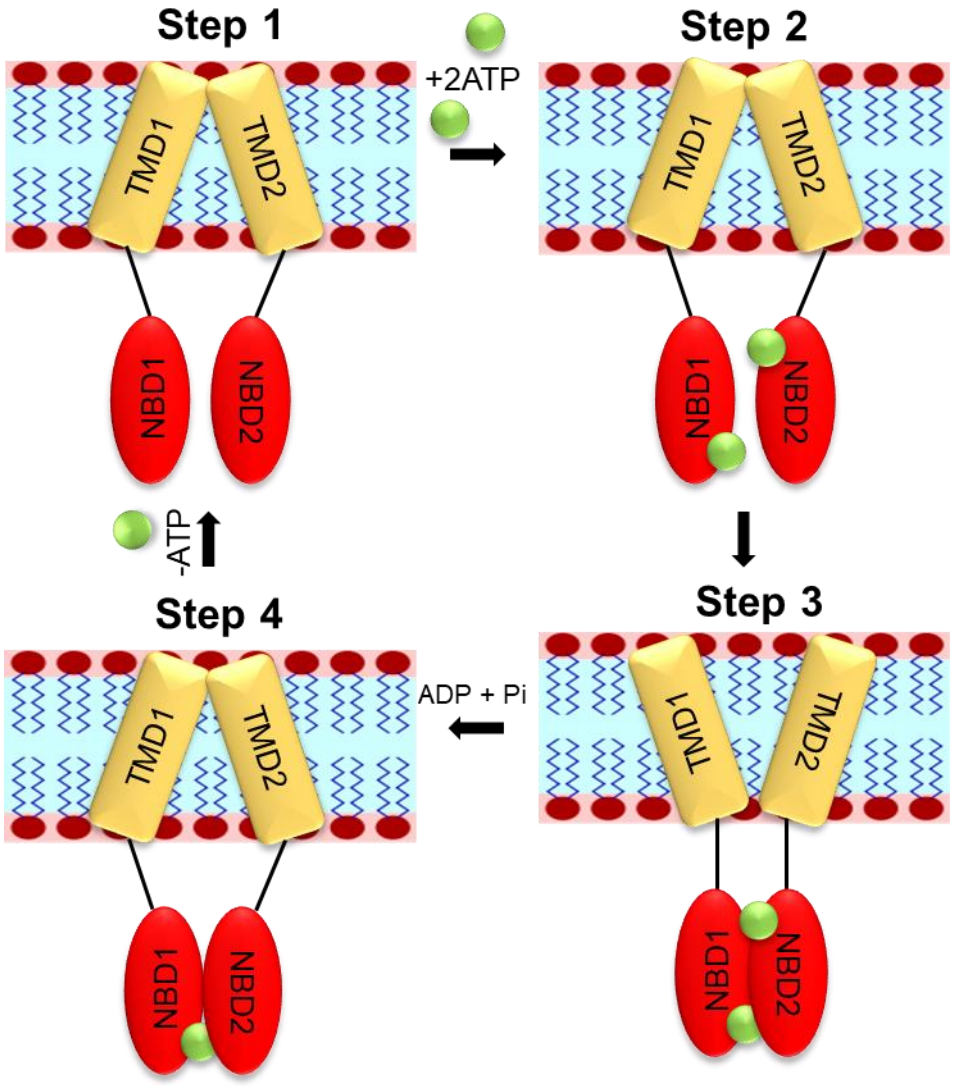

Figure 1. 19 CFTR channel gating. A simplified diagram presenting dominant gating transitions from Step 1 to Step 4, including the engagement and disengagement of the two TMDs and NBDs. Adapted from Hwang and Kirk, (2013).

1.8.4 CFTR and regulation of ROMK ion channel activity in kidneys

The renal outer medullary potassium (ROMK) ion channel is critical for restoration of K^+ levels in the lumen of thick ascending limbs of Henle's loop (TAL) and K^+ excretion in the cortical collecting duct (CCD) of human kidneys (Wang et al., 1997) (Figure 1.20). ROMK is a member of the inward-rectifier K^+ channels or K_{ir}. All members of this ion channel subfamily share common features, including two transmembrane domains, the cytoplasmic N- and C-terminal regions and a conserved selectivity filter for K^+ (Welling and Ho, 2009).

Restoration of K^+ across the apical membrane of TAL is crucial for NaCl reabsorption, which consequently results in accumulation of solutes in the renal medulla (Hebert and Andreoli, 1984; Greger, 1985). Three distinct significant processes are associated with K^+ restoration in kidneys. K^+ recycling causes hyperpolarization of cell membrane, which following leads to Cl^- dissemination across the basolateral membrane. Furthermore, transepithelial Na^+ reabsorption is regulated by K^+ restoration due to the generated lumen-positive potential. Moreover, K^+ are provided to Na-K-Cl co-transporter because of K^+ recycling (Giebisch, 1998; Souza-Menezes and Morales, 2009). It has been identified that K^+ transportation across the apical membrane of the CCD is controlled by ROMK ion channel (Wang, 1999).

Previous studies have shown that inhibition of the ABC transporter family member SUR by the pharmacological agent Glibenclamide results in inhibition of ROMK2, an isoform of ROMK (Inagaki et al., 1995). Based on these findings, an accessory protein might be important for the function of ROMK2. According to Aguilar-Bryan et al., (1998) both subtypes of SUR, SUR1 and SUR2, interact with ROMK2 although there is no expression of SUR1 or SUR2 in kidneys. Fuller and Benos, (1992) suggested that CFTR is abundantly expressed in kidney epithelial cells and might form a renal low-conductance ATP-sensitive K^+ channel with the ROMK ion channel. It is also demonstrated that the presence of Glibenclamide impedes the function of ROMK2, when ROMK2 is co-expressed with CFTR (McNicholas et al. 1996). Further investigations revealed that NBD1 of CFTR ion channel is critical for the interaction between ROMK2 and CFTR (McNicholas et al., 1997). Additional studies have

demonstrated that ROMK1 was not sensitive to Mg-ATP, whereas in the presence of CFTR, the ion channel sensitivity to ATP changed (Ruknudin et al., 1998). These findings proposed that CFTR might be critical in human kidneys, where ROMK ion channels are also expressed (Souza-Menezes and Morales, 2009).

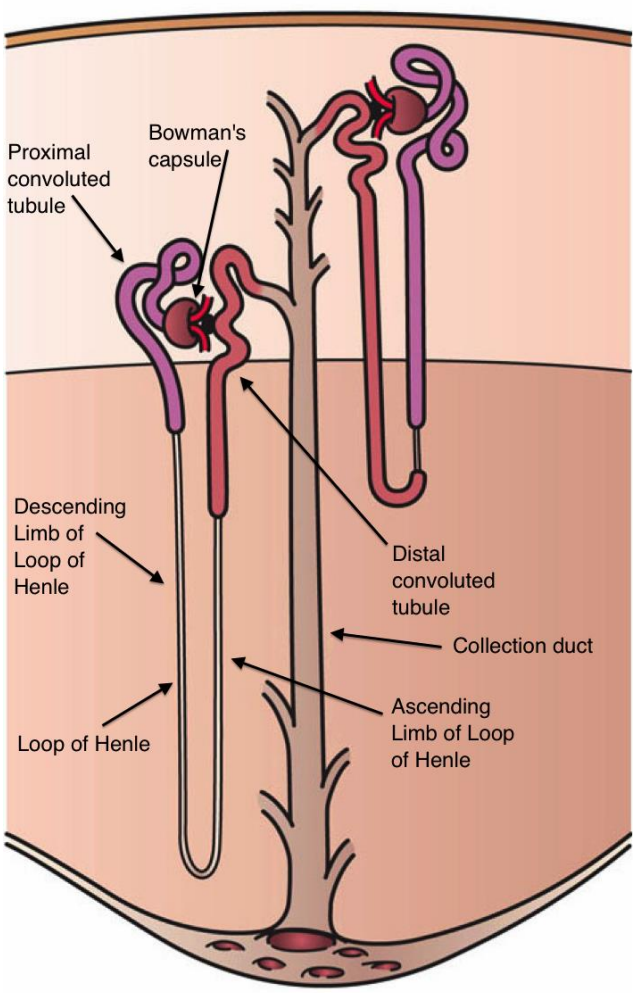

Figure 1. 20 Structure of a human nephron. Schematic representation of a human nephron showing its different parts (Pocock and Richards, 2006).

1.8.5 CFTR ion channel inhibitory compounds

Open channel blockers were the first CFTR inhibitory compounds (Schultz et al., 1999; Hwang and Sheppard, 1999). These compounds act physically by entering the open pore of the channel and temporally blocking of Cl^- flow (Linsdell, 2014). Inhibitors that share this common mechanism of CFTR ion channel inhibition are sulfonylureas including Glibenclamide, diphenylamine-2-carboxylate (DPC) and 5-nitro-2-(3-phenylpropyl-amino) benzoate (NPPB) (Figure 1.21) (Verkman et al., 2013). Glibenclamide is one of the most widely utilized compound for Cl^- inhibition and is identified as an antidiabetic drug, which targets ATP-sensitive K^+ channels in pancreatic islet beta cells (Verkman et al., 2013).

Biophysical analysis of these compounds revealed details about the mechanism of their action. Each inhibitor binds to sites inside the pore only from the cytoplasmic end causing a voltage-dependent blockade, which is stronger in more hyperpolarized voltages. However, the channel inhibition is affected by the extracellular Cl^- concentration. At low extracellular Cl^- concentration, the ion channel inhibition is stronger, whereas at higher Cl^- is weaker (Linsdell, 2014). Previous studies have also suggested that CFTR might possess an asymmetric structure since inhibitors reach the pore of the channel only from the cytoplasmic side. The narrow extracellular entrance does not permit the entry of larger compounds, although the inner side is accessible for substances from the cytoplasm (Hwang and Sheppard, 1999; Linsdell and Hanrahan, 1996).

Other studies have identified novel inhibitors with a more potent effect on CFTR (Figure 1.19) (Verkman and Galietta, 2009). Thiazolidinone, CFTR172, blocks CFTR ion channel from the cytoplasmic side at a sub-micromolar level (Ma et al., 2002) and in a voltage-independent manner (Taddei et al., 2004; Kopeikin et al., 2010). Furthermore glycine hydrazides, such as GlyH-101, impact on CFTR ion channel in a voltage-dependent manner from the extracellular environment and at a low micromolar concentration (Muanprasat et al., 2004). These two recent identified compounds cause inhibition of CFTR ion channel by a different mechanism in comparison with the open channel blockers (Linsdell, 2014). In particular, CFTR172

binds to the open ion channel preferentially, which results in conformational changes of CFTR (Kopeikin et al., 2010). GlyH-101 works as an open channel blocker, although reaches the ion channel pore from the extracellular side through the narrow entrance blocking Cl^- flow (Muanprasat et al., 2004; Norimatsu et al., 2012). The pyrimido-pyrrolo-quinoxalinediones (PPQs) are also small molecule CFTR inhibitors and a primary screening identified PPQ-102 as the most potent among 347 commercially available PPQ analogs (Verkman et al., 2013). Unlike GlyH-101, PPQ-102 is uncharged at physiological pH and therefore acts in a voltage-independent manner (Verkman et al., 2013). A more potent CFTR modulator, compared to PPQ-102, is BP0-27 exhibiting greater metabolic stability and aqueous solubility even though it acts in voltage-independent trend similarly to PPQ-102 (Verkman et al., 2013).

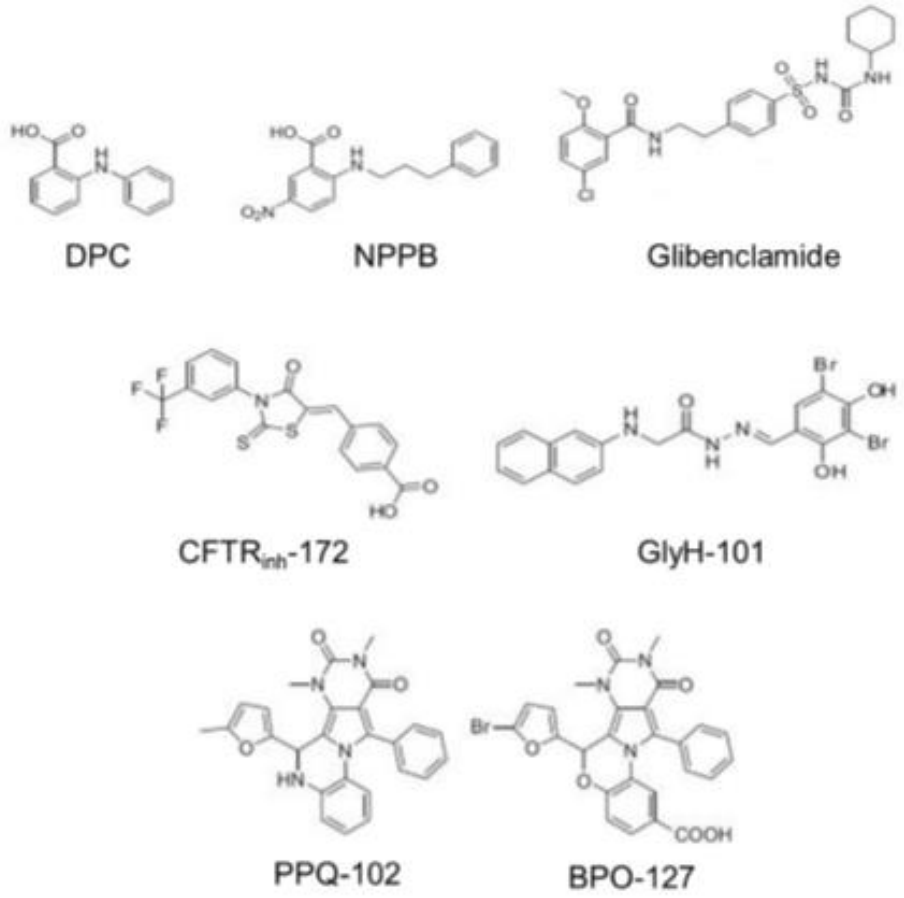

Figure 1. 21 Chemical structures of CFTR inhibitory compounds. Structure of the open channel blockers, DPC, NPPB and Glibenclamide are shown. Structure of more recent and potent inhibitors such as CFTR172, GlyH-101, PPQ-102 and BPO-127 are represented (Verkman *et al*., 2013).

1.9 Viral modulation of host ion channels

All viruses exploit host cell factors and machineries to fulfill their life cycles. It is established that several viruses generate their ion channels to monitor ion homeostasis throughout the different stages of their life cycles (Royle et al., 2015; Sze and Tan, 2015). However, many viruses do not generate a viroporin and/or manipulate host cell ion channels to regulate host ionic environment. Studies have shown that host cell ion channels are exploited by different viruses and at different stages of their life cycles (Hover et al., 2017).

1.9.1 Host ion channels and virus trafficking

Ion channels are implicated in the process of virus trafficking into the host cells and during the virus and host membrane fusion processes. It is known that Ebola virus (EBOV) and Marburg virus enter host cells through micropinocytosis (Gehring et al., 2014). Studies have demonstrated that host Ca^{2+} channels play a critical role for filoviruses cell entry since treatment with Ca^{2+} inhibitory compounds, such as verapamil, cause blockade of virus entry (Gehring et al., 2014). Two types of Ca^{2+} family, TPC1 and TPC2 are associated with EBOV entry and release from the endocytic network. Moreover, similar findings were observed for Marburg virus life cycle, suggesting a shared regulatory mechanism for filoviruses (Sakurai et al., 2015).

Recent work has identified that K^+ channels control events after the initial entry of Bunyamwera virus (BUNV) (Hover et al., 2016). K^+ channels were critical for the BUNV during the early stages of infection prior to viral RNA synthesis and blockade of this ion channel family was detrimental to BUNV (Hover et al., 2016). Further analysis revealed that the two-pore K^+ channels (K_{2P}) are required for the BUNV life cycle (Hover et al., 2016) and particularly are important within endosomal compartments (Hover et al., 2018). In addition, the requirement of K^+ channels for a successful life cycle was also observed in other bunyaviruses, such as Hazara virus and Schmallenberg virus, indicating a common regulatory mechanism shared amongst the members of this family (Hover et al., 2016).

It is also demonstrated that there is a requirement of host Cl^- channels during herpes simplex virus 1 (HSV-1) entry process. HSV-1 promotes Cl^- flow and in the presence of specific inhibitory compounds, such as NPPB and tamoxifen, blockade of HSV-1 virion binding, penetration into the host cell and nuclear translocation were observed (Zheng et al., 2014).

1.9.2 Host ion channels and virus persistence

Previous work has identified that the Hepatitis C virus (HCV) non-structural protein, NS5A, is able to block the liver-expressed voltage-gated K^+ channel 2.1 ($K_v2.1$) (Mankouri et al., 2009). Phosphorylation and activation of $K_v2.1$ are promoted by oxidative stress leading to an outward K^+ current that cause apoptotic induction (Redman et al., 2007). An increase in reactive oxygen species has been identified in HCV infected hepatocytes, thus the virus would appear capable of promoting such channel activity. To avoid this, NS5A blocks the oxidative-stress-mediated phosphorylation of $K_v2.1$ and linked apoptotic signaling (Mankouri et al., 2009). Moreover, the suppression of p38 MAPK signaling is involved in the mechanism of $K_v2.1$ inhibition (Mankouri et al., 2009). It was also demonstrated that stress-mediated neuronal cell death is blocked by NS5A through the impediment of $K_v2.1$ functionality via Src-mediated phosphorylation (Redman et al., 2007). Consequently, these findings suggested that $K_v2.1$ activation is disturbed by HCV to avoid apoptosis and permit virus survival and persistence (Norris et al., 2012). Additionally, HCV causes an increase of intracellular Cl^- flow, which can be blocked by specific pharmacological compounds (Igloi et al., 2015). Three members of Cl^- channel family, ClC-1, ClC-5 and ClC- 7 are required for HCV replication by an unknown mechanism (Igloi et al., 2015).

Studies have indicated that HIV-1 is able to modify K^+ concentration indirectly (Choi et al., 2008) and further analysis revealed that large-conductance Ca^{2+}-dependent K^+ host channels (BK_{Ca}) are blocked by Nef protein, although this modulation is still unclear (Herrmann et al., 2010; Kort and Jalonen, 1998). HIV-1 virion particles release is regulated by K^+ channel functionality through the impact of HIV-1 gp120 and viral protein U (Vpu). Direct interaction of Gp120 with the cytoplasmic C-terminus of the

ether-a-go-go K^+ channel (hERG) and its subsequently inhibition results in enhanced virus particle release, whereas it can be impeded by hERG overexpression (Herrmann et al., 2010). Moreover, resting membrane potential is manipulated by HIV-Vpu through obstruction of leak K^+ channels (Hsu et al., 2010; Strebel, 2004). Previous studies revealed that HIV-1 release is blocked by the expression of the acid-sensitive K_{2P} channel, TASK-1 via an unknown mechanism (Hsu et al., 2004). HIV release is facilitated due to the formation of inactive Vpu and TASK-1 heterodimers, which subsequently cause an inhibition of TASK-1 currents and destabilization of membrane potential to facilitate virus assembly (Hsu et al., 2004).

Furthermore, studies have shown that eight different host ion channels from K^+, Na^+, Cl^- and Ca^{2+} families are downregulated by monkeypox virus, although the distinct impact of this downregulation on virus life cycle is still uncharacterized (Alkhalil et al., 2010). Previous work has also demonstrated that Epstein-Barr virus causes an increase of the Orai1 channel expression, modifying Ca^{2+} homeostasis due to the initiation of Ca^{2+} flow into ER stores. These results indicated that intracellular host ion channels might be modulated by viruses (Dellis et al., 2011). It is also established that human T-cell leukaemia virus type 1 might stimulate an inward K^+ current for as yet unknown viral processes (Biasiotto et al., 2010).

1.9.3 Viral modulation of host ion channels in excitable cells

Chronic viral infection of the central nervous system might result in severe clinical complications, likely promoted by viral modulation of ion channels. Studies have shown that mumps virus is able to reduce the magnitude and frequency of action potentials, which might be associated with the blockade of voltage-gated Na^+ (Na_v) channel (Stauffer and Ziegler, 1989). In contrast, varicella-zoster virus promotes increase of Na_v currents mediated by the $Na_v1.6$ and $Na_v1.7$ members of this family, which might lead to neuropathic pain (Kennedy et al., 2013). Rabies virus (RABV) is also strongly linked with complications of central nervous system. Studies have shown that a reduction of inwardly-rectifying K^+ (K_{ir}) and Na_v was observed in RABV infected cells, which ultimately results in alterations of action potential firing (Iwata et al., 1999). Moreover, it is identified that RABV prohibits the inhibition of Ca^{2+} currents

in the presence of noradrenaline, an important mediator of Ca^{2+} entry that signals neurotransmitter release (Rosenblum et al., 1991). These findings suggested that alterations of K^+, Na^+ and Ca^{2+} currents might facilitate virus pathogenesis although resulting in lethal consequences to the host (Iwata et al., 1999).

Previous work has also demonstrated that there are distinct interactions between coxsackievirus B3 (CVB3) and hERG1 channels, L-type Ca^{2+} channels and K_vLQT1 (K_v7.1) channels during infection (Steinke et al., 2013). Further analysis in mice revealed that CVB3 replicated in higher titres in the heart of Kir6.1-deficient mice, indicating that ATP-sensitive K^+ channel deregulation might play a crucial role in innate anti-viral immunity in the heart. Therefore, ion channel alterations promoted by CVB3 might impact on the arrhythmia observed in CVB3 patients and may be required for virus persistence as well (Steinke et al., 2013). Thus, host cell ion channel activity appears to be a key virus-host interaction during several viruses' life cycle and since some of these ion channel modulators are currently clinically available, further studies may reveal intriguing insights into their potential anti-viral therapeutic.

1.10 Aims and Objectives

Preliminary data from our group had proposed that inhibition of host cell K^+ channels, using specific inhibitory compounds, could impair the BKPyV life cycle by a mechanism which was uncharacterized. The main aim of this research project was to validate the preliminary data and to investigate whether host ion channels could be potential anti-viral drugs against BKPyV. To this end the objectives of this project were:

1. To establish a primary renal proximal epithelial cell culture model for the study of the BKPyV life cycle.

2. To perform and establish a high-throughput technique for BKPyV titration.

3. To validate and characterize the impact of host cell ion channels on BKPyV life cycle.

4. To identify at which stage of BKPyV life cycle there is a potential requirement of host ion channels.

5. To investigate whether the same ion channel is required by other polyomaviruses.

2 Materials and Methods

2.1 Bacterial cell culture

2.1.1 Preparation of competent bacteria cells

NEB5α bacteria cells were prepared to become chemically competent. SOB-media (10 mM NaCl, 0.5% yeast extract, 2% peptone, 2.5 mM KCl, pH 7.5) was used for the growth of single bacterial colonies. Single colonies were grown at 18^{o}C to reach an optical density at 600 nm (OD_{600}) of approximately 0.6. Cultures were incubated on ice and then centrifuged at 2500 x g for 10 minutes to harvest bacterial cells. The harvested bacterial cells were then washed in transformation buffer containing 15 mM $CaCl_2$, 10 mM PIPES, 55 mM $MnCl_2$, 250 mM KCl, pH 6.7. Following this, the bacterial cells were resuspended in cold transformation buffer containing 7% dimethyl sulphoxide (DMSO). Prepared aliquots of competent bacteria cells were placed at -80^{o}C for long-term storage.

2.1.2 Transformation of plasmid DNA into bacteria

Competent bacteria NEB5α cells were used in all transformation experiments. An aliquot of bacteria was thawed on ice and 1.5 ml tubes were pre-chilled. Thawed bacteria (50 µl) were mixed with 1 µl of DNA and incubated in the pre-chilled tubes on ice for 30 minutes. The mixture was next heat shocked at 42^{o}C for 45 seconds and placed back on ice to recover for 2 minutes. LB-Broth (200 µl) was added to the bacterial mixture, which was then incubated at 37^{o}C and 180 rpm for 1 hour. The bacterial culture was spread on agar plates in the presence of the appropriate antibiotics (100 µg/ml) and incubated at 37^{o}C overnight.

2.1.3 Preparation of plasmid DNA

2.1.3.1 Small scale bacterial culture

Small scale bacterial cultures were set up to a final volume of 5 ml LB-Broth media. In 50 ml universal falcon tubes 5 ml of LB-Broth containing the appropriate antibiotics (100 µg/ml) was inoculated with a scrape from a glycerol stock or a single colony from a cultured agar plate. Bacterial inoculum was incubated in an orbital shaker at 180 rpm and 37^{o}C from 4 hours to overnight incubation depending on the experiment and the use of the bacterial culture.

2.1.3.2 Large scale bacterial culture

Large scale bacterial cultures were set up to a final volume of 100 ml LB-Broth media. In 500 ml sterile conical flasks, 100ml of sterile LB-Broth media containing the appropriate antibiotics (100 µg/ml) was inoculated with 5 ml of overnight bacterial culture. Bacterial culture was incubated in an orbital shaker at 180 rpm and 37^{o}C overnight. Following, bacterial culture centrifuged at 4,000 x g for 15 minutes at 4^{o}C to pellet bacterial cells. Plasmid DNA extraction was performed according to manufacturer's instructions (Qiagen, Germany). Plasmid DNA was eluted by adding 100-800 µl nuclease-free water and quantified using the Nanodrop (Thermo Fisher Scientific, USA).

2.2 Mammalian cell culture

2.2.1 Growing, maintaining and passaging mammalian cells

African green monkey kidney (Vero) cells (kindly provided by Dr Holly Shelton-The Pirbright Institute, UK) were cultured and seeded in Dulbecco's Modified Eagle Medium (DMEM) (Sigma Aldrich, USA) supplemented with 1% (v/v) Penicillin/Streptomycin and 10% (v/v) Foetal bovine serum (FBS). Vero cells were grown in T75 cm^2 flasks in the tissue culture incubator at 37^{o}C and 5% CO_2 (Ammerman et al., 2008). To passage Vero cells, growth media was decanted, and

the cells washed with Phosphate Buffered Saline (PBS). Cells were trypsinised to remove them from the flask and passaged at 1:10 dilution in fresh complete media.

Human foetal glial (SVG-A) cells (kindly provided by Dr Walter Atwood-Brown University, USA) were cultured and seeded in Dulbecco's Modified Eagle Medium (DMEM) (Sigma Aldrich, USA) supplemented with 1% (v/v) Penicillin/Streptomycin, 1% (v/v) non-essential amino acids (Life Technologies, USA) and 10% (v/v) Foetal bovine serum (FBS). SVG-A cells were grown in T75 cm^2 flasks in the tissue culture incubator at 37^oC and 5% CO_2. To passage SVG-A cells, growth media was decanted, and cells were washed with Phosphate Buffered Saline (PBS). Cells were trypsinised to remove them from the flask and passaged at 1:8 dilution in fresh complete media.

Human embryonic kidney (HEK293TT) cells (HEK293T are HEK293 cells stably transfected with SV40 genome and they express tAg and low amount of TAg. HEK293TT are HEK293T cells that are stably transfected with SV40 TAg cDNA and they express high levels of TAg) (kindly provided by Dr Chris Buck- NIH, USA) were cultured and seeded in Dulbecco's Modified Medium (DMEM) (Sigma Aldrich, USA) supplemented with 1% (v/v) Penicillin/Streptomycin and 10% Foetal bovine serum (FBS) (Russell et al., 1977). HEK293TT cells were grown in T75 cm^2 flasks in the tissue culture incubator at 37^oC and 5% CO_2. To passage HEK293TT cells, growth media were decanted and washed with Phosphate Buffered Saline (PBS). Cells were trypsinised to remove them from the flask and passaged at 1:10 dilution in fresh complete media.

Primary Human Renal Proximal Tubular Epithelial cells (RPTE) were obtained from Lonza and cultured in REBM Medium (Lonza, UK). Essential supplements including FBS, insulin, gentamicin sulphate, epidermal growth factor, epinephrine, hydrocortisone, triiodothyonine and transferrin (purchased as a kit-Lonza, UK) were added to the media before use. RPTE cells were seeded onto a T175 flask and manipulated according to the supplier's instructions. To allow a flask to become confluent the media was changed every 3 days due to the low amount of FBS. After each passage, 1 x 10^6 RPTE cells per ml in 1 ml fresh media were frozen down as aliquots (Taub, 1997).

2.2.2 Cell counting

Mammalian cells were counted using a haemocytometer. Cell suspension (10 µl) was mixed with 10 µl of Trypan Blue solution (Sigma Aldrich, USA) and applied to the haemocytometer slide. The average cell count from each set of corner squares was taken and multiplied by 2 x 10^4 to represent the number of cells per ml.

2.2.3 Freezing and thawing mammalian cells

Following cell harvesting, 5 x 10^5-10^6/ml cells were resuspended in 1 ml of complete fresh media in the presence of 10% (v/v) DMSO. Cell solutions were added to cryovials and placed in a freezer container (Mr Frosty) containing isopropanol and incubated at -80^{o}C overnight. The following day, cells were transferred to liquid nitrogen for long-term storage.

Frozen cells were thawed at 37^{o}C and transferred to a universal falcon tube. Approximately 10 ml of fresh complete media was added to cells. This suspension centrifuged at 1,100 rpm at 4^{o}C for 5 minutes to pellet the cells. The supernatant was carefully discarded, and cells were resuspended in 2 ml of fresh complete growth media. Resuspended cells were transferred to a T75 cm^2 flask and 8 ml of fresh growth media was added. Flasks were placed in the tissue culture incubator at 37^{o}C and 5% CO_2.

2.2.4 Transient transfections with NanoJuice

Vero cells were seeded into 6-well dishes (Sarstedt, Germany) at a density of 2 x 10^5 cells/ml and incubated overnight. Plasmid DNA (0.5 µg) was added per reaction to each well. The transfection mixture was prepared in 1.5 ml tubes and for each reaction, 50 µl of Opti-MEM was added to 1 µl of NanoJuice Core transfection reagent and 1.5 µl of NanoJuice Transfection Booster (Merck Millipore, USA) and mixed thoroughly before a 15 minute-incubation at room temperature. Next, DNA was added, and the transfection mixture was incubated for 15 minutes at roomtemperature. The transfection mixture (50 µl) was then added to each well of

cells (in complete growth media). Growth media was replaced with fresh 16 hours post-transfection (Panou et al., 2018). Transfected cells were incubated for further 48-72 hours depending on the specific experimental procedure.

2.2.5 Transfecting siRNA into RPTE cells

RPTE cells were seeded into 6-well dishes (Sarstedt, Germany) at a density of 2 x 10^5 cells/ml and incubated overnight. RPTE cells were transfected with a pool of 4 different Flexitube siRNA (Table 2.1) (Qiagen, Germany) molecules specifically targeted to CFTR, and an AllStars negative control siRNA (Qiagen, Germany). Each of the 4 different Flexitube siRNA (100 nM each) and 10 µl of Santa Cruz siRNA Transfection Reagent (Santa Cruz, USA) were dissolved in 100 µl of Opti-MEM in 2 different 1.5 ml tubes, respectively. This was then incubated at room temperature for 5 minutes. Next, the 2 solutions were combined, mixed gently and incubated for 30-45 minutes at room temperature. Approximately 800 µl of complete fresh media was added to the transfection mixture. Cells were washed once with 1 ml of Opti-MEM before the transfection mixture was added. The siRNA transfection mixture was removed from cells around 6-8 hours post-transfection and replaced with 2 ml of fresh media. Cells were incubated for 48 hours prior to analysis.

Table 2. 1 CFTR-specific FlexiTube siRNA sequences

Product name	siRNA sequence
Hs_CFTR_5	ATCGCGATTTATCTAGGCATA
Hs_CFTR_4	TCGATATATTACTGTCCACAA
Hs_CFTR_2	ATGGCCAACTCTCGAAAGTTA
Hs_CFTR_1	CTCGAAAGTTATGATTATTGA

2.2.6 Use of ion channel modulators

All the inhibitors used in this study were diluted to a final working concentration in 2 ml of complete fresh media (Table 2.2). Mixtures of fresh media and inhibitory compounds were mixed thoroughly and added directly to cells. Treated cells were incubated for 24-72 hours based on the experimental procedure.

Table 2. 2 List of modulatory compounds. The table indicates the ion channel family and sub-family targeted and the diluent used.

Compound	Ion channel family	Compound modulates	Diluent
Tetraethylammonium (TEA)	K^+	Non-selective K^+ channel blocker	H_2O
Potassium Chloride (KCl)	K^+	Increases extracellular K^+	H_2O
Quinidine	K^+	Reduces both Na^+ and K^+ channel currents	DMSO
Barium Chloride ($BaCl_2$)	K^+	Blocker of inward rectifier K^+ channels	H_2O
4-Aminopyridine (4AP)	K^+	Non-selective voltage-gated K^+ channel blocker	H_2O
Glibenclamide	K^+	Blocker of ATP-sensitive K^+ channels	DMSO
Tolbutamide	K^+	Blocker of ATP-sensitive K^+ channels	DMSO
Apamin	K^+	Blocker of Ca^{+2}-activated K^+ channels	Acidic buffer pH 4.8
5-Hydroxydecanoate (5HD)	K^+	Blocker of mitochondrial ATP-sensitive K^+ channels	H_2O
U-37883A	K^+	Blocker of ATP-sensitive K^+ channels (specificity to Kir6.1-type)	H_2O
Diazoxide	K^+	Activator of ATP-sensitive K^+ channels	DMSO
Pinacidil	K^+	Activator of ATP-sensitive K^+ channels	DMSO
VU591	K^+	Blocker of ROMK channels	DMSO
CFTR172	Cl^-	Blocker of CFTR ion channels	DMSO

2.2.7 Cell viability (MTT) assay

Cells were seeded into 96-well dishes at a density of 10^3 cells/ml and incubated overnight. The next day, cells were treated with ion channel modulators and incubated for the period that the drugs' effect was being assessed. Vero and RPTE cells were incubated for 48 hours, HEK293TT cells for 72 hours and SVG-A cells were incubated for 5 days. On the day of the assay, MTT Mw414 was dissolved in serum free media at 1 mg/ml concentration. Growth media was removed from wells and 100 µl of MTT solution was added per well. Cells were then incubated at 37^{o}C for 30 minutes and plates were covered in aluminium foil. After the incubation, the MTT solution was discarded and replaced with 100 µl DMSO. Plates were then placed on a shaking rocker for 5 minutes (60 rpm) to dissolve the purple precipitate and optical densities were read at 570 nm on a plate reader (Riss et al., 2004).

2.2.8 Resting membrane potential assay

Cells were seeded into 6-well dishes at a density of 2 x 10^5 cells/ml and incubated overnight. The next day, cells were treated with inhibitory compounds to a final working concentration in 2 ml of complete fresh media and incubated for the required length of time (Vero/RPTE cells-48 hours; HEK293TT cells-72 hours and SVG-A cells-5 days). Cells were then incubated with 20 µM of DiBAC4(3) (Sigma-Aldrich, USA) in 2 ml of fresh complete media for 30 minutes at 37^{o}C and protected from light (Hover et al., 2016). The DiBAC4(3) dye was removed and cells were washed once with 2 ml of 1 x PBS before being scraped into 500 µl of PBS for analysis by flow Cytometry.

2.2.9 Flow cytometry analysis of live cells

Cell suspensions of cells treated with ion channel modulators and DiBAC4(3) were analysed on an LSRFortessa (BD Biosciences, USA) flow cytometer using the accompanied (FACSDiva Version 6.2) software. All cell populations were gated to contain only live cells. The mean green fluorescence was determined for 100,000 live

cells per sample and the experiments were repeated three independent times. The resulting data were entered into an Excel file to conduct a statistical analysis.

2.2.10 Harvesting and lysing cells

Three different lysis buffers were used in our experiments, dictated by the nature of the experimental protocol.

Cells were cultured in 6-well dishes for the appropriate incubation time at 37^{o}C. Growth media was removed, and cells were washed with 1 ml of PBS and trypsinized with 1 ml of 1 x Trypsin (Lonza, UK), to remove the cells from the dish. To neutralise the 1 x Trypsin, 1 ml of growth media was added, and the cell suspension transferred to 1.5 ml tubes. The cell pellet was collected by centrifugation at 13,000 rpm for 5 minutes and the supernatant discarded, prior to washing the cell pellet with 0.5 ml of PBS. This was repeated, and the cell pellet placed at -80^{o}C for long-term storage. Cell lysis was conducted using a Triton lysis buffer (10 mM Tris (pH 7.6); 10 mM sodium phosphate; 130 mM NaCl; 1% Triton X-100, 20 mM *N*-ethylmaleimide) containing 1 x Protease inhibitor cocktail EDTA-free (Roche, Switzerland) (Hurdiss et al., 2016). Approximately 100 µl of lysis buffer was added to cell pellets and the cells were gently resuspended. Cell lysates were sonicated (20 seconds on, 20 seconds off) 3 times, then incubated on ice for 1 hour and subsequently centrifuged at 13,000 rpm for 5 minutes. Alternatively, for harsher lysis conditions, cells were lysed using 100 µl of RIPA buffer for containing 50 mM Tris-HCl (pH 7.5), 150 mM NaCl, 1% NPEO (Nonylphenol ethoxylates), 0.5% Sodium deoxycholate, 0.1% SDS and 1 x Protease inhibitor cocktail EDTA-free. Cells were gently resuspended in lysis buffer and sonicated (20 seconds on and 20 seconds off) 3 times. Then, cells were incubated on ice for 1 hour and centrifuged at 13,000 rpm for 5 minutes. Another lysis buffer that was used in this study was E1A lysis buffer containing 50 mM HEPES pH 7.0, 250 mM NaCl, 0.1% NP-40, 1 mM EDTA, 1 mM DTT and 1 x Protease inhibitor cocktail EDTA-free (Jiang et al., 2009). Approximately 100 µl of E1A lysis buffer was added to lyse the cells. Cell lysates were sonicated (20 seconds on, 20 seconds off) 3 times. Then, cells were incubated on ice for 1 hour and centrifuged at 13,000 rpm for 5 minutes. Cell lysates were contained in the supernatant.

2.3 Preparation of viral genomes

2.3.1 Preparation of BKPyV, JCPyV and SV40 genomes

Plasmid vectors containing the viral genomes were digested with 10 units of restriction enzymes (Table 2.3) in a 50 µl reaction buffer containing 1 x buffer 4 (NEB, USA) and double distilled water to final volume. Reactions were incubated at 37^{o} C for 2 hours; after 1 hour another 10 units of restriction enzymes (NEB, USA) was added to the mixture. Once digested, re-ligations of the linear genomes at a concentration of 10 ng/µl were carried out with 1 µl of T4 DNA Ligase (NEB, USA) in 100 µl of 10 x T4 Ligation Buffer (NEB, USA) and double distilled water to a final volume of 1 ml (to reduce the probability of concatemer formation). Ligation mixtures were incubated at 16^{o}C overnight and subsequently purified. Both digested and ligated samples were analysed by agarose gel electrophoresis.

Table 2. 3 List of viral genomes. The name of each plasmid containing the viral genome, the amount of DNA and the restriction enzyme used in each enzymatic restriction reaction are listed.

Plasmid	Amount of maxi-prepped DNA	Restriction enzyme	Source
pGem7 BKPyV Dunlop (re-arranged form-lab strain)	10 µg	BamHI-HF	Kindly provided by Professor Michael Imperiale, University of Michigan, USA
pBR322 JCPyV Mad-1	10 µg	EcoRI-HF	Kindly provided by Professor Michael Imperiale, University of Michigan, USA
pUC SV40	4 µg	KpnI-HF	Kindly provided by Professor Daniel DiMaio, Yale University, USA

2.3.2 DNA purification and quantification

A commercially available PCR Purification Kit (Qiagen, Germany) was used to purify ligated DNA products, based on the protocol's instructions. Briefly, 3-parts of Buffer PB were added to 1-part of DNA solution (3 ml of Buffer PB was added to 1 ml of DNA solution). Approximately 650 µl of sample was loaded onto a silica column inside a provided 2 ml collection tube, which following was centrifuged at 13,000 rpm for 60 seconds. The flow-through was discarded. That step was repeated to wash the whole sample volume. A further wash was conducted by adding 750 µl of Buffer PE to the silica column. Samples were centrifuged at 13,000 rpm for 60 seconds and flow-through was discarded. Another centrifugation at 13,000 rpm for 60 seconds was carried out to remove any remaining wash Buffer PE. Following this, the silica column was removed from the 2 ml collection tube and transferred to a new sterile 1.5 ml tube. Nuclease-free distilled water (30 µl) was added to the silica column to elute DNA samples. Nuclease-free distilled water was left in the column for 60 seconds at room temperature to increase the concentration of DNA sample after the purification. Samples were centrifuged at 13,000 rpm for 60 seconds to elute DNA from the silica column. Eluted DNA was quantified using a Nanodrop spectrophotometer (Thermo Fisher Scientific, USA) through the Nanodrop 1000 computer software. Double distilled water (1.5 µl) was used as a blank and 1 µl of sample was measured. Each DNA concentration was calculated by measuring the optical density at 260 nm wavelength relative to the double distilled water control.

Alternatively, an ethanol precipitation was carried out to purify ligated DNA products. For this, 2.5 ml of 100% ethanol and 100 µl of 3 M sodium acetate pH 5.2 were added to each ligation reaction. Samples were placed at -80^{o}C for 1 hour, then centrifuged at 2,500 rpm for 30 minutes and the cell pellets were washed with 70% ethanol. A second centrifugation step followed at 2,500 rpm for 5 minutes. The supernatants were discarded, and the DNA pellets were allowed to dry briefly and resuspended in 200 µl of double distilled water.

2.3.3 Agarose gel electrophoresis

Agarose gels (1% w/v in 1 x TAE buffer) containing, 1 x SYBRsafe Gel Stain (Invitrogen, USA) were used to analyse 8 µl of each sample (3 µl of genomic DNA; 3 µl of double distilled water; 2 µl of loading dye (NEB, USA)). HyperLadder I (NEB, USA) (200-10,000 bp) (6 µl) was also loaded onto the agarose gels and served as a molecular weight marker. Agarose gels were run for approximately 40 minutes at 80 V and DNA bands were visualized using the Syngene gel imager.

2.4 Generation of viral stocks

2.4.1 Generation of BKPyV stocks

Vero cells were seeded into 2 T75 cm^2 flasks (Sarstedt, Germany) at a density of 1 x 10^6 cells/ml and incubated overnight. The following day, cells were transfected with BKPyV genomes and 800 µl of Opti-MEM, 8 µl of Core reagent and 12 µl of Booster (NanoJuice transfection kit) were required for each flask. All the reagents were mixed thoroughly and incubated at room temperature for 5 minutes. Then, 4 µg of ligated BKPyV DNA genome was added to transfection mixture and incubated for 15 minutes at room temperature. Approximately 800 µl of this mixture was next distributed to each flask in complete growth media at an even distribution. The following morning, media was replaced with fresh and cells were incubated for 10 days at 37^{o}C. Transfected Vero cells were harvested by scraping the cells into the growth media of each flask and stored at -80^{o}C.

The frozen harvested cell suspension from BKPyV transfected Vero cells thawed out using a sequential freeze-thaw protocol. Briefly, the suspension exposed to liquid N_2 and a 40^{o}C water bath for 3 times, which bursts the infected cells. The lysate was then added to naïve Vero cells in T75 cm^2 flasks for 2 hours at 37^{o}C rocking the flask every 30 minutes to ensure even coverage. After this period, suspensions were removed and replaced with fresh complete growth media. Cells were incubated for 14 days without adding any fresh growth media and prior to harvesting by scraping the cells into the growth media of each flask. Samples were placed at -80^{o}C for long-term storage (Figure 2.1) (Hurdiss et al., 2016).

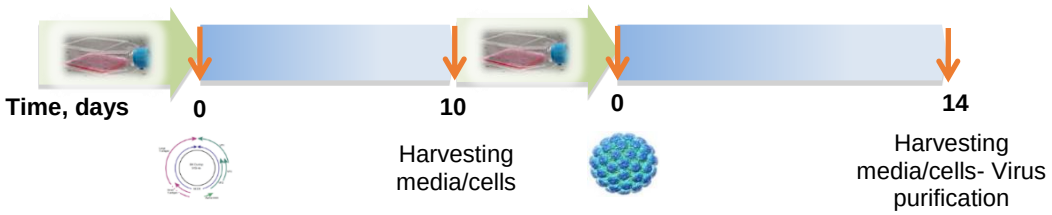

Figure 2. 1 Schematic representation of the preparation of BKPyV virus stock. Vero cells were transfected with 4 µg of ligated BKPyV genomes and incubated overnight at 37ºC. Media was replaced with fresh and transfected Vero cells were incubated for 10 days at 37ºC. Cell suspension was harvested and used to further infect naïve Vero cells for 2 hours at 37ºC. Infected Vero cells were incubated for 14 days at 37ºC, then cell suspension was harvested and purified.

2.4.2 Generation of JCPyV stocks

SVG-A cells were seeded into 2 T75 cm^2 flasks (Sarstedt, Germany) at a density of 1 x 10^6 cells/ml and incubated overnight. The following day, cells were transfected with JCPyV genomes. Approximately 400 µl of Opti-MEM with 8 µg of ligated JCPyV DNA genome and 400 µl of Opti-MEM with 16 µl of Lipofectamine 2000 (Invitrogen, USA) were mixed and incubated for 5 minutes, separately, for each flask. Then, both mixtures were combined in one and incubated for 20 minutes at room temperature. Approximately 800 µl of transfection mixture was distributed to each flask at an even distribution containing complete growth media. The following morning, media was replaced with fresh and cells were incubated for 20 days at 37ºC. Transfected SVG-A cells were harvested by scraping them into the media of each flask and stored at -80ºC.

2.4.3 Generation of SV40 stocks

Vero cells were seeded into 2 T75 cm^2 flasks (Sarstedt, Germany) at a density of 1 x 10^6 cells/ml and incubated overnight. The following day, cells were transfected with SV40 genomes and 800 µl of Opti-MEM, 8 µl of Core reagent and 12 µl of Booster (NanoJuice transfection kit) were required for each flask. All the reagents were mixed thoroughly and incubated at room temperature for 5 minutes. Then, 4 µg of ligated SV40 DNA genomes was added to this mixture and incubated for 15 minutes at room temperature. Approximately 800 µl of the transfection mixture was distributed to each flask in complete growth media at an even distribution. The following morning, media containing the transfection mixture was replaced with fresh and cells were incubated for 7 days prior harvesting by scraping them into the media of each flask. Samples were placed at -80ºC for long-term storage.

2.4.4 Purification of BKPyV stocks

Cell suspensions were collected from infected Vero cells and centrifuged at 8,000 x g for 30 minutes. The supernatants were saved on ice and cell pellets resuspended in 10 ml of Buffer A (10 mM HEPES, pH 7.9; 1 mM $CaCl_2$; 1 mM $MgCl_2$; 5 mM KCl; water) and sonicated in a water bath for 5 minutes. The pH of the resuspended samples was adjusted to 6.0 with 0.5 M HEPES pH 5.4 and 10 U of neuraminidase from *Clostridium perfringens (C. welchii)* (Sigma Aldrich, USA) was added prior to a 1 hour-incubation time at 37ºC. Neuraminidase cleaves the sialic acid groups from host cell glycoproteins for the virus to be released from host cells. The pH of the samples was next adjusted to 7.4 with 0.5 M HEPES pH 8 and the samples were heated to 40ºC for 5 minutes prior to centrifugation at 16,000 x g for 5 minutes. Supernatants were placed on ice, whilst cell pellets were resuspended in 10 ml of Buffer A and 100 µl of sodium deoxycholate (Sigma Aldrich, USA) was added to the mixture. Samples were incubated at 37ºC for 15 minutes with occasional vortexing within the incubation time before a 5 minute-centrifugation at 16,000 x g; supernatants were placed on ice. After the last centrifugation, all the supernatants that were collected during the process, were combined and added over a layer of 4 ml of 20% sucrose. Samples were centrifuged at 25,000 rpm (85,500 x g) for 3 hours and then

the pellets (containing the virus) were resuspended in 10 ml of Buffer A and sonicated for 5 minutes. Samples were then centrifuged at 4,000 rpm for 5 minutes to pellet the insoluble fraction, collect the supernatant and place it over a preformed CsCl (Sigma Aldrich, USA) gradient (3 ml of light (1.2 g/cm^3) CsCl; then added 3 ml of heavy (1.4 g/cm^3) CsCl underneath). All the samples were centrifuged at 35,000 rpm (155,000 x g) for 16 hours at 15^{o}C and subsequently dialyzed against 1 L of Buffer A overnight at 4^{o}C. All the solutions were made up in Buffer A (Light CsCl solution: 1.2 g/cm^3; Heavy CsCl solution: 1.4 g/cm^3; 20% sucrose: 10 g/50 ml) (Jiang et al., 2009).

2.4.5 Titration of purified BKPyV or crude BKPyV, SV40 and JCPyV

Cells (RPTE, Vero and SVG-A, respectively) were seeded into 96-well dishes (Sarstedt, Germany) at a density of 2 x 10^3 cells/ml and incubated overnight. Approximately 90 µl (for the purified virus titration) or 50 µl (for the crude virus titration) of Opti-MEM was mixed with 10 µl of purified BKPyV or 50 µl crude cell suspension containing virus, into the first well of the 96-well dish, respectively. All the other wells of the same row across the plate contained 50 µl of Opti-MEM. Then, two-fold serial dilutions into the existing Opti-MEM of each well across the plate were carried out. The final volume into each well was 50 µl totally. Cells were incubated with the purified or crude virus for 2 hours at 37^{o}C, then one wash with 1 x PBS was performed and 100 µl of complete growth media was added to each well. Infected cells were incubated for 48 hours before the detection of viral proteins using the IncuCyte ZOOM equipment (Stewart et al., 2015).

2.4.6 Immunofluorescence and use of the IncuCyte ZOOM for determination of virus titres

Infected cells on 96-well plates were washed once with 1 x PBS for 5 minutes and fixed with 4% paraformaldehyde for 10 minutes at room temperature. Then followed extensive washes with 1 x PBS and the cell monolayer was permeabilized with 0.1% Triton-X100 in PBS (v/v) for 15 minutes. Next, cells were washed once with 1 x PBS and blocked with 1% BSA (Sigma Aldrich, USA) in PBS for 30 minutes. Another wash

with 1 x PBS was followed and primary anti-VP1 (1:250) antibody was added to cells and incubated overnight at 4^{o}C. The following day cells were washed with 1 x PBS twice and anti-mouse alexa fluor 488-conjugated secondary (1:250) antibody (Thermo Fisher Scientific, USA) was added for 1 hour at 37^{o}C. Approximately 4 washes with 1 x PBS were carried out and cells were stored in 1 x PBS prior to visualization. After the immunofluorescence staining, the 96-well plates were imaged with the IncuCyte ZOOM machine (Essen Bioscience, USA) and the appropriate IncuCyte software was utilized to calculate the mean confluence from non-overlapping bright phase images of each well. Following, the number of positive-infected cells per well was calculated and based on these results, viral titres were calculated as well. All the titres were represented as infectious units per ml (IU/ml) (Stewart et al., 2015).

2.5 Infection of cells using viral stocks

2.5.1 Infection of cells with virus stocks

Cells were seeded into 6-well dishes (Sarstedt, Germany) at a density of 2 x 10^5 cells/ml and incubated overnight. The following day cells at approximately 70% confluency were infected with virus stock at an MOI of 0.5 or 5 (dependent on the experiment). Virus was diluted in 2 ml of Opti-MEM or the appropriate amount of crude media of infected virus added to cells for approximately 2 hours at 37^{o}C. For a synchronised infection of cells, virus was diluted in 2 ml of Opti-MEM and added to cells for 2 hours at 4^{o}C to allow virus attachment to host cell receptors. Once the virus was removed, infected cells were washed once with 1 ml of 1 x PBS and 2 ml of fresh media was added. Infected cells were incubated for further 24-72 hours dependent on the specific experiment (Figure 2.2).

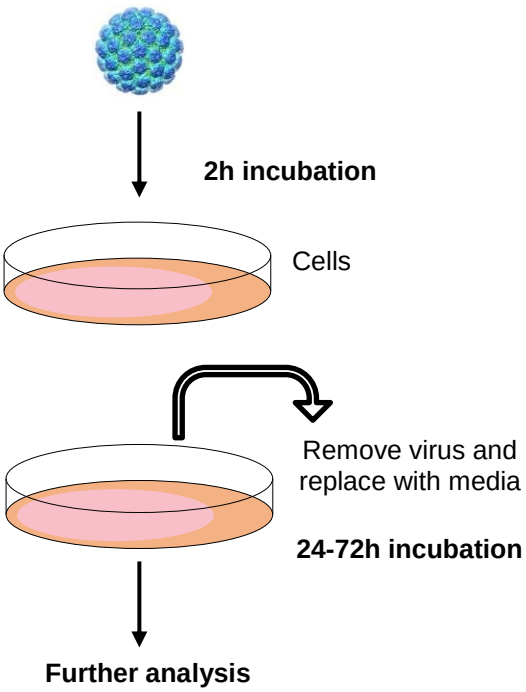

Figure 2. 2 Schematic representation of the methodology of cells' infection. Cells were infected with purified or crude virus stock at an MOI of 0.5 or 5 and incubated for 2 hours at 37ºC. Once the virus was removed, fresh media was added to cells and further incubated for 24 up to 72 hours.

2.5.2 Time-of-addition experiments using inhibitory compounds

RPTE cells were seeded into 6-well dishes at a density of 2 x 10^5 cells/ml and incubated overnight. The following day cells at approximately 70% confluency were infected with virus stock. BKPyV stock (MOI of 0.5) was diluted in 2 ml of Opti-MEM and added on cells for approximately 2 hours at 4ºC. Once the virus was removed, infected cells were washed once with 1 ml of 1 x PBS. All the inhibitors that used in this experiment were diluted to a final working concentration in 2 ml of complete fresh media and added to infected RPTE cells at indicated time-points as described below: 0, 1, 2, 4, 6, 8, 10, 12 and 24 hours post-infection, respectively. A treatment was carried out 1-hour pre-infection and during the incubation time of infection. Once the virus-inhibitory compound mixture was removed, cells were washed twice with 2 ml of 0.5% Trypsin in 1 x PBS to wash off any residual of the ion channel modulators in

the wells and 2 ml of fresh media was added. Infected and treated RPTE cells were incubated for a total 48 hour-incubation time.

2.5.3 Infection assays using media from infected cells

RPTE cells were grown and infected as it is described in Section 2.5.2 and incubated for a total 48 hour-incubation time. Following this period, cell pellets were harvested for further analysis and media of each treatment was collected and placed at -80^{o}C for long-term storage.

RPTE cells were seeded into 96-well dishes at a density of 2 x 10^3 cells/ml and incubated overnight. The following day cells at approximately 70% confluency were infected with 100 µl of media that was collected and incubated for a 48 hour-incubation period and further analysed using the IncuCyte ZOOM equipment (Figure 2.3).

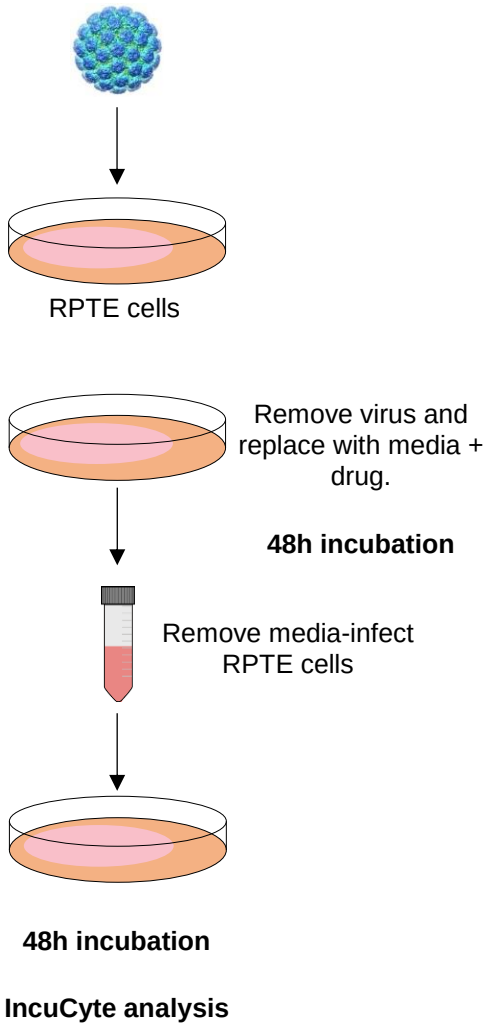

Figure 2. 3 Schematic representation of infection assay. Cells were infected with purified or crude virus stock at an MOI of 0.5 and incubated for 2 hours at 37ºC. Once the virus was removed, fresh media was added to cells and further incubated for 48 hours in the presence of modulatory compounds. Media samples were used to further infect naïve RPTE cells prior a 48-hour incubation time. Infected RPTE cells were analysed by the IncuCyte ZOOM equipment.

2.6 Production of Virus-like particles (VLPs)

2.6.1 Transfection of HEK293TT cells

HEK293TT cells (1 x 10^6 cells/ml) were seeded into T75 cm^2 flasks (Sarstedt, Germany) so that they were at 60% confluency by the next day. The following day, 38 µg of DNA (19 µg of maxi-prepped plasmid (pIaw, expressing VP1-kindly provided by Dr Chris Buck, NIH, USA) and 19 µg of GFP-C1 (Addgene, USA) plasmid) were mixed with 2 ml of Opti-MEM. In separate tubes, 85 µl of Lipofectamine 2000 (Invitrogen, USA) were mixed with 2 ml of Opti-MEM and incubated separately at room temperature for 5 minutes. Then the 2 mixtures were combined and incubated for an additional 20-minute incubation time. The resulting lipid/DNA complexes were added directly to the pre-plated HEK293TT cells and incubated overnight at 37^{o}C. The next morning, the lipid/DNA complexes were removed, and fresh media was added to the upper surface of the flask to avoid any dislodging cells. Upon media change, flasks were returned to the incubator for an additional 30-hour incubation time. A total incubation period of 48 hours will have passed after the initial addition of the lipid/DNA transfection mixtures (Buck et al., 2004).

2.6.2 Harvesting and maturation of generated VLPs

Cells were collected by trypsinization 48 hours post-transfection. Floating cells were collected from the culture by centrifugation as well. Cell pellets were resuspended in up to 10 ml of complete growth media and transferred to conical tubes and the flask was rinsed with 4 ml of fresh media to collect any residual cells. Supernatants were discarded, and cell pellets were resuspended in the residual fluid by gently agitating the conical tubes and transferred into siliconized screw-cap tubes. The original tubes were rinsed with 0.5 ml DPBS/0.8 M salt (20 ml of 10 x PBS; 25 ml of 5 M NaCl; 90 µl of 2 M $CaCl_2$; 50 µl of 2 M $MgCl_2$; 420 µl of 1 M KCl; 153.5 ml of double distilled water) and combined with the suspended cells. Then, cells were centrifuged in the siliconized tubes and supernatants were discarded. Instead of counting cells, an estimation of the volume of the cell pellet was performed and 1.2 pellet volume of DPBS/0.8 M salt was added to the siliconized tube to resuspend the cell pellet. Next, 2 U/ml of neuraminidase from *Clostridium perfringens (C. welchii)* (Sigma Aldrich,

USA) was added to the suspended cells and tubes were mixed briefly by vortexing prior to a 30-minute incubation time at 37^{o}C. To lyse the cells, 1/20th of a volume of 10% Triton X-100 was also added to the mixture. Following, 0.2% benzonase and 1/40th volume of 1 M ammonium sulfate pH 9 (final concentration of 25 mM) were added to cell suspension for an overnight incubation at 37^{o}C for VLPs maturation (Buck et al., 2004).

2.6.3 Purification and collection of VLPs

The next morning, 0.17 volumes of 5 M NaCl was added to the cell lysates and incubated for 10 minutes on ice. Salt lysates were clarified by centrifugation at 5,000 x g for 5 minutes at 4^{o}C and the clarified supernatants were transferred into fresh siliconized screw-cap tubes. Pellet materials were re-extracted by re-suspending them into two pellet volumes of DPBS/0.8 M NaCl. Another centrifugation step followed at 5,000 x g for 5 minutes and the second clarified supernatants were transferred into the same tubes with the first supernatants, respectively. A third centrifugation step was carried out to re-clarify the pooled supernatants at 5,000 x g for 5 minutes. The double-clarified supernatants were layered onto an Optiprep (Sigma Aldrich, USA) gradient to purify the VLPs and samples were centrifuged at 16^{o}C at 50,000 rpm (234,000 x g) for 3.5 hours in an SW55Ti rotor. Acceleration and deceleration were set to minimum. The Optiprep gradient was made up as described below using the following buffers: Optiprep (60% wt/vol iodixanol solution); 50 ml 46% Optiprep in PBS/0.8 M salt (38.3 ml of 60% Optiprep; 5 ml of 10 x PBS; 6.5 ml of 5 M NaCl; 23 µl of 2 M $CaCl_2$; 13 µl of 2 M $MgCl_2$; 100 µl of 1M KCl); 27% Optiprep in PBS/0.8 M salt (9.3 ml of DPBS/0.8 M salt and 13.2 ml of 46% Optiprep in PBS/0.8 M salt); 33% Optiprep in PBS/0.8 M salt (6.4 ml of DPBS/0.8 M salt and 16.1 ml of 46% Optiprep in PBS/0.8 M salt); 39% Optiprep in PBS/0.8 M salt (3.4 ml of DPBS/0.8 M salt and 19 ml of 46% Optiprep in PBS/0.8 M salt). Optiprep gradients were placed in thin polyallomer (Beckman Coulter, USA) 5 ml tubes by underlaying 27%, then 33% and then 39% Optiprep gradients at approximately 1.4 ml steps using a 3 ml syringe fitted with a long needle. The Optiprep gradients were allowed to set between 1 to 4 hours before adding the double-clarified supernatants on the top. After the centrifugation, gradient fractions were collected by puncturing the bottom of the tube

slightly of centre with a syringe needle (25-26-gauge needles). Drip fractions were collected into siliconized microcentrifuge tubes (the first 750 µl as one fraction and 6 to 8 drop fractions up to fraction 10; the top 2 ml of the gradient were discarded) (Buck et al., 2004).

2.7 Protein Biochemistry

2.7.1 Bicinchoninic acid assay for protein quantification

The bicinchoninic acid (BCA) assay (Thermo Fisher Scientific, USA) was used for protein quantification of cell lysates according to manufacturer's instructions. Diluted albumin standards (BSA) at known concentrations were made up in the appropriate diluent (0 µg/ml-2 µg/ml). To make up the working solution, 50-parts of BCA Reagent 1 and 1-part of BCA Reagent 2 were mixed and 5 µl of each BSA standard and each sample was added to wells on a 96-well plate. Also, 50 µl of the working solution was added to each well for a 15-minute incubation time at room temperature. The plate was read at 562 nm on a PowerWave XS2 Microplate Spectrophotometer (BioTek, UK) and the optical densities of each of the standards were used to create a standard curve using the accompanying software (Gen5 1.07.5, BioTek, UK). The optical densities of each sample were then plotted against this standard curve to calculate protein concentrations.

2.7.2 Bradford assay for protein quantification

The Bradford assay (Sigma-Aldrich, USA) was used for protein quantification of cell lysates according to manufacturer's instructions. Diluted albumin standards (BSA) at known concentrations were made up in the appropriate diluent (0 µg/ml-2 µg/ml). Approximately 5 µl of each BSA standard and each sample were added to wells on a 96-well plate. Also, 100 µl of the working solution was added to each well for 15 minutes at room temperature. Then, the plate was read at 595 nm on a PowerWave XS2 Microplate Spectrophotometer (BioTek, UK) and the optical densities of each of the standards were used to create a standard curve using the accompanying software

(Gen5 1.07.5, BioTek, UK). The optical densities of each sample were plotted against this standard curve to calculate protein concentrations.

2.7.3 Preparation of SDS polyacrylamide gel electrophoresis (SDS-PAGE)

Proteins from cell lysates were separated according to molecular weight using a minigel system (BioRAD, USA). SDS-polyacrylamide (8%, 10%, 12.5% and 15%) gels were prepared according to required protein resolution and allowed to set an appropriate amount of time (separating gel: 8%, 10%, 12.5%, 15% Acrylamide, 0.1% SDS, 375 mM Tris/HCl pH 8.8, 0.1% APS and 0.01% TEMED). Stacking gels were allowed to set above the separating gels with a 10-well comb (BioRAD, USA) inserted. SDS-polyacrylamide gels were inserted into a Mini-PROTEAN Tetra System (BioRAD, USA) and 30 µl of protein samples with 10 µl of lithium dodecyl sulphate (LDS) sample buffer (Invitrogen, USA) and 0.1% β-mercaptoethanol were loaded. Approximately 5 µl of Blue Protein Standard Blue Range Protein Marker (NEB, USA) or Color Protein Standard Broad Range Protein Marker (NEB, USA) was used as a marker for protein molecular weight. SDS-polyacrylamide gel electrophoresis was conducted at 120 V for approximately 80 minutes until the protein loading dye reached the bottom of the gel. 1 x SDS running buffer contains 250 mM Tris Base, 1.92 M Glycine and 34.7 mM SDS.

2.7.4 Western Blot Analysis

Proteins separated on the SDS-polyacrylamide gel were transferred onto HybondTM-C Extra mixed ester nitrocellulose membranes (Amersham BioSciences, UK) on a wet transfer XCell II^{TM} Blot Module (Invitrogen, USA) or on a semi-dry Turbo-Blot Transfer Blot (BioRAD, UK) using soaking membranes and sponges that had been pre-soaked in 1 x transfer buffer (20% methanol, 192 mM Glycine and 25 mM Tris base). Next, the sponges, membranes and gels were incubated at 25 V for 1 hour to allow the protein bands to be transferred from the SDS-polyacrylamide gel to the nitrocellulose membrane. Then, membranes were blocked in TBS/T buffer (25 mM Tris/HCl pH 7.5, 138 mM NaCl and 0.1% Tween-20) containing 5% (w/v) Marvel dry

skimmed milk powder on a rocker (30 rocks/min) for 1 hour at room temperature. All antibodies were diluted in TBS/T containing 5% (w/v) Marvel dry skimmed milk. Membranes were incubated in primary antibody for 1 hour at room temperature or overnight at 4^{o}C with constant rocking (Table 2.4). Membranes were washed 3 times in TBS/T buffer for 5 minutes and after the washes, secondary antibodies (1: 5000) were added to membranes for 1 hour at room temperature. Then, 4 further washes in TBS/T were carried out. To detect the chemiluminescent signal, membranes were incubated with enhanced chemiluminescent solutions (WesternBright^{TM} ECL-spray (Advansta, USA), ECL Select^{TM} Western Blotting Detection Reagent (GE Healthcare, UK)) for 1 minute at room temperature. Following, membranes were placed on a protective plastic sleeve in a Hypercassette (Amersham Biosciences, UK) and were exposed to CL-XPosure^{TM} Films (Thermo Fisher Scientific, USA). Exposure times varied depending on the primary antibody that had used. The films were automatically developed on a table top developer (Konica SRX-101A) and after detecting viral proteins, blots were stripped and washed by Restoring buffer A and B (Millipore, UK) for 10 and 15 minutes, respectively, and allowed to be re-probed.

Table 2. 4 List of antibodies. A detailed list of antibodies used in this study is shown below.

Antibody	Manufacturer	Description	Size of target	Dilution used
anti-agnoprotein (pAb81038)	Kindly provided by Professor Ugo Moens, The Arctic University of Norway	Rabbit	11 kDa	1:10000 in WB
anti-CFTR (sc-376683)	Santa Cruz, USA	Mouse	165 kDa	1:100 in WB
anti-GAPDH (sc-47724)	Santa Cruz, USA	Mouse	37 kDa	1:5000 in WB
anti-VP1 (P5G6)	Kindly provided by Dr Denise Galloway, University of Washington, USA	Mouse	42 kDa	1:1000 in WB
anti-VP1 (pAb597)	Kindly provided by Dr Chris Buck, NIH, USA	Mouse	42 kDa	1:250 in WB
anti-VP2/VP3 (ab53983)	Abcam, UK	Rabbit	38, 26 kDa	1:1000 in WB

2.7.5 Densitometry analysis of Western blots

Western blot films were scanned on Photo Scanner as an 8-bit image and protein levels were quantified using ImageJ (National Institutes of Health, USA). Protein bands were selected with a square and the same square was used to select every protein band on the same film. This was repeated for each protein band of interest and protein band of loading control, following band intensity was determined with the measure function. The resulting data were entered into an Excel file to conduct a statistical analysis.

2.8 Quantitative PCR

Total DNA was extracted from RPTE cells using the E.Z.N.A Tissue DNA Kit (Omega Bio-Tek, USA) following the manufacturer's protocol and approximately 5 ng/μl of the total extracted DNA was used per reaction. Quantitative PCR was performed using the QuantiFast SYBR Green PCR kit (Qiagen, Germany) and specific primers against the, BK Dunlop genome (FW:*TGTGATTGGGATTCAGTGCT;* RV:*AAGGAAAGGCTGGATTCTGA*). The PCR reaction was carried out on a Corbett Rotor-Gene 6000 (Qiagen, Germany) following three different steps. The initial activation step for 10 minutes at 95^{o}C and a three-step cycle of denaturation of 10 seconds at 95^{o}C; the second step of annealing for 15 seconds at 60^{o}C and the step of extension for 20 seconds at 72^{o}C. All the three steps were repeated 40 times and concluded by melting curve analysis (Panou et al., 2018).

3 BKPyV life cycle

3.1 Introduction

3.1.1 The BKPyV life cycle in its natural host

Currently it is poorly understood how BKPyV establishes an infection in its natural host, completes a replication cycle and persists for a lifelong subclinical infection or becomes active again under immunosuppressive conditions. Therefore, the establishment of an *in vitro* cell system, which could be similar to *in vivo* conditions is required to study the virus life cycle in depth. Previous studies on BKPyV have been carried out using human embryonic kidney cells, human embryonic fibroblast cells or monkey-derived Vero cells, although these cell lines are not the most physiologically relevant host cell type for BKPyV *in vivo* (Maraldi et al., 1975; Seehafer et al., 1975). In other studies, human primary renal epithelial (RPTE) cells have been used in order to study the virus life cycle due to the fact that BKPyV is able to infect tubular epithelium in humans (Randhawa et al., 1999). RPTE cells regulate different cellular functions, including the maintenance of essential non-waste blood products, the regulation of blood volume and blood pressure, the production of vitamin precursors and the involvement in the release of cytokines upon infections or in the presence of molecules, which cause cell toxicity (Daha and van Kooten, 2000). Humes et al., (2002) reported that a model system has been developed in which human RPTE cells are capable of differentiation, *in vitro,* as they can be passaged up to six times. By using this primary cell system, we have the advantages to study many aspects of the virus life cycle that are still uncharacterized and to determine interactions between the virus and host cell factors in a known cell type susceptible to BKPyV.

BKPyV must enter host cell to establish a successful infection, where it manipulates the host cellular machinery for transcription, replication and protein synthesis (Bennett et al., 2012). Studies have shown that the expression of early viral genes starts to be

detectable about 24 hours post-infection, with the expression levels to be increasing out to 72 hours post-infection (Low et al., 2004). Also, viral DNA replication and expression of late viral genes begin approximately 36 hours post-infection, with expression levels to be gradually increasing throughout later stages of the time-course of BKPyV infection in RPTE cells. Thus, the release of the newly synthesized viral progeny initiates at later stages, approximately 48 hours post-infection (Low et al., 2004).

3.1.2 Chapter aims

The main aims of this Chapter are to highlight each stage of the generation of purified BKPyV and the establishment of a high-throughput method to measure the BKPyV titres. The time-course of the BKPyV life cycle in human primary RPTE cells is also studied in order to form a basis for further research on the virus life cycle and other host factors that could be potentially involved in a successful BKPyV infection.

3.2 Results

3.2.1 Generation of purified BKPyV

3.2.1.1 Enzymatic digestions and re-ligations of the BKPyV genome

Preparation of BKPyV genome was required to generate a purified and infectious stock of BKPyV that could be used in further experiments. For that reason, 10 µg of pGem7 BKPyV Dunlop plasmid (951 ng/µl) was digested by the restriction enzyme BamHI-HF in order to separate the BKPyV genomic DNA from the plasmid DNA. The same enzyme reaction was repeated 4 independent times. Digested products were analysed on an 0.8% agarose gel and bands were visualized confirming that the BKPyV genome was separated from the backbone plasmid DNA (Figure 3.1A).

The digested linearized products were re-ligated before they could be used in further experiments. This was carried out by setting up ligation enzymatic reactions using the T4 DNA ligase enzyme. The same enzymatic reaction was performed 4 independent times. After the overnight incubation time of the digested products with the T4 DNA ligase enzyme, the re-ligated products were purified using a purification kit (See Section 2.3.2) following manufacturer's instructions. Purified samples were quantified using a spectrophotometer and further analysed on an 0.8% agarose gel. Bands of the products were visualized indicating that the BKPyV genome was separately re-ligated from the backbone plasmid DNA, whilst other ligated products were generated (Figure 3.1B).

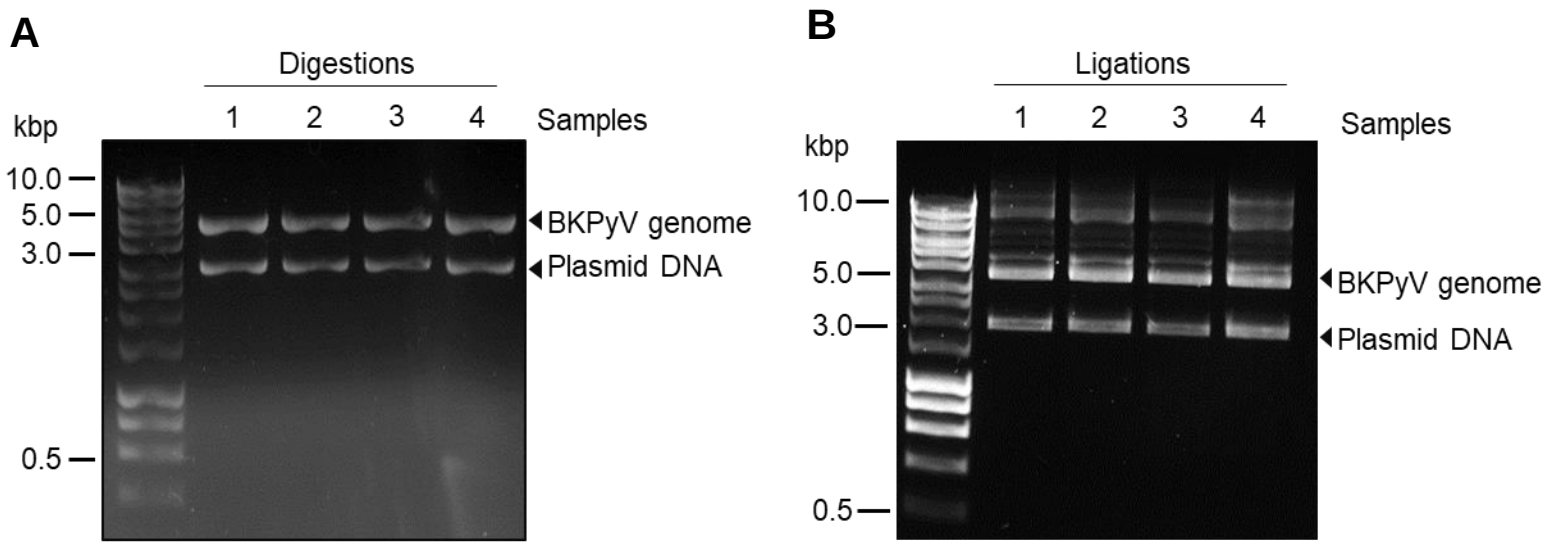

Figure 3. 1 Digestions and ligations of the BKPyV genome. A. Four independent digestions of pGem7 BKPyV Dunlop plasmid (10 µg each) were loaded onto an 0.8% agarose gel and run for 40 minutes at 80 V. Lane 1: 6 µl of DNA ladder 1 kb; Lane 2-5: 6 µl of digested pGem7 BKPyV Dunlop. B. Re-ligated products were loaded onto an 0.8% agarose gel and run for 40 minutes at 80 V. Lane 1: 6 µl of DNA ladder 1 kb; Lane 2-5: 6 µl of purified and ligated products (n= 3).

3.2.1.2 Transfections of the BKPyV genome into Vero cells

The methodology to generate an infectious BKPyV stock is summarized in Figure 3.2. Initially, Vero cells were transfected with 4 µg of BKPyV genome using the NanoJuice transfection kit in a ratio 1-part of DNA: 2-parts of Core reagent: 3-parts of Booster (See Section 2.4.1) (Figure 3.3A). Cells were harvested 10 days post-transfection, and cell suspensions were stored. Samples of both cell pellets and media were analysed to identify the presence of intracellular and secreted BKPyV virions. The major capsid protein, VP1, was used as an indication marker of viral protein expression.

Total protein of both cell lysates and media samples were separated by SDS-PAGE. The corresponding Western blots were probed with a monoclonal VP1 antibody and with a commercial GAPDH antibody as a protein loading control. The presence of VP1 in every sample, both cell pellets and media, respectively, was confirmed showing a clear band at the expected molecular weight of approximately 42 kDa (Figure 3.3B). Clear bands of GAPDH at the expected molecular weight of approximately 37 kDa (Figure 3.3B) were also detected confirming the equal amount of loaded total protein.

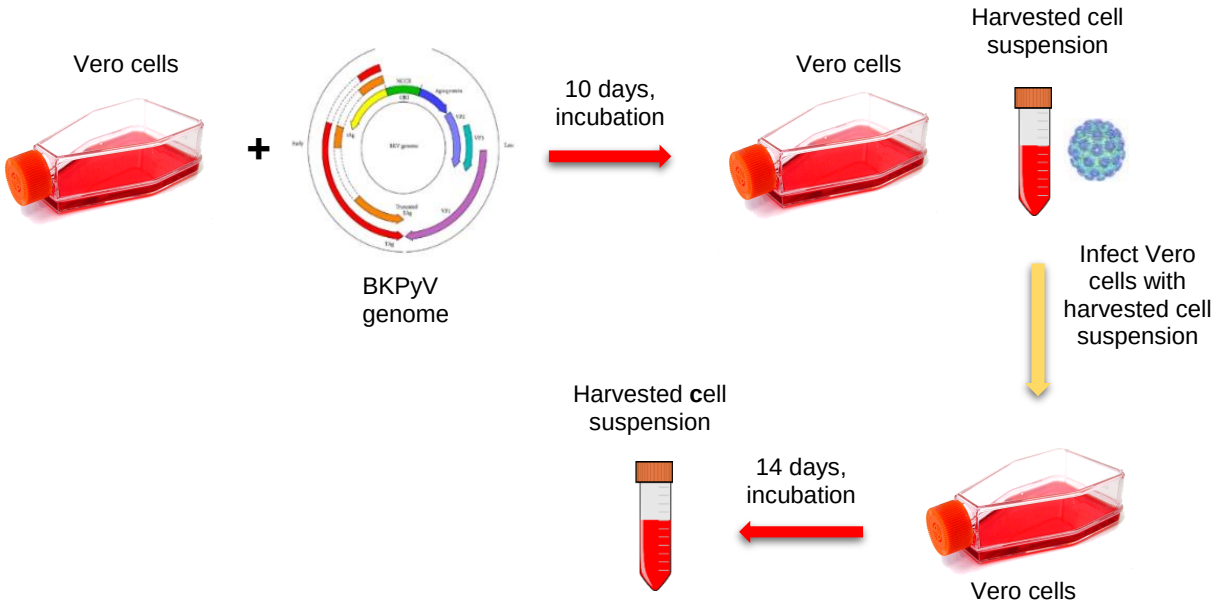

Figure 3. 2 Schematic representation of the two distinct stages of the BKPyV generation. In the first stage, Vero cells were transfected with 4 µg of the BKPyV genome and incubated for 10 days. Cell suspension was harvested and used to further infect naïve Vero cells. This step initiates the second stage of the experimental procedure. Cells infected with BKPyV crude cell suspension were incubated for 14 days. Cell suspension was harvested and further analysed for BKPyV VP1 protein expression.

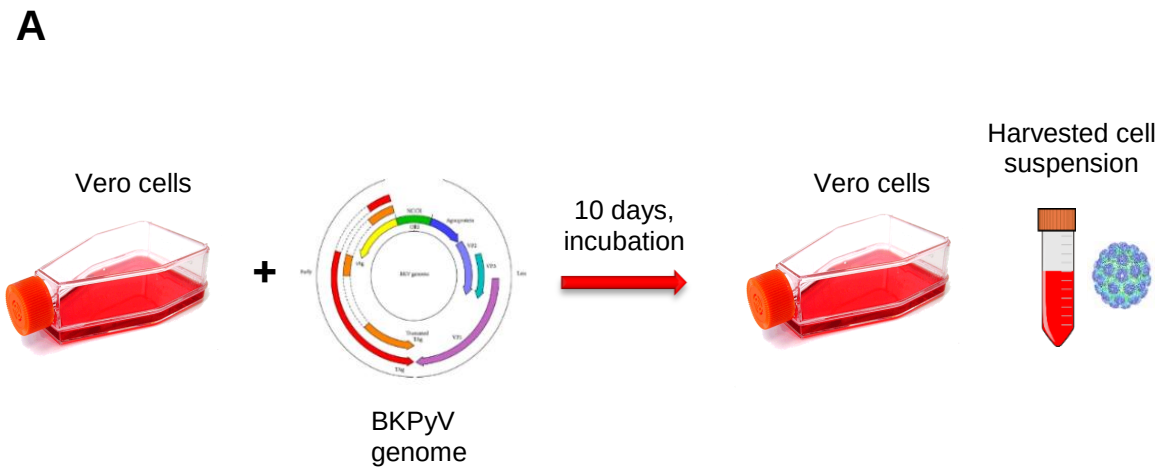

Figure 3. 3 Transfections of Vero cells with the BKPyV genome. A. Schematic representation of the first stage of the generation of BKPyV stock. Vero cells were transfected with 4 µg of the BKPyV genome and incubated for 10 days. B. Total protein of cell lysates and media samples from the collected cell suspension were separated by SDS-PAGE and probed for VP1 (P5G6) as a marker of BKPyV transfection, and GAPDH as a loading control. Representative blots are shown from 2 independent flasks containing transfected Vero cells with BKPyV genome (n= 3).

3.2.1.3 Infections of Vero cells with the crude BKPyV cell suspension

Collected cell suspension from the first stage of the process and confirmed by Western blot analysis that VP1 was present both intracellularly and extracellularly (Figure 3.3B) was used in this second stage. Prior to Vero infections, the frozen harvested cell suspension thawed out using a sequential freeze-thaw protocol. Briefly, the suspension exposed to liquid N_2 and a 40^{o}C water bath for 3 times, which bursts the infected cells to release any intracellular BKPyV virions. Vero cells were infected with the crude BKPyV cell suspension and incubated for 14 days. Cell suspensions were stored and samples of both cell pellets and media were analysed to identify the presence of intracellular and secreted virions.

Total protein of both cell lysates and media samples were separated by SDS-PAGE and the corresponding Western blots were probed with a monoclonal VP1 antibody and a GAPDH antibody as a loading control. The presence of VP1 in every sample, both cell pellets and media, respectively, was confirmed showing a clear band at the expected molecular weight (Figure 3.4B) suggesting that BKPyV virions positive to VP1 were produced.

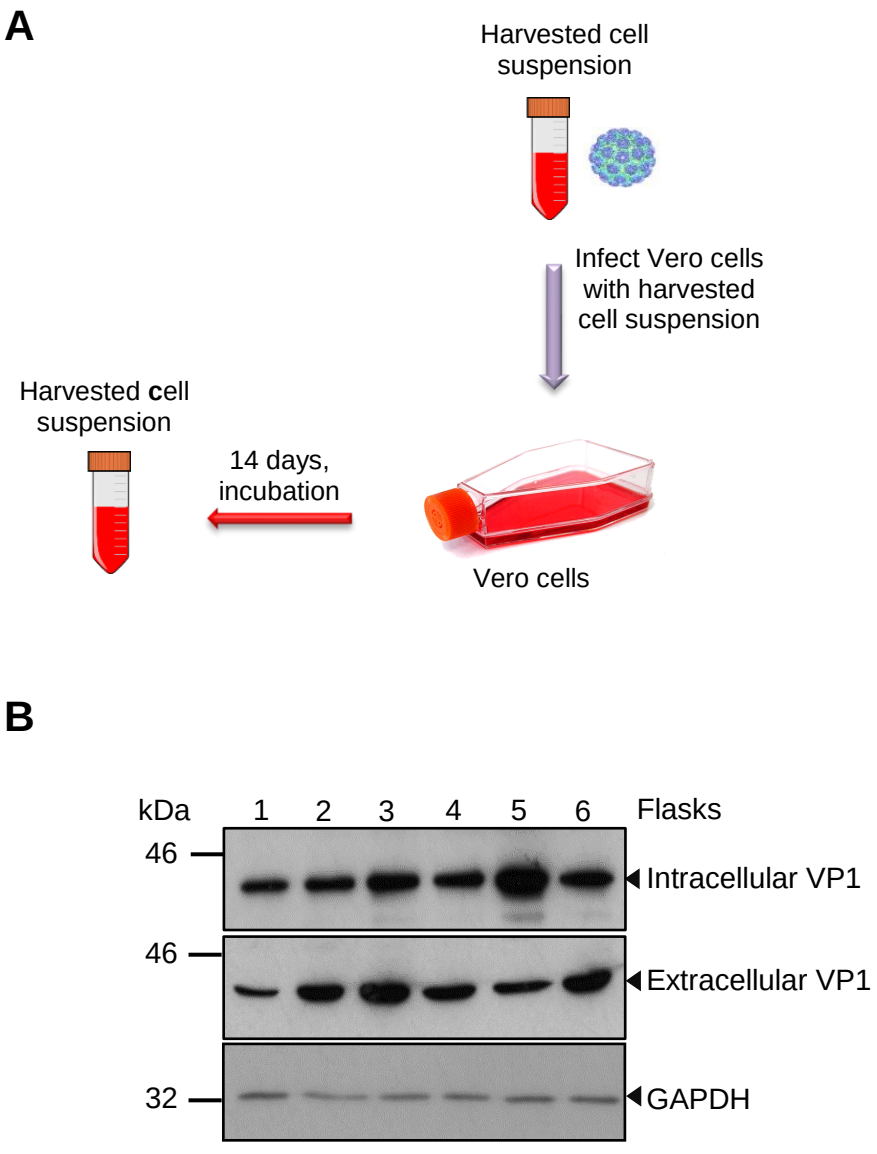

Figure 3. 4 Infections of Vero cells with the BKPyV crude cell suspension. A. Schematic representation of the second stage of the generation of BKPyV stock. Vero cells were infected with BKPyV crude cell suspension and incubated for 14 days. B. Total protein of cell lysates and media samples from the collected cell suspension were separated by SDS-PAGE and probed for VP1 (P5G6) as a marker of BKPyV infection, and GAPDH as a loading control. Representative blots are shown from 6 independent flasks (n= 3).

3.2.1.4 Purification of BKPyV virions to generate a stock of infectious BKPyV

In order to use the collected crude cell suspension after the long process of the virus production, a virus purification was required. For that reason, we performed a virus purification, which was based on ultracentrifugation. Two different ultracentrifugation spins were carried out to separate the viral particles and other macromolecules into different component parts using sucrose and caesium chloride (CsCl) gradients (Jiang et al., 2009). After the overnight ultracentrifugation of the sample, 2 distinct bands were appeared in the heavy CsCl gradient, which were collected carefully using an 18-gauge syringe (Figure 3.5A).

Before the collected BKPyV was used in further experiments, the extracted sample was examined whether it was positive for BKPyV viral proteins. To achieve this, total protein from pure collected samples was separated by SDS-PAGE and the corresponding Western blot was probed with a monoclonal VP1 antibody, as a BKPyV marker (Figure 3.5B). The presence of VP1 in the extracted sample was confirmed, suggesting that BKPyV virions positive for VP1 were collected after the virus purification. Samples from the collected virus were assessed by cryo-EM (Conducted by Daniel Hurdiss), which demonstrated the identical size and morphology to native BKPyV virions (Figure 3.5C).

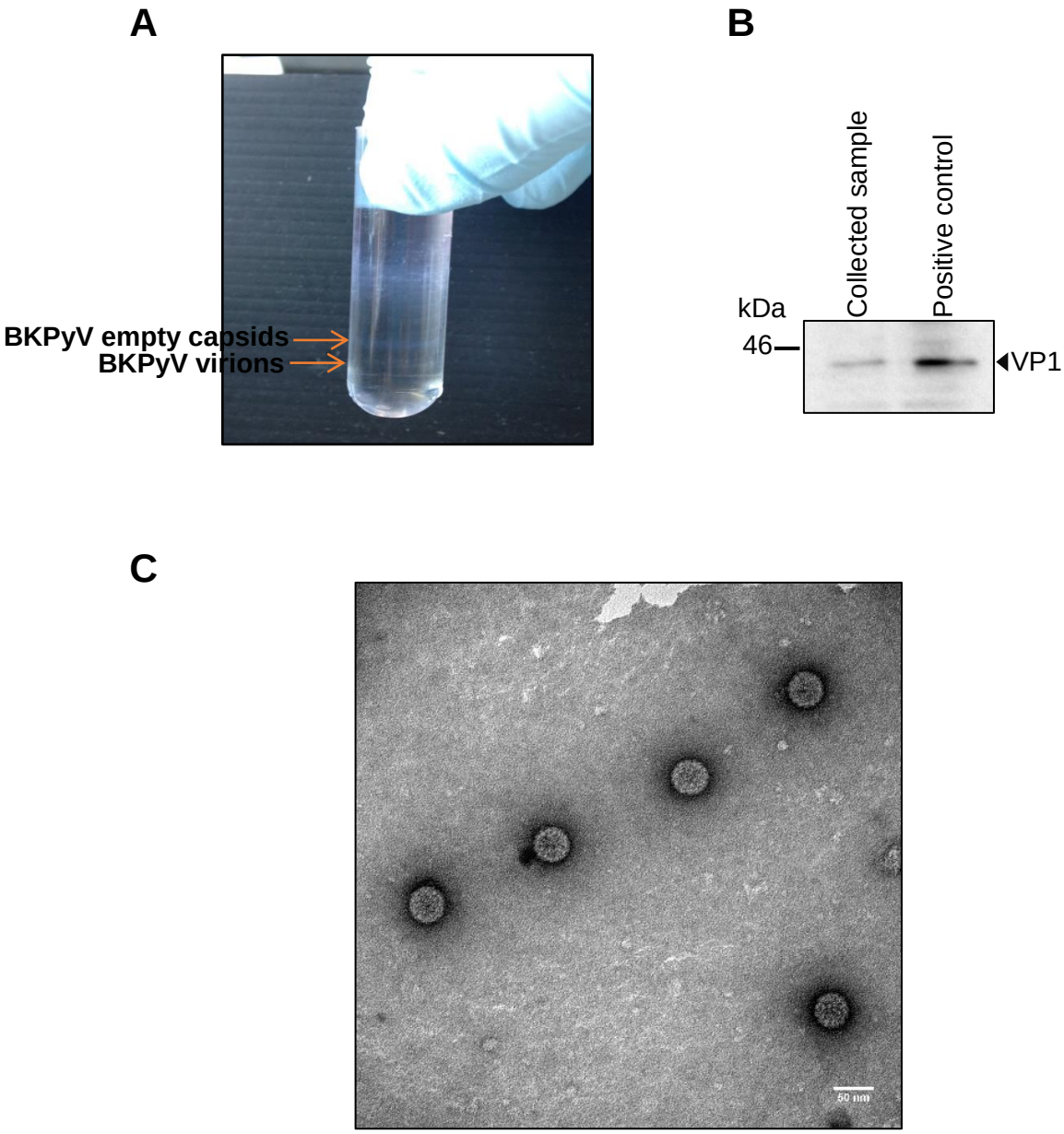

Figure 3. 5 Purification of BKPyV stock. A. Image after the virus purification. Collected crude BKPyV cell suspension containing VP1 positive viral particles was purified under 2 ultracentrifugation steps using sucrose and CsCl gradients. Following the overnight ultracentrifugation, 2 distinct bands of BKPyV were collected (indicated red arrows). B. 5 µl of the purified and collected virus and 5 µl of a confirmed infectious sample (positive control) were separated by SDS-PAGE and probed for VP1 (P5G6) as a BKPyV marker. C. Cryo-electron micrograph of purified BKPyV sample suspended in vitreous ice. Scale bars, 50 nm.

3.2.2 Establishment of a high-throughput method to measure BKPyV infectivity

Our next experimental objective was to examine whether the purified BKPyV stock was infectious and to determine the viral titres in order to perform our following experimental procedures under identical conditions.

Methods to quantify viral amounts accurately might be carried out based on different ways as described below. Determination of levels of virus infectivity and measurement of the presence or function of viral proteins can be performed. Also, detection of viral or marker nucleic acid within the viral genome and counting physical viral particles, whether labeled or unmarked can be done (Heider and Metzner, 2014). However, most of current methods are labour-intensive and susceptible to human error. Accurate determination of the BKPyV titres was conducted using the IncuCyte ZOOM machine (Stewart et al., 2015). Purified BKPyV stock in 1:10 dilution was added to the first well and then 2-fold serially diluted BKPyV was used to infect cells in the wells across the plate. RPTE cells were infected with BKPyV for 2 hours at 37^{o}C and subsequently incubated for 48 hours. Cells were then fixed, permeablized and BKPyV infection assayed through staining for VP1 as a marker of virus production. Using IncuCyte ZOOM analysis, the number of positive infected cells was measured. Results revealed an accumulation of VP1 in the nucleus of infected RPTE cells (Figure 3.6A). Three different batches of purified BKPyV were used in this experiment, although only the data of one batch is presented below as a representative example. The number of infected cells per well of the first three wells of the first row of the 96-well plate was presented (Figure 3.6B). A decrease in the number of infected cells per well was observed across the plate due to the serial dilutions performed. Based on the number of infected cells, the infectious units per ml (IU/ml) were calculated for each sample of purified BKPyV. Also, the number of IU/ml of the first three wells of a row was presented (Figure 3.6C). Approximately, 5 x 10^5 IU/ml was the value of infectious units using the most concentrated sample.

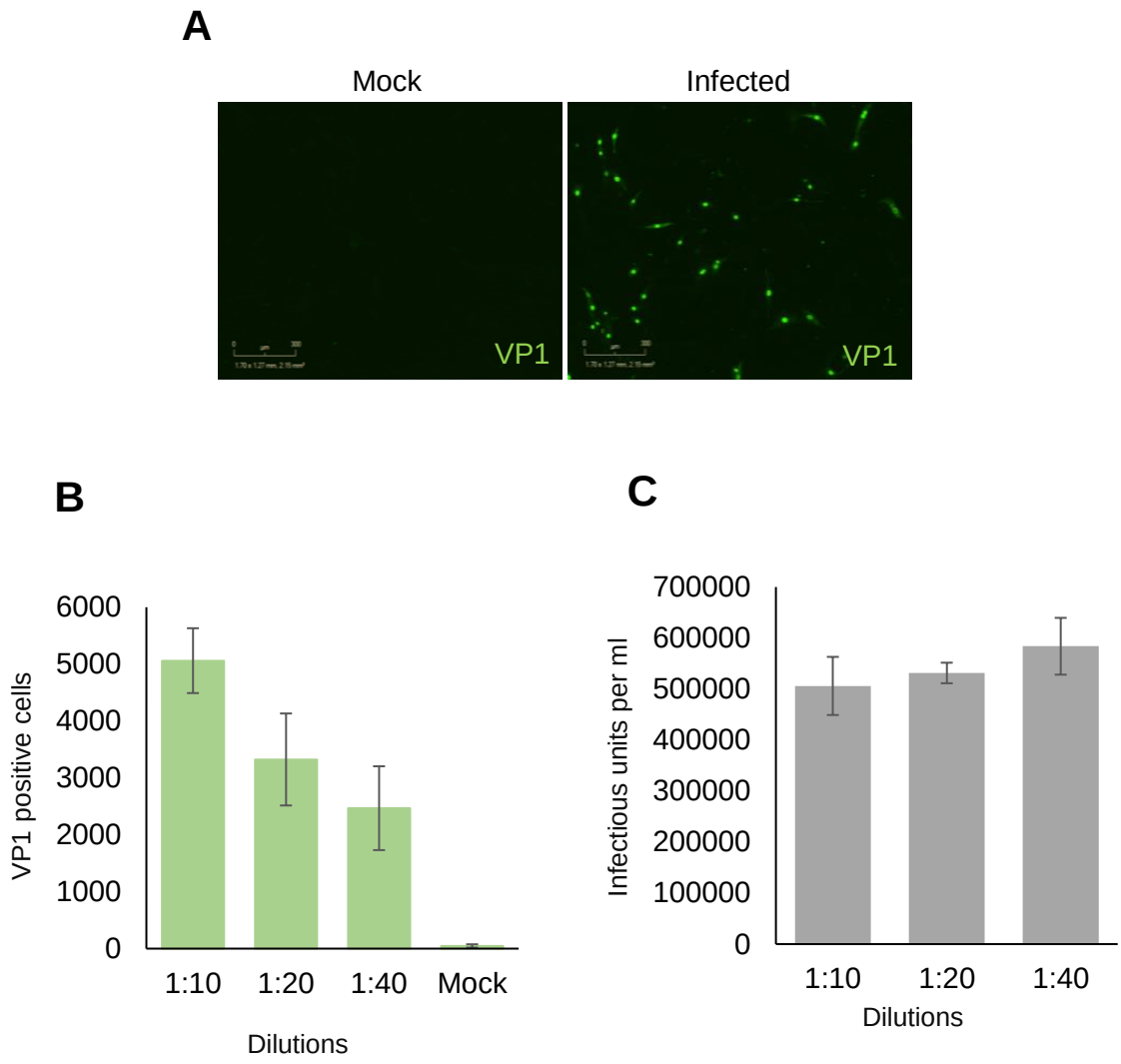

Figure 3. 6 Titration of the purified BKPyV. RPTE cells were infected with a batch of purified BKPyV for 2 hours at 37^{o}C. Purified BKPyV in 1:10 dilution was added to the first well. Then followed a 2-fold serially dilution of BKPyV across the plate and infected cells were incubated for 48 hours. RPTE cells were fixed and stained with a primary anti-VP1 (1:250) antibody (pAb597) and a secondary anti-mouse alexa fluor-conjugated 488. BKPyV VP1 was used as a marker of BKPyV infection. A. Subcellular localization of VP1 protein was detected in the nucleus of BKPyV infected cells. B. Positive infected cells per well were calculated for the first three serial dilutions of BKPyV across the plate. Values represent the mean ±SD of positive infected cells (n= 3) C. Positive infected cells were calculated by the IncuCyte ZOOM and extrapolated to produce BKPyV infectious units per ml (IU/ml). Values represent the mean ±SD of IU/ml (n= 3).

3.2.3 Profile of the BKPyV course of infection

The BKPyV life cycle is poorly characterized and there are several aspects that needs to be elucidated. To identify the protein expression profile of the different viral proteins during the BKPyV life cycle, infection assays were performed. RPTE cells were infected with BKPyV at an MOI of 0.5 for 2 hours at 37^{o}C. Infected cells were incubated over a course of 72 hours and harvested every 12 hours from the starting point of 12 hours post-infection to the ending time-point of 72 hours post-infection.

Isolated total protein from lysates and media samples over the course of 72 hours post-infection were separated by SDS-PAGE and assayed for the late viral proteins by Western blotting (Figure 3.7A and C). The corresponding Western blots were probed with a monoclonal VP1 antibody, a commercial SV40 VP2/VP3 antibody, an agnoprotein antibody and a GAPDH antibody as a protein loading control.

The presence of intracellular VP1, VP2/VP3 and agnoprotein was confirmed 48 hours post-infection by showing clear bands at the appropriate molecular weight of approximately, 42 kDa, 38 kDa, 26 kDa and 11 kDa, respectively. Much higher levels of the late proteins were detected between 60 and 72 hours post-infection, respectively (Figure 3.7A). Secreted viral capsid proteins were detected 60 hours post-infection with the highest level of expression detected at the end of the experimental time-course (Figure 3.7C).

The same secreted samples were used to further infect RPTE cells in order to examine whether the released virus was infectious. Infected cells were incubated for 48 hours at 37^{o}C. Following to this, cells were fixed and stained for VP1 protein using the respective antibody and IncuCyte ZOOM analysis was conducted. Data revealed that the released virus was infectious. Interestingly, RPTE cells infected with the 48 hours-sample were also positive for VP1 expression, even though viral capsid proteins were not detectable in the media samples by Western blotting at the 48 hours-time-point (Figure 3.7D). Also, a greater number of VP1 positive cells were detected towards the end of the time-course (Figure 3.7D).

Another crucial stage of the BKPyV life cycle is the viral genome replication. To study the BKPyV replication, the time-course of infection was repeated using the same critical time-points as described above. Total DNA was extracted from each harvested

sample and analysed by quantitative PCR using specific primers against the viral genome. Due to the very low but detectable levels of viral DNA seen during the first 24 hours post-infection, it was speculated that this was an artifact from the input virus. The first greater increase in viral genome copy numbers occurred 36 hours post-infection, whilst they were constantly increased throughout the time-course, peaking 72 hours post-infection (Figure 3.7B).

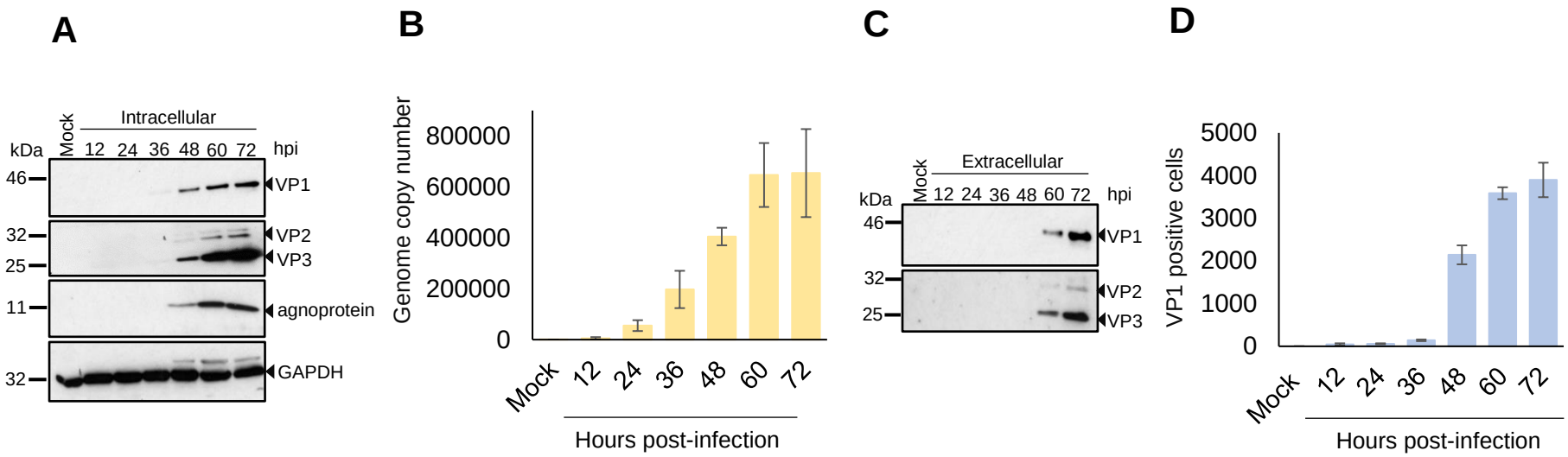

Figure 3. 7 Viral protein expression and DNA replication in the BKPyV life cycle. A. RPTE cells were infected with BKPyV at an MOI of 0.5. Infected cells were incubated over a time-course (72 hpi) and harvested at the indicated time-points (12, 24, 36,48, 60 and 72 hpi, respectively). Total protein of cell lysates from infected RPTE cells was separated by SDS-PAGE. VP1 (P5G6), VP2/VP3, agnoprotein and GAPDH were detected on the corresponding Western blots with the respective antibodies. Representative blots are shown from 3 independent repeats. B. RPTE cells were infected with BKPyV at an MOI of 0.5. Infected cells were incubated over a time-course and harvested at the indicated time-points as described above. Quantitative PCR analysis of DNA viral genome was performed. Values represent the mean ±SD of viral genome copy numbers (n= 3). C. Total protein of media samples was separated by SDS-PAGE. VP1, VP2/VP3 were detected on the corresponding Western blots with the respective antibodies. Representative blots are shown from 3 independent repeats. D. Collected media samples from each of the indicated time-points of the time-course were used to further infect RPTE cells for 48 hours. Cells were fixed and stained with a primary anti-VP1 (1:250) (pAb597) antibody and a secondary anti-mouse alexa fluor-conjugated 488. BKPyV VP1 protein was used as an infection marker. Positive infected cells were calculated by IncuCyte ZOOM and data represent the mean ±SD of positive infected cells (n= 3).

3.3 Discussion

3.3.1 Generation of purified BKPyV stock

Generation of a purified and infectious stock of BKPyV was required in order to be used in further infection assays (Chapter 4 and Chapter 5). Initially, the re-circularized BKPyV genome was prepared, which was transfected into Vero cells. At every step and in particularly following digestions and re-ligations of the BKPyV genome, digested and re-ligated products, respectively, were analysed on 0.8% agarose gels and bands were visualized. It was confirmed that BKPyV genome of approximately 5.0 kbp was separated from the backbone plasmid DNA (Figure 3.1A). Also, as it is shown in Figure 3.1B by visualizing the re-ligated products, the BKPyV genome was separately re-ligated from the backbone plasmid DNA which was at an approximate size of 3.0 kbp.

Vero cells were transfected with the re-ligated BKPyV genome and incubated for 10 days. Following to this incubation time, cell suspensions were harvested and further analysed. The presence of both intracellular and extracellular VP1 protein with higher levels of VP1 protein detected in cell lysates were confirmed by Western blot analysis (Figure 3.3B). This suggested that BKPyV virions positive for the major capsid protein VP1 were present in Vero cells and there was a release of BKPyV virions in media samples to a certain extend. Harvested cell suspensions from transfected Vero cells were freezed and thawed using liquid nitrogen in order to burst the transfected cells and release any intracellular BKPyV virions into the media. Next, crude cell suspensions were used to further infect naïve Vero cells. Infected Vero cells were incubated for 14 days and harvested samples of cell lysates and media were further analysed. By Western blot analysis (Figure 3.4B) it was confirmed that VP1 protein was present in both cell lysates and media samples, suggesting the presence of both intracellular and secreted BKPyV virions. Crude cell suspensions collected from the last stage of this experimental procedure were purified under two ultracentrifugations using sucrose and CsCl gradients (Moriyama and Sorokin, 2009). Collected and purified virus was analysed by Western blotting and cryo-EM, suggesting that BKPyV virions positive for VP1 were collected after the virus purification (Figure 3.5B).

3.3.2 Titration of purified BKPyV

In this study, we established a novel high-throughput method to measure the BKPyV infectivity. The determination of viral titres is necessary to carry out each experiment in identical conditions. We adopted and optimized a method, which was previously published for the measurement of the Hepatitis C virus titres utilizing the IncuCyte ZOOM equipment (Stewart et al., 2015). By this method we quantified accurately the BKPyV titres performing infections of 2-fold serially diluted BKPyV on human RPTE cells (Figure 3.6B and C). This method is based on fluorescence microscopy and gives us the advantages to quantify accurately the number of positive infected cells and to detect the subcellular localization of the major capsid protein, VP1, as it was used as a BKPyV infection marker.

Previous studies have described methods that involve lengthy assays by labour-intensive counting of infected cells manually. Moriyama and Sorokin (2009) described the standard plaque assay for determination of the BKPyV titres; this has been improved and consists the basis of Fluorescent focus assay (FFA). The difference between FFA and plaque assay is that the number of infected cells could be detected by using antibodies against the BKPyV TAg. Low et al., (2004) and Abend et al., (2007) conducted FFA to measure the BKPyV infectivity by performing 10-fold dilutions of BKPyV and incubating the cells for 4 days. The BKPyV titres were determined as fluorescent forming units (FFU) by counting manually five random fields of view. However, only a 48 hour-incubation is required, and a fully automated data analysis is performed using the IncuCyte ZOOM equipment. By this method we could have more accurate and precise results, the reproducibility is higher as well and the processivity is also increased. It is known that $TCID_{50}$ and focus-forming unit methods require and end point dilution, although this is not essential for the method that we described in our study. Thus, an extensive number of viral dilutions for each tested sample is not required and that leads to a reduced reagent cost per assay (Stewart et al., 2015).

Alternative methods for BKPyV titration, such as core protein Elisa assay, have been utilized previously but all of them show significant disadvantages. These assays are high-throughput techniques, although there is no distinguish between defective viral particles and infectious virions or antigen released from dead cells. The same

downside is observed using the hemagglutination assay. Studies have shown that JCPyV VP1 protein is responsible for red blood cell agglutination and HA inhibition and consequently hemagglutination assays have been utilized to determine the JCPyV infectious titres. However, the hemagglutination assay is poorly sensitive and measurement of JCPyV viral load is often impossible *in vitro*. It is also known that this method cannot be efficient under certain experimental conditions, such as using microtiter and transwell plates (Chapagain et al., 2006). Quantitative and Real-Time PCRs have also been described as methods to identify the JCPyV infectious titres with more accurate results compared to hemagglutination and HA inhibition assays (Chapagain et al., 2006).

The IncuCyte ZOOM analysis can also be applied in multiple areas of BKPyV studies as most of them require sensitive and accurate measurements of viral infectivity. By using this method, we could identify and validate novel anti-viral compounds having as an infection marker, VP1 protein expression (Chapter 4 and 5). In conclusion, we established and optimized a novel high-throughput method to determine the BKPyV titres on human primary kidney cells by using the IncuCyte ZOOM equipment and the appropriate software. This assay is a powerful tool for all the basic research involving not only BKPyV, but also other closely related polyomaviruses and the identification of innovative anti-viral compounds targeting host cell factors that are essential in different stages of the viral life cycle.

3.3.3 Time-course of the BKPyV life cycle

BKPyV is a human pathogen that establishes a persistent infection. The main site into the hosts that BKPyV reactivates and complete its life cycle is within kidneys and the urinary tract (Bennett et al., 2012). This leads to an establishment of an *in vitro* cell system that is similar to *in vivo* conditions. Most of our studies have been carried out using human primary kidney epithelial cells (RPTE) cells, which is the most physiologically relevant cell system to study the virus life cycle.

Virus attachment to the host cell surface results in internalization of BKPyV into the host cell, which in turn leads to a successful infection. BKPyV traffics through the cytoplasm towards the nucleus, where the uncoated double-stranded DNA genome

manipulates the cellular machinery for early genes transcription, genome replication and late genes transcription. We performed infection assays on human RPTE cells to investigate the profile of BKPyV viral protein expression and genome replication over a specific period.

Previous studies have examined the time-course of the BKPyV life cycle as well (Low et al., 2004). Infection assays, over the course of 11 days, identified that TAg expression was first detected approximately 24 hours post-infection and its expression levels peaked at 7 days post-infection and remained at the same levels throughout the rest of the incubation time (Low et al., 2004). In our studies, we failed to detect TAg by Western blotting (Data not shown), therefore we focused on the expression of the late viral proteins.

Following to early genes transcription, the viral genome replication occurs. To examine the time-course of viral DNA replication, we performed infection assays of human RPTE cells over a time-course of 72 hours. Total DNA was extracted from infected RPTE cells and quantitative PCR analysis was performed. Very low levels of BKPyV DNA were detected during the first 12 and 24 hours post-infection, respectively (Figure 3.7B). This suggested that it was observed as an artifact from the DNA of input virus. The first higher increase in viral genome copy numbers was observed 36 hours post-infection, which was expected due to the initiation of TAg expression approximately 24 hours post-infection, as it was previously demonstrated from other studies (Low et al., 2004). The viral DNA levels were constantly increased and peaked towards the end of the time-course. Previous studies demonstrated that viral DNA levels were detected approximately 36 hours post-infection showing an increasing trend throughout the course of infection and reaching their highest levels 9 days post-infection (Low et al., 2004), supporting our findings.

After identifying the stages of the early viral genes transcription, and the viral DNA replication, we determined the stage of the BKPyV life cycle that the late viral proteins were expressed. Total intracellular and secreted proteins were isolated from infected RPTE cells over a time-course of infection. The late viral proteins were detectable intracellularly approximately 48 hours post-infection (Figure 3.7A). Previous studies demonstrated the presence of VP1 between 36 and 48 hours post-infection by Western blot analysis. It was also suggested that VP1 expression levels were

increased throughout the course of infection peaking approximately 11 days post-infection (Low et al., 2004). These findings are partially agreed with our data, as we detected the VP1 expression approximately 48 hours after infection.

Progeny viral particles formed when viral capsomeres assemble around newly synthesized viral genomes, although the mechanism of viral egress is not fully defined (Bennett et al., 2012). To identify the stage that newly synthesized viral progeny was secreted, infection assays were performed under identical conditions as previously described. It was identified that secreted late viral proteins were detectable at later stages of the viral life cycle, approximately 60 hours post-infection (Figure 3.7C). In addition to that, we examined whether the released virus over this time-course was infectious. Notably, the released viral progeny was infectious, and it was also found that there was release of BKPyV virions approximately 48 hours post-infection, even though that was not detected by Western blotting (Figure 3.7C and D). This might be due to higher sensitivity of the IncuCyte ZOOM analysis compared to Western blotting. A greater number of infected cells was observed towards the end of the time-course peaking approximately 72 hours post-infection (Figure 3.7D). Due to very low numbers of infected cells seen during the initial 36 hours post-infection, we suggested that this was an artifact from the input virus.

By examining and determining all the critical steps of the BKPyV life cycle, we could have assayed inhibitory compounds that target host cell factors at specific time-points and study their effect on the virus life cycle. These studies are clearly defined in the following Chapters (Chapter 4 and 5).

4 Host ion channels and the BKPyV life cycle

4.1 Introduction

4.1.1 Targeting host cell factors as potential anti-viral therapy

Viruses as obligate intracellular parasites require host cellular machineries to complete their life cycles. In order to transport their genetic material through the host cells, attachment of the virions to host cell receptors and/or additional co-receptor(s) is required (Bhattacharjee, 2015). Following successful binding to host cell receptor, the internalization is mediated by endocytic transport pathways, which are distinct to each virus (Bhattacharjee, 2015). There are several mechanisms of virus entry; by exemplification many enveloped viruses, including members of *Paramyxoviridae*, enter host cells via activation of viral fusion proteins, whereas influenza virus utilizes a receptor-mediated endocytic pathway for a successful entry (Kielian, 2014). On the other hand, the entry mechanism of non-enveloped viruses may significantly vary; from disruption of endosomes at low pH levels, which observed during adenovirus infection, or pore formation at plasma membrane during poliovirus infection and via caveolae, which is identified during SV40 infection (Marsh and Helenius, 2006; Mudhakir and Harashima, 2009). Recent accumulating evidence reveals a clathrin-independent endocytic pathway, micropinocytosis, which is utilized by several viruses from different families including Ebola virus, influenza virus A, adenovirus 35, Kaposi's sarcoma-associated herpesvirus, Nipah virus and Old World Arenaviruses (Kunz, 2009; Mercer and Helenius, 2012). Then, viruses enter host cell nucleus to replicate their genome by exploiting host cellular machineries.

Specific viral proteins and enzymes can be targeted as a conventional therapeutic approach against viral infections, although by this approach there is always the risk of targeting viral factors that are evolved to resistant varieties due to the ability of viruses for rapid genetic changes and evolution (Bhattacharjee, 2015). Therefore, there is an urgent need to identify a novel therapeutic strategy that avoids selection of resistant viral strains and shows greater efficiency and specificity. This implies to

target critical virus-host interactions that are required for a successful viral infection. Currently, there are few promising drugs that target host proteins and are ready to be commercially available; including Maraviroc which is a CCR5 co-receptor antagonist as a therapy for HIV and DAS181, a recombinant sialidase fusion protein that acts against influenza virus and TSG101 (de Chassey et al., 2012). Thus, investigating and understanding of virus and host interactions is a prerequisite to identify novel druggable cellular targets.

4.1.2 Chapter Aims

Ion channels have emerged as essential host factors in the life cycles of a number of human viruses (Hover et al., 2017). The main aim of this Chapter is to determine the role of host ion channels in the BKPyV life cycle and to validate their potential as a target for novel anti-viral therapeutics to treat PVAN, the leading cause of kidney transplant rejection worldwide. Preliminary data from our group showed that blockade of host cell K^+ channels impedes the BKPyV life cycle by an uncharacterized mechanism. K^+ channels were selected for initial investigations as they represent the largest ion channel family distributed in most cell types and an array of blockers to specific K^+ channel family members are available and well characterized.

4.2 Results

4.2.1 Examination of host K^+ channels as potential targets against BKPyV

4.2.1.1 Host K^+ channels might be critical for BKPyV infection

Previous studies from our group suggested that the host cell K^+ channel family is involved in the BKPyV life cycle by an unknown mechanism. The initial experimental objective was to validate these findings. Primary renal proximal tubular epithelial cells (RPTE cells) were infected with BKPyV at an MOI of 0.5 for 2 hours at 37^{o}C and then were treated with tetraethylammonium (TEA), which is a broad-spectrum K^+ channel blocker, at a range of concentrations for 48 hours post-infection. Cells were then fixed and BKPyV infection assayed through staining for VP1 as a marker of virus production. Using IncuCyte ZOOM analysis, an accumulation of VP1 was observed in the nucleus of infected cells 48 hours post-infection (Figure 4.1A). A decrease of BKPyV VP1 expression in a dose-dependent manner was revealed upon treatment with TEA. The highest dose of TEA (20 mM) caused a greater than 60% reduction of VP1 expression (Figure 4.1B).

More chemical compounds that impact on K^+ channel family were next used to study their effect on BKPyV production. RPTE cells were infected with BKPyV at an MOI of 0.5 for 2 hours at 37^{o}C. Following infections, cells were treated with 20 mM of TEA and 30 mM of potassium chloride (KCl), which collapses K^+ gradient across cellular membrane and inhibits K^+ channels indirectly. Cells were also treated with 30 mM of sodium chloride (NaCl) for 48 hours as a control for osmolarity (Figure 4.2A). Cell pellets were lysed, and total protein was separated by SDS-PAGE. The corresponding Western blots were probed with a polyclonal VP1 antibody and a GAPDH antibody as a loading control. The presence of VP1 was confirmed at the expected molecular weight (42 kDa). Both TEA and KCl caused a decrease of VP1 protein expression, although there was no effect upon treatment with NaCl (Figure 4.2B).

Pharmacological analysis with identical treatments were repeated with the addition of 15 µg/ml of Cidofovir, which is an anti-viral agent, as a positive control (Figure 4.2A). Treated cells were incubated for 48 hours, then were fixed, and BKPyV infection assayed through staining for VP1 as a marker of virus production. Using IncuCyte

ZOOM analysis, the level of VP1 expression was measured. An accumulation of VP1 was observed in the nucleus of infected cells 48 hours post-infection (Figure 4.2C). Results revealed that TEA caused a decrease of BKPyV VP1 expression of approximately 70% and both KCl and Cidofovir had a similar effect on VP1 protein levels causing 40% reduction. NaCl did not affect VP1 expression levels (Figure 4.1D). Taken together, these data suggest that K^+ channels might impact on the BKPyV life cycle.

Modulators that were used in this study have been examined by cell toxicity assay and there was no detrimental effect on cell viability suggesting that their effect is caused by the actual modulator and not because of cell mortality (Figure 4.2E).

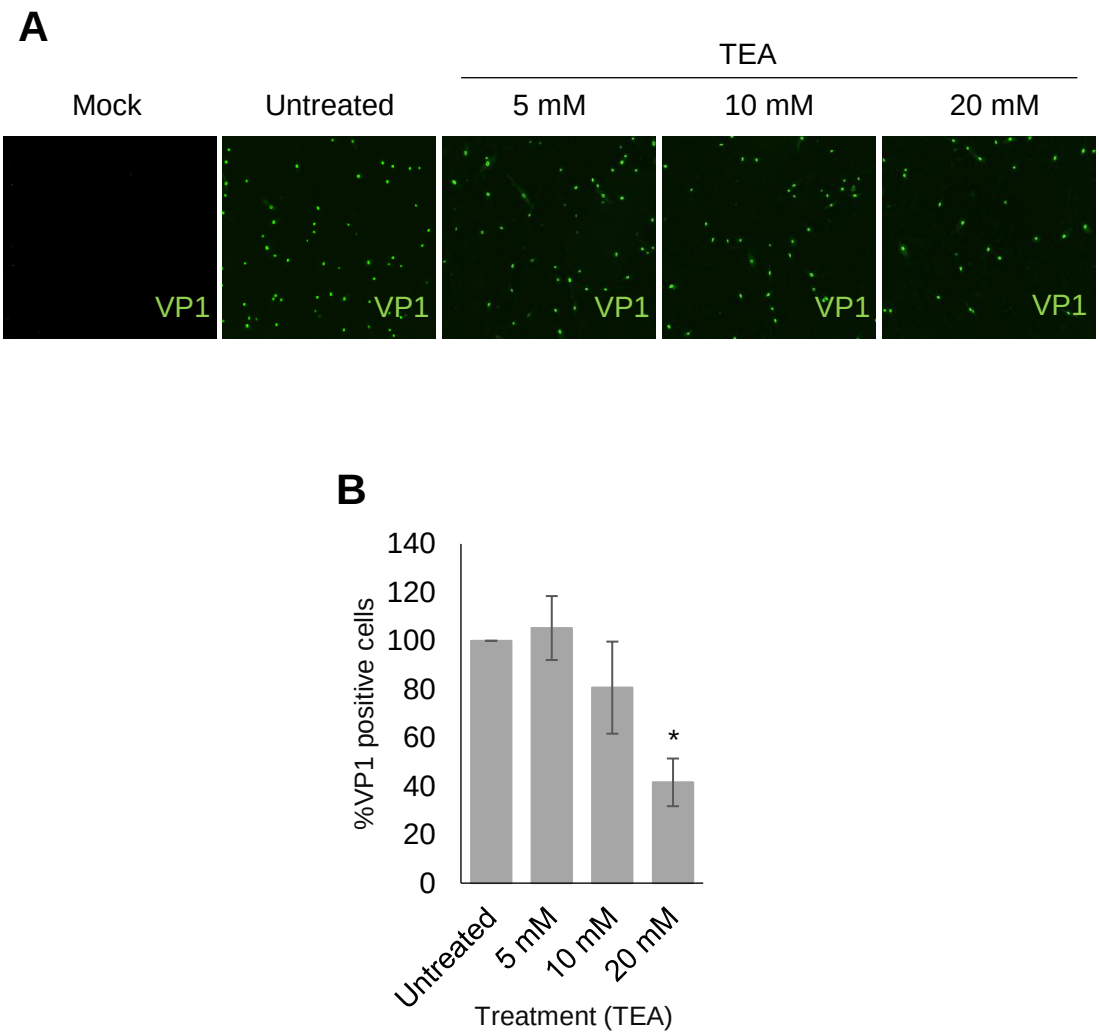

Figure 4. 1 TEA inhibits BKPyV infection in RPTE cells. A. RPTE cells were infected with BKPyV at an MOI of 0.5 and treated with 5 mM, 10 mM and 20 mM of TEA, respectively for 48 hours. RPTE cells were fixed and stained with a primary anti-VP1 (1:250) (pAb597) antibody and a secondary anti-mouse alexa fluor-conjugated 488. BKPyV VP1 was used as marker of BKPyV infection. Subcellular localization of VP1 protein was detected in the nucleus of BKPyV infected cells. B. Positive infected cells were calculated by IncuCyte ZOOM and normalized to the no-drug control sample. Values represent the mean ±SD of positive infected cells (n= 3) (*, significant difference at the $p \leq 0.05$ level).

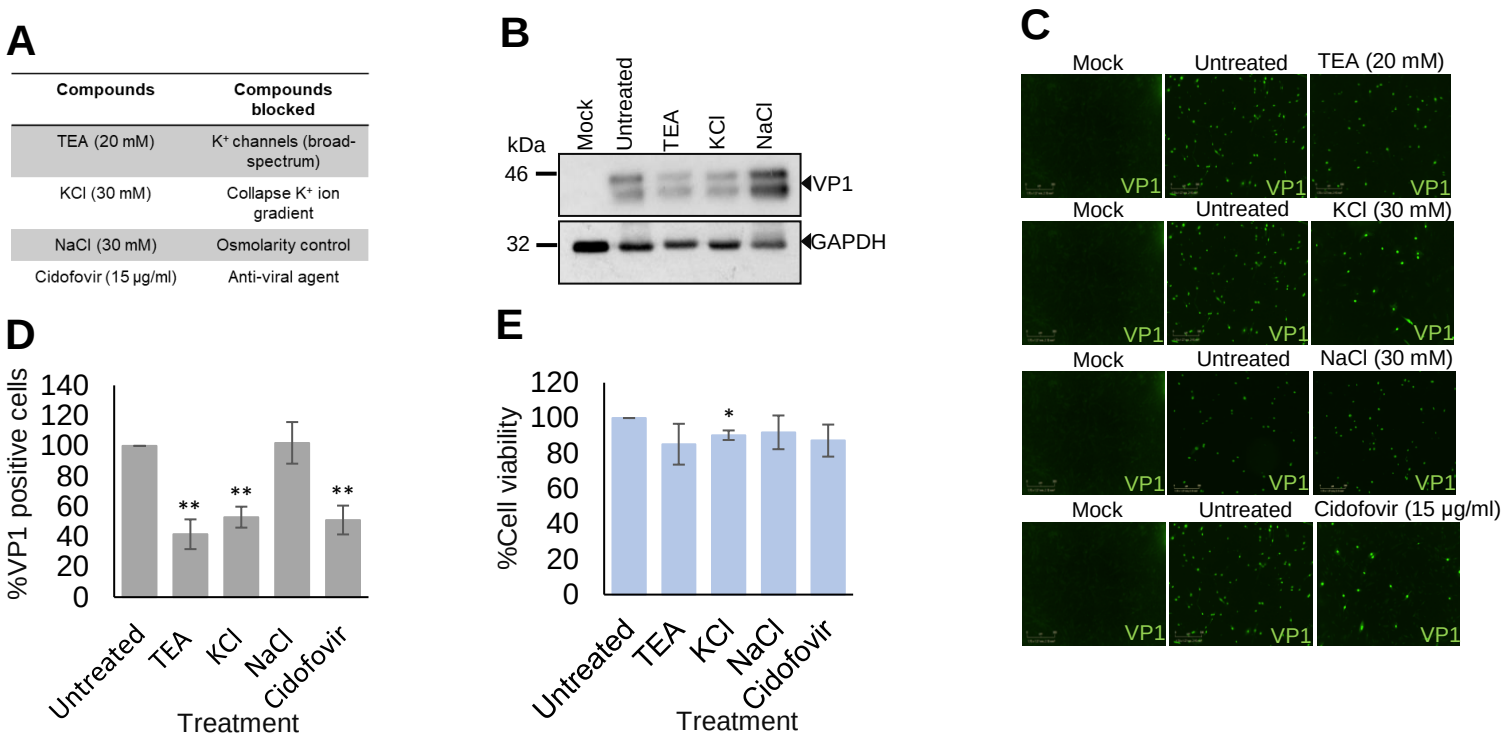

Figure 4. 2 K^+ channels inhibition reduces BKPyV infection in RPTE cells. A. Table presenting chemical compounds and concentration applied to cells. B. RPTE cells were infected with BKPyV at an MOI of 0.5 and treated with chemical modulators presented on the table for 48 hours. Total protein of cell lysates from infected cells was separated by SDS-PAGE and probed for VP1 (pAb597) as a BKPyV infection marker, and GAPDH as a loading control. Representative blots are shown from two independent infections. C. RPTE cells were infected with BKPyV at an MOI of 0.5 and treated with chemical compounds presented on the table for 48 hours. RPTE cells were fixed and stained with a primary anti-VP1 antibody (pAb597) and a secondary anti-mouse alexa fluor-conjugated 488. BKPyV VP1 was used as marker of BKPyV infection. Subcellular localization of VP1 protein was detected in the nucleus of BKPyV infected cells. D. Positive infected cells were calculated by IncuCyte ZOOM and normalized to the no-drug control. Values represent the mean ±SD of positive infected cells (n= 3) (TEA and KCl treatments were performed at the same time- NaCl and Cidofovir were performed at different times, respectively). E. RPTE cells were treated under identical treatment conditions and cell viability assessed via MTT assays. Values represent the mean ±SD normalized to the untreated controls (n= 3) (*, significant difference at the $p \leq 0.05$ level; **, significant difference at the $p \leq 0.01$ level).

4.2.1.2 ATP-sensitive K^+ channels are required for a productive BKPyV infection

K^+ channel family can regulate several cellular processes and is the largest ion channel family consisting of a number of different K^+ channel subfamilies (Table 4.1). To identify which subfamily of this wide group might be required for a productive life cycle, a more detailed pharmacological analysis was performed. To achieve this, RPTE cells were infected with BKPyV at an MOI of 0.5 for 2 hours at 37^{o}C. Cells were treated with a panel of K^+ channel modulators that target different K^+ channel subfamilies. Cells were treated with 20 mM of TEA and 50 µM of Quinidine, which are broad-spectrum inhibitors of K^+ channels. Infected RPTE cells were also treated with 1 mM of barium chloride ($BaCl_2$), which blocks the function of inward rectifier K^+ channels. 4-Aminopyridine (4AP) was also used at 0.5 mM; this organic compound inhibits voltage-gated K^+ channels; 20 µM of Glibenclamide, which impedes the function of ATP-sensitive K^+ channels, and 0.5 µM of Apamin, which blocks Ca^{+2}-activated K^+ channels were utilized (Figure 4.3A). Cells were lysed 48 hours post-infection, and VP1 expression assessed by Western blot analysis. Treatment with TEA and Glibenclamide caused a decrease of VP1 protein expression levels, with Glibenclamide showing a more potent effect. In contrast, there was no effect upon treatment with the other ion channel modulators (Figure 4.3B and C). These results suggested that ATP-sensitive K^+ channels, as a major Glibenclamide target, might play a role in the BKPyV life cycle.

Ion channel blockers that were used have been examined by cell toxicity assay to identify whether the resulting effect was due to loss of cell viability. Findings from toxicity assays reveal that Quinidine and Glibenclamide at the applied concentration reduced cell viability by approximately 25%, respectively. Although, Quinidine did not cause any decrease of VP1 protein expression levels and Glibenclamide had a greater impact on VP1 expression, which was not occurred due to loss of cell viability entirely (Figure 4.3D).

Table 4. 1 Potassium channel family. K+ channel classes , subclasses, function and pharmacology are shown below (Rang, 2003).

Class	*Subclasses*	*Function*	*Blockers*	*Activators*
Ca^{2+}-activated 6T & 1T	• BK channel • SK channel • IK channel	Inhibition in response to rising intracellular Ca^{2+}	• Charybdotoxin, Iberiotoxin • Apamin	• 1-EBIO • NS309 • CyPPA
Inwardly rectifying 2T &1P	• ROMK	• Recycling and secretion of K^+ in nephrons	• Non-selective Ba^{2+}, Cs^+	• none
	• GPCR regulated	• Mediate the inhibitory effect of many GPCRs	• GPCR antagonists • Ifenprodil	• GPCR agonists
	• ATP-sensitive	• Close when ATP is high to promote insulin secretion	• Glibenclaimde • Tolbutamide	• Diazoxide • Pinacidil • Minoxidil • Nicorandil
Tandem pore domain 4T & 2P	• TWIK • TREK • TASK • TALK • THIK • TRESK	• Contribute to resting potential	• Bupivacaine • Quinidine	• Halothane
Voltage-gated 6T &1P	• Herg • KvLQT1	• Action potential repolarization • Limits frequency of action potentials	• Tetraethylammonium • 4-Aminopyridine • Dendrotoxins	• Retigabine

A

Compounds	K^+ channels blocked
TEA (20 mM)	K^+ channels (broad spectrum)
Quinidine (50 µM)	K^+ channels (broad spectrum)
$BaCl_2$ (1 mM)	Inward rectifier K^+ channels
4AP (0.5 mM)	Voltage-gated K^+ channels
Glibenclamide (20 µM)	ATP sensitive K^+ channels
Apamin (0.5 µM)	Ca^{+2}-activated K^+ channels

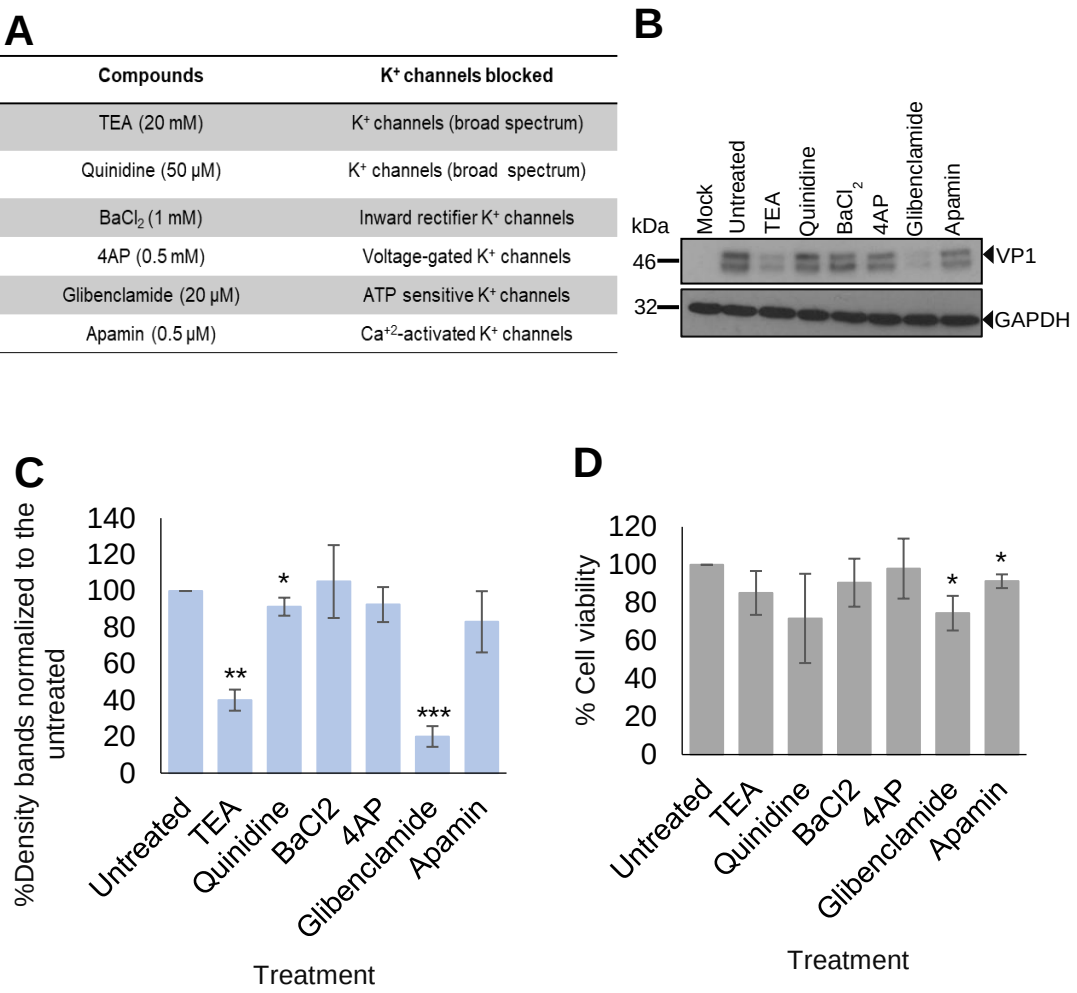

Figure 4. 3 ATP-sensitive K^+ channels are required for BKPyV production in RPTE cells. A. Table presenting chemical compounds and concentration applied to cells. B. RPTE cells were infected with BKPyV at an MOI of 0.5 and treated with chemical modulators for 48 hours. Total protein of cell lysates from infected cells was separated by SDS-PAGE and probed for VP1 (pAb597) as a marker of BKPyV infection, and GAPDH as a loading control. Representative blots are shown from three independent infections. C. Densitometry analysis of Western blots was performed. Values represent the mean ±SD normalized to the no-drug control (n= 3). D. RPTE cells were treated as above and cell viability assessed via MTT assays. Values represent the mean ±SD normalized to the untreated control (n= 3) (*, significant difference at the $p \leq 0.05$ level; **, significant difference at the $p \leq 0.01$ level; ***, significant difference at the $p \leq 0.001$).

4.2.2 Targeting ATP-sensitive K^+ channels to study their impact on the BKPyV life cycle

ATP-sensitive K^+ channel complexes are regulated by intracellular nucleosides, such as ATP and ADP. They are composed of an inward rectifier K_{ir}6.x-type (1, 2) subunit and the sulfonylurea receptor-type (SUR1, SUR2A, SURS2B) subunits (Stephan et al., 2006). Sulfonylurea pharmacological compounds, including Glibenclamide, can inhibit the ATP-sensitive K^+ channels by binding to sulfonylurea regulatory subunits (Serrano-Martín et al., 2006). Tolbutamide is also a sulfonylurea inhibitor, blocks the function of ATP-sensitive K^+ channels and shows a higher specificity to ion channel complexes composed of SUR1-type subunits (Walker and Parrish, 1988).

Previous findings revealed that ATP-sensitive K^+ channels might play an important role in the BKPyV life cycle, because inhibition of these ion channel complexes impedes viral protein expression. Pharmacological analysis using other chemical modulators that target specifically the same family member was performed. RPTE cells were infected with BKPyV at an MOI of 0.5 for 2 hours at 37^{o}C. Cells were treated with two different sulfonylurea inhibitors, including 20 µM of Glibenclamide and 150 µM of Tolbutamide for 48 hours (Figure 4.4A). Cells were fixed, and BKPyV infection assayed through staining for VP1 as a marker of virus infection using IncuCyte ZOOM analysis. Results showed an accumulation of VP1 within the nucleus of infected RPTE cells (Figure 4.4B). There was an ~83% decrease in VP1 positive cells compared to the untreated control sample upon treatment with Glibenclamide. However, a more modest effect of Tolbutamide was observed, causing a 20% reduction of VP1 expression levels, even though both chemical modulators target the same family member (Figure 4.4C). These findings suggest that the potential ATP-sensitive K^+ channel complex, which is expressed in RPTE cells and affects BKPyV is likely less sensitive to Tolbutamide. Both inhibitors have been examined by cell toxicity assay to identify whether the resulting effect was due to loss of cell viability. Findings from toxicity assays revealed that Tolbutamide did not cause any effect on cell viability. Glibenclamide at the applied concentration reduced cell viability by approximately 25% (Figure 4.4D).

Plasma membrane channels play a critical role in regulating the resting membrane potential, which can become hyperpolarized (more negatively charged) or depolarized (more positively charged) depending on specific stimuli that regulates the channel activity. DiBAC4(3) is a fluorescent dye that has been used to monitor changes in the resting membrane potential over short time periods (Bräuner et al., 1984). In cells treated with DiBAC4(3), increased fluorescence is indicative of membrane depolarization, whilst a decrease in fluorescence over time indicates membrane hyperpolarization (Baxter et al., 2002). To support the pharmacological data, the effects of both modulators on the resting membrane potential of RPTE cells were investigated, DiBAC4(3) was added to RPTE cells treated with 20 μM of Glibenclamide or 150 μM of Tolbutamide for 48 hours and DiBAC4(3) fluorescence assessed by flow cytometry. Glibenclamide led to a depolarization of plasma membrane evidenced by the 0.2-fold increase in fluorescence observed following drug treatments, compared to no-drug controls (Figure 4.4E). However, there was no effect of Tolbutamide treatment on plasma membrane polarization as no shift of the fluorescence dye was observed (Figure 4.4E) in comparison with the untreated control sample, suggesting that at the applied concentrations only Glibenclamide was able to alter resting membrane potential.

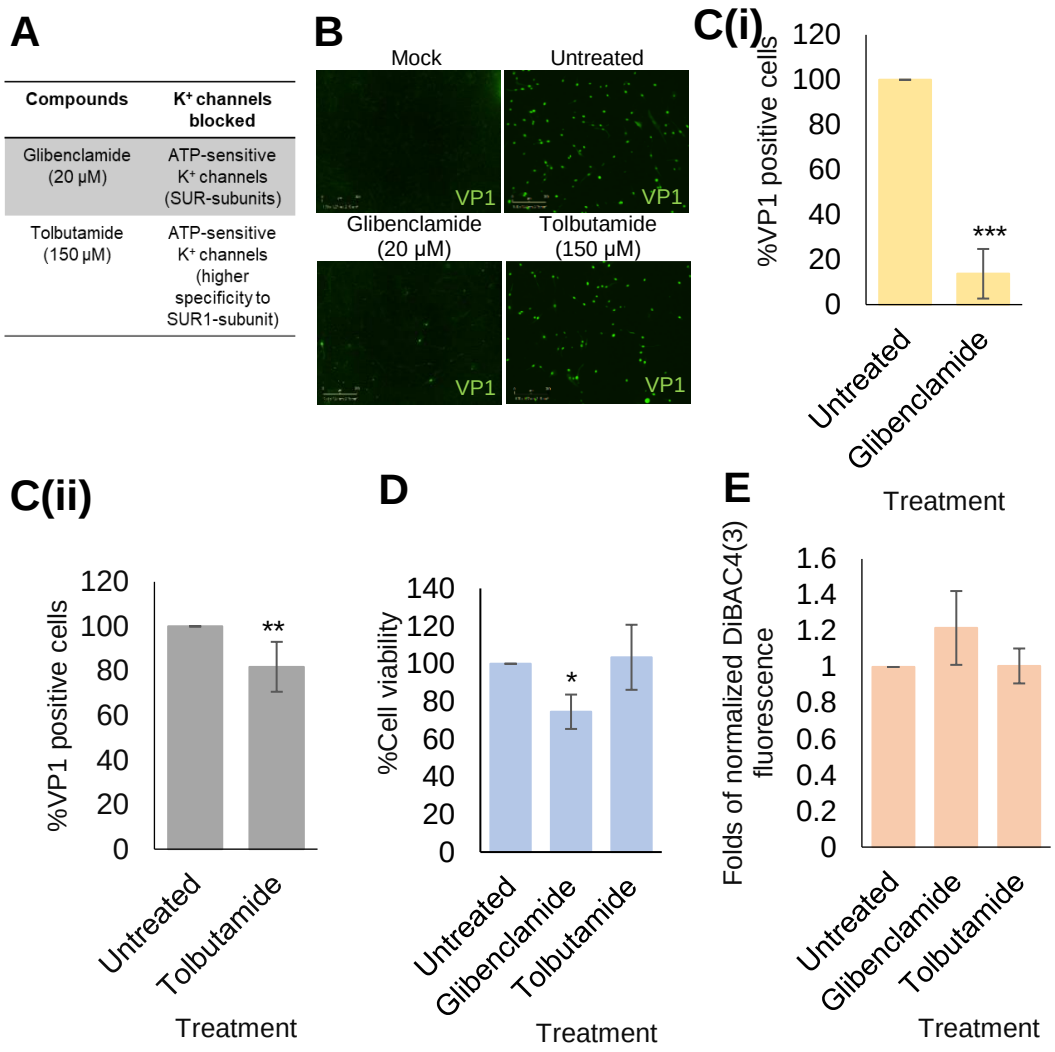

Figure 4. 4 ATP-sensitive K^+ channels expressed in RPTE cells are more sensitive to Glibenclamide compared to Tolbutamide. A. Table presenting chemical compounds and concentration applied to cells. B. RPTE cells were infected with BKPyV at an MOI of 0.5 and treated with chemical modulators for 48 hours. Cells were fixed and stained with a primary anti-VP1 (pAb597) antibody and a secondary alexa fluor-conjugated 488. BKPyV VP1 was used as marker of BKPyV infection. Subcellular localization of VP1 protein was detected in the nucleus of BKPyV infected cells. C. Positive infected cells were normalized to the untreated control sample. Values represent the mean ±SD of positive infected cells (n= 3). D. RPTE cells were treated as above, and cell viability assessed via MTT assays. Values represent the mean ±SD normalized to the untreated control (n= 3). E. RPTE cells were treated with 20 µM of Glibenclamide or 150 µM of Tolbutamide and incubated for 48 hours. 20 µM of DiBAC4(3) was added to treated cells and flow cytometry analysis of total cell fluorescence was measured. Values represent the mean ±SD normalized to the untreated control (n= 3) (*, significant difference at the $p \leq 0.05$ level; **, significant difference at the $p \leq 0.01$ level; ***, significant difference at the $p \leq 0.001$).

To test more chemical compounds which modulate ATP-sensitive K^+ channels either by inhibiting or activating them, further pharmacological-based analysis was conducted. ATP-sensitive K^+ channels are located on the plasma membrane, although previous studies have identified that these ion channel complexes can also be found on subcellular membranes including mitochondrial, sarcolemmal and nuclear membranes (Stephan et al., 2006). Studies have shown that Glibenclamide and Tolbutamide exhibit different potencies for the different SUR subunits. It is also known that the chemical compound U-37883A inhibits selectively ATP-sensitive K^+ channels containing K_{ir}6.1-type subunits and has no inhibitory impact on ATP-sensitive K^+ channels composed of K_{ir}6.2-type subunits, regardless of the co-expressed SUR-type subunits (Teramoto, 2006).

RPTE cells were infected with BKPyV at an MOI of 0.5 for 2 hours at 37^{o}C and treated with compounds that target ATP-sensitive K^+ channels located on mitochondrial membranes (5-Hydroxydecanoate (5HD)) and ATP-sensitive K^+ channels containing K_{ir}6.1-type subunits (U-37883A). 500 µM of 5HD or 50 µM of U-37883A were added to infected RPTE cells for 48 hours (Figure 4.5A). Cells were then fixed, and BKPyV infection examined through staining for BKPyV VP1 as a marker of infection. Results showed an accumulation of VP1 within the nucleus of infected RPTE cells (Figure 4.5B). However, there was no effect on VP1 expression upon treatment with the modulators (Figure 4.5C). These findings suggest that the potential ATP-sensitive K^+ channel complex, which is expressed in RPTE cells and affects BKPyV is not located on mitochondrial membranes or composed of K_{ir}6.1-type subunits. Both inhibitors have been assessed by cell toxicity assays and findings revealed that neither 5HD or U-37883A cause reduction of cell viability (Figure 4.5D). The ability of both modulators to influence the resting membrane potential of RPTE cells was investigated. To determine this, RPTE cells were treated with 500 µM of 5HD or 50 µM of U-37883A for 48 hours and DiBAC4(3) was added to treated cells. Flow cytometry analysis showed that 5HD caused a very modest effect on membrane polarization of RPTE cells as evidenced by the 0.1-fold increase in fluorescence compared to no-drug controls. Notably, U-37883A had a higher impact on resting membrane potential of RPTE cells as revealed by the 0.7-fold increase in DiBAC4(3) fluorescence in treated

cells compared to the untreated controls (Figure 4.5E), suggesting that U-37883A treatment at the applied concentration is able to cause depolarization of RPTE cells.

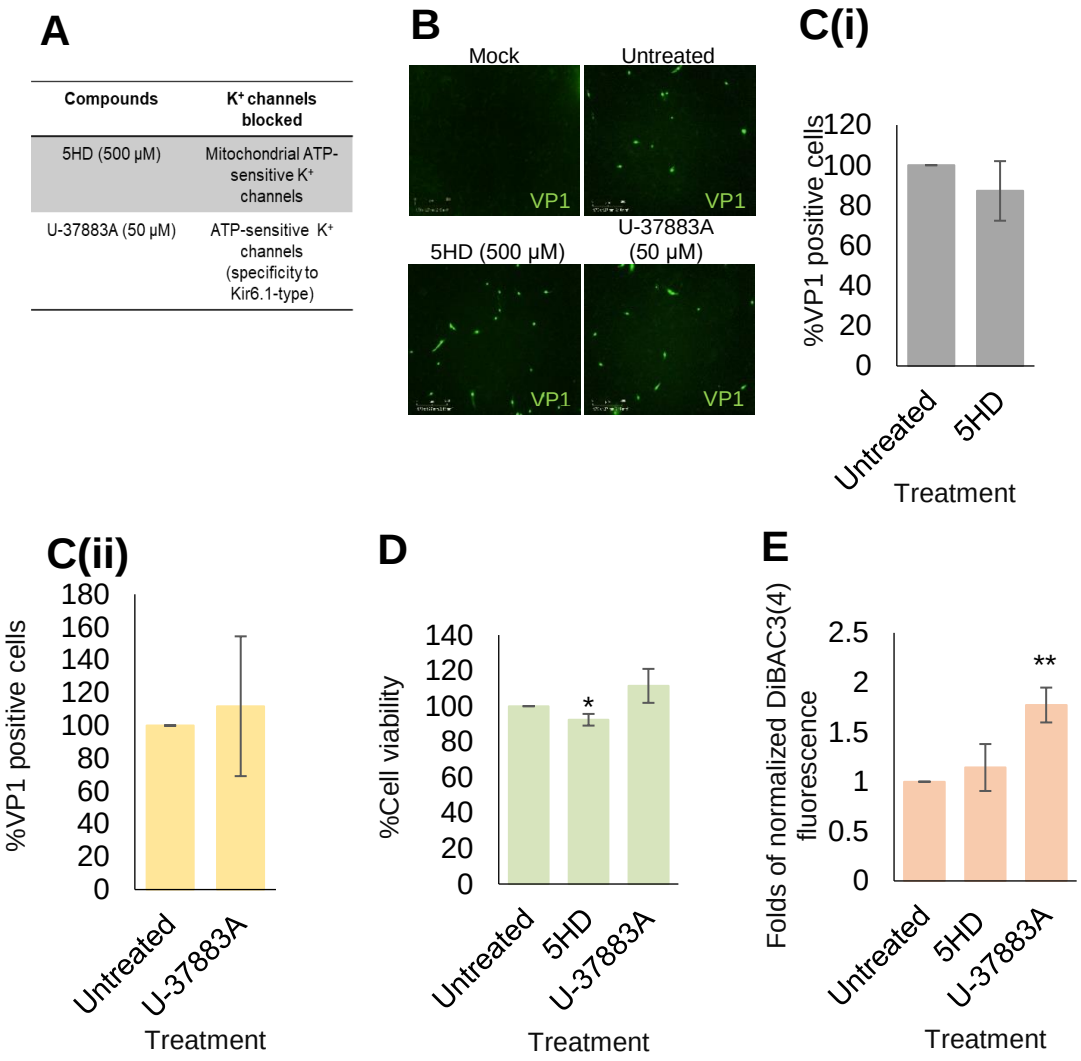

Figure 4. 5 Mitochondrial or K_{ir}6.1-type-ATP-sensitive K^+ channel blockers do not reduce BKPyV infection in RPTE cells. A. Table presenting chemical compounds and concentration applied to cells. B. RPTE cells were infected with BKPyV at an MOI of 0.5 and treated with 5HD and U-37883A for 48 hours. Cells were fixed and stained with a primary anti-VP1 (pAb597) antibody and a secondary anti-mouse alexa fluor-conjugated 488. VP1 protein was detected by IncuCyte ZOOM screening as a marker of infection. VP1 protein was detected in the nucleus of BKPyV infected cells. C. Positive infected cells were calculated by IncuCyte ZOOM and normalized to the untreated control. Values represent the mean ±SD of positive infected cells (n= 3). D. RPTE cells were treated as above for 48 hours and cell viability assessed via MTT assays. Values represent the mean ±SD of three independent experiments and normalized to the untreated control. E. RPTE cells were treated as above for 48 hours. 20 µM of DiBAC4(3) was added to treated cells and flow cytometry analysis of total cell fluorescence was measured. Values represent the mean ±SD normalized to the no-drug control (n= 3) (*, significant difference at the $p \leq 0.05$ level; **, significant difference at the $p \leq 0.01$ level).

There are well characterized ATP-sensitive K^+ channel openers, such as Diazoxide and Pinacidil (Chowdhury et al., 2013; Gollasch et al., 1995) and their function were assessed to investigate their effect on BKPyV production. RPTE cells were infected with BKPyV (MOI 0.5) for 2 hours at 37^{o}C and treatment with 50 μM of Diazoxide or 20 μM of Pinacidil was performed for 48 hours (Figure 4.6A). Cells were lysed 48 hours post-infection, and VP1 expression assessed by Western blot analysis. Results from Western blotting confirmed the expression of VP1. Interestingly, there was a reduction of VP1 protein expression in the presence of Diazoxide, whereas no effect was observed upon treatment with Pinacidil (Figure 4.6B). Findings from toxicity assays revealed that neither Diazoxide or Pinacidil caused metabolic changes (Figure 4.6C).

A

Compounds	K^+ channels activated
Diazoxide (50 µM)	ATP-sensitive K^+ channels
Pinacidil (20 µM)	ATP-sensitive K^+ channels

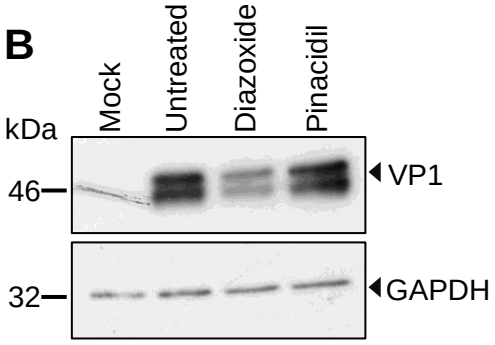

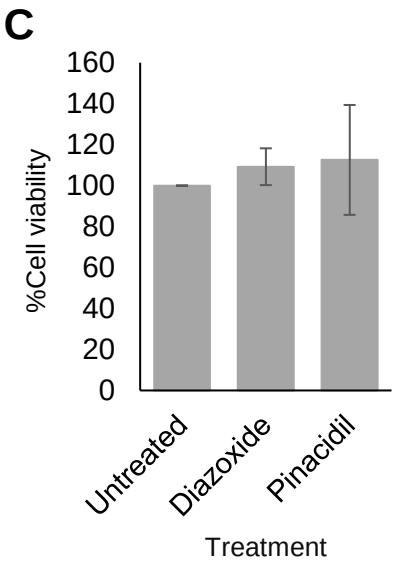

Figure 4. 6 ATP-sensitive K^+ channel openers and BKPyV production. A. Table presenting chemical compounds and concentration applied to cells. B. RPTE cells were infected with BKPyV at an MOI of 0.5 and treated with ion channel activators for 48 hours. Total protein of cell lysates from infected cells was separated by SDS-PAGE and probed for VP1 (pAb597) as a BKPyV infection marker, and GAPDH as a loading control. Representative blots are shown from two independent infections. C. RPTE cells were treated as above for 48 hours and cell viability assessed via MTT assays. Values represent the mean ±SD normalized to the untreated control (n= 3).

Taken together all the previous data, Glibenclamide causes a reduction of VP1 expression suggesting that ATP-sensitive K^+ channels which are targeted by Glibeclamide might be involved in the BKPyV life cycle by an unknown mechanism. However, pharmacological analysis using other chemical modulators which also target this family member indicate that there is no effect on viral protein expression upon treatments. Therefore, ATP-sensitive K^+ channels might not be required for a successful BKPyV life cycle in RPTE cells. Although, Glibenclamide might target another host factor which is essential for BKPyV production and a more in-depth analysis was performed to identify the target of this compound.

4.2.3 Glibenclamide reduces BKPyV infection in RPTE cells

4.2.3.1 Glibenclamide blocks BKPyV in a dose-dependent fashion

To identify the highest dose of Glibenclamide that could be applied to cells without causing cell toxicity and the lowest dose that could be applied to minimize its effect on BKPyV, titration of Glibenclamide was carried out. RPTE cells were infected with BKPyV at an MOI of 0.5 for 2 hours at 37^{o}C and then treated with Glibeclamide for 48 hours; 10 µM, 20 µM, 35 µM and 50 µM, respectively. Cells were lysed and BKPyV infection assessed through the expression of VP1 by Western blotting.

Results from Western blotting indicated that the presence of VP1 was confirmed in the untreated control sample showing a clear band at the expected molecular weight of approximately 42 kDa. Faint bands of VP1 were identified in the other samples suggesting that even lower doses of Glibenclamide (10 µM) can cause detrimental effects on VP1 protein expression (Figure 4.7A). Cell viability assays were also performed to examine whether this loss of VP1 expression was due to toxicity caused by the increasing doses of Glibenclamide. Data suggested that doses higher than 20 µM of Glibenclamide lead to decrease of cell viability. (Figure 4.7B).

In order to determine the minimum concentration at which Glibenclamide can inhibit VP1 expression, a more detailed titration was conducted. RPTE cells were infected with BKPyV at an MOI of 0.5 for 2 hours at 37^{o}C and then treated with different doses of Glibenclamide for 48 hours; 0.5 µM, 1 µM, 2 µM, 4 µM, 6 µM, 8 µM, 10 µM, 15 µM

and 20 μM, respectively. Cells were fixed, and BKPyV infection assayed through staining for VP1 as a marker of virus production using IncuCyte ZOOM analysis. BKPyV VP1 staining was again observed in the nucleus of infected cells, 48 hours post-infection (Figure 4.7C). There was approximately 25% reduction of VP1 expression upon treatment with the lowest concentration of Glibenclamide. A significant and proportional decreasing trend of VP1 expression levels was observed upon the gradually higher doses of Glibenclamide (Figure 4.7D). Taken together, these data suggest that Glibenclamide inhibits BKPyV production in a dose-dependent manner.

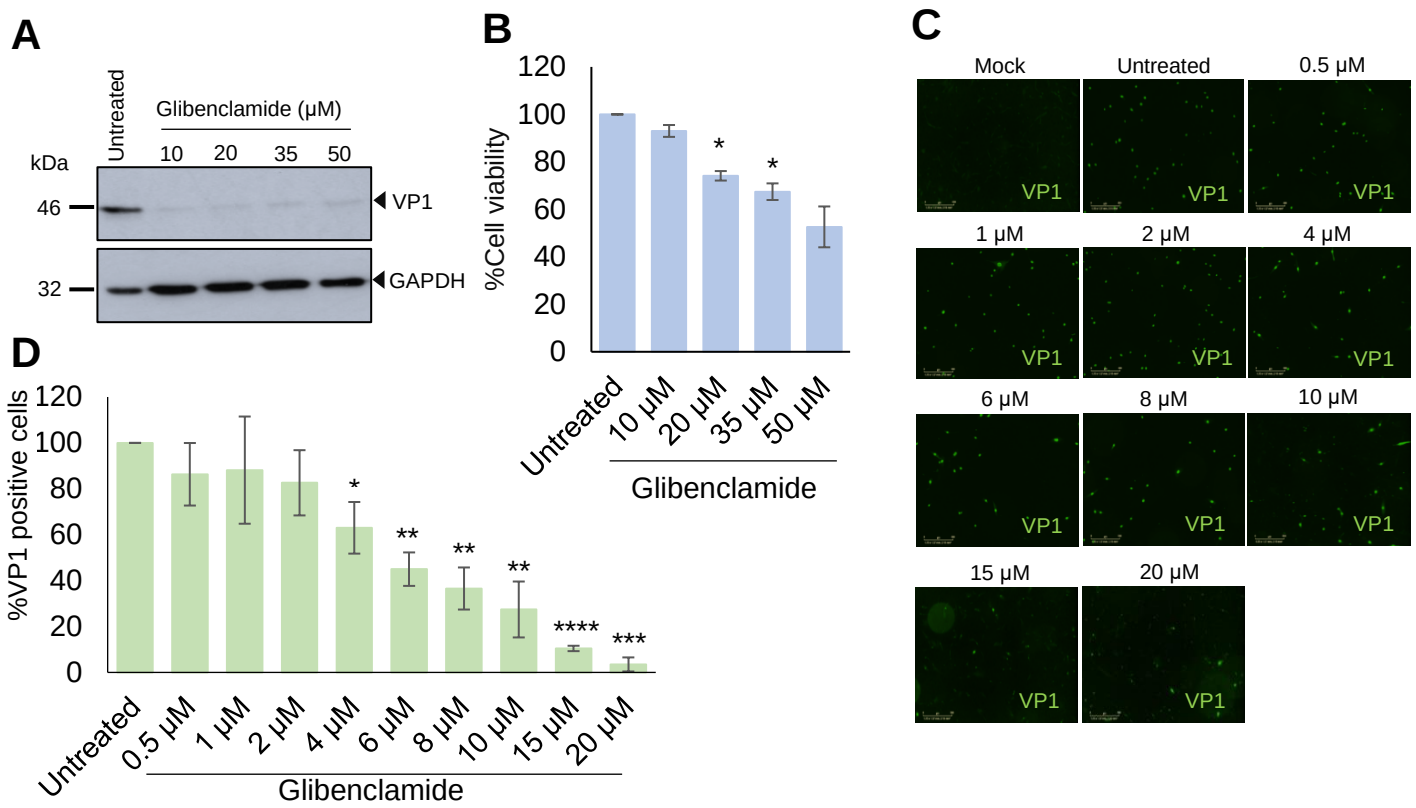

Figure 4. 7 Glibenclamide reduces BKPyV production in a dose-dependent manner. A. RPTE cells were infected with BKPyV at an MOI of 0.5 and treated with 10 μM, 20 μM, 35 μM and 50 μM of Glibenclamide, respectively for 48 hours. Total protein of cell lysates from infected cells was separated by SDS-PAGE and probed for VP1 (P5G6) as a marker of BKPyV infection, and GAPDH as a loading control. Representative blots are shown from two independent infections. B. RPTE cells were treated as above for 48 hours and cell viability assessed via MTT assays. Values represent the mean ±SD normalized to the no-drug control (n= 3). C. RPTE cells were infected with BKPyV at an MOI of 0.5 and treated with 0.5 μM, 1 μM, 2 μM, 4 μM, 6 μM, 8 μM, 10 μM, 15 μM and 20 μM of Glibenclamide, respectively for 48 hours. Cells were fixed and stained with a primary anti-VP1 (1:250) (pAb597) antibody and a secondary anti-mouse alexa fluor-conjugated 488. BKPyV VP1 was used as marker of BKPyV infection. Subcellular localization of VP1 protein was detected in the nucleus of BKPyV infected cells. D. Positive infected cells were normalized to the untreated control sample. Values represent the mean ±SD of positive infected cells (n= 3) (*, significant difference at the $p \leq 0.05$ level; **, significant difference at the $p \leq 0.01$ level; ***, significant difference at the $p \leq 0.001$ level; ****, significant difference at the $p \leq 0.0001$ level).

4.2.3.2 Glibenclamide inhibits BKPyV production in an MOI-independent manner

To identify whether the effect of Glibenclamide was dependent on the amount of infectious virus that was added to cells, infection assays using different MOIs of BKPyV were conducted. To achieve this, RPTE cells were infected with BKPyV at an MOI of 0.5 and 5, respectively, for 2 hours at 37^{o}C and treated with 20 μM of Glibenclamide for 48 hours. Then, infected cells were fixed, and BKPyV infection assayed through staining for VP1 as a marker of virus production using IncuCyte ZOOM analysis. BKPyV VP1 staining was observed in the nucleus of infected cells, 48 hours post-infection (Data not shown). Results demonstrated that there was a significant reduction (~ 80%) of VP1 expression regardless of the different amount of virus that was added to cells (Figure 4.8 A and B).

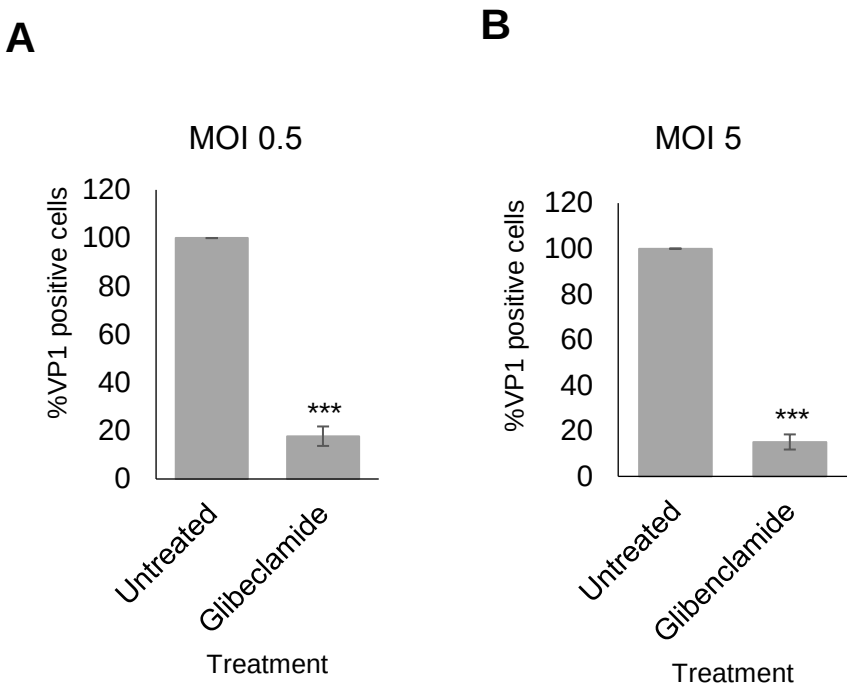

Figure 4. 8 The Glibenclamide effect is BKPyV MOI-independent. A. RPTE cells were infected with BKPyV at an MOI of 0.5 and treated with 20 μM of Glibenclamide for 48 hours. Cells were fixed and stained with a primary anti-VP1 (1:250) (pAb597) antibody and a secondary anti-mouse alexa fluor-conjugated 488. BKPyV VP1 protein was used as a marker of BKPyV infection. Positive infected cells were normalized the untreated control. Data represent the mean ±SD of positive infected cells (n= 3). B. RPTE cells were infected with BKPyV at an MOI of 5 and treated with 20 μM of Glibenclamide for 48 hours. Cells were fixed and stained with a primary anti-VP1 (1:250) (pAb597) antibody and a secondary anti-mouse alexa fluor-conjugated 488. Positive infected cells were normalized to the no-drug control. Values represent the mean ±SD of positive infected cells (n= 3) (***, significant difference at the $p \leq 0.001$ level).

4.2.3.3 Glibenclamide reduces BKPyV viral proteins expression and genome replication

In previous experiments BKPyV VP1 was used as an infection marker, therefore we next investigated the effect of Gliblenclamide on other aspects of the life cycle including viral protein expression and genome replication. For that reason, RPTE cells were infected with BKPyV (MOI 0.5) for 2 hours at 37^{o}C and treated with 20 μM of Glibenclamide for 48 hours. Isolated total protein from lysates was separated by SDS-PAGE and assayed for viral protein expression by Western Blotting. The corresponding Western blots were probed with a hybridoma polyclonal VP1 antibody, a commercial polyclonal VP2/VP3 antibody, which detects both late proteins, and GAPDH as a loading control. Results showed that Glibenclamide decreases not only VP1 expression but also other late proteins including VP3; VP2 was not successfully detected on the corresponding Western blots (Figure 4.9A).

To examine whether Glibenclamide has an impact on viral genome replication, quantitative PCR analysis was carried out. RPTE cells were infected with BKPyV (MOI 0.5) for 2 hours at 37^{o}C and treated with 20 μM of Glibenclamide or 15 μg/ml of Cidofovir, as a positive control, for 48 hours. Total DNA was extracted from each sample and analyzed by quantitative PCR using specific primers against the viral genome. Data extracted following the qPCR analysis indicated that both Glibenclamide and Cidofovir caused a significant decrease on viral DNA levels. There was approximately 80% decrease of viral genome copy numbers upon treatment with Glibenclamide and about 75% reduction in the presence of Cidofovir (Figure 4.9B). Taken together these data suggest that Glibenclamide decreases BKPyV infection not only at a protein level, but also at a DNA level.

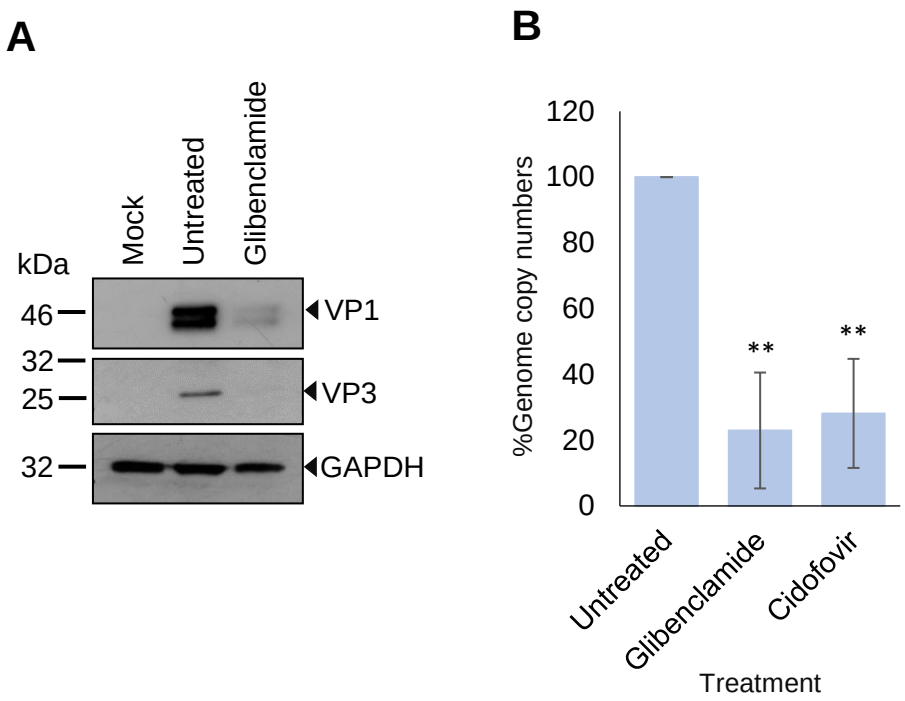

Figure 4. 9 Glibenclamide decreases BKPyV viral protein expression and genome replication. A. RPTE cells were infected with BKPyV at an MOI of 0.5 and treated with 20 µM of Glibenclamide for 48 hours. Total protein of cell lysates from infected cells was separated by SDS-PAGE. VP1 (pAb597), VP3 and the loading control GAPDH were detected on the Western blot with the appropriate antibodies. Representative blots are shown from two independent infections. B. RPTE cells were infected with BKPyV at an MOI of 0.5 and treated with 20 µM of Glibenclamide or 15 µg/ml of Cidofovir for 48 hours. Quantitative PCR analysis of DNA viral genome was performed. Values represent the mean ±SD of viral genome copy numbers normalized to the untreated control sample (n= 3) (**, significant difference at the $p \leq 0.01$ level).

4.2.3.4 Glibenclamide decreases the titres of the released viral progeny

To identify whether Glibenclamide treatment affects the release of viral progeny from infected cells, infection assays were carried out. RPTE cells were infected with BKPyV at an MOI of 0.5 for 2 hours at 37^{o}C and then treated with 20 μM of Glibenclamide or 15 μg/ml of Cidofovir, as a control, for 48 hours. Supernatants were collected 48 hours post-infection and utilized to further infect RPTE cells for 48 hours (Figure 4.10A). Cells were then fixed, and BKPyV infection assayed through staining for VP1 as a marker of virus production. Using IncuCyte ZOOM analysis, it was demonstrated that the released viral progeny was infectious as an accumulation of BKPyV VP1 was observed in the nucleus of infected cells, 48 hours post-infection (Figure 4.10B). Interestingly, both Glibenclamide and Cidofovir caused a decrease in the titres of the synthesized viral progeny. There was approximately an 80% reduction of VP1 expression in infected cells with the supernatant sample from the Glibenclamide treatment and 90% from the Cidofovir treatment, respectively (Figure 4.10C).

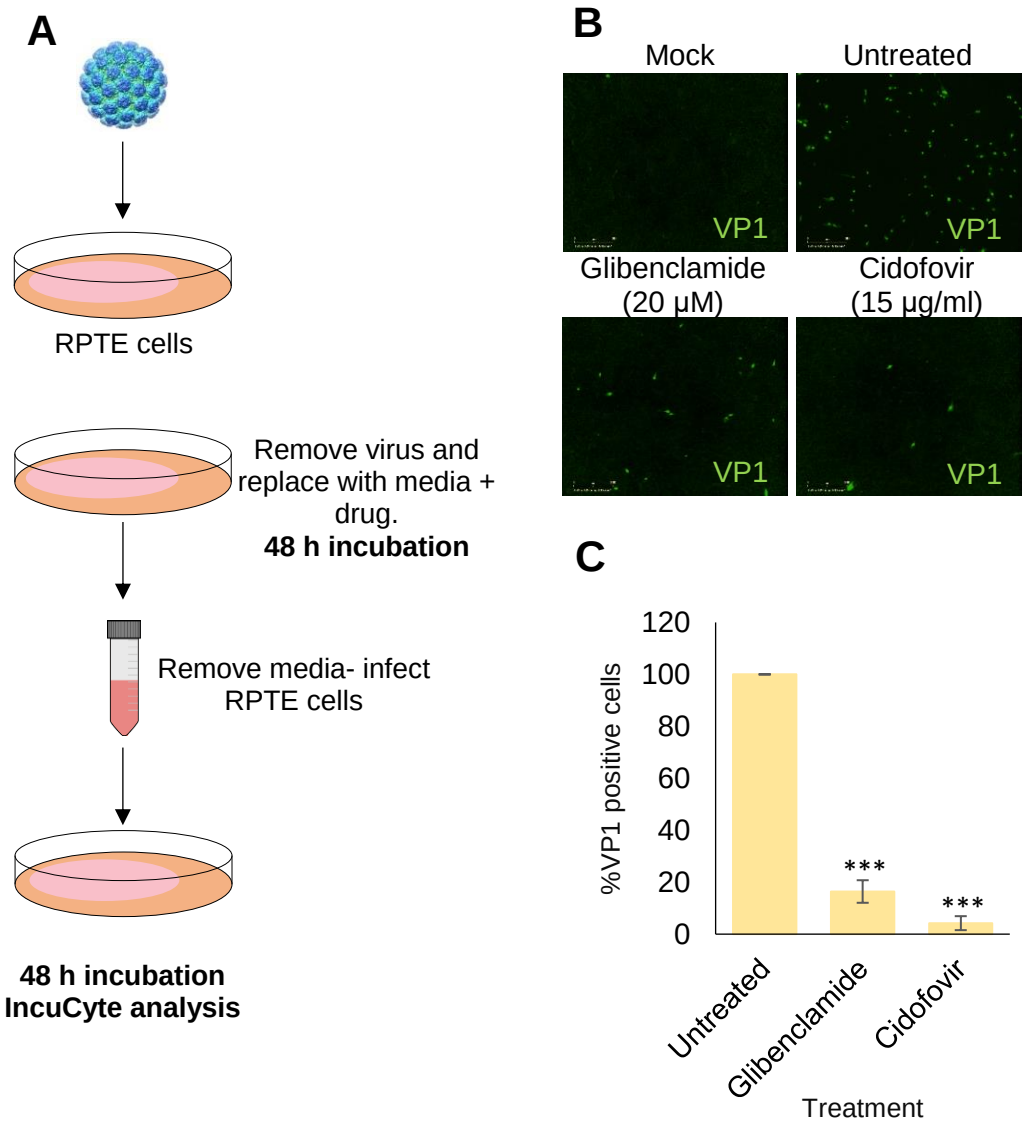

Figure 4. 10 Glibenclamide treatment decreases the titres of released viral progeny. A. Schematic representation of the infection assay. B. RPTE cells were infected with BKPyV at an MOI of 0.5 and treated with 20 µM of Glibenclamide or 15 µg/ml of Cidofovir for 48 hours. Supernatants were collected and used to further infect RPTE cells for 48 hours. Cells were fixed and stained with a primary anti-VP1 (pAb597) (1:250) antibody and a secondary anti-mouse alexa fluor-conjugated 488. BKPyV VP1 protein was used as a marker of BKPyV infection. Subcellular localization of VP1 protein was detected in the nucleus of BKPyV infected cells. C. Positive infected cells were calculated by IncuCyte ZOOM and normalized to the untreated control. Data represent the mean ±SD of positive infected cells (n= 3) (***, significant difference at the $p \leq 0.001$ level).

It is known that Glibenclamide acts as a non-selective inhibitor of ATP-sensitive K^+ channels by binding to SUR subunits. Taken together our pharmacological data, Glibenclamide treatment impacts on the BKPyV life cycle, but not through directly targeting ATP-sensitive K^+ channels. Glibenclamide can inhibit other ABCC transporters, which the SUR subunits belong to. Therefore, the next experimental objective was to test more compounds that target other members of the ABCC subfamily.

4.2.4 CFTR172 impacts on the BKPyV life cycle

The SURs belong to the subfamily ABCC of the ABC-transporters and are involved in several processes, such as neuronal and muscle function and insulin secretion (Dean et al., 2001). Amongst the thirteen ABCC members, the Cystic fibrosis transmembrane conductance regulator (CFTR) is characterized as a chloride (Cl^-) channel permitting the influx and efflux of Cl^- across epithelial cell membranes (Riordan et al., 1989). Mutation or loss of CFTR function is strongly related to a genetic disorder, the Cystic fibrosis (Dean et al., 2001). It is also established that CFTR is abundantly expressed in human renal epithelial cells (Souza-Menezes and Morales, 2009), thus given that CFTR is sensitive to Glibenclamide we focused on studying and investigating a potential implication of CFTR in the BKPyV life cycle.

4.2.4.1 CFTR172 inhibits BKPyV infection in a dose-dependent manner

To examine whether CFTR plays an essential role in the BKPyV life cycle, pharmacological assays were performed. For that reason, RPTE cells were infected with BKPyV (MOI 0.5) for 2 hours at 37^{o}C and then treated with a range of concentrations of CFTR172, which inhibits specifically CFTR, for 48 hours. Treatments of 10 μM, 20 μM, 30 μM, and 40 μM of CFTR172, respectively, were performed. Cells were lysed 48 hours post-infection, and VP1 expression assessed by Western blot analysis. When VP1 expression was assessed ±CFTR172, there was a reduction of VP1 expression, suggesting that CFTR might impede a successful BKPyV infection (Figure 4.11A).

Cell toxicity assays were also performed in order to identify whether this potent effect of CFTR172 was due to loss of cell viability. Results revealed that doses higher than 30 μM of CFTR172 caused a decrease up to 30% of cell viability. Whereas, lower concentration, such as 10 μM and 20 μM of CFTR172, were not toxic to RPTE cells (Figure 4.11B).

A more detailed CFTR172 titration was carried out to identify the minimum concentration at which CFTR172 can inhibit VP1 expression. RPTE cells were infected with BKPyV (MOI 0.5) for 2 hours at 37^{o}C and treated with 1 μM, 2 μM, 4 μM, 6 μM, 8 μM and 10 μM of CFTR172, respectively for 48 hours. Cells were fixed, and BKPyV infection assayed through staining for VP1 as a marker of virus infection. Using IncuCyte ZOOM analysis, an accumulation of VP1 was again observed in the nucleus of infected cells, 48 hours post-infection (Figure 4.11C). Moreover, we demonstrated that at the lowest concentration of CFTR172, 1μM, there was approximately 30% reduction of VP1 expression compared to the untreated control sample. A statistical significant decrease of VP1 was observed upon the gradually higher doses of CFTR172 showing approximately more than 80% decrease of VP1 expression at the highest concentration of 10 μM (Figure 4.11D). Taken together these data suggest that CFTR172 inhibits BKPyV infection in a dose-dependent manner indicating a potential implication of CFTR in the BKPyV life cycle.

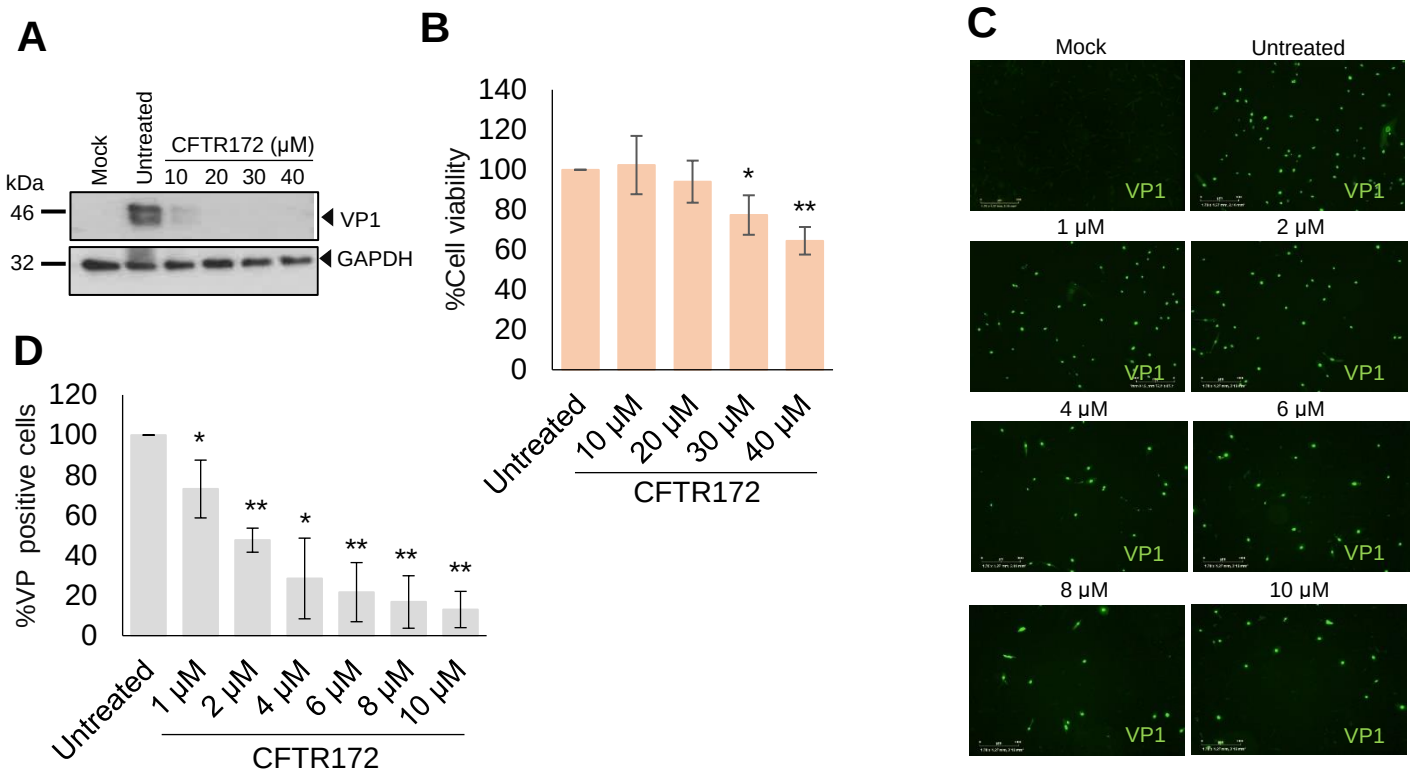

Figure 4. 11 CFTR172 reduces BKPyV infection in a dose-dependent manner. A. RPTE cells were infected with BKPyV at an MOI of 0.5 and treated with 10 μM, 20 μM, 30 μM and 40 μM of CFTR172, respectively for 48 hours. Total protein of cell lysates from infected cells was separated by SDS-PAGE and corresponding blots were probed for VP1 (pAb597) as a BKPyV infection marker, and GAPDH as a loading control. Representative blots are shown from two independent infections. B. RPTE cells were treated as above for 48 hours, and cell viability assessed via MTT assays. Values represent the mean ±SD normalized to the untreated control (n= 3). C. RPTE cells were infected with BKPyV at an MOI of 0.5 and treated with 1 μM, 2 μM, 4 μM, 6 μM, 8 μM and 10 μM of CFTR172, respectively for 48 hours. Cells were fixed and stained with a primary anti-VP1 (1:250) (pAb597) antibody and a secondary anti-mouse alexa fluor-conjugated 488. VP1 protein was used as a marker of BKPyV infection. D. Positive infected cells were calculated by IncuCyte ZOOM and normalized to the untreated control. Data represent the mean ±SD of positive infected cells (n= 3) (*, significant difference at the $p \leq 0.05$ level; **, significant difference at the $p \leq 0.01$ level).

4.2.4.2 CFTR172 inhibits BKPyV production in an MOI-independent manner

Our next experimental objective was to investigate whether the effect of CFTR172 varied depending on the amount of virus that cells were exposed to. To achieve this, RPTE cells were infected with BKPyV at an MOI of 0.5 and 5, respectively, for 2 hours at 37ºC. Following to this, infected cells were treated with 10 µM of CFTR172 for 48 hours and fixed. BKPyV infection assayed through staining for VP1 as a marker of BKPyV production. Using IncuCyte ZOOM analysis, an accumulation of VP1 was observed in the nucleus of infected cells, 48 hours post-infection (Data not shown). Results indicated that CFTR172 had a drastic effect on VP1 levels in an MOI-independent manner, causing ~ 80% reduction of VP1 positive infected cells compared to the untreated control sample (Figure 4.12A and B).

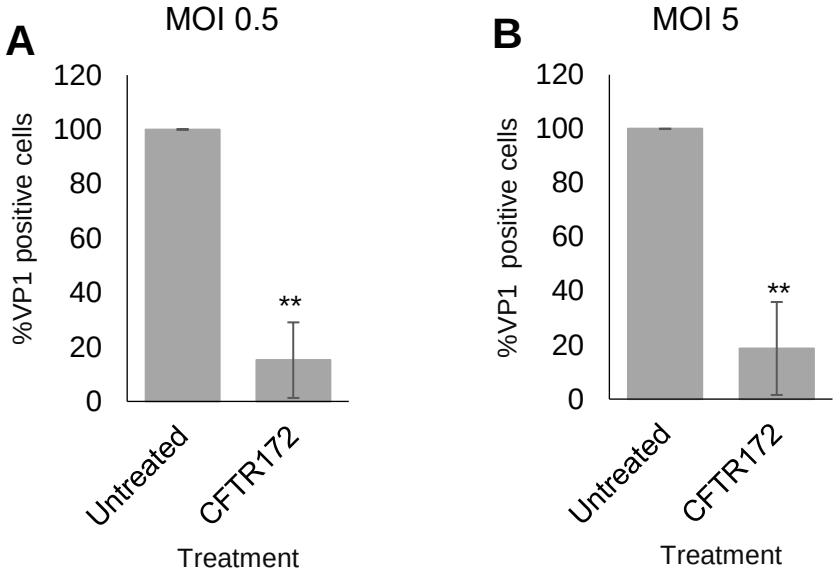

Figure 4. 12 CFTR172 affects BKPyV at an MOI-independent manner. RPTE cells were infected with BKPyV at an MOI of 0.5 (A) or 5 (B), respectively, and treated with 10 µM of CFTR172 for 48 hours. Cells were fixed and stained with a primary anti-VP1 (1:250) (pAb597) antibody and a secondary anti-mouse alexa fluor-conjugated 488. VP1 protein was used as a marker of BKPyV production and positive infected cells were calculated by IncuCyte ZOOM and normalized to the no-drug control. Data represents the mean ±SD of positive infected cells (n= 3) (**, significant difference at the $p \leq 0.01$ level).

4.2.4.3 CFTR172 reduces BKPyV genome replication

Our previous findings suggested that CFTR172 causes a reduction in BKPyV protein expression. Following to this, quantitative PCR analysis was conducted in order to identify whether CFTR172 has an impact on BKPyV genome levels as well. To achieve this, RPTE cells were infected with BKPyV (MOI 0.5) for 2 hours at 37ºC and treated with 10 μM of CFTR172 or 15 μg/ml of Cidofovir, as a positive control sample. Infected and treated cells were incubated for 48 hours prior to total DNA extraction.

Data collected after the quantitative PCR analysis showed that CFTR172 caused a significant decrease on BKPyV genome replication. About 80% decrease of viral genome copy numbers compared to the untreated control sample was observed upon treatment with 10 μM of CFTR172. Cidofovir, the positive control, caused approximately 70% reduction of viral DNA levels (Figure 4.13). Given this, inhibition of CFTR function results in reduction of BKPyV genome replication.

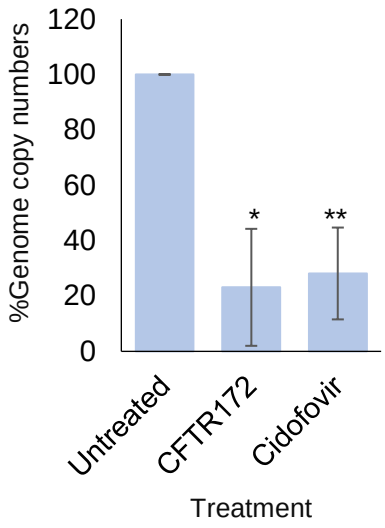

Figure 4. 13 CFTR172 treatment decreases BKPyV genome replication. RPTE cells were infected with BKPyV at an MOI of 0.5 and treated with 10 μM of CFTR172 or 15 μg/ml of Cidofovir. Infected and treated cells were incubated and harvested 48 hours post-infection prior to quantitative PCR analysis. Data represent the mean ±SD of genome copy numbers normalized to the no-drug control from three independent experiments (*, significant difference at the $p \leq 0.05$ level; **, significant difference at the $p \leq 0.01$ level).

4.2.4.4 CFTR172 decreases the titres of the BKPyV released progeny

To determine the impact of CFTR on the released BKPyV viral progeny, infection assays were performed. For that reason, RPTE cells were infected with BKPyV (MOI 0.5) for 2 hours at 37^{o}C and then treated with 10 μM of CFTR172 or 15 μg/ml of Cidofovir, as a positive control, for 48 hours. Collected supernatants from these treatments were utilized to further infect RPTE cells for an additional 48 hour-incubation period (Figure 4.14A). Cells were then fixed, and BKPyV infection assayed through staining for VP1 as a marker of virus production. Data collected following IncuCyte ZOOM analysis indicated that the released viral progeny was infectious since an accumulation of VP1 protein was observed in infected RPTE cells 48 hours post-infection (Figure 4.14B). Interestingly, both agents, CFTR172 and Cidofovir caused a statistical significant reduction of the titres of the synthesized viral progeny. Only 20% of cells were positive for VP1 expression after infections with supernatant from CFTR172 treatment and approximately 10% of cells that were infected with supernatant from Cidofovir treatment, respectively (Figure 4.14C).

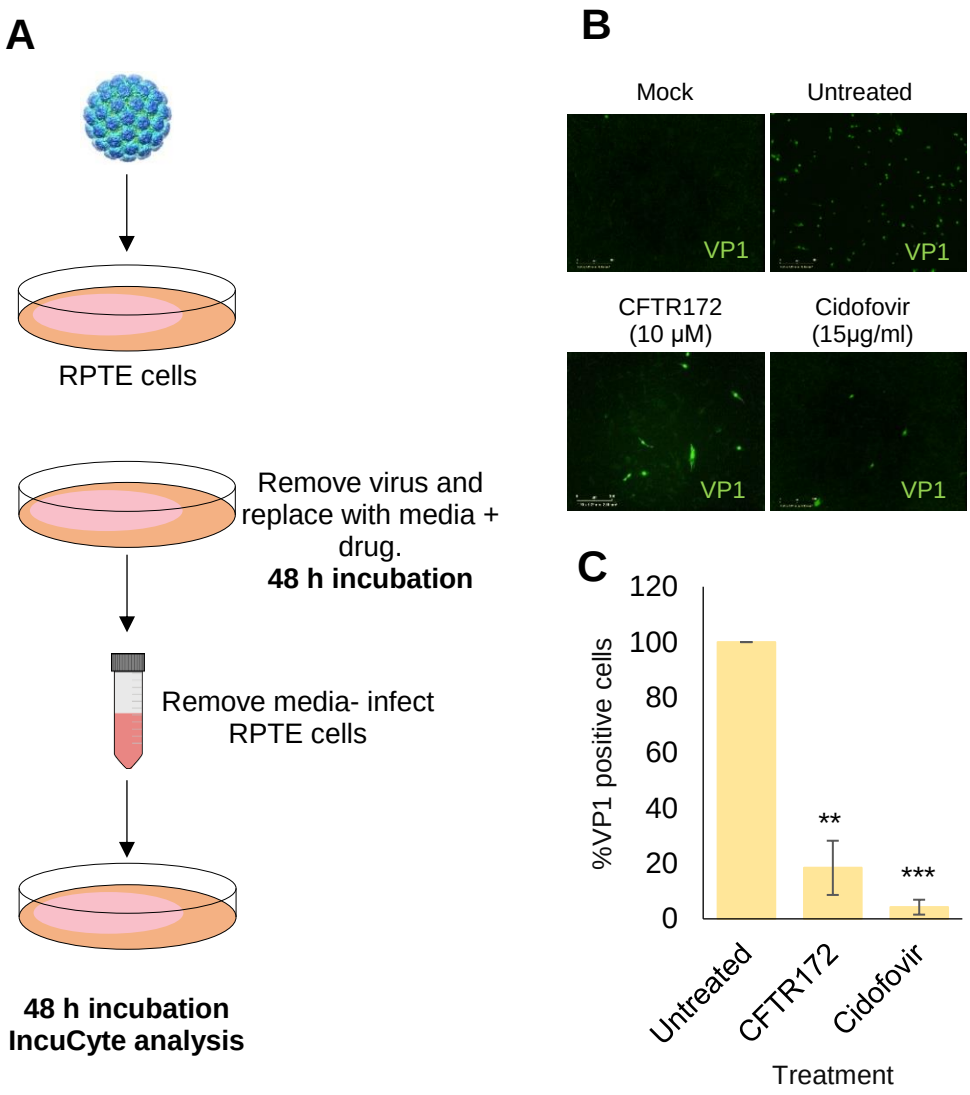

Figure 4. 14 CFTR172 reduces the titres of the released BKPyV progeny. A. Schematic representation of the protocol for infection assays. B. RPTE cells were infected with BKPyV at an MOI of 0.5 and treated with 10 µM of CFTR172 or 15 µg/ml of Cidofovir for 48 hours. Supernatants were collected 48 hours post-infection and used to further infect RPTE cells. Infected cells were incubated for another 48 hours. Cells were fixed and stained with a primary anti-VP1 (1:250) (pAb597) antibody and a secondary anti-mouse alexa fluor-conjugated 488. BKPyV VP1 was used as a marker of BKPyV production. Subcellular localization of VP1 protein was detected in the nucleus of BKPyV infected cells. C. Positive infected cells were calculated by IncuCyte ZOOM and normalized to the no-drug control. Data represent the mean ±SD of positive infected cells (n= 3) (**, significant difference at the $p \leq 0.01$ level; ***, significant difference at the $p \leq 0.001$ level).

4.2.5 ROMK does not affect BKPyV production

The general and canonical ATP-sensitive K^+ channel complex consists of an ABC family member and a K_{ir} family member (Welling and Ho, 2009). It is known that the renal outer medullary K^+ channel (ROMK) is a member of the inward-rectifier K^+ channel subfamily and forms a type of ATP-sensitive K^+ channel with the CFTR subunit (Welling and Ho, 2009). Previous studies have shown that the chemical compound VU591 blocks the function of ROMK (Swale et al., 2015).

Our next experimental objective was to examine whether an ATP-sensitive K^+ channel complex composed by the CFTR and ROMK subunits plays a role in a successful BKPyV infection. To identify the importance of ROMK function for a BKPyV infection, pharmacological analysis was performed using the VU591 modulator. RPTE cells were infected with BKPyV (MOI 0.5) for 2 hours at 37^{o}C and treated with a range of concentrations of VU591 for 48 hours; 5 μM, 10 μM, 15 μM and 20 μM of VU591, respectively. Cells were lysed 48 hours post-infection, and VP1 expression assessed by Western blot analysis. Data showed that there was no effect on VP1 expression upon treatment with 5 μM, 10 μM and 15 μM of VU591, respectively. A decrease of VP1 levels after treatment with the highest concentration of VU591 was observed, although levels of GAPDH were lower in this sample compared to the untreated control sample (Figure 4.15A). To investigate whether VU591 cause a real effect on BKPyV, cell viability assays were performed. RPTE cells were treated under identical treatment conditions prior to toxicity analysis.

Data from toxicity assay revealed that 5 μM and 10 μM of VU591 did not cause any effect on cell viability. However, there was a decrease of cell viability of approximately 40% upon treatment with 20 μM of VU591 (Figure 4.15B). This indicated that the decrease of VP1 expression levels after treatment with 20 μM of VU591 was due to reduction of cell viability. Moreover, VU591 compound at the applied concentration was not able to affect resting membrane potential assessed through DiBAC4(3) fluorescence in RPTE cells (Figure 4.15C). Thus, it is likely that ROMK does not impact on BKPyV production.

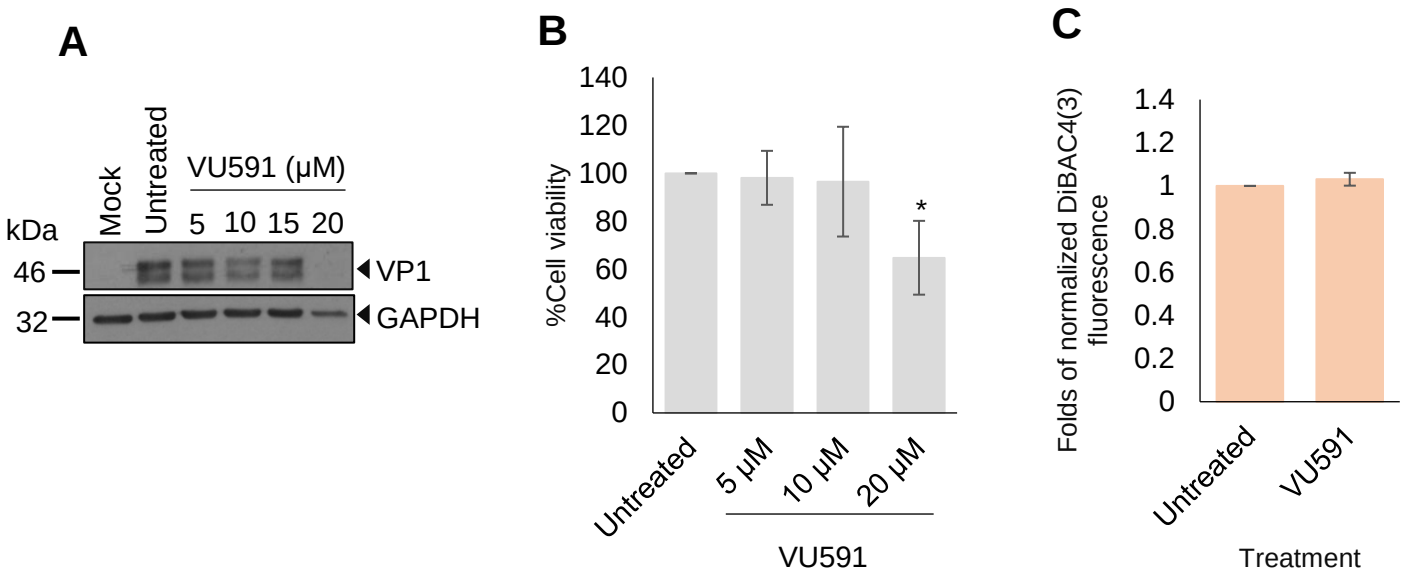

Figure 4. 15 VU591 does not affect a BKPyV successful infection. A. RPTE cells were infected with BKPyV at an MOI of 0.5 and treated with 5 μM, 10 μM, 15 μM and 20 μM of VU591, respectively for 48 hours. Total protein of cell lysates from infected cells was separated by SDS-PAGE and probed for VP1 (pAb597) as a BKPyV infection marker, and GAPDH as a loading control. Representative blots are shown from three independent infections. B. RPTE cells were treated as above for 48 hours and cell viability assessed via MTT assays. Values represent the mean ±SD normalized to the untreated control (n= 3). C. RPTE cells were treated with 10 μM of VU591 and incubated for 48 hours. 20 μM of DiBAC4(3) was added to treated cells and flow cytometry analysis of total cell fluorescence was measured. Values represent the mean ±SD normalized to the untreated control (n= 3) (*, significant difference at the $p \leq 0.05$ level).

4.2.6 BKPyV exploits host ion channels

4.2.6.1 CFTR is required at an early stage of the BKPyV life cycle

Findings from our pharmacological data suggested that CFTR might be important for the establishment of a successful BKPyV life cycle into host cells. To identify at which stage of the virus life cycle, CFTR might play a role, time-of-addition experiments were conducted. To achieve this, RPTE cells were infected with BKPyV at an MOI of 0.5 at 4^{o}C for 2 hours. Cells were placed at 4^{o}C in the presence of virus to achieve a synchronized infection. Following to that period, cells were transferred at 37^{o}C and treated with 20 μM of Glibenclamide or 10 μM of CFTR172 at specific time-points; 0, 12 and 24 hours post-infection, respectively (Figure 4.16A). Infected and treated cells were incubated for a total 48 hour-incubation period before harvesting. To examine whether CFTR channel was required for the initial binding of BKPyV to host cell receptors, treatment under certain conditions was performed. RPTE cells were treated with 20 μM of Glibenclamide or 10 μM of CFTR172 for 1 hour before and during the synchronized infection as well. Then, both compounds were removed and replaced with fresh complete growth media for a total incubation of 48 hours. Cells were lysed, and VP1 expression assessed by Western blot analysis.

Results from Western blotting demonstrated that both Glibenclamide and CFTR172 caused a reduction of VP1 expression during the first 12 hours of the BKPyV life cycle. However, there was no effect when either drug was added at the stage of the binding of BKPyV to host cell receptors, suggesting that CFTR channel is required at an early stage of the life cycle but following virus internalization Figure 4.16B).

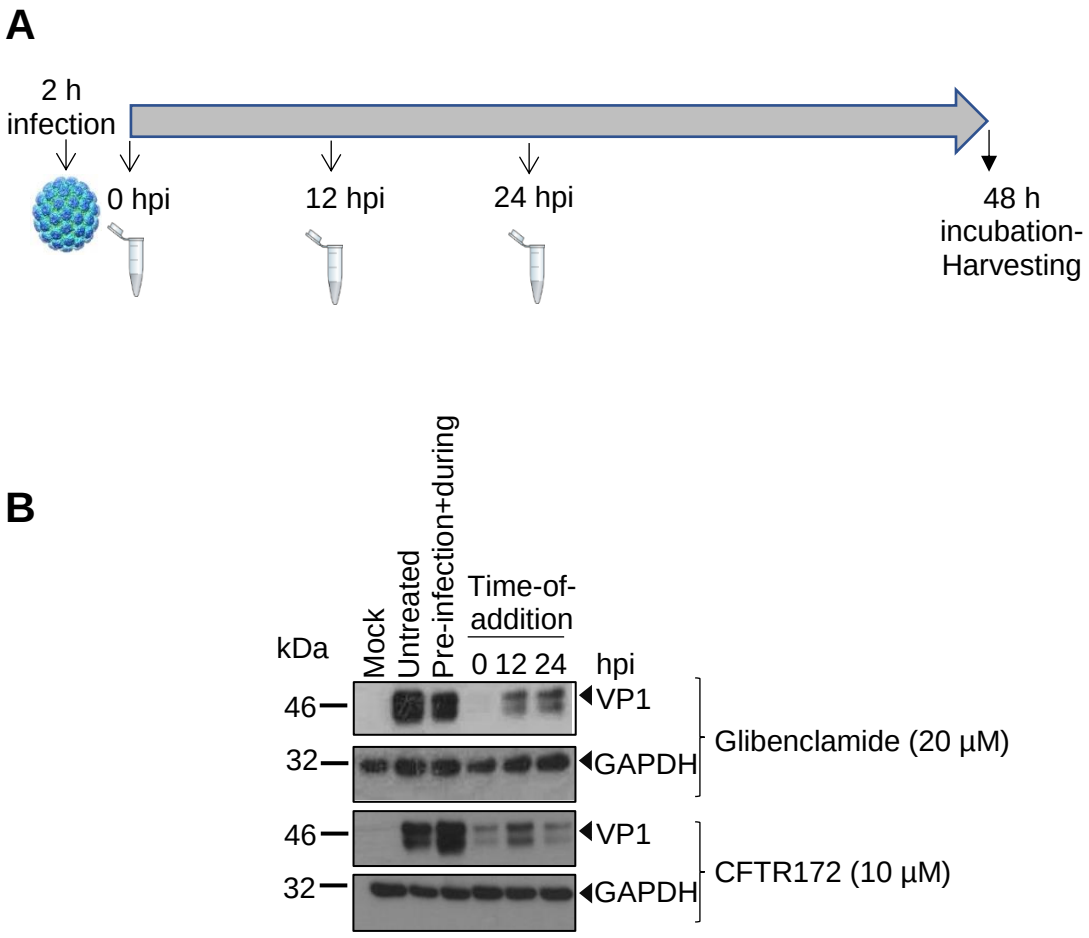

Figure 4. 16 CFTR is required during the first 12 hpi. A. Schematic representation of the treatments performed at the indicated time-points of the life cycle. B. RPTE cells were infected with BKPyV at an MOI of 0.5 for 2 hours at 4ºC and treated with 20 µM of Glibenclamide or 10 µM of CFTR172, respectively, before and during synchronized infection, 0, 12 and 24 hpi, respectively. Infected and treated RPTE cells were incubated for 48 hours in total. Total protein of cell lysates from infected cells was separated by SDS-PAGE and probed for VP1 (pAb597) as a marker of BKPyV infection, and GAPDH as a loading control. Blots are shown from independent infections (Glibenclamide- n= 3; CFTR172- n= 1).

4.2.6.2 CFTR is required at a very early stage of the BKPyV life cycle

Findings from time-of-addition experiments suggested that CFTR plays a critical role for BKPyV infection during the first 12 hours of the life cycle. A more detailed time-course with shorter time-points was performed to identify the specific time-point of the life cycle that CFTR function is essential. For that reason, RPTE cells were infected with BKPyV at an MOI of 0.5 for 2 hours at 4^{o}C to achieve a synchronized infection. Cells were treated with 20 μM of Glibenclamide or 10 μM of CFTR172 at the indicated time-points; 0, 1, 2, 4, 6, 8 and 10 hours post-infection, respectively, and incubated for 48 hours totally before harvesting (Figure 4.17A). Cells were lysed and VP1 expression assessed by Western blot analysis. Data showed that both chemical modulators caused a reduction of VP1 expression during the first 4 hours post-infection. Given this, CFTR is involved in a process occurring at a very early stage and its blockade affects BKPyV infection (Figure 4.17B).

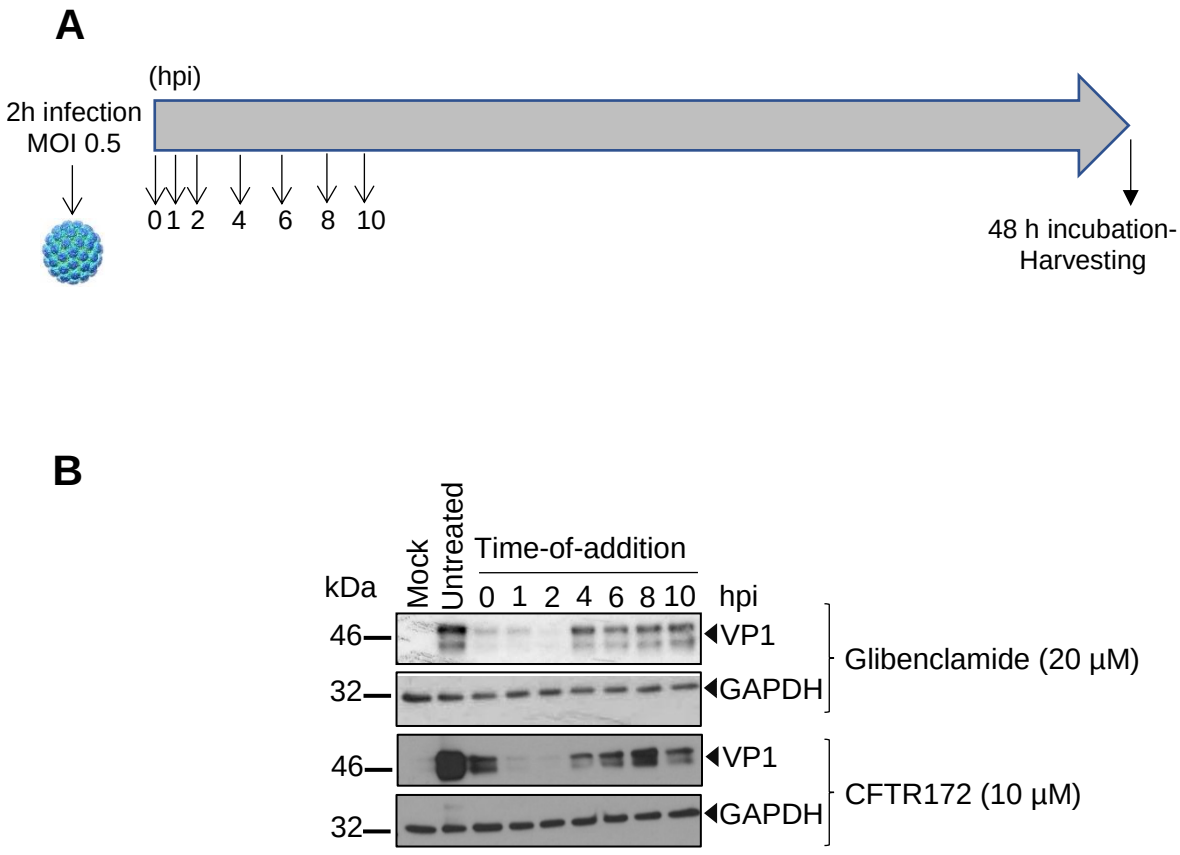

Figure 4. 17 CFTR is required within the first 4 hpi. A. Schematic representation of the treatments that performed at the indicated time-points of the life cycle. B. RPTE cells were infected with BKPyV at an MOI of 0.5 for 2 hours at 4°C and treated with 20 µM of Glibenclamide or 10 µM of CFTR172, at 0, 1, 2, 4, 6, 8 and 10 hpi, respectively. Infected and treated RPTE cells were incubated for 48 hours in total. Total protein of cell lysates from infected cells was separated by SDS-PAGE and probed for VP1 (pAb597) as a BKPyV infection marker, and GAPDH as a loading control. Blots are shown from independent infections (Glibenclamide- n= 3; CFTR172- n= 1).

4.2.6.3 A low-pH step is critical for BKPyV infection

To investigate the intracellular trafficking pathway of BKPyV into RPTE cells, a pharmacological analysis by treating RPTE cells with chemical compounds that are known to block distinct cellular processes was performed. It is known that BKPyV requires a low-pH environment into the host cells for a successful infection (Jiang et al., 2009). The next experimental objective was to determine whether a low-pH microenvironment is essential in the BKPyV life cycle. RPTE cells were infected with BKPyV at two different MOIs; 0.5 and 5, respectively, for 2 hours at 37^{o}C and then treated with 6.25 mM of NH_4Cl for 48 hours. NH_4Cl is a lysosomotropic compound that enters only intracellular compartments with low internal pH and increases the level of pH, disrupting their internal acidification. Cells were then fixed, and BKPyV infection assayed through staining for VP1 as a marker of virus production.

Data following IncuCyte ZOOM analysis revealed that there was a statistically significant reduction of approximately 40% of VP1 positive infected cells upon treatment with NH_4Cl compared to the untreated control, regardless of the amount of virus that cells were exposed to (Figure 4.18A and B). These findings suggest that low pH in intracellular compartments is essential for BKPyV infection irrespective of BKPyV MOIs.

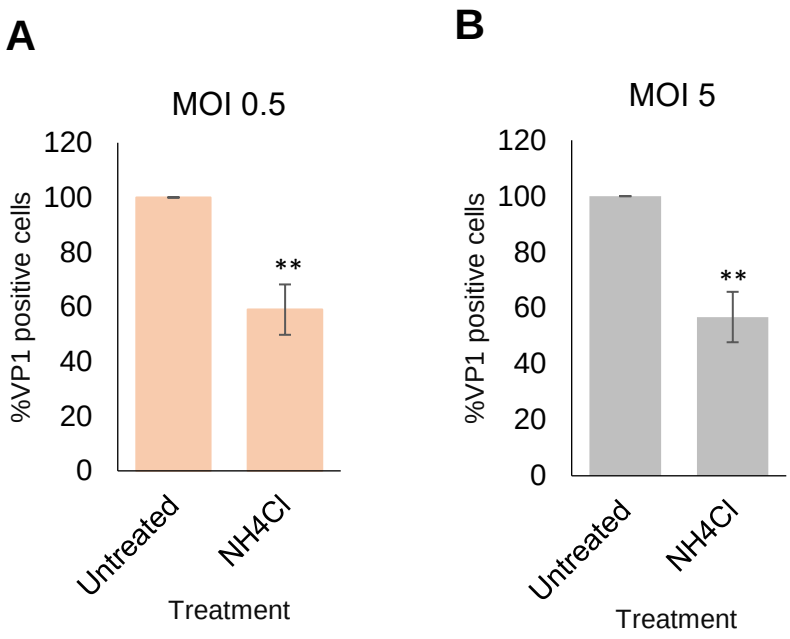

Figure 4. 18 BKPyV requires low-pH for a successful infection in an MOI-independent manner. A. RPTE cells were infected with BKPyV at an MOI of 0.5 (A) or 5 (B) and treated with 6.25 mM of NH_4Cl for 48 hours. Cells were fixed and stained with a primary anti-VP1 (1:250) (pAb597) antibody and a secondary anti-mouse alexa fluor-conjugated 488. BKPyV VP1 was used as a marker of BKPyV infected cells. Positive infected cells were calculated by IncuCyte ZOOM and normalized to the no-drug control. Values represent the mean ±SD of positive infected cells (n= 3) (**, significant difference at the $p \leq 0.01$ level).

4.2.6.4 Low-pH is critical at an early stage of the BKPyV life cycle

To gain a better understanding of the pH-requirement for a successful BKPyV infection, time-of-addition experiments were carried out. To achieve this, RPTE cells were infected with BKPyV at an MOI 0.5 for 2 hours at 4^{o}C to synchronize the infection and entry of the virus was initiated by transferring the cells to 37^{o}C. Following to this, infected cells were treated with 6.25 mM of NH_4Cl at the indicated time-points; 0, 1, 2, 4, 6, 8 and 10 hours post-infection, respectively, and incubated for 48 hours in total prior to harvesting. (Figure 4.19A). Cells were lysed and VP1 expression assessed by Western blot analysis.

Results after Western blotting showed that there was a reduction of VP1 expression upon treatment with NH_4Cl at various time-points throughout the time course. Given the data suggest that the requirement of a low-pH environment is crucial for BKPyV during the early stages of the life cycle (Figure 4.19B).

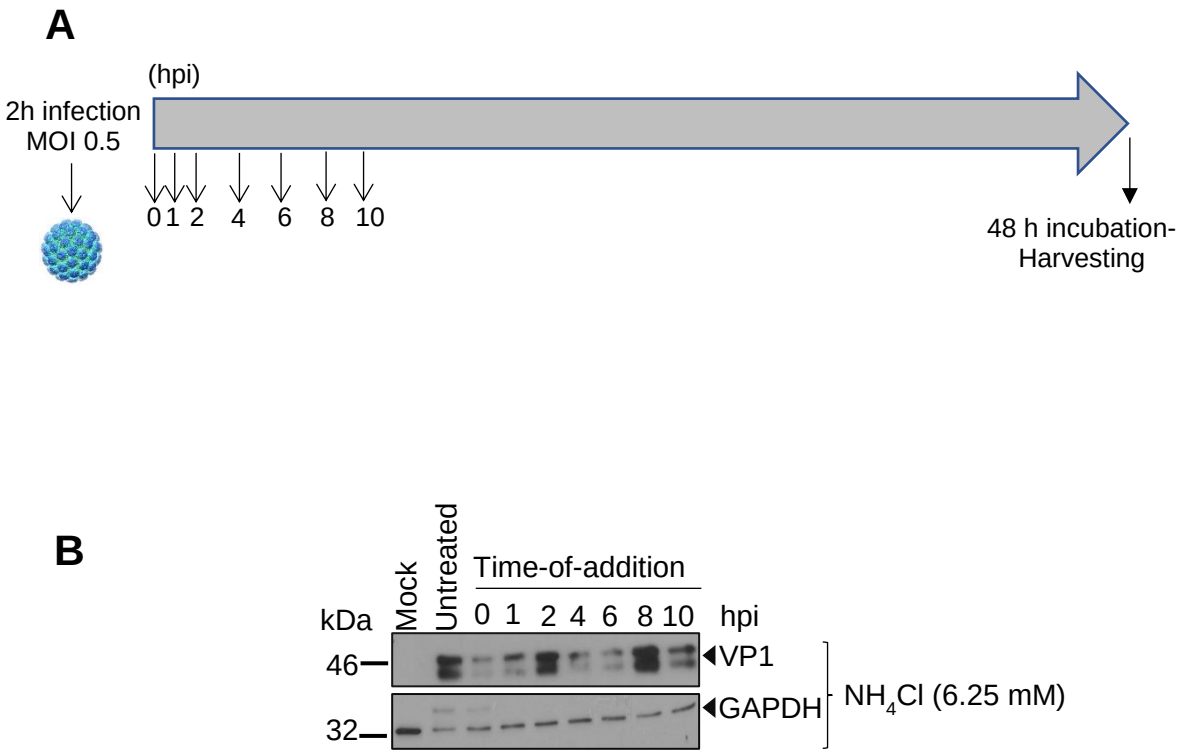

Figure 4. 19 Low pH-environment is required at an early stage of the BKPyV life cycle. A. Schematic diagram of the treatments that performed at the indicated time-points of the life cycle. B. RPTE cells were infected with BKPyV at an MOI of 0.5 for 2 hours at 4ºC and treated with 6.25 mM of NH_4Cl at 0, 1, 2, 4, 6, 8 and 10 hpi, respectively. Infected and treated RPTE cells were incubated for 48 hours in total. Total protein of cell lysates from infected cells was separated by SDS-PAGE and probed for VP1 (pAb597) as a BKPyV infection marker, and GAPDH as a loading control. Representative blots are shown from independent infections (n= 2).

4.2.6.5 CFTR knocked down leads to inhibition of BKPyV production

Based on our pharmacological data, it is proposed that CFTR is involved in the BKPyV life cycle by an unknown mechanism. Molecular-based techniques were performed to validate the implication of CFTR in the virus life cycle. To determine this, RPTE cells were transfected with a pooled siRNA (400 nM), that target specifically CFTR mRNA molecules, and with non-targeting Scramble siRNA molecules, as a negative control. Transfected RPTE cells were incubated for 48 hours at 37^{o}C to ensure that silencing of CFTR successfully occurred. Following to that incubation period, transfected RPTE cells were infected with BKPyV (MOI of 0.5) for 2 hours at 37^{o}C and incubated for a 48 hour-incubation period prior to harvesting.

Isolated total protein from lysates was separated by SDS-PAGE and assayed for VP1, as a marker of BKPyV infection, and CFTR expression by Western Blotting. The corresponding Western blots were probed with a hybridoma polyclonal VP1 antibody, a commercial CFTR antibody and a GAPDH antibody as a loading control. Data revealed that silencing of CFTR mRNA occurred to a certain extend (Figure 4.20A). CFTR expression was reduced by approximately 50% (Figure 4.20B). In parallel, we identified that by knocking down CFTR expression, VP1 expression was also decreased by more than 20% (Figure 4.20A and B). Taken together these data suggest that CFTR is implicated in the BKPyV life cycle and plays a significant role for a successful infection into host cells.

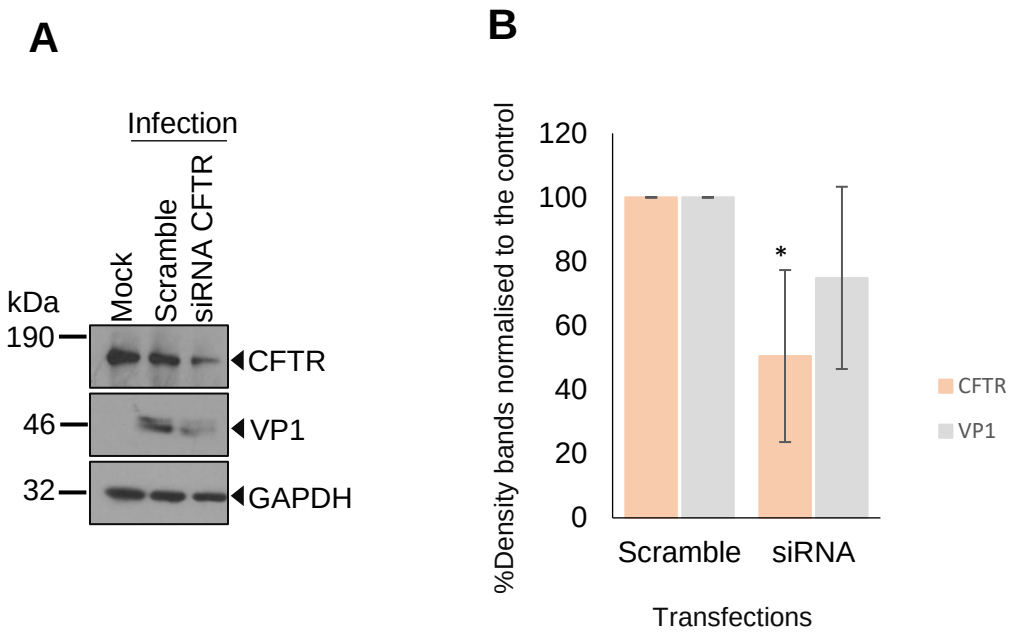

Figure 4. 20 Silencing of CFTR causes reduction of BKPyV infection. A. RPTE cells were transfected with pooled siRNA molecules against CFTR (400 nM) and Scramble siRNAs, as a negative control. Transfected RPTE cells were incubated for 48 hours and then infected with BKPyV at an MOI of 0.5 for 2 hours at 37ºC. Infected RPTE cells were incubated for 48 hours. Total protein of cell lysates from infected cells was separated by SDS-PAGE and probed for VP1 (pAb597) as a marker of BKPyV infection, CFTR, and GAPDH as a loading control. Representative blots are shown from three independent infections. B. Densitometry analysis of Western blots was performed. Values represent the mean ±SD normalized to the Scramble control (*, significant difference at the $p \leq 0.05$ level).

4.3 Discussion

4.3.1 Host cell CFTR is required for a successful BKPyV infection

Ion channels are pore-forming proteins composed of multiple subunits and are located on cellular membranes. It is established that selective influx and efflux of ions across all cell membranes are controlled by ion channels (Yu et al., 2005). Ion channels are expressed in all cell types, both excitable and non-excitable cells and localized on both cell plasma membranes and membranes of intracellular organelles, regulating several functions, including cellular ion homeostasis (Hover et al., 2017). Due to their significant implication in numerous cellular processes, ion channel malfunction can lead to the onset and progression of diseases named channelopathies (Kim, 2014).

Viruses manipulate the intracellular machineries of host cells in order to complete their life cycles; to replicate, release their viral progeny and survive into the host organism. Previous studies have identified that host cell ion channels are manipulated by viruses at different stages of their life cycles (Hover et al., 2017). Therefore, a new strategy to identify novel anti-viral targets is to examine through which mechanism(s) viruses exploit host ion channels and then to validate whether these interactions could be targeted.

Potassium (K^+) channels, were initially identified as the molecular entities that allow the influx and efflux of K^+ across nerve membranes (Miller, 2000). Currently, they have been detected in most cell types of all organisms and are known to control several physiological functions (Miller, 2000). The genomes of humans, *Drosophila*, and *Caenorhabditis elegans* contain 30-100 K^+ channel genes each, and some of these are subject to elaborate alternative splicing (Miller, 2000). Disruption of K^+ channel genes leads to pathologies, including deafness, diabetes, mis-regulation of blood pressure and cardiac arrhythmias (Miller, 2000).

Preliminary data produced in our group suggested that host K^+ channels might be required for a productive BKPyV infection. Thus, the main aim of this Chapter was to identify a potential role of host ion channels in the BKPyV life cycle (Table 4.2). A rational panel of broad spectrum K^+ channel modulators were used to examine the impact of K^+ channel family on BKPyV infection. We identified that upon treatment

with 20 mM of Tetraethylammonium (TEA) there was a significant decrease of BKPyV VP1 expression in infected RPTE cells of approximately 70% (Figure 4.2). Previous studies have shown that extracellular addition of TEA can inhibit K^+ channels by binding in the pore of the channel (Armstrong, 1966; Armstrong and Hille, 1972; Kirsch et al., 1991). K^+ channels are composed by four distinct protein subunits that form a single channel and TEA is able to interact with all of them (Kavanaugh et al., 1992). Thus, based on previous studies and our pharmacological analysis, we speculated that host K^+ channels might be important for a BKPyV infection. It is also reported that Cidofovir can block BKPyV load in RPTE cells in a dose-dependent manner showing a 90% reduction after treatment with 40 µg/ml (Bernhoff et al., 2008). Based on our studies, Cidofovir caused a statistically significant decrease of BKPyV VP1 expression levels in infected RPTE cells supporting previous published findings (Figure 4.2).

A pharmacological analysis was carried out using a panel of modulators that target different subfamilies of the K^+ channel family to identify the candidate family member, which might be required for a successful BKPyV life cycle. Data showed that Glibenclamide caused a decrease of BKPyV VP1 expression (Figure 4.3). Glibenclamide is a clinically available drug that is used as a therapy for diabetes mellitus type 2 and is known as a second-generation sulfonylurea inhibitor (Marble, 1971). Studies have shown that Glibenclamide acts by inhibiting ATP-sensitive K^+ channels located on cell plasma membranes. These are complexes consisted by two types of subunits, the pore-forming subunits which are the inwardly rectifier K_{ir}6.x-type and the sulfonylurea receptors, SURs-type (Ashcroft and Gribble, 1998; Aguilar-Bryan and Bryan, 1999). There are two types of SURs and are classified as members of the ATP-binding cassette protein superfamily (Sakura et al., 1995; Tusnády et al., 1997). SUR1 is predominantly expressed in pancreatic β-cells and in brain, whereas SUR2-type is mainly found in muscles (Sakura et al., 1995). It is known that SUR2 is expressed in two isoforms which they have a 42 amino acid-difference in their last exon. SUR2A is mainly expressed in striated and SUR2B in smooth muscles (Isomoto et al., 1996; Inagaki et al., 1996). Glibenclamide binds to SUR1-type with higher affinity compared to SUR2-type and this is because to a serine in position 1206 in SUR1-type, which is replaced with a tyrosine in the same position in SUR2 (Ashfield et al., 1999).

Barium ions inhibit K^+ channels (Piasta et al., 2011; Neyton and Miller, 1988) and particularly the inwardly rectifying K^+ channels (Alagem et al., 2001). Quayle et al., (1988) stated that there was a voltage-dependent blockade of ATP-sensitive K^+ channels expressed in frog skeletal muscle in the presence of barium ions. However, we interestingly did not detect any effect of $BaCl_2$ on BKPyV VP1 expression at the applied concentration (Figure 4.3). Higher concentrations than 1mM of $BaCl_2$ could not be applied to RPTE cells since $BaCl_2$ was cytotoxic causing approximately 60% decrease of cell viability (Data not shown).

Based on our pharmacological data, we hypothesized that ATP-sensitive K^+ channels might be implicated in the BKPyV life cycle as upon treatment with Glibenclamide there was a reduction of VP1 expression levels. Following to this, other chemical modulators that target the same family member, either by inhibiting or activating it, were also utilized in order to study their effect on a BKPyV infection. Infected RPTE cells were treated with Glibenclamide and Tolbutamide, which is a sulfonylurea compound classified as a first-generation sulfonylurea inhibitor. Interestingly, results from IncuCyte ZOOM analysis revealed that Tolbutamide caused a significant decrease on BKPyV production compared to the no-drug control, but not as potent as Glibenclamide treatment (Figure 4.4). Previous studies have suggested that there is a tissue specificity of sulfonylureas (Gribble et al., 1998; Babenko et al., 1999). It is proposed that ATP-sensitive K^+ channels expressed in cardiac muscles and beta-cells are composed by the same pore-forming subunit, $K_{ir}6.2$, although SUR1-type is expressed in beta-cells and SUR2A-type in cardiac muscles. Tolbutamide could inhibit the function of the $K_{ir}6.2$/SUR1 ion channel complex with high affinity, but not the $K_{ir}6.2$/SUR2A ion channel complex. However, Glibenclamide treatment causes the blockade of both combinations of ion channel complexes with high affinity. These findings could support our data and indicate a potential SUR-type composition of the ATP-sensitive K^+ channel complex that might be expressed in RPTE cells and affect the BKPyV life cycle. Moreover, at the applied concentrations only Glibenclamide could alter resting membrane potential of RPTE cells.

Several studies have shown that 5-Hydroxydecanoate (5HD) is a fatty acid and is characterized as a specific inhibitor of mitochondrial ATP-sensitive K^+ channels (Hanley et al., 2005; Garlid and Halestrap, 2012; Vadzyuk and Kosterin, 2018). Vadzyuk and Kosterin, (2018) stated that 200 μM of 5HD blocked the function of

mitochondrial ATP-sensitive K^+ channels. In our studies, 500 μM of 5HD did not cause any effect on BKPyV VP1 expression in infected RPTE cells, suggesting that mitochondrial ATP-sensitive K^+ channels might not be involved in the BKPyV life cycle, even though this treatment was able to cause a modest change on resting membrane potential (Figure 4.5). Moreover, treatment with U-37883A compound did not have a potent effect on VP1 expression, suggesting that the ATP-sensitive K^+ channel complex that possibly expressed in RPTE cells might not consist of the $K_{ir}6.1$-type subunit (Figure 4.5). Although, U-37883A treatments caused depolarization of plasma membranes suggesting that the compound at the applied concentrations was actually blocking the ion channels composed of the $K_{ir}6.1$-type subunit. Quantitative RT-PCR analysis using specific primers against all the SUR-types and Kir6.x-types of subunits in infected RPTE cells, failed to detect any levels of the canonical subunits of a typical ATP-sensitive K^+ channel (Data not shown).

Given these data, we hypothesized that a non-canonical combination of an ATP-sensitive K^+ channel complex might be expressed in RPTE cells or that Glibenclamide could target another type of host ion channel. For that reason, a more in-depth investigation of Glibenclamide on infected RPTE cells was carried out. We identified that 20 μM of Glibenclamide can cause approximately 90% reduction of VP1 expression in infected RPTE cells without causing any detrimental effect on cell viability (Figure 4.7) and is able to block BKPyV production at an MOI-independent manner (Figure 4.8). Furthermore, Glibenclamide treatment decreases not only BKPyV VP1 expression but also other viral proteins, including VP3, and can reduce viral genome replication by approximately 80% compared to the untreated sample (Figure 4.9). We also showed that Glibenclamide decreases the titres of the released viral progeny by 80% following IncuCyte ZOOM analysis (Figure 4.10). Taken together, we demonstrated that Glibenclamide impacts on a successful BKPyV production in RPTE cells.

Several studies suggested that Glibenclamide acts not only as a non-selective ATP-sensitive K^+ channel blocker, but also as an inhibitor of the cystic fibrosis transmembrane conductance regulator (CFTR) (Sheppard and Welsh, 1992; Sheppard and Robinson, 1997; Melin et al., 2007; Hwang and Kirk, 2013). CFTR is classified as a Cl^- channel, which is controlled by the cAMP-dependent phosphorylation and the intracellular ATP, like the ATP-sensitive K^+ channels

(Sheppard and Welsh, 1992). Both CFTR and SURs belong to the same ABCC subfamily, therefore modulators could act on them in similar ways. Studies have examined the effect of K^+ channel modulators on cells expressing recombinant CFTR (Sheppard and Welsh, 1992; Sheppard and Robinson, 1997; Melin et al., 2007). Both Glibenclamide and Tolbutamide could inhibit the function of CFTR, with Glibenclamide having a greater effect. Also, even though Diazoxide is a well characterized K^+ channel opener, studies have shown that it causes the opposite effect on CFTR as its function was blocked upon treatment with Diazoxide (Sheppard and Welsh, 1992). These studies could also support our findings as shown in Figure 4.6.

Furthermore, quaternary ammonium compounds, including tetraethylammonium ion (TEA) and its derivatives, have been extensively used to identify the implication of K^+ channels in physiological processes in several tissues (Armstrong, 1974; Stanfield, 1983; Hille, 1978). However, not all of the K^+ channels are inhibited by TEA, whilst other non-K^+ channels are blocked in the presence of TEA (Sanchez and Blatz, 1992). Studies have demonstrated that TEA blocks rat neuronal Cl^-- selective channels at concentrations similar to that are used to inhibit K^+ channels (Sanchez and Blatz, 1992; Sanchez and Blatz, 1994). Other studies have reported that Cl^--selective channels of lobster walking nerve have been inhibited upon treatment with TEA (Lukács and Moczydlowski, 1990). It is also reported that a commonly used pharmacological compound to determine the implication of K^+ channels, is the 4-Aminopyridine (4AP), which did not block fast Cl^- channels at concentrations up to 5 mM (Sanchez and Blatz, 1992). Whereas, other derivatives of quaternary ammonium compounds inhibited fast Cl^- channels (Sanchez and Blatz, 1992). Tetra-methylammonium ion (TMA) decreased single Cl^- channel currents at concentrations higher than 100 mM (Sanchez and Blatz, 1992). These findings suggest that a blocking effect by TEA itself, cannot be used as a sufficient indicator of a K^+ channels implication in a process (Sanchez and Blatz, 1992).

Taking account previous studies and our pharmacological data as an overall, Glibenclamide might affect the BKPyV life cycle not through the inhibition of K^+ channels, but rather by blockade of another ion channel, such as CFTR. For that reason, a more-detailed pharmacological analysis was performed using modulators of CFTR in order to study a potential requirement of CFTR in the BKPyV life cycle.

High-throughput screening has identified very potent and selective inhibitors of CFTR including, the thiazolidinone, CFTR172, and the glycine hydrazides, GlyH-101 (Caci et al., 2008; Tang et al., 2009; Linsdell, 2014; Ehrhardt et al., 2016). An in-depth investigation of CFTR172 inhibitor in infected RPTE cells was performed and interestingly we identified that CFTR172 causes similar effects on a BKPyV infection as Glibenclamide. Firstly, we demonstrated that 10 μM of CFTR172 could cause a significant decrease of BKPyV VP1 positive cells and not due to cytotoxicity effect (Figure 4.11). Furthermore, that effect occurred at an MOI-independent way, as is shown in Figure 4.12, following IncuCyte ZOOM analysis. CFTR172 modulator caused a decrease on BKPyV infection not only at a protein level, but also at a DNA level. Approximately 80% reduction of viral genome copy numbers was observed upon treatment with CFTR172 (Figure 4.13). CFTR172 treatment also decreased the titres of the released BKPyV progeny by approximately 80% compared to the no-drug control, as is shown in Figure 4.14. Based on these findings, we suggest that CFTR might be involved in the BKPyV life cycle.

CFTR silencing experiments, using siRNA molecules against CFTR mRNA, showed that by knocking down 50% of CFTR expression, there is a greater than 20% reduction of BKPyV VP1 expression (Figure 4.20). These results strongly support our hypothesis about a CFTR-requirement for a successful BKPyV infection into RPTE cells. In a recent study a high-throughput siRNA screen for BKPyV was performed in order to identify host cell factors that are involved in BKPyV entry and intracellular trafficking (Zhao and Imperiale, 2017). A whole-genome siRNA screen for BKPyV infection was carried out in RPTE cells, utilizing more than 18,000 human siRNA pools. The same host gene was targeted by four unique siRNAs contained in each pool. Data revealed that by targeting CFTR there was an approximately 22.3% decrease of BKPyV infection in its natural host cells (Zhao and Imperiale, 2017). These findings were in agreement with our data supporting the hypothesis that CFTR is required for a successful BKPyV infection in RPTE cells. Although, further investigation is required in order to improve the level of CFTR knocking down, since 50% reduction of protein expression was achieved in this work. Whilst, inhibitors that target specifically CFTR are likely to block all of the CFTR activity in cells and for that reason the effect on BKPyV infection is more profound compared to the data from the silencing experiments.

Another type of ion channel that play significant roles in kidneys is the renal outer medullary K^+ channel (ROMK). ROMK or $K_{ir}1.1$ is a member of the inwardly-rectifier K^+ channels and is an ATP-dependent ion channel that regulates the transportation of K^+ in and out of cells (Welling and Ho, 2009). ROMK can also control K^+ secretion in the cortical collecting duct (CCD) and K^+ recycling in the thick ascending limb (TAL) of the nephron (Ho et al., 1993). Molecular and gene knockout studies suggested that an ABC protein is essential as a co-factor for ROMK. A combination of SUR with ROMK can lead to a weakly inwardly-rectifier ion channel, which is ATP-dependent showing similar properties as the native ion channel complex. However, CFTR is more important than SUR in kidneys and both ROMK and CFTR are expressed in the TAL and CCD membranes (Crawford et al., 1991). As CFTR regulates ROMK and are closely linked, the potential role of ROMK in the BKPyV life cycle was also examined. VU591 is a chemical compound that targets selectively ROMK and was utilized in order to examine a potential requirement of ROMK for a successful BKPyV infection. Infected RPTE cells were treated with VU591, although no effect on BKPyV VP1 was observed after Western blot analysis (Figure 4.15). However, we could not conclude whether ROMK is critical for the BKPyV life cycle, since we provided evidences based on only a pharmacological analysis using one ROMK modulator. Zhao and Imperiale, (2017) performing a whole-genome siRNA screen for BKPyV infection, they indicated that there was an approximately 70% decrease of BKPyV infection by targeting *KCNJ1* (ROMK gene). Therefore, a more detailed investigation is required in order to identify whether CFTR acts synergistically with ROMK in BKPyV infected RPTE cells and are both critical for a BKPyV infection.

Table 4. 2 List of ion channel modulators used in this study. Infected RPTE cells were treated with the following ion channel modulators and their impact on BKPyV life cycle, VP1 protein production, viral progeny, BKPyV genome replication and cell viability are shown below.

Ion channel	Inhibitor	Inhibition of life cycle	BKPyV VP1 protein	BKPyV progeny	BKPyV genome replication	Reduced cell viability
Broad-spectrum K^+ channel	TEA (20mM)	Yes	60% reduction			No
Broad-spectrum K^+ channel	KCl (30mM)	Yes	50% reduction			10% reduction
Broad-spectrum K^+ channel	NaCl (30mM)	No	No			No
Broad-spectrum K^+ channel	Quinidine (50µM)	No	No			25% reduction
Inward-rectifier K^+ channel	$BaCl_2$ (1mM)	No	No			No
Votage-gated K^+ channel	4-Aminopyridine (0.5mM)	No	No			No
ATP-sensitive K^+ channel	Glibenclamide (20µM)	Yes	80% reduction	80% reduction	80% reduction	25% reduction
Ca^{2+}-activated K^+ channel	Apamin (0.5µM)	No	No			10% reduction
ATP-sensitive K^+ channel	Tolbutamide (150µM)	Yes	20% reduction			No
Mitochondrial ATP-sensitive K^+ channel	5-Hydroxydecanoate (500µM)	No	No			10% reduction
Kir6.1 ATP-sensitive K^+ channel	U-37883A (50µM)	No	No			No
ATP-sensitive K^+ channel	Diazoxide (Activator) (50µM)	Yes	Reduction			No
ATP-sensitive K^+ channel	Pinacidil (Activator) (20µM)	No	No			No
CFTR	CFTR172 (10µM)	Yes	80% reduction	80% reduction	80% reduction	Reduction (≥30µM)
ROMK	VU591 (5-20µM)	No	No			Reduction (≥20µM)
Change in pH	NH_4Cl (6.25mM)	Yes	40% reduction			No (Data not shown)
CFTR	siRNA	Yes	>20% reduction			Not tested

4.3.2 CFTR is critical at an early stage of the BKPyV life cycle

BKPyV does not encode polymerases and for that reason is dependent on host cell DNA machinery to replicate its genome and complete its life cycle. BKPyV must enter the nucleus to reach the host DNA replication machinery by travelling through the cytoplasm. As a result, the exploitation of host cell factors is essential for BKPyV (Zhao and Imperiale, 2017). Previous studies have proposed that several host cell factors play significant roles in BKPyV entry into the host cells and the intracellular trafficking. For the initiation of a successful BKPyV infection, BKPyV binds to GD1b or GT1b on host cell membrane and enters host cell (RPTE cells) through a clathrin/caveolin-independent way (Low et al., 2006; Zhao et al., 2016). Following the step of endocytosis, BKPyV enters to endosomes, as other polyomaviruses, in order to traffic through the ER (Querbes et al., 2006; Liebl et al., 2006; Engel et al., 2011; Ashok and Atwood, 2003). An acidic microenvironment and maturation of endosomes are also a critical next step for a BKPyV infection (Jiang et al., 2009) which, in turn, leads to activation of sorting intracellular machinery that includes the recruitment of Rab5, Rab7, Rab9, Rab11 and Rab18 proteins (Liebl et al., 2006; Qian et al., 2009; Engel et al., 2011; Zhao and Imperiale, 2017) Following sorting through the late endosomes, trafficking vesicles reach the ER along with microtubules between 8 to 12 hours post-infection (Eash and Atwood, 2005; Jiang et al., 2009).

To gain a better understanding of the importance of CFTR in the BKPyV life cycle, time-of-addition experiments were carried out. Western blot analysis revealed that upon treatment with both Glibenclamide or CFTR172, there was a decrease of BKPyV VP1 expression during the first 12 hours post-infection and not at a later stage of the virus life cycle or during virus binding/entry (Figure 4.16). These results suggested that host cell CFTR is involved in a process occurred before BKPyV reaches the ER but after initial BKPyV binding and penetration. To have a more in-depth understanding of this time-course, a more detailed time-of-addition assay was performed. Infected RPTE cells were treated with Glibenclamide or CFTR172 at different time-points of this early stage. Western blot analysis indicated that CFTR plays a crucial role during the first 4 hours of the course of infection, since blockade

of CFTR at these time-points caused a decrease of BKPyV VP1 which was recovered upon treatment at later time-points (Figure 4.17).

Previous studies have shown that a low-pH step is essential for BKPyV soon after internalization. It has been reported that acidification occurred in the adenovirus endosomal escape process as well (Jiang et al., 2009; Wiethoff et al., 2005). This acidification facilitates conformational changes of the viral capsid, which leads to further virion disassembly (Jiang et al., 2009). Alternatively, this low-pH microenvironment might be important for BKPyV so as certain proteases to be functional as it was reported during reovirus capsid disassembly (Ebert et al., 2002). To achieve a characterization of the intracellular trafficking pathway of BKPyV in its natural host, a pharmacological analysis was performed by treating infected cells with agents that block distinct cellular processes. Members of the polyomavirus family, including JCPyV and MPyV, require a low-pH step for a successful infection (Ashok and Atwood, 2003; Liebl et al., 2006). However, it is demonstrated that SV40 is not dependent on an acidification step since is known to enter the caveosome, a pH-neutral organelle (Ashok and Atwood, 2003; Pelkmans et al., 2001). Studies have shown that BKPyV infection in Vero cells requires an acidification step (Eash et al., 2004). To identify the pH dependence of a BKPyV infection in RPTE cells, treatment with NH_4Cl was performed. NH_4Cl is known to disrupt the acidification of intracellular compartments. Data revealed that NH_4Cl inhibits BKPyV infection and the inhibitory effect was independent of BKPyV MOIs (Figure 4.18). Similar results were observed when treatments under identical conditions were carried out in previous studies (Jiang et al., 2009), supporting our findings.

To have a better insight into BKPyV trafficking, time-of-addition assays were performed in the presence of NH_4Cl. Treatments were carried out at various time-points post-absorption. Results after Western blot analysis showed that the low-pH requirement occurred early during infection, within the first 8 hours of infection (Figure 4.19). Similar time-of-addition assays have been conducted under identical treatment conditions in previous studies. The low-pH requirement occurred very early during infection, between the first 2 hours of BKPyV infection. Beyond this time-point, NH_4Cl was no longer able to block BKPyV infection (Jiang et al., 2009). These findings are partially in agreement with our proposed time-course since the inhibitory effect was observed at later time-points as well (Figure 4.19).

Electron microscopy studies have shown that BKPyV is localized in caveosome-like vesicles (Drachenberg et al., 2003). Moreover, colocalization of caveolin 1, which is the main component of caveosome, with labelled BKPyV (Moriyama et al., 2007), suggest that BKPyV enters caveosome, which is a pH-neutral compartment, en route to the nucleus (Pelkmans et al., 2001). The colocalization of BKPyV and caveolin 1 peaks at about for 4 hours post-infection according to Moriyama et al., (2007), therefore an acidic endosomal/lysosomal compartment is likely to be involved in BKPyV transportation before entering the caveosome. Taken together previous studies and our time-of-addition assays, we suggest that CFTR is required at an event that occurs at a very early stage of the BKPyV life cycle, which coincides with the stage that acidification occurs. In addition to this, studies have reported that CFTR is critical for vesicular acidification since it counteracts proton pumps in endosomes and facilitates further acidification (Bradbury, 1999), which also support our hypothesis about the CFTR requirement for a productive BKPyV infection.

Previous studies have demonstrated that host ion channels are involved in virus intracellular trafficking and particularly in the critical step of vesicles acidification (Hover et al., 2016). A member of K^+ channel family, K_{2P} is required for a successful bunyavirus (BUNV) infection. Time-of-addition assays indicated that K^+-sensitive steps are critical within the first 6 hours post-infection without including the initial virus binding/penetration or later stages of the virus life cycle including the mRNA transcription and translation (Hover et al., 2016). This implicated the functionality of host K^+ channels during BUNV transportation through the endocytic pathway (Hover et al., 2016). A more recent study revealed that BUNV traffics through endosomes containing high [K^+], which impacts on virions infectivity (Hover et al., 2018). Moreover, blockade of K^+ channels may lead to alteration of K^+ distribution across the endosomal system, which results in arrest of BUNV trafficking in endosomes (Hover et al., 2018). Other studies have also indicated that endosomal pH and [K^+] are critical for an influenza A virus (IAV) infection (Stauffer et al., 2014). There is a K^+ gradient from the intracellular to extracellular environment and the [K^+] is increased with trafficking along the intracellular endocytic pathway (Scott and Gruenberg, 2011). Thus, a decrease of pH and a gradual change in the overall ionic milieu in endocytic vesicles were critical for an IAV infection (Stauffer et al., 2014).

Here, we show for the first time that BKPyV requires cellular CFTR channels to infect its natural host, RPTE cells. Time-of-addition assays revealed that CFTR is critical for the virus during a very early stage of the BKPyV life cycle after virus penetration, but before BKPyV reaches the nucleus. It was also determined that a low-pH step, occurring within the initial hours post-infection, is critical for the BKPyV life cycle. Accumulating evidences suggest that host ion channels control the overall ionic milieu and pH of endocytic vesicles, indicating their importance. Several viruses exploit host ion channels in order to facilitate their trafficking along the endocytic network. Therefore, a more in-depth investigation is required to dissect the exact mechanism(s) by which CFTR impacts on the BKPyV life cycle in RPTE cells.

4.3.3 CFTR inhibitors as potential therapeutics against BKPyV

To this date, the cornerstone of PVAN therapy is the reduction of immunosuppressive regimen, indicating the importance of host's immune system to battle the reactivation of BKPyV in renal transplant recipients (Thangaraju et al., 2016; Wojciechowski and Chandran, 2016). Unfortunately, tailoring of immunosuppression leaves the risk of kidney acute rejection (Johnston et al., 2010). Currently, there is no clinical evidence to support any particular treatment against PVAN, although many approaches are suggested based on evidenced anti-viral activity *in vitro* (Lamarche et al., 2016). Several of the current therapeutic regimens have been characterized as highly nephrotoxic and have not been undergone clinical trials. Hence, there is an urgent need to identify novel anti-viral drugs to treat PVAN, without risking a transplant acute rejection.

Here, we reported for the first time the requirement of host cell CFTR for a successful BKPyV infection in its natural host, RPTE cells, *in vitro*. For the first time, it is reported that Glibenclamide, a clinically available drug, inhibits BKPyV infection. Glibenclamide is a sulfonylurea anti-diabetic drug for type 2 diabetes (Balsells et al., 2015) and is an intermediate-acting drug with its active metabolites to be eliminated by the liver by approximately 50% (Jönsson et al., 1994; Jönsson et al., 1998). It does not exhibit any severe side effects and the mechanism of its action as an anti-diabetic implicates the direct secretory effect on the pancreatic islet beta-cells. Glibenclamide treatment

causes the closing of ATP-sensitive K^+ channels on the cell membranes of pancreatic beta-cells, which leads to depolarization and opening of voltage-dependent Ca^{2+} channels. Therefore, Ca^{2+} influx is mediated which results in subsequent stimulation of insulin release (Aguilar-Bryan et al., 1995).

Moreover, studies have shown that the potency and pharmacological properties of other CFTR inhibitors, including CFTR172, and their efficacy in various pre-clinical models, support further development for therapy of Polycystic Kidney Disease (PKD) and enterotoxin-mediated secretory diarrheas (Verkman et al., 2013). Accumulating evidence suggest that CFTR is the major apical membrane Cl^- pathway in secretory diarrheas caused by the bacterial enterotoxins released in cholera and Travelers' diarrhea (Field, 1979; Venkatasubramanian et al., 2010). *In vivo* studies have reported that dosage of µg of CFTR172 can block intestinal fluid secretion in a rat-model (Ma et al., 2002) and in mice (Thiagarajah et al., 2004) indicating a potential novel treatment for secretory diarrheas. PKD is one of the most common human genetic diseases and is the main cause of chronic kidney failure. In PKD massive enlargement cysts filled with fluid are observed, which ultimately result in destruction of normal renal tissue progressively (Torres et al., 2007). The cyst growth implicates fluid secretion into the cyst lumen and alterations in morphology of surrounding epithelial cells, which express CFTR and are of tubular origin (Brill et al., 1996). Studies have identified that CFTR172 completely blocked the growth of cysts in mouse embryonic kidney cyst models (Yang et al., 2008).

In this work, we identified that two CFTR inhibitory compounds block the BKPyV life cycle at a very early stage, *in vitro*, by a yet unknown mechanism which might implies on intracellular vesicular acidification. CFTR172 has potential clinical applications and Glibenclamide is already a clinically available drug. Thus, we suggest at least one potential therapeutic agent pharmacologically safe for a potential PVAN treatment.

5 Polyomaviruses and host ion channels

5.1 Introduction

5.1.1 Investigation of polyomavirus' life cycles

It is of great importance to study human polyomaviruses as primary infection is usually asymptomatic, although under certain circumstances including immunosuppression, severe diseases can occur. Two major examples are JCPyV/BKPyV-associated diseases and Trichodysplasia Spinulosa (TS), a rare skin disease that occurs in immunosuppressed patients infected with Trichodysplasia Spinulosa virus (TSPyV). Some polyomaviruses have been reported to encode oncogenic proteins and are therefore linked with human cancers. Merkel cell polyomavirus (MCPyV) for example, was first detected in individuals with an aggressive malignant skin cancer, Merkel cell carcinoma (Feng et al., 2008).

JCPyV is closely related to BKPyV and SV40 showing approximately 70-80% homology in the coding regions, however regulatory non-coding regions are considerably divergent (Frisque and White, 1992). Studies have shown that the variation in the regulatory region determines the tissue or species specificity of each polyomavirus (Bollag et al., 1989; Haggerty et al., 1989). Epidemiological studies have identified seven types of JCPyV, each with multiple subtypes which are linked with distinct human populations (Cubitt et al., 2001). JCPyV is the causative agent of PML, a clinical complication that cause visual deficit, cognitive impairment and motor dysfunction. This severe disease progresses slowly causing death within 4-6 months, although symptoms may vary due to the different size and location of the lesion (Major, 2011; Saribas et al., 2011). PML is characterized by progressive damage or inflammation of the white matter of the brain and occurs amost exclusively in patients with sever immune deficiency, including AIDS sufferers, individuals receiving chemotherapy and other patients suffering from autoimmune diseases (Major, 2011).

MCPyV was first identified in 2008 (Feng et al., 2008) using digital transcriptome subtraction (Feng et al., 2007) and its viral genome shares higher similarities with the African Green Monkey lymphotropic polyomavirus, although it is classified in the *Alphapolyomavirus* genus which includes mammalian virus species (Calvignac-Spencer et al., 2016). MCPyV is strongly correlated with a rare but malignant and aggressive form of skin cancer, Merkel cell carcinoma (MCC) (Arora et al., 2012; Spurgeon and Lambert, 2013). MCC is mainly diagnosed in the elderly receiving immunomodulatory therapies, such as transplant recipients and AIDS sufferers (Engels et al., 2002). MCPyV is mainly detected on human skin, however the mode of virus transmission is unclear (Schowalter et al., 2010). Two mutational events are critical for MCPyV induced MCC. Firstly, the MCPyV genome is integrated into the host. Secondly, mutated TAg is unable to initiate DNA replication due to the loss of helicase function (Shuda et al., 2008).

SV40 or simian vacuolating virus 40 causes a lifelong infection in rhesus macaque monkeys and was first discovered in 1960 (Sweet and Hilleman, 1960). SV40 causes an asymptomatic infection in immunocompetent rhesus monkeys, but causes a severe disease in immunosuppressed monkeys. Primary kidney cells extracted from rhesus macaques were used to manufacture inactivated polio vaccines in the 1950s. During the process of the inactivation, SV40 was more resistant than poliovirus and as a result, polio vaccines were contaminated with live SV40 stocks. Several million people worldwide, were vaccinated with these polio vaccines and exposed to SV40 inoculum (Shah and Nathanson, 1976). The correlation of SV40 and tumour formation in humans is a controversial research area and there is no strong epidemiological evidence that implicates SV40 in cancer development (Strickler et al., 1998). However, SV40 genomic sequences have been detected in several tumour types in humans such as mesotheliomas, brain tumours, lymphomas and osteosarcomas (Bergsagel et al., 1992; Pepper et al., 1996; Wong et al., 2002). It is suggested that the prevalence of SV40 tumour positivity may be variable due to the differing sources and geographical areas of specimens (Butel, 2012).

5.1.2 Chapter Aims

In our previous studies, host factors required during a BKPyV infection were investigated. Use of the inhibitors Glibenclamide and CFTR172 led to a significant decrease of both viral proteins and DNA levels, suggesting that CFTR plays a critical role during the BKPyV life cycle. Based on the pharmacological data, CFTR was observed as required during an early event of an infection, following binding and initial entry of BKPyV into the host cells but prior to virus reaching the nucleus. Thus, CFTR modulation was revealed as a druggable target to inhibit the BKPyV entry process.

BKPyV is classified as a member of the *Betapolyomavirus* genus that also includes JCPyV and SV40, which cause severe clinical complications (Calvignac-Spencer et al., 2016). Moreover, MCPyV is an emerging pathogen which is strongly associated with a malignant form of cancer (Arora et al., 2012; Spurgeon and Lambert, 2013). Therefore, there is also a need to identify therapeutics, which target specifically these viruses. In the previous Chapter, we demonstrated a potential druggable target to block the BKPyV life cycle in its natural host cells, thus the effects of CFTR modulation on JCPyV, SV40 and MCPyV were investigated and described in this Chapter.

5.2 Results

5.2.1 Examination of CFTR expression in different cell lines

It was first necessary to confirm that CFTR is expressed in cells that are susceptible to infection by the viruses under investigation. Cell lysates from RPTE, Vero, HEK293TT and SVG-A cells were produced and CFTR expression assessed by Western blot analysis. Human primary renal proximal tubular epithelial (RPTE) cells were used in pharmacological analysis as is the most physiologically relevant cell line to study the BKPyV life cycle, but they can also be used to investigate the SV40 life cycle. Vero cells are kidney cells extracted from the African green monkey and utilized as a commonly used cell line as previous studies have suggested that are susceptible to infection by both BKPyV and SV40. Moreover, human embryonic kidney cells (HEK293TT) were utilized to determine the impact of CFTR modulation on MCPyV infection, as they are one of the few cell lines that can be efficiently transduced with VLPs. In addition, human foetal glial cells (SVG-A) were used to investigate the JCPyV life cycle as they are the most physiologically relevant cell line to its natural host cells.

The corresponding Western blots were probed with a CFTR antibody and GAPDH as a loading control. An approximate 165 kDa band was identified in all samples presenting the CFTR expression (Figure 5.1). The expression levels of CFTR were comparable across the different cell lines, although lower levels were observed in RPTE cells. In addition to this, lower expression levels of GAPDH were detected in the same sample suggesting that less total protein was loaded from RPTE sample (Figure 5.1-Lane 1). These results suggest that all tested cell lines display CFTR expression providing the potential to target CFTR function during virus infection of these cultured cell lines.

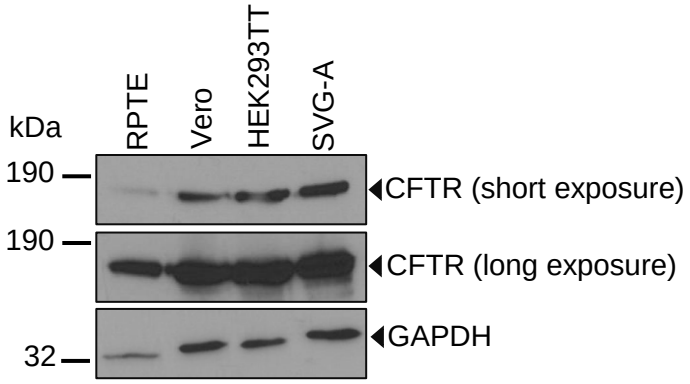

Figure 5. 1 CFTR expression in different cell lines. RPTE, Vero, HEK293TT and SVG-A cells were lysed, and total protein from cell lysates was separated by SDS-PAGE. CFTR and the loading control GAPDH were detected for each cell line by Western blot analysis. Blots are shown (n= 1).

5.2.2 Generation of crude JCPyV and SV40 virus

5.2.2.1 Enzymatic digestions and re-ligation of the JCPyV genome

Appropriate preparation of JCPyV genome was necessary in order to generate infectious JCPyV that could be used in subsequent experiments. Approximately 10 µg of pBR322 Mad-1 JCPyV plasmid was digested with the EcoRI-HF and re-ligated by the T4 DNA ligase following the same methodology as previously described (see Section 3.2.1.1) for the preparation of the BKPyV genome. Digested products were run on 0.8% agarose gels and separation of the JCPyV genome from the backbone plasmid DNA was confirmed (Figure 5.2A). It was also identified that the JCPyV genome was separately re-ligated from the backbone plasmid DNA (Figure 5.2B).

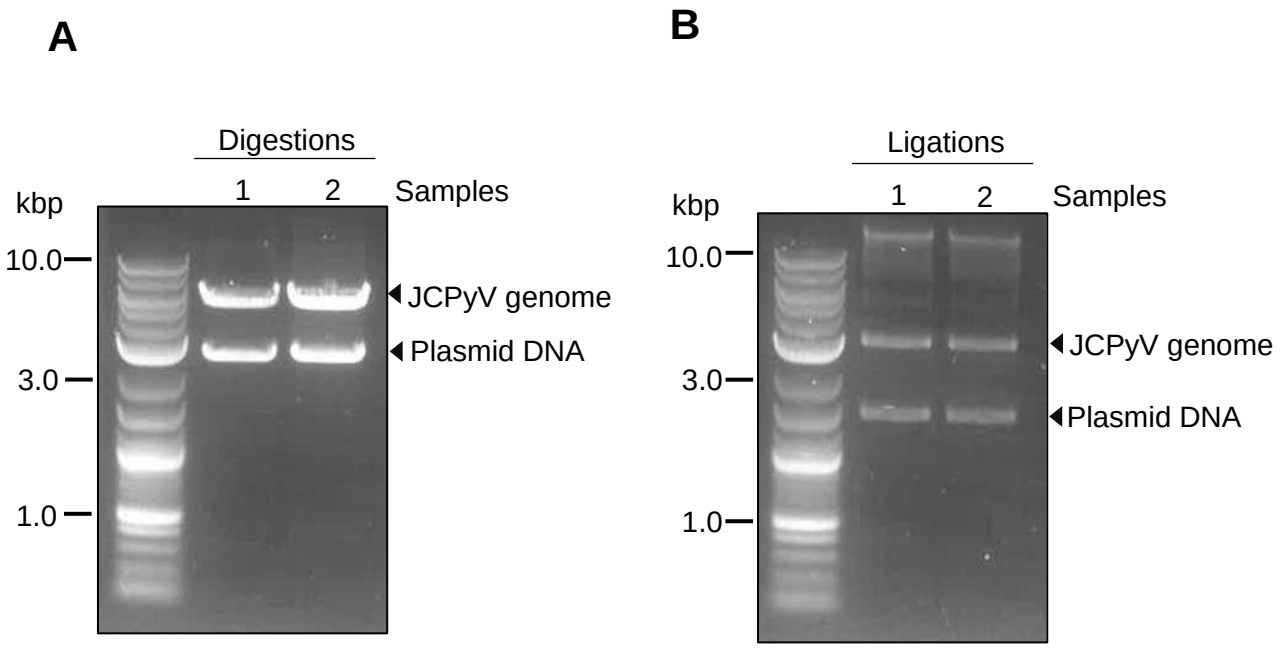

Figure 5. 2 Digestions and ligations of JCPyV genome. A. Two independent digestions of pBR322 Mad-1 JCPyV plasmid (10 µg each) were loaded onto a 0.8% agarose gel and run for 40 minutes at 80 V. Lane 1: 6 µl of DNA ladder 1 kb; Lane 2, 3: 6 µl of digested pBR322 Mad-1 JCPyV plasmid. B. Re-ligated products were loaded onto a 0.8% agarose gel and run for 40 minutes at 80 V. Lane 1: 6 µl of DNA ladder 1 kb; Lane 2, 3: 6 µl of purified and ligated products (n= 2).

5.2.2.2 Transfection of the JCPyV genome into SVG-A cells

The methodology to generate an infectious JCPyV stock is summarized in Figure 5.3A. Initially, 8 µg of re-ligated JCPyV genome was transfected into SVG-A cells using Lipofectamine 2000 in a ratio 1-part of DNA: 2-parts of Lipofectamine (see Section 2.4.2) and incubated for a total 20 days. Cell supernatants were collected, cells lysed and stored for the analysis of intracellular and secreted viral proteins. The major capsid protein, VP1, was used as a marker of infection.

Cell pellets were lysed, and total protein was separated by SDS-PAGE. Released proteins in media samples were also separated by SDS-PAGE. The corresponding Western blots were probed with a hybridoma VP1 antibody and with a GAPDH antibody as a loading control. The presence of VP1 in every sample of cell pellets was confirmed showing a clear band at the expected molecular weight of approximately 42 kDa (Figure 5.3B). However, secreted VP1 protein was not detected in cell supernatants (Data not shown).

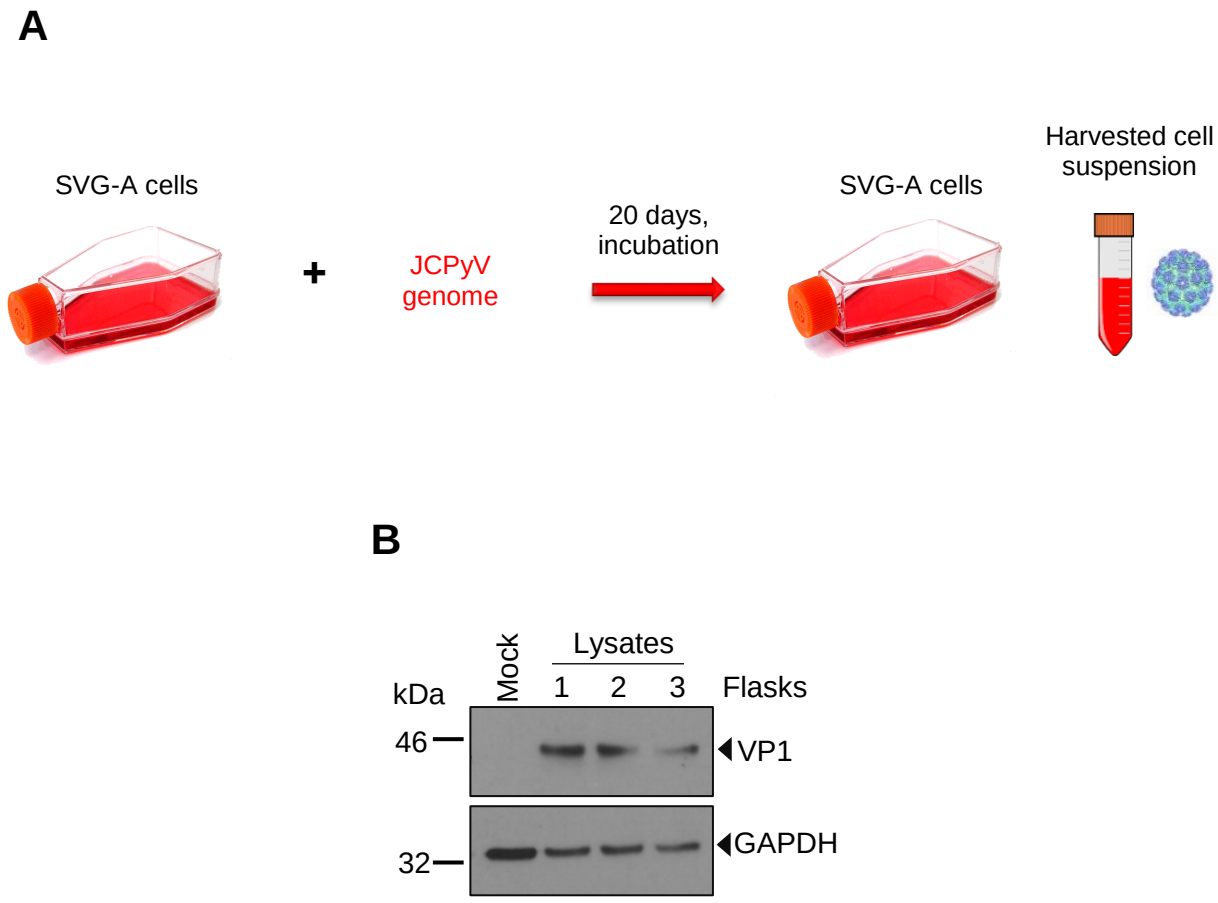

Figure 5. 3 JCPyV production in SVG-A cells. A. Schematic representation of the JCPyV production protocol. SVG-A cells were transfected with 8 µg of JCPyV genome and incubated for 20 days. B. Total protein of cell lysates from transfected cells was separated by SDS-PAGE and probed for VP1 (pAb597) as a marker of JCPyV transfection, and GAPDH as a loading control. Representative blots are shown from 3 flasks of transfected SVG-A cells (n= 2).

5.2.2.3 Digestions and re-ligation of the SV40 genome

Preparation of the SV40 genome was performed to generate infectious stock that could be used in virus assays. Initially, 4 µg of pUC-SV40 was digested with the restriction enzyme KpnI-HF and re-ligated by the T4 DNA ligase following the same methodology as previously described (Section 3.2.1.1) for the preparation of the BKPyV genome. Digested products were run on 0.8% agarose gels and bands were visualized under UV to confirm that the SV40 genome was separated from the backbone plasmid DNA (Figure 5.4). Re-ligated products were purified by ethanol precipitation, quantified using a spectrophotometer and run on 0.8% agarose gels. Bands were visualized under UV light to confirm that SV40 genomes were re-ligated from the backbone plasmid DNA (Figure 5.4).

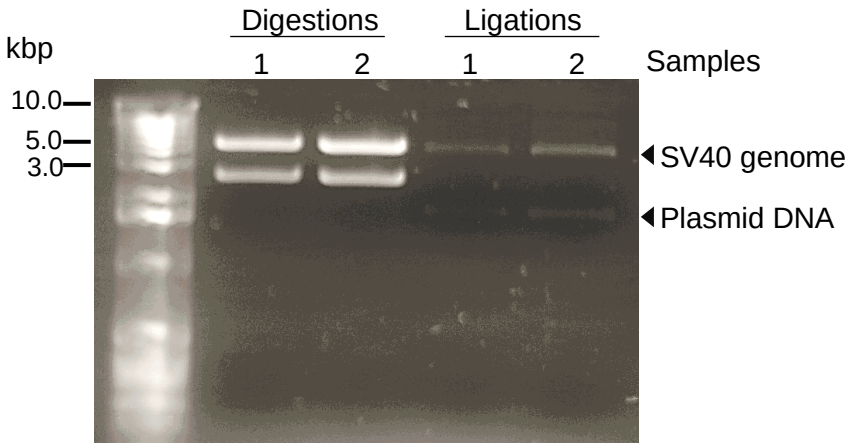

Figure 5. 4 Preparation of SV40 genomes. Two independent digestions (4 µg each) and re-ligations of pUC-SV40 plasmid were loaded onto a 0.8% agarose gel and run for 40 minutes at 80 V. Lane 1: 6 µl of DNA ladder 1 kb; Lane 2, 3: 6 µl of digested pUC-SV40 plasmid. Lane 4, 5: 6 µl of purified and ligated products.

5.2.2.4 Transfections of SV40 genomes into Vero cells

To generate an infectious SV40 stock, Vero cells were transfected with 4 µg of re-ligated SV40 genomes, using the NanoJuice transfection kit in a ration 1-part of DNA: 2-parts of Core reagent: 3-parts of Booster (see Section 2.4.3) and incubated for 7 days (Figure 5.5A). Cell suspensions were collected, and cells were lysed for the assessment of intracellular and extracellular VP1 expression as an indicator of virus production. VP1 expression was confirmed in cell lysates and supernatants of transfected cells as indicating the presence of intracellular and secreted virus (Figure 5.5B).

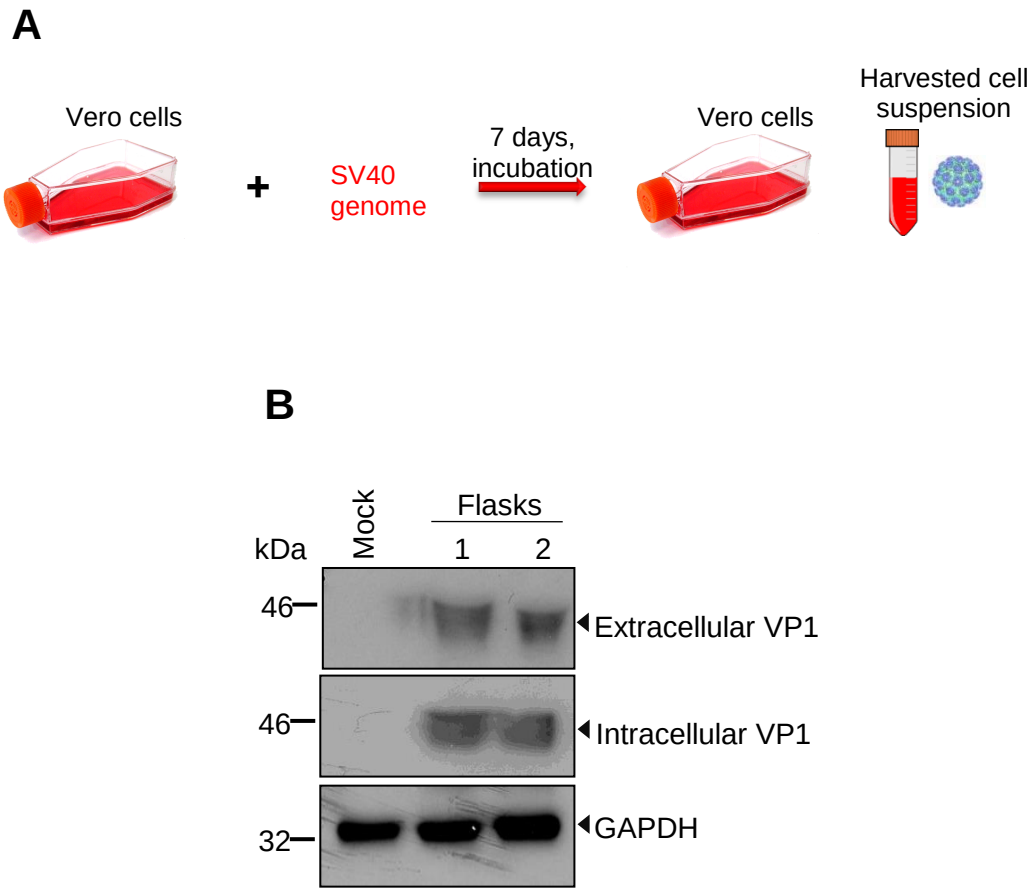

Figure 5. 5 SV40 production in Vero cells. A. Schematic representation of the SV40 production protocol. Vero cells were transfected with 4 µg of SV40 genome and incubated for 7 days. B. Total protein of cell lysates and supernatants collected from transfected cells was separated by SDS-PAGE. VP1 (pAb597) expression was assessed as a marker of SV40 transfection. GAPDH was probed as a loading control. Representative blots are shown (n= 3).

5.2.3 CFTR ion channel is required for a successful JCPyV infection

Previous studies demonstrated a requirement for the CFTR channel during the BKPyV life cycle. It was therefore investigated whether this requirement was also essential for a closely related polyomavirus, JCPyV. JCPyV infectious supernatants were generated and human foetal glial cells (SVG-A cells) were infected with JCPyV at an MOI of 0.5 for 2 hours at 37^{o}C. Following infection, cells were treated with 20 μM of Glibenclamide or 10 μM of CFTR172 for a total of 5 days post-infection. Cells were lysed and JCPyV infection assessed through the expression of VP1. Both CFTR modulators decreased VP1 protein expression compared to no-drug controls, with CFTR172 causing a greater decrease in virus infections (Figure 5.6A). CFTR172 caused approximately 40% reduction of VP1, whilst Glibenclamide led to a 30% decrease in VP1 expression (Figure 5.6B). The concentrations that were inhibitory to JCPyV did not cause any effect on cell health when assessed via cell viability assays (Figure 5.6C). Taken together, these data suggest that CFTR dependence is conserved during the BKPyV and JCPyV life cycles into their natural host cells, respectively.

To support the pharmacological data, the effects of Glibenclamide on the resting membrane potential of SVG-A cells was investigated, DiBAC4(3) was added to SVG-A cells treated with 20 μM of Glibenclamide for 5 days and DiBAC4(3) fluorescence assessed by flow cytometry. Glibenclamide led to a depolarization of plasma membrane evidenced by the 0.4-fold increase in fluorescence observed following drug treatments, compared to no-drug controls (Figure 5.6D). These results indicate that Glibenclamide treatment leads to depolarization of SVG-A cells.

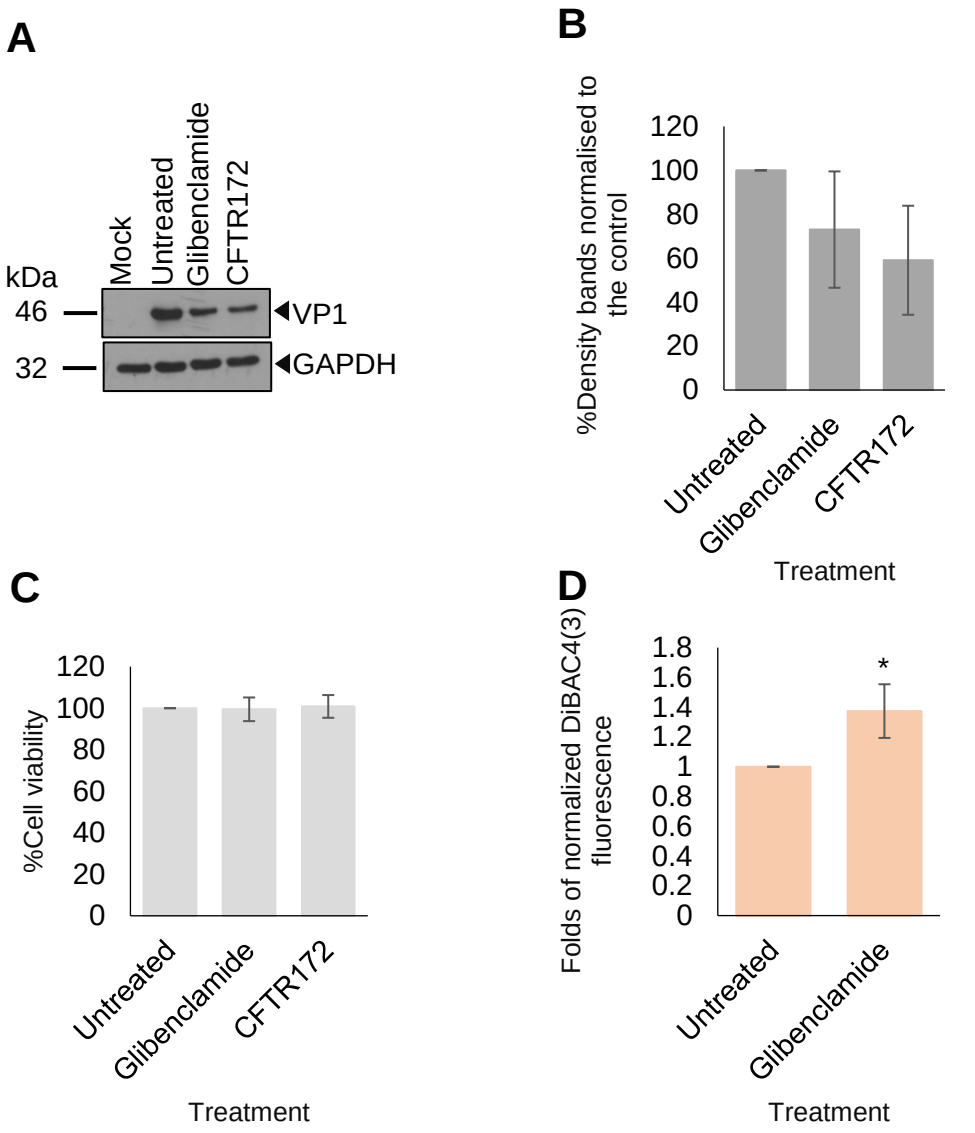

Figure 5. 6 CFTR inhibition reduces JCPyV infection. A. SVG-A cells were infected with JCPyV at an MOI of 0.5 and treated with 20 μM of Glibenclamide or 10 μM of CFTR172 for 5 days. Total protein of cell lysates from infected cells was separated by SDS-PAGE and probed for VP1 (pAb597) as a marker of JCPyV infection, and GAPDH as a loading control. Representative blots are shown from three independent infections. B. Densitometry analysis was performed of Western blots. Values represent the mean ±SD normalized to the no-drug control (n= 3). C. SVG-A cells were treated as above, and cell viability assessed via MTT assays. Values represent the mean ±SD normalized to the no-drug control (n= 3). D. SVG-A cells were treated with 20 μM of Glibenclamide and incubated for 5 days. 20 μM of DiBAC4(3) was added to treated cells and flow cytometry analysis of total cell fluorescence was measured. Values represent the mean ±SD normalized to the untreated control (n= 3) (*, significant difference at the $p \leq 0.05$ level).

5.2.4 Role of CFTR channel during SV40 and BKPyV infection of Vero cells

To determine if there was also a role for the CFTR channel during the SV40 life cycle, we first studied infection of Vero cells, which are a cell line routinely used in the study of BKPyV and SV40. For this reason, Vero cells were infected with SV40 at an MOI of 0.5 for 2 hours and subsequently treated with 20 μM of Glibenclamide or 10 μM of CFTR172 for 48 hours. Cells were then fixed, and SV40 infection assayed through staining for VP1 as a marker of virus production. Using IncuCyte ZOOM analysis, an accumulation of VP1 was observed in the nucleus of infected cells, 48 hours post-infection, the expression of which was unaffected by Glibenclamide and approximately 10% reduced by CFTR172 treatment (Figure 5.7A). Since functional analysis of CFTR has not been performed in Vero cells, it was important to confirm the impact of CFTR modulation in this cell line. To achieve this, the anti-BKPyV activity of Glibenclamide or CFTR172 was re-assessed in Vero cells. Cells were infected with BKPyV (MOI of 0.5) for 2 hours and then treated with Glibenclamide or CFTR172 under identical conditions. Cells were lysed 48 hours post-infection, and VP1 expression assessed by Western blot analysis. When VP1 expression was assessed ± CFTR modulation, no impact on VP1 expression upon treatment with the modulators was observed (Figure 5.7C). Thus, it is likely that the CFTR is not an essential host factor for BKPyV/SV40 infection of Vero cells.

Cell toxicity was also assayed in Vero cells, which were treated with 20 μM of Glibenclamide or 10 μM of CFTR172. Treated cells were incubated for 48 hours before the MTT analysis. Since both drugs did not have any effect on VP1 expression, data as it was expected indicated that both CFTR modulators did not have an effect on cell viability (Figure 5.7D).

Given these data, the ability of Glibenclamide to influence the resting membrane potential of Vero cells was investigated. Vero cells were treated with 20 μM of Glibenclamide for 48 hours and DiBAC4(3) was added to treated cells. Flow cytometry analysis revealed that Glibenclamide retained the ability to cause depolarization of Vero cells as evidenced by the 0.3-fold increase in fluorescence in Glibenclamide treated cells compared to no-drug controls (Figure 5.7E). These results indicate that whilst Glibenclamide can modulate ion channel function in Vero cells, the

Glibenclamide sensitive channels are not required for SV40/BKPyV production in this cell line.

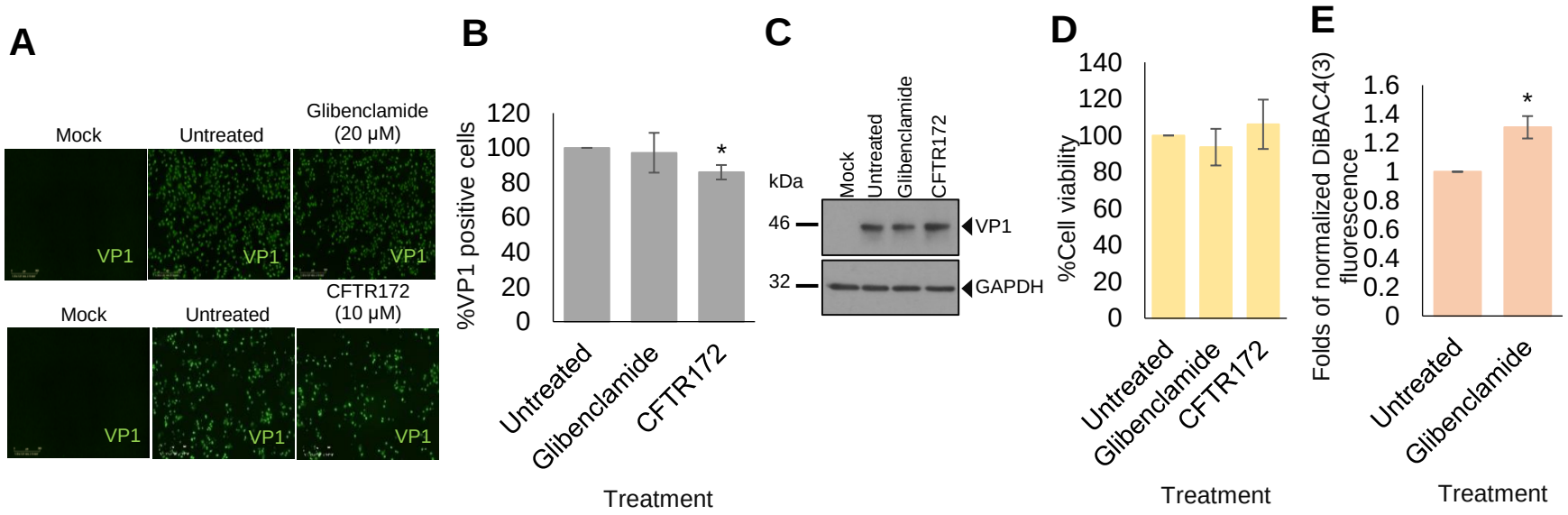

Figure 5. 7 CFTR inhibition does not reduce SV40 or BKPyV infection of Vero cells. A. Vero cells were infected with SV40 at an MOI of 0.5 and treated with 20 μM of Glibenclamide or 10 μM of CFTR172 for 48 hours. Vero cells were fixed and stained with a primary anti-VP1 (1:250) (pAb597) antibody and a secondary anti-mouse alexa fluor-conjugated 488. SV40 VP1 was used as a marker of SV40 infection. Subcellular localization of VP1 protein was detected in the nucleus of SV40 infected cells. B. Positive infected cells were calculated by IncuCyte ZOOM and normalized to the no-drug control. Values represent the mean ±SD of positive infected cells (n= 3). C. Vero cells were infected with BKPyV at an MOI of 0.5 and treated with 20 μM of Glibenclamide or 10 μM of CFTR172 for 48 hours totally. Total protein of cell lysates from infected cells was separated by SDS-PAGE and probed for VP1 (pAb597) as a BKPyV infection marker, and GAPDH as a loading control. Representative blots are shown from three independent infections. D. Vero cells were treated as above, and cell viability assessed via MTT assays. Values represent the mean ±SD normalized to the no-drug control sample (n= 3). E. Vero cells were treated with 20 μM of Glibenclamide and incubated for 48 hours. 20 μM of DiBAC4(3) was added to treated cells and flow cytometry analysis of total cell fluorescence was measured. Values represent the mean ±SD normalized to the no-drug control (n= 3) (*, significant difference at the $p \leq 0.05$ level).

5.2.5 Role of CFTR ion channel during SV40 infection of RPTE cells

Given the surprising lack of effects of CFTR modulation in Vero cells, we next tested whether CFTR was required during SV40 infection of primary human RPTE cells. Cells were infected with SV40 at an MOI of 0.5 for 2 hours and 20 μM of Glibenclamide or 10 μM of CFTR172 added to infected cells for a further 48 hours. Cells were fixed, and SV40 infection assayed through staining for VP1 as a marker of virus production using IncuCyte ZOOM analysis. SV40 VP1 staining was again observed in the nucleus of infected cells, 48 hours post-infection (Figure 5.8A). Interestingly, an approximate 40%-50% reduction of VP1 expression was observed upon treatment with Glibenclamide or CFTR172, respectively, compared to no-drug control sample (Figure 5.8B). Glibenclamide was also confirmed to cause membrane depolarization assessed through DiBAC4(3) fluorescence in these cells (Figure 5.8C). Taken together, these data suggest that host cell CFTR channels are similarly required for SV40 infection in RPTE cells.

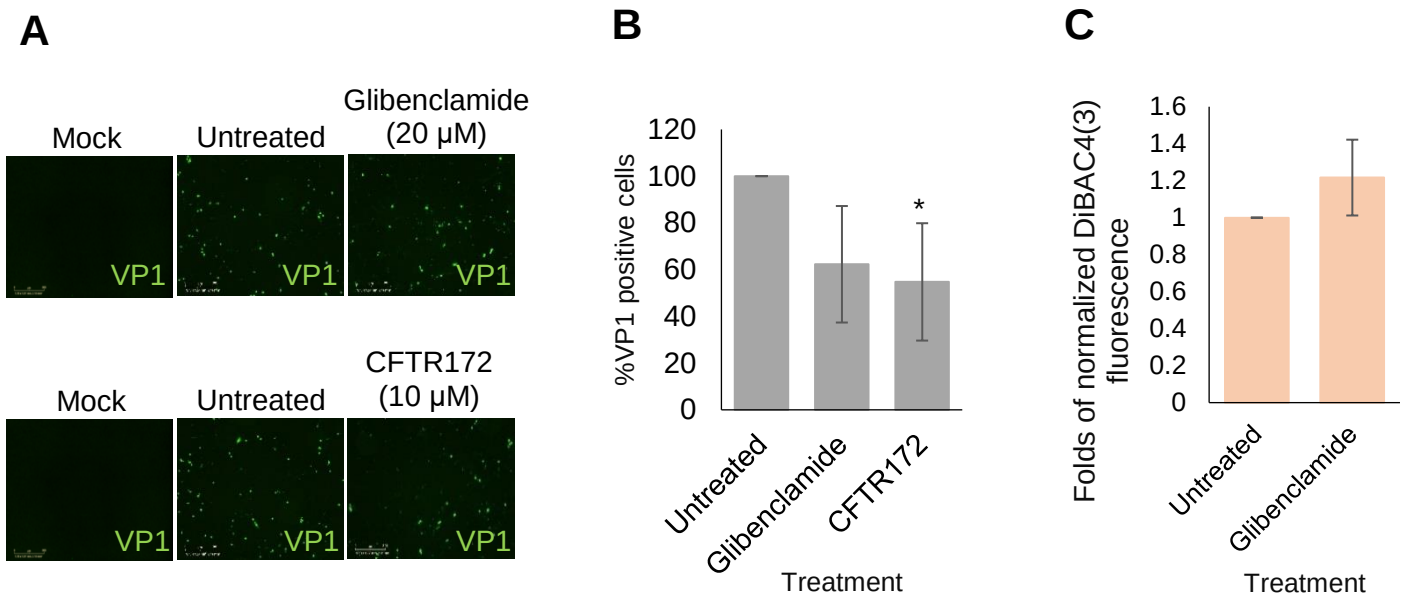

Figure 5. 8 CFTR blockade decreases SV40 infection of RPTE cells. A. RPTE cells were infected with SV40 at an MOI of 0.5 and treated with 20 μM of Glibenclamide or 10 μM of CFTR172 for 48 hours. RPTE cells were fixed and stained with a primary anti-VP1 (1:250) (pAb597) antibody and a secondary anti-mouse alexa fluor-conjugated 488. SV40 VP1 was used as a marker of SV40 infection. Subcellular localization of VP1 protein was detected in the nucleus of SV40 infected cells. B. Positive infected cells were normalized to the no-drug control sample. Values represent the mean ±SD of positive infected cells (n= 3). C. RPTE cells were treated with 20 μM of Glibenclamide and incubated for 48 hours. 20 μM of DiBAC4(3) was added to treated cells and flow cytometry analysis of total cell fluorescence was measured. Values represent the mean ±SD normalized to the untreated control (n= 3) (*, significant difference at the $p \leq 0.05$ level).

5.2.6 Role of CFTR channel during SV40 and BKPyV infection of HEK293TT cells

To identify the effect of CFTR modulation on SV40 infection, HEK293TT cells were infected with SV40 (MOI of 0.5) and treatments of 20 μM of Glibenclamide or 10 μM of CFTR172 were performed. Cells were lysed, total protein was separated by SDS-PAGE and probed for SV40 VP1 as previously described. In the HEK293TT cell system, neither Glibenclamide or CFTR172 influenced VP1 protein expression differing from the data obtained from primary RPTE cells (Figure 5.9A). Thus, in contrast to primary kidney models, SV40 infection does not require functional CFTR channels in HEK293TT cells.

To confirm drug activity in HEK293TT cells, BKPyV infection assays were performed in the presence of Glibenclamide or CFTR172. HEK293TT cells were infected with BKPyV (MOI of 0.5) for 2 hours in the presence of both CFTR modulators and VP1 expression assessed by Western blot analysis from cell lysates 48 hours post-infection. VP1 expression decreased by approximately 50% in the presence of CFTR172, whilst a more modest decrease of approximately 10% of VP1 expression was observed upon treatment with Glibenclamide, compared to no-drug controls (Figure 5.9B and C). Cell viability assays in these cell lines confirmed that the reduction in VP1 expression was not due to cell toxicity, as cell viability was unaffected in both treatment conditions (Figure 5.9D). Furthermore, Glibenclamide led to depolarization of the HEK293TT cell membrane to levels consistent with those observed in Vero/RPTE cells (Figure 5.9E). These results indicate that CFTR modulation can regulate ion channel function in HEK293TT cells, but CFTR channel influences only BKPyV production and not SV40 in this cell line.

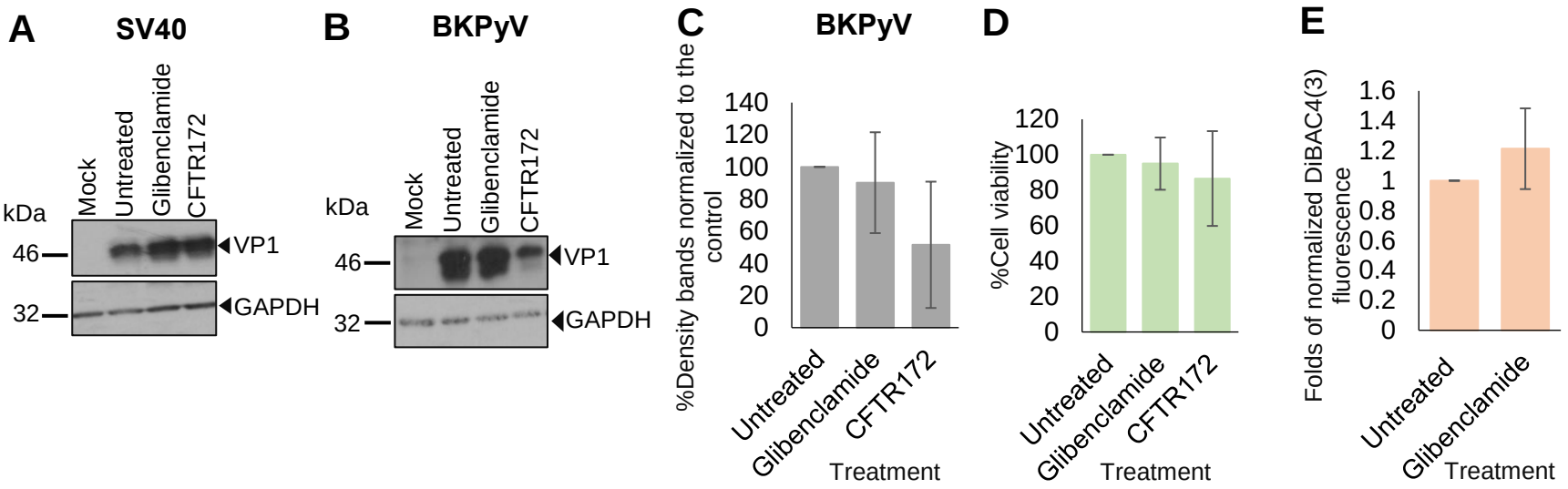

Figure 5. 9 CFTR is required for a successful BKPyV infection but not for an SV40 infection of HEK293TT cells. A. HEK293TT cells were infected with SV40 at an MOI of 0.5 and treated with 20 μM of Glibenclamide or 10 μM of CFTR172 for 48 hours. Total protein of cell lysates from infected cells was separated by SDS-PAGE and probed for VP1 (pAb597) as a marker of SV40 infection, and GAPDH as a loading control. Representative blots are shown from three independent infections. B. HEK293TT cells were infected with BKPyV at an MOI of 0.5 and treated with 20 μM of Glibenclamide or 10 μM of CFTR172 for 48 hours. Total protein of cell lysates from infected cells was separated by SDS-PAGE and probed for VP1 (pAb597) as a marker of BKPyV infection, and GAPDH as a loading control. Representative blots are shown from three independent infections. C. Densitometry analysis of Western blots was performed. Values represent the mean ±SD normalized to the no-drug control (n= 3). D. HEK293TT cells were treated as above and cell viability assessed via MTT assays. Values represent the mean ±SD normalized to the untreated control sample (n= 3). E. HEK293TT cells were treated with 20 μM of Glibenclamide and incubated for 48 hours. 20 μM of DiBAC4(3) was added to treated cells and flow cytometry analysis of total cell fluorescence was measured. Values represent the mean ±SD normalized to the untreated control (n= 3).

5.2.7 The role of CFTR ion channel in the MCPyV life cycle

5.2.7.1 Generation of BKPyV VLPs

To examine the role of host cell CFTR during the MCPyV life cycle, more pharmacological-based experiments were performed. MCPyV VLPs were kindly provided to our group (Samuel Dobson) and were generated from a codon-modified MCPyV expression plasmid for dual expression of VP1/VP2 (pwM2m) together with a reporter plasmid encoding EGFP (pEGFP-C1). Before the analysis using MCPyV VLPs, BKPyV VLPs were also generated.

HEK293TT cells were transfected with a reporter plasmid encoding for EGFP (pEGFP-C1) together with a codon-modified BK polyomavirus expression plasmid for VP1 genotype Ia (pIaw) in order to generate VLPs, which their capsids consist of VP1 protein only and EGFP encapsidated. Transfected cells were harvested 48 hours post-transfection and VLPs purified using Optiprep gradients. Following the purification, fractions were collected by gravity flow (Hurdiss et al., 2016). Seventeen samples were collected and 20 µl of each fraction separated by SDS-PAGE to detect VP1. VP1 was detected in most of the fractions at the expected molecular mass (42 kDa) (Figure 5.10A). To examine the infectivity of BKPyV VLPs, naïve HEK293TT were transduced with 10 µl of each of the collected fractions and analysed using the IncuCyte ZOOM screening 48 hours post-transduction. The results revealed that only the HEK293TT transduced with the 6^{th} and 7^{th} fractions were positive for EGFP expression (approximately 60%), suggesting that only BKPyV VLPs collected from the 6^{th} and 7^{th} fractions encapsidated EGFP (Figure 5.10B). Samples from these 6^{th} and 7^{th} fractions were assessed by cryo-EM (Performed by Daniel Hurdiss), which demonstrated that BKPyV VLPs have identical size and morphology to native BKPyV virions (Figure 5.10C).

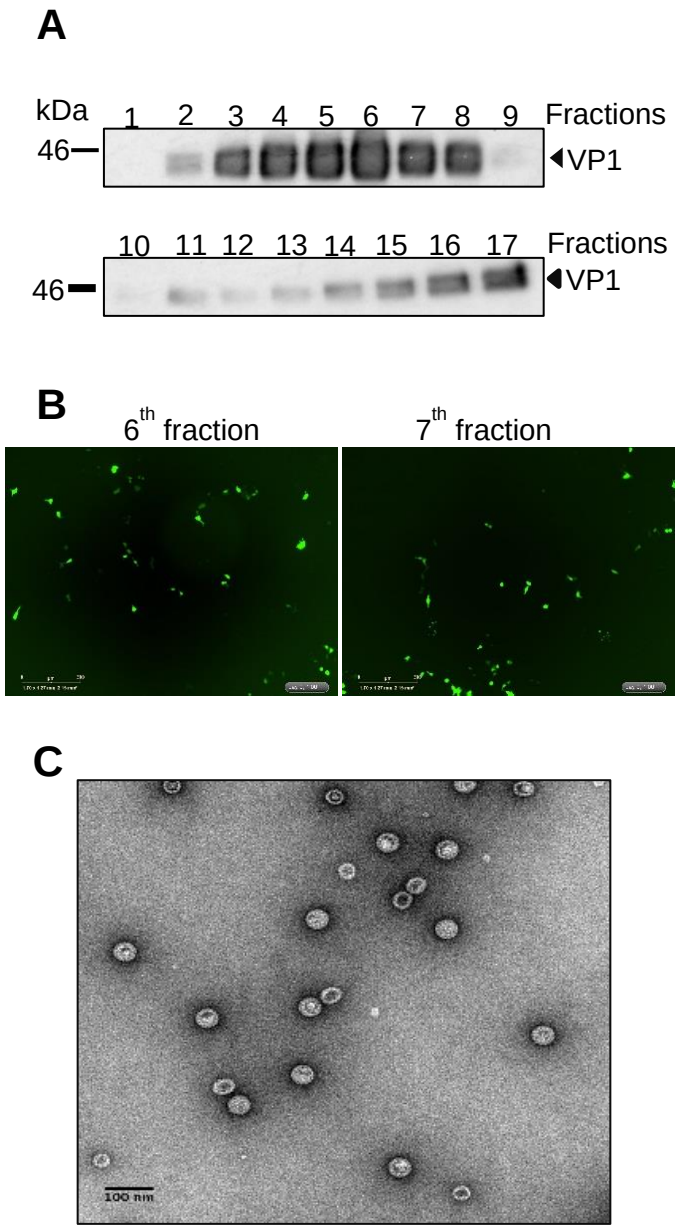

Figure 5. 10 Generation and purification of BKPyV VLPs. HEK293TT cells were co-transfected with pIaw and pEGFP-C1 and incubated for 48 hours. Samples were collected, BKPyV VLPs were purified by Opriprep gradients and fractions collected by gravity flow and further analysed. A. 20 µl of each fraction was separated by SDS-PAGE. VP1 (pAb597) was detected as a marker of BKPyV infection. Representative blots are shown (n= 2). B. 10 µl of each fraction was used to transduce naïve HEK293TT cells for 48 hours. The presence of EGFP protein was detected in the 6th and 7th fractions by IncuCyte ZOOM screening. Representative images are shown. C. Cryo-electron micrograph of purified VLPs suspended in vitreous ice. Scale bars, 100 nm.

5.2.7.2 CFTR channel is required for MCPyV and BKPyV VLPs transduction of HEK293TT cells

MCPyV VLPs were used to study the effect of CFTR modulators on MCPyV VLPs transduction in a cell line that is susceptible to this virus. BKPyV VLPs were also utilized in order to perform a pharmacological analysis for both polyomaviruses under identical conditions. HEK293TT cells were used to set up the VLP system. Firstly, HEK293TT cells were transduced with MCPyV VLPs for 2 hours and subsequently treated with 20 μM of Glibenclamide or 10 μM of CFTR172 for 72 hours. Cells were imaged using IncuCyte ZOOM analysis to assess the EGFP expression, since EGFP was encapsidated in MCPyV VLPs virions containing both VP1 and VP2 proteins in their capsids. The data revealed an approximate 30% and 40% reduction of transduced cells in the presence of Glibenclamide or CFTR172, respectively, compared to no-drug control samples (Figure 5.11A). These data implicate a role of CFTR during a successful MCPyV VLPs transduction.

Similar experiments were carried out using BKPyV VLPs as a control. HEK293TT cells were transduced with BKPyV VLPs and Glibenclamide or CFTR172 were added under identical treatment conditions. IncuCyte ZOOM analysis of EGFP showed that both modulators led to a modest reduction in cells transduced with BKPyV VLPs, but these effects were not as potent as those observed for MCPyV VLPs (10% decrease of EGFP upon treatment with Glibenclamide and 20% reduction in the presence of CFTR172) (Figure 5.11B). Taken together these data suggest that both modulators did not work as potent using the BKPyV VLP system compared to native BKPyV virions.

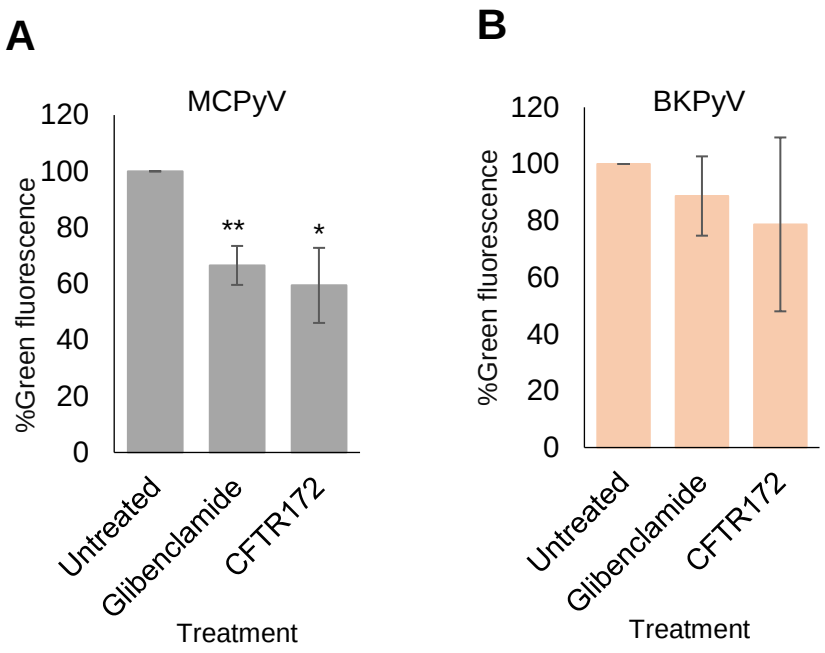

Figure 5. 11 Effect of CFTR modulation on HEK293TT cells transduced with MCPyV and BKPyV VLPs. HEK293TT cells were transduced with MCPyV (A) and BKPyV (B) VLPs for 2 hours at 37ºC. Cells were treated with 20 µM of Glibenclamide or 10 µM of CFTR172 and incubated for 72 hours. Live cells were imaged using the IncuCyte ZOOM equipment and EGFP fluorescence measured. Data represent the mean ±SD of fluorescent intensity normalized to the untreated control samples (n= 3) (*, significant difference at the $p \leq 0.05$ level; **, significant difference at the $p \leq 0.01$ level).

5.3 Discussion

5.3.1 A requirement for CFTR activity during the JCPyV life cycle

In the Chapter 4 it was shown that BKPyV requires the function of host cell CFTR channels to complete its infectious life cycle in RPTE cells. Based on time-of-addition experiments it was proposed that CFTR is important at a post-entry stage of the virus life cycle, which may include endosome acidification that is critical for a successful viral infection. The main aim of the experiments described in this Chapter was to study the involvement of host cell CFTR channels in other polyomaviruses' life cycles (Table 5.1).

JCPyV is an emerging human pathogen that is closely related to BKPyV, that causes severe clinical complications in immunosuppressed individuals. JCPyV infectious stocks were generated (Figure 5.3) and CFTR protein expression was confirmed in a JCPyV susceptible cell line, SVG-A cells (Figure 5.1). Stages of the JCPyV infection cycle have been well defined including viral attachment to the host cell serotonin receptor $5HT_{2A}$ and alpha (2-6)-linked sialic acids (Elphick et al., 2004; Gee et al., 2004). Pho et al., (2000) demonstrated that JCPyV enters through a clathrin-dependent endocytic pathway, although the mechanism of virion transportation to the nucleus is less well understood. T antigens are produced and TAg initiates viral genome replication and regulates the viral late promoter (Lynch and Frisque, 1990; Lashgari et al., 1989). The translation of late viral genes follows, which leads to the generation of structural proteins, VP1, VP2 and VP3 and non-structural but regulatory protein, the agnoprotein. Structural proteins form the virion capsid and along with viral DNA genomes are packaged and newly synthesized viral progeny is released by a poorly defined process (Seth et al., 2004).

As JCPyV enters endosomes the virions are exposed to a low pH-environment leading to conformational changes and virion uncoating (Bayer et al., 1998; Mellman et al., 1986; Suzuki et al., 2001). Ashok and Atwood, (2003) determine the role of acidification in the JCPyV life cycle. There was an approximate 60-80% reduction of JCPyV infection upon treatment with ammonium chloride (NH_4Cl), known to neutralize endosomal pH. These results suggested that JCPyV requires an acidification step at a very early stage of the course of infection to complete its life cycle successfully. The

acidification step is similarly critical to BKPyV infection. Time-of-addition assays suggested that viral entry was the stage of life cycle requiring CFTR functionality (Chapter 4). It was demonstrated that the inhibition of CFTR resulted in a reduction of JCPyV infection (Figure 5.6). Performing time-of-addition experiments in JCPyV infected glial cells combined with an assessment of CFTR modulation on endosomal pH may reveal if CFTR channel function influences endosome acidification explaining its contribution to the JCPyV life cycle.

Table 5. 1 Effect of CFTR modulators on other polyomaviruses' life cycle. Impact of Glibenclamide (20 μM) and CFTR172 (10 μM) on VP1 protein expression and cell viability are shown below.

	Vero cells			HEK293TT cells			RPTE cells			SVG-A cells		
	Glib	**CFTR172**	**Cell viability**	**Glib**	**CFTR172**	**Cell viability**	**Glib**	**CFTR172**	**Cell viability**	**Glib**	**CFTR172**	**Cell viability**
BKPyV	No	No	No	10% reduction	50% reduction	No	80% reduction	80% reduction	No			
BKPyV VLP				10% reduction	20% reduction	No						
JCPyV										30% reduction	40% reduction	No
SV40	No	10% reduction	No				40% reduction	50% reduction	No			
MCPyV VLP				30% reduction	40% reduction	No						

5.3.2 Host cell CFTR channels modulation inhibits SV40 production in a cell type-dependent manner

Simian virus 40 (SV40) is also a closely related polyomavirus to BKPyV. During virus entry, SV40 binds to the major histocompatibility complex class I antigens on the host cell surface (Atwood and Norkin, 1989; Breau et al., 1992) and is internalized via a caveolae-dependent endocytosis (Anderson et al., 1996; Kartenbeck et al., 1989). Live fluorescence microscopy in CV-1 cells (derived from Cercopithecus aethiops monkey kidneys) revealed that SV40 is transported from plasma membrane into vesicles positive for caveolin 1. These organelles were not co-stained with intracellular markers of lysosomes/endosomes or ER/Golgi apparatus. Following this step, SV40 is localized in larger organelles with a non-acidic pH environment, prior to sorting into tubular vesicles. These tubular vesicles facilitate transportation along microtubules to the smooth ER compartment (Pelkmans et al., 2001). It has been also demonstrated that treatment with NH_4Cl on SV40 infected glial cells (SVG-A cells) does not impact on SV40 production, implicating no requirement for an acidic pH environment during virus entry in glial cells (Ashok and Atwood, 2003). To determine the role of host cell CFTR channels during SV40 infection, pharmacological analysis was first performed in Vero cells (African green monkey kidney cells), an SV40 cell line in which CFTR expression was confirmed (Figure 5.7A and B). Given the lack of pH dependence of SV40 entry in these cells, it was speculated that a lack of requirement of endosome acidification, renders SV40 entry independent of CFTR function and is thus insensitive to CFTR modulation.

There is accumulating evidence that SV40 can infect humans (Butel et al., 1999; Garcea and Imperiale, 2003) leading to analysis of the SV40 life cycle in human cell lines. Low et al., (2004) performed infection assays on RPTE cells to identify if SV40 is capable of infecting human primary kidney cells. They identified that SV40 could not successfully enter RPTE cells without the exogenous expression of GM1 gangliosides. Further investigations (Low et al., 2004) suggested that SV40 can infect RPTE cells as SV40 DNA was detected in infected RPTE cells by Southern blot, but whether this SV40 remained on cell surface or was internalized was not investigated. In this study, infection assays in two human cell lines that express CFTR were

performed (Figure 5.1). SV40 was shown to infect human RPTE cells (Figure 5.8) and HEK293TT cells (Figure 5.9A) as SV40 VP1 protein was detectable following infection of both cell lines. Furthermore, differences in the impact of CFTR channel inhibition on SV40 production were observed. A significant decrease of SV40 VP1 expression occurred in infected RPTE cells upon treatment with CFTR modulators (Figure 5.8). Conversely, no effects on SV40 infection in HEK293TT cells was observed (Figure 5.9A). The discrepancy between the cell lines may suggest that SV40 is internalized and trafficked to the nucleus through cell type-specific mechanisms, some of which are CFTR dependent.

Similarly, Vero and HEK293TT cells were infected with BKPyV and treated with CFTR modulators. BKPyV VP1 expression was detected in both Vero (Figure 5.7C) and HEK293TT cells (Figure 5.9B), suggesting that BKPyV can infect both monkey-derived cell lines (Figure 5.7C) and human cells (Chapter 4 and Figure 5.10B). However, blockade of CFTR function had an impact on BKPyV production only in HEK293TT cells (Figure 5.9B) and not in Vero cells (Figure 5.7C). These results may strengthen the hypothesis that cell type-specific endocytic pathways are co-opted by polyomaviruses *en* route to the nucleus.

Polyomaviruses are dependent on different endocytic pathways to infect their hosts. SV40 enters host cells using a caveolar-mediated endocytic pathway (Anderson et al., 1996; Pelkmans et al., 2002; Stang et al., 1997), whereas JCPyV utilizes a clathrin-mediated endocytic pathway (Pho et al., 2000). Murine polyomavirus (MPyV) is found to enter host cells via a caveolar/or clathrin-independent endocytic pathway (Gilbert and Benjamin, 2000). Disruption of caveolar function had no impact on the successful MPyV infection in primary baby mouse kidney (BMK) epithelial cells and NIH 3T3 fibroblasts, whereas SV40 infection was inhibited in the same cell lines. These data highlighted that two related viruses enter the same cell lines following different endocytic pathways as dictated by the virus (Richterova et al., 2001).

Notably, the same virus may utilize different cellular endocytic pathways for uptake in different cell lines (Gilbert et al., 2003). Cytoskeletal elements are most likely involved in the directed trafficking of a virus (Sodeik, 2000). Studies have shown that intracellular trafficking may vary significantly amongst different viruses of the same or related groups (Kasamatsu and Nakanishi, 1998). Receptor-mediated endocytosis

occurs during adenovirus infection and following penetration of endosomal membrane, the viral particles are released into the cytoplasm. Then adenovirus utilizes microtubules to reach the nucleus (Miles et al., 1980; Suomalainen et al., 1999). Previous studies have demonstrated that in cells with disrupted microtubules, adenovirus relies on a transportation mechanism independent on microtubules (Glotzer et al., 2001). Moreover, ecotropic murine leukemia virus has been found to utilize actin cytoskeleton in both NIH 3T3 fibroblasts and XC cells, although microtubules were also required for transportation only in XC cells (Kizhatil and Albritton, 1997). These findings highlighted that the cell type can influence the mechanism by which the same virus traffics within different cells, (Kizhatil and Albritton, 1997; Glotzer et al., 2001) supporting our hypothesis as well. Furthermore, a virus may have the ability to use different pathways to enter host cells. A successful influenza virus infection is dependent on an acidification step early during infection, using a clathrin-mediated endocytic pathway as a primary route (Marsh and Helenius, 1989). However, blockade of both clathrin- and caveola-mediated endocytic pathways did not stop the influenza virus to infect cells (Sieczkarski and Whittaker, 2002). Influenza virus utilizes sialic acid as the primary host cell receptor, similar to MPyV and the relative lack of specificity of the primary receptors for a specific endocytic route may contribute to the use of alternative entry pathways (Gilbert et al., 2003).

5.3.3 CFTR inhibition influences MCPyV infection

Merkel cell polyomavirus (MCPyV) is one of the most recently identified human polyomavirus and is strongly linked with Merkel cell carcinoma (Spurgeon and Lambert, 2013). Currently little is known about the life cycle and viral genome replication of MCPyV, consequently, events occurring following virus penetration into host cells up to the delivery of viral genome into the nucleus are not fully understood (Schowalter et al., 2012).

Previous studies have identified that gangliosides GT1b might be a potential host cell receptor for MCPyV (Erickson et al., 2009). However, following studies revealed that MCPyV pseudovirions require sulfated glycosaminoglycans and particularly heparan sulfate for a successful entry in A549 cells (Schowalter et al., 2011). It is shown that

in Lec2 cells lacking sialylated glycans, MCPyV pseudovirions efficiently bound to host cell receptor, although there was no gene transduction. These data led to the hypothesis that glycosaminoglycan might be a primary receptor and sialylated glycan serves as a post-attachment co-receptor for an efficient MCPyV pseudovirion entry and gene transduction (Schowalter et al., 2011).

Schowalter et al., (2012) performed infectivity assays using MCPyV pseudovirions on a panel of 60 different cancer cell lines. They identified that in transformed melanocyte cell lines and human skin-derived primary keratinocytes, MCPyV entry occurred. However, MCPyV pseudovirus could not successfully enter the transformed keratinocytes (HaCat) and primary melanocytes did not support an infection. As a result, a cautious approach to cell line models to examine the MCPyV life cycle was proposed, with skin cells representing the most preferential sites for MCPyV infection (Spurgeon and Lambert, 2013). A more recent study identified that human dermal fibroblasts are able to sustain MCPyV replication in a cell culture system (Liu et al., 2016).

To determine the role of host cell CFTR channels in the MCPyV life cycle, pharmacological analysis of CFTR modulators using MCPyV pseudovirions was performed. MCPyV pseudovirions were generated in HEK293TT cells and transduced cells were treated with CFTR modulators. Both Glibenclamide and CFTR172 were found to decrease virus transduction (Figure 5.11A) suggesting that CFTR influences MCPyV pseudovirus transduction. However, to identify the exact role of CFTR in the MCPyV life cycle, infection assays using native MCPyV could be required. Moreover, further pharmacological analyses could be performed in a more physiologically relevant cell system, which would be more relevant to MCPyV natural hosts.

In this study, we also used BKPyV VLPs as a control to the VLP system. BKPyV pseudovirus was generated in HEK293TT cells using an EGFP expression vector and a VP1 modified expression vector. The presence of VP1 protein after VLPs purification and morphological features of generated VLPs were confirmed by Western blotting and cryo-electron microscopy, respectively (Figure 5.10). HEK293TT cells were transduced with BKPyV VLPs and treated with CFTR modulators, further analysed by IncuCyte ZOOM analysis for the EGFP expression. Interestingly, data showed that BKPyV transduction in HEK293TT cells was

moderately inhibited by CFTR modulation (Figure 5.11B), which was in contrast with the level of reduction of VP1 expression in infection assays using BKPyV native virions.

Accumulating evidences that implicate host ion channels in the life cycles of many viruses suggest that CFTR or other host ion channels might influence the *Polyomaviridae* life cycle in a cell type-specific manner. Further studies are now required to fully dissect the role of CFTR channels during virus entry to reveal the mechanism(s) behind its cell type-specific effects, and its cell type-specific inhibition as a potential pan *Polyomaviridae* inhibitor.

5.3.4 Glibenclamide affects resting membrane potential

Membrane excitability in cell-based assays requires accurate and precise measurements. Patch-clamp recording is the gold standard for monitoring ion channel modulations (Hamill et al., 1981). This technique allows the monitoring of ion channel gating, activation, inactivation, drug effects and ion selectivity, although the ease of use of patch-clamp is low and is not a high-throughput technique (Baxter et al., 2002). Current technologies used for monitoring ion channels include radioactive flux assays, automated patch-clamp techniques, radioligand binding and optical recording techniques such as fluorescence and bioluminescence detection (Baxter et al., 2002). Optical readouts of ion channel functionality are sensitive and versatile and for that reason are favorable for high-throughput screening among the other methods (Denyer et al., 1998; González et al., 1999). Intracellular ion concentrations, as well as measurement of membrane potentials can be monitored by fluorescence readouts (Denyer et al., 1998). Modifications of ion channels leading to fluctuations of intracellular Ca^{2+} concentration can be measured using fluorescent probes including Calcium Green and Fluo-3 (Denyer et al., 1998). Furthermore, there are several fluorescent dyes that indicate changes in membrane potential, such as bisoxonol, styryl and fluorescence resonance energy transfer-based voltage-sensitive dyes (González et al., 1999).

The bisoxonol fluorescent dye, bis-(1,3-dibutylbarbituric acid) trimethine oxonol, or DiBAC4(3) (Epps et al., 1994), has been the reagent used in this study to measure

membrane potential. Redistribution of the dye indicates changes in the membrane potential. An increase in fluorescence intensity indicates cell depolarization (membrane potential become more positive), while a decrease in fluorescence indicates hyperpolarization (membrane potential become more negative) (Baxter et al., 2002).

Cl^- channels contribute to membrane potential and control cell volume and intracellular pH (Okada et al., 2004). Studies have shown that cell cycle and proliferation are regulated by Cl^- currents (Kunzelmann, 2005). CFTR is an ATP-gated Cl^- channel and controls ion fluxes across the cell membrane (Li and Naren, 2010; Hallows et al., 2000). It is demonstrated that several membrane transport proteins are controlled by CFTR, such as the outwardly-rectifying Cl^- channel (Gabriel et al., 1993), Ca^{2+}-activated Cl^- channel (Wei et al., 2001), the epithelial sodium channel (ENaC) (Stutts et al., 1997), sodium/hydrogen exchanger (Ahn et al., 2001), the anion exchanger (Lee et al., 1999) and aquaporin 9 water channel (Pietrement et al., 2008). Thus, CFTR function is critical for the fluctuation of membrane potential (Zhu et al., 2018). Recent studies revealed that a significant decrease in DiBAC4(3) fluorescence intensity was observed upon treatment with the CFTR inhibitor GlyH-101, suggesting that CFTR inhibition leads to cell membrane hyperpolarization (Zhu et al., 2018). Whereas, agonist-mediated activation of CFTR results in cell membrane depolarization (Maitra et al., 2013).

In this study, screening of CFTR channel modulations was performed using the DiBAC4(3) fluorescence dye. RPTE, SVG-A, Vero and HEK293TT cells, respectively, were treated with 20 µM of Glibenclamide and fluorescence intensity of DiBAC4(3) dye was measured by flow cytometry. Similar shifts were observed in all cell lines upon treatment with Glibenclamide (Figure 5.8C; Figure 5.6D; Figure 5.7E; Figure 5.9E). An increase of fluorescence intensity was observed suggesting that Glibenclamide, the CFTR inhibitor, cause cell membrane depolarization. However, at this stage of the study we could not suggest whether this shift caused through CFTR inhibition or another Glibenclamide sensitive channels since Glibenclamide targets K^+ channels as well. Further screening of membrane potential upon treatment with the inhibitory compound CFTR172 is required to fully dissect the role of CFTR as a determinant of cell membrane potential.

6 Summary and Conclusion

BK polyomavirus (BKPyV) is a pathogen infecting the majority of the population worldwide. Whilst a primary infection is usually asymptomatic in healthy individuals, BKPyV can cause severe clinical complications in immunocompromised individuals, including polyomavirus-associated nephropathy (PVAN) in renal transplant recipients. Currently, there is no clinically available therapeutic intervention against BKPyV and the number of kidney transplants is increasing significantly. Therefore, there is an urgent need to study the BKPyV life cycle in order to identify potential targets that can be exploited for anti-viral therapeutic development.

Ion channels play critical roles in kidney physiology and regulate a number of processes. In addition, they are required during the life cycles of several viruses, implicating them as attractive candidate proteins required for a successful BKPyV infection. The main aims of this work were to investigate the roles of host ion channels in the BKPyV life cycle and to validate them as potential novel anti-viral therapeutics.

This study established a cell culture system using human primary kidney epithelial cells (RPTE) to study the BKPyV life cycle in the most physiological relevant cell system to BKPyV host cells. It also identified and optimized a method for measurement of infectious BKPyV titres using a fluorescent-based microscopy technique, the IncuCyte ZOOM analysis. This high-throughput method provided us with sensitive and accurate measurements of viral infectivity and was used to assess and validate pharmacological compounds having BKPyV VP1 expression as an infection marker.

Notably, time-course of BKPyV infection indicated the time-points during the BKPyV life cycle in which genome replication and late viral gene expression occur. Moreover, it was also identified at which time-point the newly synthesized viral progeny is released from infected RPTE cells. These findings were supported by previous published studies and determined all the critical steps of the BKPyV life cycle.

It is established in the literature that viruses manipulate host intracellular machineries to favour their life cycles. Several viruses encode their own ion channels known as viroporins highlighting the need for regulation of ion homeostasis during their life cycles. However, other viruses exploit host ion channels to facilitate different processes. Therefore, a strategy to identify novel anti-viral targets is to study virus and host interactions, including interactions with host ion channels, and to investigate their importance in viruses' life cycle. K^+ channel family is the most widely distributed ion channel family across all the different cell types and regulates several intracellular processes in kidneys. In addition, an array of modulatory compounds to K^+ channel family members are available and well-characterized. Therefore, K^+ channel family was selected for initial investigations.

Initial screening revealed that tetraethylammonium (TEA), a broad-spectrum K^+ channel blocker impacted on BKPyV infection causing a decrease on BKPyV VP1 production. A more detailed pharmacological analysis showed the potential molecular identity of specific K^+ channels required for a successful BKPyV infection. Pharmacological data suggested that the clinically available drug, Glibenclamide, the ATP-sensitive K^+ channel blocker caused a drastic inhibition of BKPyV VP1 production at concentrations that did not impact on cell viability. Moreover, there was experimental evidence that Glibenclamide inhibited BKPyV VP1 expression in a dose-dependent manner regardless of the multiplicity of BKPyV infection. It was also demonstrated that Glibenclamide had an impact not only at a protein level but also at a DNA level causing a significant reduction of viral genome replication. Notably, Glibenclamide was found to decrease the infectivity of the newly synthesized viral progeny. Taken together these data identify a requirement for Glibenclamide sensitive ion channels during the BKPyV life cycle in human primary RPTE cells.

Glibenclamide is known to cause blockade of ATP-sensitive K^+ channels. Although by utilizing other pharmacological compounds that target, specifically, components of this ion channel complex, no effect on a BKPyV infection was observed. Consequently, it was speculated that Glibenclamide inhibits BKPyV through a different mechanism and not due to the inhibition of ATP-sensitive K^+ channels. Glibenclamide is an open-channel blocker of the cystic fibrosis transmembrane conductance regulator (CFTR), a Cl^- permeable channel, as well. As CFTR is abundantly expressed in human kidneys, a potential role for CFTR in the BKPyV life

cycle was investigated through performing pharmacological analysis in the presence of CFTR172, a specific inhibitor of CFTR channel. Findings showed that CFTR172 affected the BKPyV life cycle similarly with Glibenclamide, suggesting for the first time that renal expressed CFTR is sensitive to Glibenclamide and a host factor required during a successful BKPyV infection. Knock down experiments supported the importance of CFTR in the BKPyV life cycle, as a decrease in CFTR expression also led to a reduction in VP1 production.

A major finding was that CFTR is required at very early stage of the BKPyV life cycle confirmed by performing time-of-addition experiments. Data demonstrated that CFTR was critical for BKPyV infection within the first 4 hours of infection without affecting the stage of binding/penetration to host cell. It was suggested that CFTR might be implicated in early events occurring during the endosomal transportation of BKPyV towards the ER compartment.

There is experimental evidence that CFTR is expressed in different cell types, which are susceptible to other polyomaviruses, including JC polyomavirus (JCPyV), SV40 and Merkel cell polyomavirus (MCPyV). Pharmacological analysis in the presence of Glibenclamide or CFTR172 indicated that there was a requirement of host CFTR ion channel for a successful BKPyV, JCPyV, SV40 and MCPyV infection, respectively, in certain cell lines *in vitro*. It was proposed that polyomaviruses studied in this work, followed different endocytic pathways towards the nucleus, which might be cell type-dependent showing a requirement for CFTR in a cell type-dependent manner as well.

In conclusion, host CFTR ion channel is highly likely to be crucial for BKPyV since blockade of the channel's functionality results in inhibition of BKPyV infection. CFTR might be implicated in early events within the first 4 hours post-infection, including events occurring during the endocytic trafficking pathway of BKPyV and particularly during the transportation to the ER. Previous studies demonstrated that host ion channels are involved in acidification occurring at early stages during a viral infection. CFTR, potentially, might be involved in acidification of intracellular compartments to facilitate partial uncoating and further conformational changes of BKPyV virions before reaching the ER. Further research is needed to identify the exact role and mechanism(s) of CFTR function during a BKPyV infection. Exploiting host CFTR ion channel as potential drug target could help to combat other polyomavirus-related

diseases since there could be experimental evidence for a CFTR requirement during other polyomaviruses infection.

Bibliography

Abend, J.R., Joseph, A.E., Das, D., Campbell-Cecen, D.B. and Imperiale, M.J. 2009. A truncated T antigen expressed from an alternatively spliced BK virus early mRNA. *The Journal of general virology*. [Online]. **90**(Pt 5), pp.1238–45. [Accessed 18 July 2018]. Available from: http://www.ncbi.nlm.nih.gov/pubmed/19264611.

Abend, J.R., Low, J.A. and Imperiale, M.J. 2010. Global effects of BKV infection on gene expression in human primary kidney epithelial cells. *Virology*. [Online]. **397**(1), pp.73–79. [Accessed 20 July 2018]. Available from: http://www.ncbi.nlm.nih.gov/pubmed/19945725.

Abend, J.R., Low, J.A. and Imperiale, M.J. 2007. Inhibitory effect of gamma interferon on BK virus gene expression and replication. *Journal of virology*. [Online]. **81**(1), pp.272–9. [Accessed 21 July 2018]. Available from: http://www.ncbi.nlm.nih.gov/pubmed/17035315.

Aguilar-Bryan, L. and Bryan, J. 1999. Molecular Biology of Adenosine Triphosphate-Sensitive Potassium Channels [1]. *Endocrine Reviews*. [Online]. **20**(2), pp.101–135. [Accessed 21 July 2018]. Available from: http://www.ncbi.nlm.nih.gov/pubmed/10204114.

AGUILAR-BRYAN, L., CLEMENT, J.P., GONZALEZ, G., KUNJILWAR, K., BABENKO, A. and BRYAN, J. 1998. Toward Understanding the Assembly and Structure of K_{ATP} Channels. *Physiological Reviews*. [Online]. **78**(1), pp.227–245. [Accessed 20 July 2018]. Available from: http://www.ncbi.nlm.nih.gov/pubmed/9457174.

Aguilar-Bryan, L., Nichols, C.G., Wechsler, S.W., Clement, J.P., Boyd, A.E., González, G., Herrera-Sosa, H., Nguy, K., Bryan, J. and Nelson, D.A. 1995. Cloning of the beta cell high-affinity sulfonylurea receptor: a regulator of insulin secretion. *Science (New York, N.Y.)*. [Online]. **268**(5209), pp.423–6. [Accessed 23 July 2018]. Available from: http://www.ncbi.nlm.nih.gov/pubmed/7716547.

Ahn, W., Kim, K.H., Lee, J.A., Kim, J.Y., Choi, J.Y., Moe, O.W., Milgram, S.L., Muallem, S. and Lee, M.G. 2001. Regulatory Interaction between the Cystic Fibrosis Transmembrane Conductance Regulator and HCO Salvage Mechanisms in Model Systems and the Mouse Pancreatic Duct. *Journal of Biological Chemistry*. [Online]. **276**(20), pp.17236–17243. [Accessed 23 July 2018]. Available from: http://www.ncbi.nlm.nih.gov/pubmed/11278980.

Alagem, N., Dvir, M. and Reuveny, E. 2001. Mechanism of Ba(2+) block of a mouse inwardly rectifying K+ channel: differential contribution by two discrete residues. *The Journal of physiology*. [Online]. **534**(Pt. 2), pp.381–93. [Accessed 22 July 2018]. Available from: http://www.ncbi.nlm.nih.gov/pubmed/11454958.

Alkhalil, A., Hammamieh, R., Hardick, J., Ait Ichou, M., Jett, M. and Ibrahim, S. 2010. Gene expression profiling of monkeypox virus-infected cells reveals novel interfaces for host-virus interactions. *Virology Journal*. [Online]. **7**(1), p.173. [Accessed 21 July 2018]. Available from: http://www.ncbi.nlm.nih.gov/pubmed/20667104.

Allander, T., Andreasson, K., Gupta, S., Bjerkner, A., Bogdanovic, G., Persson, M.A.A., Dalianis, T., Ramqvist, T. and Andersson, B. 2007. Identification of a Third Human Polyomavirus. *Journal of Virology*. [Online]. **81**(8), pp.4130–4136. [Accessed 17 July 2018]. Available from: http://www.ncbi.nlm.nih.gov/pubmed/17287263.

Alméras, C., Foulongne, V., Garrigue, V., Szwarc, I., Vetromile, F., Segondy, M. and Mourad, G. 2008. Does Reduction in Immunosuppression in Viremic Patients Prevent BK Virus Nephropathy in De Novo Renal Transplant Recipients? A Prospective Study. *Transplantation*. [Online]. **85**(8), pp.1099–1104. [Accessed 17 July 2018]. Available

from: http://www.ncbi.nlm.nih.gov/pubmed/18431228.

Ambalathingal, G.R., Francis, R.S., Smyth, M.J., Smith, C. and Khanna, R. 2017. BK Polyomavirus: Clinical Aspects, Immune Regulation, and Emerging Therapies. *Clinical Microbiology Reviews*. [Online]. **30**(2), pp.503–528. [Accessed 17 July 2018]. Available from: http://www.ncbi.nlm.nih.gov/pubmed/28298471.

Ammerman, N.C., Beier-Sexton, M. and Azad, A.F. 2008. Growth and maintenance of Vero cell lines. *Current protocols in microbiology*. [Online]. **Appendix 4**, Appendix 4E. [Accessed 21 July 2018]. Available from: http://www.ncbi.nlm.nih.gov/pubmed/19016439.

An, P., Sáenz Robles, M.T. and Pipas, J.M. 2012. Large T Antigens of Polyomaviruses: Amazing Molecular Machines. *Annual Review of Microbiology*. [Online]. **66**(1), pp.213–236. [Accessed 18 July 2018]. Available from: http://www.ncbi.nlm.nih.gov/pubmed/22994493.

Anderson, H.A., Chen, Y. and Norkin, L.C. 1996. Bound simian virus 40 translocates to caveolin-enriched membrane domains, and its entry is inhibited by drugs that selectively disrupt caveolae. *Molecular biology of the cell*. [Online]. **7**(11), pp.1825–34. [Accessed 23 July 2018]. Available from: http://www.ncbi.nlm.nih.gov/pubmed/8930903.

Anderson, M.P., Rich, D.P., Gregory, R.J., Smith, A.E. and Welsh, M.J. 1991. Generation of cAMP-activated chloride currents by expression of CFTR. *Science (New York, N.Y.)*. [Online]. **251**(4994), pp.679–82. [Accessed 20 July 2018]. Available from: http://www.ncbi.nlm.nih.gov/pubmed/1704151.

Andrews, C.A., Shah, K. V, Daniel, R.W., Hirsch, M.S. and Rubin, R.H. 1988. A serological investigation of BK virus and JC virus infections in recipients of renal allografts. *The Journal of infectious diseases*. [Online]. **158**(1), pp.176–81. [Accessed 17 July 2018]. Available from: http://www.ncbi.nlm.nih.gov/pubmed/2839580.

Armstrong, C.M. 1974. Ionic pores, gates, and gating currents. *Quarterly Reviews of Biophysics*. [Online]. **7**(02), p.179. [Accessed 23 July 2018]. Available from: http://www.journals.cambridge.org/abstract_S0033583500001402.

Armstrong, C.M. 1966. Time course of TEA(+)-induced anomalous rectification in squid giant axons. *The Journal of general physiology*. [Online]. **50**(2), pp.491–503. [Accessed 21 July 2018]. Available from: http://www.ncbi.nlm.nih.gov/pubmed/11526842.

Armstrong, C.M. and Hille, B. 1972. The inner quaternary ammonium ion receptor in potassium channels of the node of Ranvier. *The Journal of general physiology*. [Online]. **59**(4), pp.388–400. [Accessed 21 July 2018]. Available from: http://www.ncbi.nlm.nih.gov/pubmed/4112955.

Arora, R., Chang, Y. and Moore, P.S. 2012. MCV and Merkel cell carcinoma: a molecular success story. *Current Opinion in Virology*. [Online]. **2**(4), pp.489–498. [Accessed 23 July 2018]. Available from: http://www.ncbi.nlm.nih.gov/pubmed/22710026.

Ashcroft, F.M. and Gribble, F.M. 1998. Correlating structure and function in ATP-sensitive K+ channels. *Trends in neurosciences*. [Online]. **21**(7), pp.288–94. [Accessed 21 July 2018]. Available from: http://www.ncbi.nlm.nih.gov/pubmed/9683320.

Ashfield, R., Gribble, F.M., Ashcroft, S.J. and Ashcroft, F.M. 1999. Identification of the high-affinity tolbutamide site on the SUR1 subunit of the K(ATP) channel. *Diabetes*. [Online]. **48**(6), pp.1341–7. [Accessed 22 July 2018]. Available from: http://www.ncbi.nlm.nih.gov/pubmed/10342826.

Ashok, A. and Atwood, W.J. 2003a. Contrasting roles of endosomal pH and the cytoskeleton in infection of human glial cells by JC virus and simian virus 40. *Journal of virology*. [Online]. **77**(2), pp.1347–56. [Accessed 18 July 2018]. Available from:

http://www.ncbi.nlm.nih.gov/pubmed/12502851.

Ashok, A. and Atwood, W.J. 2003b. Contrasting Roles of Endosomal pH and the Cytoskeleton in Infection of Human Glial Cells by JC Virus and Simian Virus 40. *JOURNAL OF VIROLOGY*. **77**(2), pp.1347–1356.

Atwood, W.J. and Norkin, L.C. 1989. Class I major histocompatibility proteins as cell surface receptors for simian virus 40. *Journal of virology*. [Online]. **63**(10), pp.4474–7. [Accessed 23 July 2018]. Available from: http://www.ncbi.nlm.nih.gov/pubmed/2476575.

Awadalla, Y., Randhawa, P., Ruppert, K., Zeevi, A. and Duquesnoy, R.J. 2004. HLA Mismatching Increases the Risk of BK Virus Nephropathy in Renal Transplant Recipients. *American Journal of Transplantation*. [Online]. **4**(10), pp.1691–1696. [Accessed 17 July 2018]. Available from: http://www.ncbi.nlm.nih.gov/pubmed/15367226.

Azzi, A., De Santis, R., Ciappi, S., Leoncini, F., Sterrantino, G., Marino, N., Mazzorta, F., Laszlo, D., Fanci, R. and Bosi, A. 1996. Human polyomaviruses DNA detection in peripheral blood leukocytes from immunocompetent and immunocompromised individuals. *Journal of Neurovirology*. [Online]. **2**(6), pp.411–416. [Accessed 18 July 2018]. Available from: http://www.ncbi.nlm.nih.gov/pubmed/8972423.

Babenko, A.P., Gonzalez, G. and Bryan, J. 1999. The tolbutamide site of SUR1 and a mechanism for its functional coupling to K(ATP) channel closure. *FEBS letters*. [Online]. **459**(3), pp.367–76. [Accessed 22 July 2018]. Available from: http://www.ncbi.nlm.nih.gov/pubmed/10526167.

Bacia, K., Schwille, P. and Kurzchalia, T. 2005. From The Cover: Sterol structure determines the separation of phases and the curvature of the liquid-ordered phase in model membranes. *Proceedings of the National Academy of Sciences*. [Online]. **102**(9), pp.3272–3277. [Accessed 18 July 2018]. Available from: http://www.ncbi.nlm.nih.gov/pubmed/15722414.

Bagchi, P., Walczak, C.P. and Tsai, B. 2015. The Endoplasmic Reticulum Membrane J Protein C18 Executes a Distinct Role in Promoting Simian Virus 40 Membrane Penetration T. S. Dermody, ed. *Journal of Virology*. [Online]. **89**(8), pp.4058–4068. [Accessed 18 July 2018]. Available from: http://www.ncbi.nlm.nih.gov/pubmed/25631089.

Balsells, M., García-Patterson, A., Solà, I., Roqué, M., Gich, I. and Corcoy, R. 2015. Glibenclamide, metformin, and insulin for the treatment of gestational diabetes: a systematic review and meta-analysis. *BMJ (Clinical research ed.)*. [Online]. **350**, p.h102. [Accessed 23 July 2018]. Available from: http://www.ncbi.nlm.nih.gov/pubmed/25609400.

Bär, S., Daeffler, L., Rommelaere, J. and Nüesch, J.P.F. 2008. Vesicular egress of non-enveloped lytic parvoviruses depends on gelsolin functioning. *PLoS pathogens*. [Online]. **4**(8), p.e1000126. [Accessed 20 July 2018]. Available from: http://www.ncbi.nlm.nih.gov/pubmed/18704167.

Barcena-Panero, A., Echevarria, J.E., Van Ghelue, M., Fedele, G., Royuela, E., Gerits, N. and Moens, U. 2012. BK polyomavirus with archetypal and rearranged non-coding control regions is present in cerebrospinal fluids from patients with neurological complications. *Journal of General Virology*. [Online]. **93**(Pt_8), pp.1780–1794. [Accessed 11 November 2018]. Available from: http://www.ncbi.nlm.nih.gov/pubmed/22552944.

Bauman, Y., Nachmani, D., Vitenshtein, A., Tsukerman, P., Drayman, N., Stern-Ginossar, N., Lankry, D., Gruda, R. and Mandelboim, O. 2011. An Identical miRNA of the Human JC and BK Polyoma Viruses Targets the Stress-Induced Ligand ULBP3 to Escape

Immune Elimination. *Cell Host & Microbe*. [Online]. **9**(2), pp.93–102. [Accessed 18 July 2018]. Available from: http://www.ncbi.nlm.nih.gov/pubmed/21320692.

Baxter, D.F., Kirk, M., Garcia, A.F., Raimondi, A., Holmqvist, M.H., Flint, K.K., Bojanic, D., Distefano, P.S., Curtis, R. and Xie, Y. 2002. A Novel Membrane Potential-Sensitive Fluorescent Dye Improves Cell-Based Assays for Ion Channels. *Journal of Biomolecular Screening*. [Online]. **7**(1), pp.79–85. [Accessed 21 July 2018]. Available from: http://www.ncbi.nlm.nih.gov/pubmed/11897058.

Bayer, N., Schober, D., Prchla, E., Murphy, R.F., Blaas, D. and Fuchs, R. 1998. Effect of bafilomycin A1 and nocodazole on endocytic transport in HeLa cells: implications for viral uncoating and infection. *Journal of virology*. [Online]. **72**(12), pp.9645–55. [Accessed 23 July 2018]. Available from: http://www.ncbi.nlm.nih.gov/pubmed/9811698.

Bear, C.E., Li, C.H., Kartner, N., Bridges, R.J., Jensen, T.J., Ramjeesingh, M. and Riordan, J.R. 1992. Purification and functional reconstitution of the cystic fibrosis transmembrane conductance regulator (CFTR). *Cell*. [Online]. **68**(4), pp.809–18. [Accessed 20 July 2018]. Available from: http://www.ncbi.nlm.nih.gov/pubmed/1371239.

Bechert, C.J., Schnadig, V.J., Payne, D.A. and Dong, J. 2010. Monitoring of BK Viral Load in Renal Allograft Recipients by Real-Time PCR Assays. *American Journal of Clinical Pathology*. [Online]. **133**(2), pp.242–250. [Accessed 17 July 2018]. Available from: http://www.ncbi.nlm.nih.gov/pubmed/20093233.

Beimler, J., Sommerer, C. and Zeier, M. 2007. The influence of immunosuppression on the development of BK virus nephropathy does it matter? *Nephrology Dialysis Transplantation*. [Online]. **22**(Supplement 8), pp.viii66-viii71. [Accessed 17 July 2018]. Available from: http://www.ncbi.nlm.nih.gov/pubmed/17890267.

Bennett, S.M., Broekema, N.M. and Imperiale, M.J. 2012. BK polyomavirus: Emerging pathogen. *Microbes and Infection*., pp.672–683.

Bennett, S.M., Jiang, M. and Imperiale, M.J. 2013. Role of cell-type-specific endoplasmic reticulum-associated degradation in polyomavirus trafficking. *Journal of virology*. [Online]. **87**(16), pp.8843–52. [Accessed 20 July 2018]. Available from: http://www.ncbi.nlm.nih.gov/pubmed/23740996.

Bennett, S.M., Zhao, L., Bosard, C. and Imperiale, M.J. 2015. Role of a nuclear localization signal on the minor capsid Proteins VP2 and VP3 in BKPyV nuclear entry. *Virology*. [Online]. **474**, pp.110–116. [Accessed 20 July 2018]. Available from: http://www.ncbi.nlm.nih.gov/pubmed/25463609.

Bergsagel, D.J., Finegold, M.J., Butel, J.S., Kupsky, W.J. and Garcea, R.L. 1992. DNA Sequences Similar to Those of Simian Virus 40 in Ependymomas and Choroid Plexus Tumors of Childhood. *New England Journal of Medicine*. [Online]. **326**(15), pp.988–993. [Accessed 23 July 2018]. Available from: http://www.ncbi.nlm.nih.gov/pubmed/1312224.

Bernacchi, S., Mueller, G., Langowski, J. and Waldeck, W. 2004. Characterization of simian virus 40 on its infectious entry pathway in cells using fluorescence correlation spectroscopy. *Biochemical Society Transactions*. [Online]. **32**(5), pp.746–749. [Accessed 18 July 2018]. Available from: http://www.ncbi.nlm.nih.gov/pubmed/15494004.

Bernhoff, E., Gutteberg, T.J., Sandvik, K., Hirsch, H.H. and Rinaldo, C.H. 2008. Cidofovir Inhibits Polyomavirus BK Replication in Human Renal Tubular Cells Downstream of Viral Early Gene Expression. *American Journal of Transplantation*. [Online]. **8**(7), pp.1413–1422. [Accessed 17 July 2018]. Available from: http://www.ncbi.nlm.nih.gov/pubmed/18510636.

Bernhoff, E., Tylden, G.D., Kjerpeseth, L.J., Gutteberg, T.J., Hirsch, H.H. and Rinaldo, C.H. 2010. Leflunomide inhibition of BK virus replication in renal tubular epithelial cells. *Journal of virology*. [Online]. **84**(4), pp.2150–6. [Accessed 17 July 2018]. Available from: http://www.ncbi.nlm.nih.gov/pubmed/19955306.

Bethge, T., Ajuh, E. and Hirsch, H.H. 2016. Imperfect Symmetry of Sp1 and Core Promoter Sequences Regulates Early and Late Virus Gene Expression of the Bidirectional BK Polyomavirus Noncoding Control Region L. Banks, ed. *Journal of Virology*. [Online]. **90**(22), pp.10083–10101. [Accessed 18 July 2018]. Available from: http://www.ncbi.nlm.nih.gov/pubmed/27581987.

Bethge, T., Hachemi, H.A., Manzetti, J., Gosert, R., Schaffner, W. and Hirsch, H.H. 2015. Sp1 sites in the noncoding control region of BK polyomavirus are key regulators of bidirectional viral early and late gene expression. *Journal of virology*. [Online]. **89**(6), pp.3396–411. [Accessed 18 July 2018]. Available from: http://www.ncbi.nlm.nih.gov/pubmed/25589646.

Bhaskar, P.T. and Hay, N. 2007. The Two TORCs and Akt. *Developmental Cell*. [Online]. **12**(4), pp.487–502. [Accessed 20 July 2018]. Available from: http://www.ncbi.nlm.nih.gov/pubmed/17419990.

Bhattacharjee, S. 2015. Recent advances in host–virus interactomics during entry and infection. *Virus Adaptation and Treatment*. [Online]. **7**, p.57. [Accessed 21 July 2018]. Available from: https://www.dovepress.com/recent-advances-in-hostndashvirus-interactomics-during-entry-and-infec-peer-reviewed-article-VAAT.

Biasiotto, R., Aguiari, P., Rizzuto, R., Pinton, P., D'Agostino, D.M. and Ciminale, V. 2010. The p13 protein of human T cell leukemia virus type 1 (HTLV-1) modulates mitochondrial membrane potential and calcium uptake. *Biochimica et Biophysica Acta (BBA) - Bioenergetics*. [Online]. **1797**(6–7), pp.945–951. [Accessed 21 July 2018]. Available from: http://www.ncbi.nlm.nih.gov/pubmed/20188695.

Bohl, D.L., Storch, G.A., Ryschkewitsch, C., Gaudreault-Keener, M., Schnitzler, M.A., Major, E.O. and Brennan, D.C. 2005. Donor Origin of BK Virus in Renal Transplantation and Role of HLA C7 in Susceptibility to Sustained BK Viremia. *American Journal of Transplantation*. [Online]. **5**(9), pp.2213–2221. [Accessed 17 July 2018]. Available from: http://www.ncbi.nlm.nih.gov/pubmed/16095500.

Bollag, B., Chuke, W.F. and Frisque, R.J. 1989. Hybrid genomes of the polyomaviruses JC virus, BK virus, and simian virus 40: identification of sequences important for efficient transformation. *Journal of virology*. [Online]. **63**(2), pp.863–72. [Accessed 23 July 2018]. Available from: http://www.ncbi.nlm.nih.gov/pubmed/2536108.

BRADBURY, N.A. 1999. Intracellular CFTR: Localization and Function. *Physiological Reviews*. [Online]. **79**(1), pp.S175–S191. [Accessed 20 July 2018]. Available from: http://www.ncbi.nlm.nih.gov/pubmed/9922381.

Bräuner, T., Hülser, D.F. and Strasser, R.J. 1984. Comparative measurements of membrane potentials with microelectrodes and voltage-sensitive dyes. *Biochimica et Biophysica Acta (BBA) - Biomembranes*. [Online]. **771**(2), pp.208–216. [Accessed 21 July 2018]. Available from: https://www.sciencedirect.com/science/article/pii/0005273684905352.

Breau, W.C., Atwood, W.J. and Norkin, L.C. 1992. Class I major histocompatibility proteins are an essential component of the simian virus 40 receptor. *Journal of virology*. [Online]. **66**(4), pp.2037–45. [Accessed 23 July 2018]. Available from: http://www.ncbi.nlm.nih.gov/pubmed/1312619.

Brennan, D.C., Agha, I., Bohl, D.L., Schnitzler, M.A., Hardinger, K.L., Lockwood, M., Torrence, S., Schuessler, R., Roby, T., Gaudreault-Keener, M. and Storch, G.A. 2005. Incidence of BK with Tacrolimus Versus Cyclosporine and Impact of Preemptive Immunosuppression Reduction. *American Journal of Transplantation*. [Online]. **5**(3),

pp.582–594. [Accessed 17 July 2018]. Available from: http://www.ncbi.nlm.nih.gov/pubmed/15707414.

Brill, S.R., Ross, K.E., Davidow, C.J., Ye, M., Grantham, J.J. and Caplan, M.J. 1996. Immunolocalization of ion transport proteins in human autosomal dominant polycystic kidney epithelial cells. *Proceedings of the National Academy of Sciences of the United States of America*. [Online]. **93**(19), pp.10206–11. [Accessed 23 July 2018]. Available from: http://www.ncbi.nlm.nih.gov/pubmed/8816777.

Broekema, N.M., Abend, J.R., Bennett, S.M., Butel, J.S., Vanchiere, J.A. and Imperiale, M.J. 2010. A system for the analysis of BKV non-coding control regions: application to clinical isolates from an HIV/AIDS patient. *Virology*. [Online]. **407**(2), pp.368–73. [Accessed 18 July 2018]. Available from: http://www.ncbi.nlm.nih.gov/pubmed/20869740.

Broekema, N.M. and Imperiale, M.J. 2012. Efficient propagation of archetype BK and JC polyomaviruses. *Virology*. [Online]. **422**(2), pp.235–241. [Accessed 18 July 2018]. Available from: http://www.ncbi.nlm.nih.gov/pubmed/22099377.

Broekema, N.M. and Imperiale, M.J. 2013. miRNA regulation of BK polyomavirus replication during early infection. *Proceedings of the National Academy of Sciences*. [Online]. **110**(20), pp.8200–8205. [Accessed 18 July 2018]. Available from: http://www.ncbi.nlm.nih.gov/pubmed/23630296.

Buck, C.B., Pastrana, D. V, Lowy, D.R. and Schiller, J.T. 2004. Efficient intracellular assembly of papillomaviral vectors. *Journal of virology*. [Online]. **78**(2), pp.751–7. [Accessed 12 November 2018]. Available from: http://www.ncbi.nlm.nih.gov/pubmed/14694107.

Butel, J.S. 2012. Patterns of polyomavirus SV40 infections and associated cancers in humans: a model. *Current Opinion in Virology*. [Online]. **2**(4), pp.508–514. [Accessed 23 July 2018]. Available from: http://www.ncbi.nlm.nih.gov/pubmed/22771310.

Butel, J.S., Arrington, A.S., Wong, C., Lednicky, J.A. and Finegold, M.J. 1999. Molecular Evidence of Simian Virus 40 Infections in Children. *The Journal of Infectious Diseases*. [Online]. **180**(3), pp.884–887. [Accessed 23 July 2018]. Available from: http://www.ncbi.nlm.nih.gov/pubmed/10438386.

Butin-Israeli, V., Ben-nun-Shaul, O., Kopatz, I., Adam, S.A., Shimi, T., Goldman, R.D. and Oppenheim, A. 2011. Simian virus 40 induces lamin A/C fluctuations and nuclear envelope deformation during cell entry. *Nucleus*. [Online]. **2**(4), pp.320–330. [Accessed 20 July 2018]. Available from: http://www.ncbi.nlm.nih.gov/pubmed/21941111.

Caci, E., Caputo, A., Hinzpeter, A., Arous, N., Fanen, P., Sonawane, N., Verkman, A.S., Ravazzolo, R., Zegarra-Moran, O. and Galietta, L.J.V. 2008. Evidence for direct CFTR inhibition by CFTR $_{inh}$ -172 based on Arg ^{347} mutagenesis. *Biochemical Journal*. [Online]. **413**(1), pp.135–142. [Accessed 23 July 2018]. Available from: http://www.ncbi.nlm.nih.gov/pubmed/18366345.

Calvignac-Spencer, S., Feltkamp, M.C.W., Daugherty, M.D., Moens, U., Ramqvist, T., Johne, R., Ehlers, B. and Ehlers, B. 2016. A taxonomy update for the family Polyomaviridae. *Archives of Virology*. [Online]. **161**(6), pp.1739–1750. [Accessed 17 July 2018]. Available from: http://www.ncbi.nlm.nih.gov/pubmed/26923930.

Carter, J.J., Daugherty, M.D., Qi, X., Bheda-Malge, A., Wipf, G.C., Robinson, K., Roman, A., Malik, H.S. and Galloway, D.A. 2013. Identification of an overprinting gene in Merkel cell polyomavirus provides evolutionary insight into the birth of viral genes. *Proceedings of the National Academy of Sciences*. [Online]. **110**(31), pp.12744–12749. [Accessed 17 July 2018]. Available from: http://www.ncbi.nlm.nih.gov/pubmed/23847207.

Cavallo, R., Costa, C., Bergallo, M., Messina, M., Mazzucco, G. and Segoloni, G.P. 2007. A

case of ureteral lesions in a renal transplant recipient with a co-infection of BK virus and JC virus. *Nephrology Dialysis Transplantation*. [Online]. **22**(4), pp.1275–1275. [Accessed 17 July 2018]. Available from: http://www.ncbi.nlm.nih.gov/pubmed/17164316.

Chadda, R., Howes, M.T., Plowman, S.J., Hancock, J.F., Parton, R.G. and Mayor, S. 2007. Cholesterol-Sensitive Cdc42 Activation Regulates Actin Polymerization for Endocytosis via the GEEC Pathway. *Traffic*. [Online]. **8**(6), pp.702–717. [Accessed 18 July 2018]. Available from: http://www.ncbi.nlm.nih.gov/pubmed/17461795.

Chan, L. and Schrier, R.W. 1990. Effects of Calcium Channel Blockers on Renal Function. *Annual Review of Medicine*. [Online]. **41**(1), pp.289–302. [Accessed 20 July 2018]. Available from: http://www.annualreviews.org/doi/10.1146/annurev.me.41.020190.001445.

Chand, S., Atkinson, D., Collins, C., Briggs, D., Ball, S., Sharif, A., Skordilis, K., Vydianath, B., Neil, D. and Borrows, R. 2016. The Spectrum of Renal Allograft Failure S. M. Bagnasco, ed. *PLOS ONE*. [Online]. **11**(9), p.e0162278. [Accessed 17 July 2018]. Available from: http://dx.plos.org/10.1371/journal.pone.0162278.

Chandran, K., Farsetta, D.L. and Nibert, M.L. 2002. Strategy for nonenveloped virus entry: a hydrophobic conformer of the reovirus membrane penetration protein micro 1 mediates membrane disruption. *Journal of virology*. [Online]. **76**(19), pp.9920–33. [Accessed 19 July 2018]. Available from: http://www.ncbi.nlm.nih.gov/pubmed/12208969.

Chapagain, M.L. and Nerurkar, V.R. 2010. Human Polyomavirus JC (JCV) Infection of Human B Lymphocytes: A Possible Mechanism for JCV Transmigration across the Blood-Brain Barrier. *The Journal of Infectious Diseases*. [Online]. **202**(2), pp.184–191. [Accessed 18 July 2018]. Available from: http://www.ncbi.nlm.nih.gov/pubmed/20550458.

Chapagain, M.L., Nguyen, T., Bui, T., Verma, S. and Nerurkar, V.R. 2006. Comparison of real-time PCR and hemagglutination assay for quantitation of human polyomavirus JC. *Virology journal*. [Online]. **3**, p.3. [Accessed 21 July 2018]. Available from: http://www.ncbi.nlm.nih.gov/pubmed/16398941.

de Chassey, B., Meyniel-Schicklin, L., Aublin-Gex, A., André, P. and Lotteau, V. 2012. New horizons for antiviral drug discovery from virus–host protein interaction networks. *Current Opinion in Virology*. [Online]. **2**(5), pp.606–613. [Accessed 21 July 2018]. Available from: http://www.ncbi.nlm.nih.gov/pubmed/23025912.

Chatterjee, M., Weyandt, T.B. and Frisque, R.J. 2000. Identification of archetype and rearranged forms of BK virus in leukocytes from healthy individuals. *Journal of medical virology*. [Online]. **60**(3), pp.353–62. [Accessed 17 July 2018]. Available from: http://www.ncbi.nlm.nih.gov/pubmed/10630970.

Chen, P.-L., Hsu, P.-H., Fang, C.-Y., Chang, C.-F., Ou, W.-C., Wang, M. and Chang, D. 2011. Phosphorylation of Ser-80 of VP1 and Ser-254 of VP2 is essential for human BK virus propagation in tissue culture. *Journal of General Virology*. [Online]. **92**(11), pp.2637–2645. [Accessed 18 July 2018]. Available from: http://www.ncbi.nlm.nih.gov/pubmed/21752965.

Chen, T.-Y. and Hwang, T.-C. 2008. CLC-0 and CFTR: Chloride Channels Evolved From Transporters. *Physiological Reviews*. [Online]. **88**(2), pp.351–387. [Accessed 20 July 2018]. Available from: http://www.ncbi.nlm.nih.gov/pubmed/18391167.

Choi, B., Fermin, C.D., Comardelle, A.M., Haislip, A.M., Voss, T.G. and Garry, R.F. 2008. Alterations in intracellular potassium concentration by HIV-1 and SIV Nef. *Virology Journal*. [Online]. **5**(1), p.60. [Accessed 21 July 2018]. Available from: http://www.ncbi.nlm.nih.gov/pubmed/18489774.

Chowdhury, U.R., Holman, B.H. and Fautsch, M.P. 2013. ATP-Sensitive Potassium (K_{ATP})

Channel Openers Diazoxide and Nicorandil Lower Intraocular Pressure In Vivo. *Investigative Opthalmology & Visual Science*. [Online]. **54**(7), p.4892. [Accessed 21 July 2018]. Available from: http://iovs.arvojournals.org/article.aspx?doi=10.1167/iovs.13-11872.

Clinicaltrials.gov. (2018). *Evaluate Tolerability and Safety of BD03 for Prevention of CMV and BKV Reactivation in Kidney Transplant Recipient - Full Text View - ClinicalTrials.gov*. [online] Available at: https://clinicaltrials.gov/ct2/show/NCT03576014 [Accessed 21 Nov. 2018].

Çivril, F., Wehenkel, A., Giorgi, F.M., Santaguida, S., Di Fonzo, A., Grigorean, G., Ciccarelli, F.D. and Musacchio, A. 2010. Structural Analysis of the RZZ Complex Reveals Common Ancestry with Multisubunit Vesicle Tethering Machinery. *Structure*. [Online]. **18**(5), pp.616–626. [Accessed 18 July 2018]. Available from: http://www.ncbi.nlm.nih.gov/pubmed/20462495.

Comoli, P., Azzi, A., Maccario, R., Basso, S., Botti, G., Basile, G., Fontana, I., Labirio, M., Cometa, A., Poli, F., Perfumo, F., Locatelli, F. and Ginevri, F. 2004. Polyomavirus BK-specific immunity after kidney transplantation. *Transplantation*. [Online]. **78**(8), pp.1229–32. [Accessed 17 July 2018]. Available from: http://www.ncbi.nlm.nih.gov/pubmed/15502726.

Comoli, P., Cioni, M., Basso, S., Gagliardone, C., Potenza, L., Verrina, E., Luppi, M., Zecca, M., Ghiggeri, G.M. and Ginevri, F. 2013. Immunity to Polyomavirus BK Infection: Immune Monitoring to Regulate the Balance between Risk of BKV Nephropathy and Induction of Alloimmunity. *Clinical and Developmental Immunology*. [Online]. **2013**, pp.1–6. [Accessed 17 July 2018]. Available from: http://www.ncbi.nlm.nih.gov/pubmed/24000288.

Coric, P., Saribas, A.S., Abou-Gharbia, M., Childers, W., Condra, J.H., White, M.K., Safak, M. and Bouaziz, S. 2017. Nuclear Magnetic Resonance Structure of the Human Polyoma JC Virus Agnoprotein. *Journal of Cellular Biochemistry*. [Online]. **118**(10), pp.3268–3280. [Accessed 18 July 2018]. Available from: http://www.ncbi.nlm.nih.gov/pubmed/28295503.

Costa, C. and Cavallo, R. 2012. Polyomavirus-associated nephropathy. *World journal of transplantation*. [Online]. **2**(6), pp.84–94. [Accessed 17 July 2018]. Available from: http://www.ncbi.nlm.nih.gov/pubmed/24175200.

Crawford, I., Maloney, P.C., Zeitlin, P.L., Guggino, W.B., Hyde, S.C., Turley, H., Gatter, K.C., Harris, A. and Higgins, C.F. 1991. Immunocytochemical localization of the cystic fibrosis gene product CFTR. *Proceedings of the National Academy of Sciences of the United States of America*. [Online]. **88**(20), pp.9262–6. [Accessed 20 July 2018]. Available from: http://www.ncbi.nlm.nih.gov/pubmed/1718002.

Cubitt, C.L. 2006. Molecular Genetics of the BK Virus *In*: *Polyomaviruses and Human Diseases* [Online]. New York, NY: Springer New York, pp.85–95. [Accessed 18 July 2018]. Available from: http://www.ncbi.nlm.nih.gov/pubmed/16626029.

Dadhania, D., Snopkowski, C., Ding, R., Muthukumar, T., Lee, J., Bang, H., Sharma, V.K., Seshan, S., August, P., Kapur, S. and Suthanthiran, M. 2010. Validation of Noninvasive Diagnosis of BK Virus Nephropathy and Identification of Prognostic Biomarkers. *Transplantation Journal*. [Online]. **90**(2), pp.189–197. [Accessed 17 July 2018]. Available from: http://www.ncbi.nlm.nih.gov/pubmed/20526237.

Daha, M.R. and van Kooten, C. 2000. Is the proximal tubular cell a proinflammatory cell? *Nephrology, dialysis, transplantation : official publication of the European Dialysis and Transplant Association - European Renal Association*. [Online]. **15 Suppl 6**, pp.41–3. [Accessed 21 July 2018]. Available from: http://www.ncbi.nlm.nih.gov/pubmed/11143986.

Damm, E.-M., Pelkmans, L., Kartenbeck, J., Mezzacasa, A., Kurzchalia, T. and Helenius, A. 2005. Clathrin- and caveolin-1–independent endocytosis. *The Journal of Cell Biology*. [Online]. **168**(3), pp.477–488. [Accessed 18 July 2018]. Available from: http://www.ncbi.nlm.nih.gov/pubmed/15668298.

Daniels, R., Rusan, N.M., Wadsworth, P. and Hebert, D.N. 2006. SV40 VP2 and VP3 Insertion into ER Membranes Is Controlled by the Capsid Protein VP1: Implications for DNA Translocation out of the ER. *Molecular Cell*. [Online]. **24**(6), pp.955–966. [Accessed 18 July 2018]. Available from: http://www.ncbi.nlm.nih.gov/pubmed/17189196.

Daniels, R., Sadowicz, D. and Hebert, D.N. 2007. A Very Late Viral Protein Triggers the Lytic Release of SV40. *PLoS Pathogens*. [Online]. **3**(7), p.e98. [Accessed 18 July 2018]. Available from: http://dx.plos.org/10.1371/journal.ppat.0030098.

Darbinyan, A., Siddiqui, K.M., Slonina, D., Darbinian, N., Amini, S., White, M.K. and Khalili, K. 2004. Role of JC virus agnoprotein in DNA repair. *Journal of virology*. [Online]. **78**(16), pp.8593–600. [Accessed 18 July 2018]. Available from: http://www.ncbi.nlm.nih.gov/pubmed/15280468.

Dean, M., Rzhetsky, A. and Allikmets, R. 2001. The human ATP-binding cassette (ABC) transporter superfamily. *Genome research*. [Online]. **11**(7), pp.1156–66. [Accessed 21 July 2018]. Available from: http://www.ncbi.nlm.nih.gov/pubmed/11435397.

DeCaprio, J.A. and Garcea, R.L. 2013. A cornucopia of human polyomaviruses. *Nature Reviews Microbiology*. [Online]. **11**(4), pp.264–276. [Accessed 17 July 2018]. Available from: http://www.ncbi.nlm.nih.gov/pubmed/23474680.

Dejgaard, S.Y., Murshid, A., Erman, A., Kizilay, O., Verbich, D., Lodge, R., Dejgaard, K., Ly-Hartig, T.B.N., Pepperkok, R., Simpson, J.C. and Presley, J.F. 2008. Rab18 and Rab43 have key roles in ER-Golgi trafficking. *Journal of Cell Science*. [Online]. **121**(16), pp.2768–2781. [Accessed 18 July 2018]. Available from: http://www.ncbi.nlm.nih.gov/pubmed/18664496.

Dellis, O., Arbabian, A., Papp, B., Rowe, M., Joab, I. and Chomienne, C. 2011. Epstein-Barr virus latent membrane protein 1 increases calcium influx through store-operated channels in B lymphoid cells. *The Journal of biological chemistry*. [Online]. **286**(21), pp.18583–92. [Accessed 21 July 2018]. Available from: http://www.ncbi.nlm.nih.gov/pubmed/21454636.

Denyer, J., Worley, J., Cox, B., Allenby, G. and Martyn Banks 1998. HTS approaches to voltage-gated ion channel drug discovery. *Drug Discovery Today*. [Online]. **3**(7), pp.323–332. [Accessed 23 July 2018]. Available from: https://www.sciencedirect.com/science/article/pii/S1359644698011994.

Devuyst, O., Burrow, C.R., Schwiebert, E.M., Guggino, W.B. and Wilson, P.D. 1996. Developmental regulation of CFTR expression during human nephrogenesis. *American Journal of Physiology-Renal Physiology*. [Online]. **271**(3), pp.F723–F735. [Accessed 20 July 2018]. Available from: http://www.ncbi.nlm.nih.gov/pubmed/8853436.

Devuyst, O. and Guggino, W.B. 2002. Chloride channels in the kidney: lessons learned from knockout animals. *American Journal of Physiology-Renal Physiology*. [Online]. **283**(6), pp.F1176–F1191. [Accessed 20 July 2018]. Available from: http://www.ncbi.nlm.nih.gov/pubmed/12426234.

Dharnidharka, V.R., Cherikh, W.S. and Abbott, K.C. 2009. An OPTN Analysis of National Registry Data on Treatment of BK Virus Allograft Nephropathy in the United States. *Transplantation*. [Online]. **87**(7), pp.1019–1026. [Accessed 17 July 2018]. Available from: http://www.ncbi.nlm.nih.gov/pubmed/19352121.

Doerries, K. 2006. Human Polyomavirus JC and BK Persistent Infection *In*: *Polyomaviruses and Human Diseases* [Online]. New York, NY: Springer New York, pp.102–116.

[Accessed 17 July 2018]. Available from: http://www.ncbi.nlm.nih.gov/pubmed/16626031.

Dolei, A., Pietropaolo, V., Gomes, E., Di Taranto, C., Ziccheddu, M., Spanu, M.A., Lavorino, C., Manca, M. and Degener, A.M. 2000. Polyomavirus persistence in lymphocytes: prevalence in lymphocytes from blood donors and healthy personnel of a blood transfusion centre. *Journal of General Virology*. [Online]. **81**(8), pp.1967–1973. [Accessed 18 July 2018]. Available from: http://www.ncbi.nlm.nih.gov/pubmed/10900035.

Drab, M., Verkade, P., Elger, M., Kasper, M., Lohn, M., Lauterbach, B., Menne, J., Lindschau, C., Mende, F., Luft, F.C., Schedl, A., Haller, H. and Kurzchalia, T. V 2001. Loss of Caveolae, Vascular Dysfunction, and Pulmonary Defects in Caveolin-1 Gene-Disrupted Mice. *Science*. [Online]. **293**(5539), pp.2449–2452. [Accessed 18 July 2018]. Available from: http://www.ncbi.nlm.nih.gov/pubmed/11498544.

Drachenberg, C.B., Beskow, C.O., Cangro, C.B., Bourquin, P.M., Simsir, A., Fink, J., Weir, M.R., Klassen, D.K., Bartlett, S.T. and Papadimitriou, J.C. 1999. Human polyoma virus in renal allograft biopsies: morphological findings and correlation with urine cytology. *Human pathology*. [Online]. **30**(8), pp.970–7. [Accessed 17 July 2018]. Available from: http://www.ncbi.nlm.nih.gov/pubmed/10452511.

Drachenberg, C.B., Papadimitriou, J.C., Hirsch, H.H., Wali, R., Crowder, C., Nogueira, J., Cangro, C.B., Mendley, S., Mian, A. and Ramos, E. 2004. Histological Patterns of Polyomavirus Nephropathy: Correlation with Graft Outcome and Viral Load. *American Journal of Transplantation*. [Online]. **4**(12), pp.2082–2092. [Accessed 17 July 2018]. Available from: http://www.ncbi.nlm.nih.gov/pubmed/15575913.

Drachenberg, C.B., Papadimitriou, J.C., Wali, R., Cubitt, C.L. and Ramos, E. 2003. BK polyoma virus allograft nephropathy: ultrastructural features from viral cell entry to lysis. *American journal of transplantation : official journal of the American Society of Transplantation and the American Society of Transplant Surgeons*. [Online]. **3**(11), pp.1383–92. [Accessed 18 July 2018]. Available from: http://www.ncbi.nlm.nih.gov/pubmed/14525599.

Dugan, A.S., Eash, S. and Atwood, W.J. 2005. An N-Linked Glycoprotein with (2,3)-Linked Sialic Acid Is a Receptor for BK Virus. *Journal of Virology*. [Online]. **79**(22), pp.14442–14445. [Accessed 18 July 2018]. Available from: http://www.ncbi.nlm.nih.gov/pubmed/16254379.

Dugan, A.S., Gasparovic, M.L., Tsomaia, N., Mierke, D.F., O'Hara, B.A., Manley, K. and Atwood, W.J. 2007. Identification of Amino Acid Residues in BK Virus VP1 That Are Critical for Viability and Growth. *Journal of Virology*. [Online]. **81**(21), pp.11798–11808. [Accessed 18 July 2018]. Available from: http://www.ncbi.nlm.nih.gov/pubmed/17699578.

Dupzyk, A. and Tsai, B. 2016. How Polyomaviruses Exploit the ERAD Machinery to Cause Infection. *Viruses*. [Online]. **8**(9), p.242. [Accessed 20 July 2018]. Available from: http://www.ncbi.nlm.nih.gov/pubmed/27589785.

Eash, S. and Atwood, W.J. 2005. Involvement of cytoskeletal components in BK virus infectious entry. *Journal of virology*. [Online]. **79**(18), pp.11734–41. [Accessed 18 July 2018]. Available from: http://www.ncbi.nlm.nih.gov/pubmed/16140751.

Eash, S., Querbes, W. and Atwood, W.J. 2004. Infection of vero cells by BK virus is dependent on caveolae. *Journal of virology*. [Online]. **78**(21), pp.11583–90. [Accessed 18 July 2018]. Available from: http://www.ncbi.nlm.nih.gov/pubmed/15479799.

Ebert, D.H., Deussing, J., Peters, C. and Dermody, T.S. 2002. Cathepsin L and Cathepsin B Mediate Reovirus Disassembly in Murine Fibroblast Cells. *Journal of Biological Chemistry*. [Online]. **277**(27), pp.24609–24617. [Accessed 23 July 2018]. Available

from: http://www.ncbi.nlm.nih.gov/pubmed/11986312.

Edwards, J.C. and Kahl, C.R. 2010. Chloride channels of intracellular membranes. *FEBS Letters*. [Online]. **584**(10), pp.2102–2111. [Accessed 20 July 2018]. Available from: http://www.ncbi.nlm.nih.gov/pubmed/20100480.

Ehlers, B. and Moens, U. 2014. Genome analysis of non-human primate polyomaviruses. *Infection, Genetics and Evolution*. [Online]. **26**, pp.283–294. [Accessed 17 July 2018]. Available from: http://www.ncbi.nlm.nih.gov/pubmed/24933462.

Ehrhardt, A., Chung, W.J., Pyle, L.C., Wang, W., Nowotarski, K., Mulvihill, C.M., Ramjeesingh, M., Hong, J., Velu, S.E., Lewis, H.A., Atwell, S., Aller, S., Bear, C.E., Lukacs, G.L., Kirk, K.L. and Sorscher, E.J. 2016. Channel Gating Regulation by the Cystic Fibrosis Transmembrane Conductance Regulator (CFTR) First Cytosolic Loop. *Journal of Biological Chemistry*. [Online]. **291**(4), pp.1854–1865. [Accessed 23 July 2018]. Available from: http://www.ncbi.nlm.nih.gov/pubmed/26627831.

Elder, R.T., Xu, X., Williams, J.W., Gong, H., Finnegan, A. and Chong, A.S. 1997. The immunosuppressive metabolite of leflunomide, A77 1726, affects murine T cells through two biochemical mechanisms. *Journal of immunology (Baltimore, Md. : 1950)*. [Online]. **159**(1), pp.22–7. [Accessed 17 July 2018]. Available from: http://www.ncbi.nlm.nih.gov/pubmed/9200434.

Elphick, G.F., Querbes, W., Jordan, J.A., Gee, G. V, Eash, S., Manley, K., Dugan, A., Stanifer, M., Bhatnagar, A., Kroeze, W.K., Roth, B.L. and Atwood, W.J. 2004. The Human Polyomavirus, JCV, Uses Serotonin Receptors to Infect Cells. *Science*. [Online]. **306**(5700), pp.1380–1383. [Accessed 23 July 2018]. Available from: http://www.ncbi.nlm.nih.gov/pubmed/15550673.

Engel, S., Heger, T., Mancini, R., Herzog, F., Kartenbeck, J., Hayer, A. and Helenius, A. 2011. Role of Endosomes in Simian Virus 40 Entry and Infection. *Journal of Virology*. [Online]. **85**(9), pp.4198–4211. [Accessed 23 July 2018]. Available from: http://www.ncbi.nlm.nih.gov/pubmed/21345959.

Engels, E.A., Frisch, M., Goedert, J.J., Biggar, R.J. and Miller, R.W. 2002. Merkel cell carcinoma and HIV infection. *The Lancet*. [Online]. **359**(9305), pp.497–498. [Accessed 23 July 2018]. Available from: http://www.ncbi.nlm.nih.gov/pubmed/11853800.

Epps, D.E., Wolfe, M.L. and Groppi, V. 1994. Characterization of the steady-state and dynamic fluorescence properties of the potential-sensitive dye bis-(1,3-dibutylbarbituric acid)trimethine oxonol (Dibac4(3)) in model systems and cells. *Chemistry and physics of lipids*. [Online]. **69**(2), pp.137–50. [Accessed 23 July 2018]. Available from: http://www.ncbi.nlm.nih.gov/pubmed/8181103.

Erickson, K.D., Garcea, R.L. and Tsai, B. 2009. Ganglioside GT1b is a putative host cell receptor for the Merkel cell polyomavirus. *Journal of virology*. [Online]. **83**(19), pp.10275–9. [Accessed 23 July 2018]. Available from: http://www.ncbi.nlm.nih.gov/pubmed/19605473.

Evans, G.L., Caller, L.G., Foster, V. and Crump, C.M. 2015. Anion homeostasis is important for non-lytic release of BK polyomavirus from infected cells. *Open Biology*. [Online]. **5**(8), p.150041. [Accessed 20 July 2018]. Available from: http://www.ncbi.nlm.nih.gov/pubmed/26246492.

Ewers, H., Römer, W., Smith, A.E., Bacia, K., Dmitrieff, S., Chai, W., Mancini, R., Kartenbeck, J., Chambon, V., Berland, L., Oppenheim, A., Schwarzmann, G., Feizi, T., Schwille, P., Sens, P., Helenius, A. and Johannes, L. 2010. GM1 structure determines SV40-induced membrane invagination and infection. *Nature Cell Biology*. [Online]. **12**(1), pp.11–18. [Accessed 18 July 2018]. Available from: http://www.ncbi.nlm.nih.gov/pubmed/20023649.

Fang, C.-Y., Chen, H.-Y., Wang, M., Chen, P.-L., Chang, C.-F., Chen, L.-S., Shen, C.-H.,

Ou, W.-C., Tsai, M.-D., Hsu, P.-H. and Chang, D. 2010. Global analysis of modifications of the human BK virus structural proteins by LC-MS/MS. *Virology*. [Online]. **402**(1), pp.164–176. [Accessed 17 July 2018]. Available from: http://www.ncbi.nlm.nih.gov/pubmed/20381826.

Fayard, E., Xue, G., Parcellier, A., Bozulic, L. and Hemmings, B.A. 2010. Protein Kinase B (PKB/Akt), a Key Mediator of the PI3K Signaling Pathway *In*: *Current topics in microbiology and immunology* [Online]., pp.31–56. [Accessed 20 July 2018]. Available from: http://www.ncbi.nlm.nih.gov/pubmed/20517722.

Feng, H., Shuda, M., Chang, Y. and Moore, P.S. 2008. Clonal Integration of a Polyomavirus in Human Merkel Cell Carcinoma. *Science*. [Online]. **319**(5866), pp.1096–1100. [Accessed 17 July 2018]. Available from: http://www.ncbi.nlm.nih.gov/pubmed/18202256.

Feng, H., Taylor, J.L., Benos, P. V, Newton, R., Waddell, K., Lucas, S.B., Chang, Y. and Moore, P.S. 2007. Human transcriptome subtraction by using short sequence tags to search for tumor viruses in conjunctival carcinoma. *Journal of virology*. [Online]. **81**(20), pp.11332–40. [Accessed 23 July 2018]. Available from: http://www.ncbi.nlm.nih.gov/pubmed/17686852.

Ferenczy, M.W., Marshall, L.J., Nelson, C.D.S., Atwood, W.J., Nath, A., Khalili, K. and Major, E.O. 2012. Molecular Biology, Epidemiology, and Pathogenesis of Progressive Multifocal Leukoencephalopathy, the JC Virus-Induced Demyelinating Disease of the Human Brain. *Clinical Microbiology Reviews*. [Online]. **25**(3), pp.471–506. [Accessed 17 July 2018]. Available from: http://www.ncbi.nlm.nih.gov/pubmed/22763635.

Field, M. 1979. Mechanisms of action of cholera and Escherichia coli enterotoxins. *The American Journal of Clinical Nutrition*. [Online]. **32**(1), pp.189–196. [Accessed 23 July 2018]. Available from: http://www.ncbi.nlm.nih.gov/pubmed/32766.

Forgac, M. 2007. Vacuolar ATPases: rotary proton pumps in physiology and pathophysiology. *Nature Reviews Molecular Cell Biology*. [Online]. **8**(11), pp.917–929. [Accessed 20 July 2018]. Available from: http://www.ncbi.nlm.nih.gov/pubmed/17912264.

Fotin, A., Cheng, Y., Sliz, P., Grigorieff, N., Harrison, S.C., Kirchhausen, T. and Walz, T. 2004. Molecular model for a complete clathrin lattice from electron cryomicroscopy. *Nature*. [Online]. **432**(7017), pp.573–579. [Accessed 18 July 2018]. Available from: http://www.ncbi.nlm.nih.gov/pubmed/15502812.

Frisque, R.J. and White, F.A. 1992. The Molecular Biology of JC Virus, Causative Agent of Progressive Multifocal Leukoencephalopathy *In*: *Molecular Neurovirology* [Online]. Totowa, NJ: Humana Press, pp.25–158. [Accessed 23 July 2018]. Available from: http://link.springer.com/10.1007/978-1-4612-0407-7_2.

Fu, S.-C., Imai, K. and Horton, P. 2011. Prediction of leucine-rich nuclear export signal containing proteins with NESsential. *Nucleic Acids Research*. [Online]. **39**(16), pp.e111–e111. [Accessed 18 July 2018]. Available from: http://www.ncbi.nlm.nih.gov/pubmed/21705415.

Fuller, C.M. and Benos, D.J. 1992. CFTR! *American Journal of Physiology-Cell Physiology*. [Online]. **263**(2), pp.C267–C286. [Accessed 20 July 2018]. Available from: http://www.ncbi.nlm.nih.gov/pubmed/1381146.

Fulmer, S.B., Schwiebert, E.M., Morales, M.M., Guggino, W.B. and Cutting, G.R. 1995. Two cystic fibrosis transmembrane conductance regulator mutations have different effects on both pulmonary phenotype and regulation of outwardly rectified chloride currents. *Proceedings of the National Academy of Sciences of the United States of America*. [Online]. **92**(15), pp.6832–6. [Accessed 20 July 2018]. Available from: http://www.ncbi.nlm.nih.gov/pubmed/7542778.

Gabriel, S.E., Clarke, L.L., Boucher, R.C. and Stutts, M.J. 1993. CFTR and outward rectifying chloride channels are distinct proteins with a regulatory relationship. *Nature*. [Online]. **363**(6426), pp.263–266. [Accessed 23 July 2018]. Available from: http://www.ncbi.nlm.nih.gov/pubmed/7683773.

Gadsby, D.C., Vergani, P. and Csanády, L. 2006. The ABC protein turned chloride channel whose failure causes cystic fibrosis. *Nature*. [Online]. **440**(7083), pp.477–483. [Accessed 20 July 2018]. Available from: http://www.nature.com/articles/nature04712.

Galloway, C.J., Dean, G.E., Marsh, M., Rudnick, G. and Mellman, I. 1983. Acidification of macrophage and fibroblast endocytic vesicles in vitro. *Proceedings of the National Academy of Sciences of the United States of America*. [Online]. **80**(11), pp.3334–8. [Accessed 20 July 2018]. Available from: http://www.ncbi.nlm.nih.gov/pubmed/6190176.

Garcea, R.L. and Imperiale, M.J. 2003. Simian virus 40 infection of humans. *Journal of virology*. [Online]. **77**(9), pp.5039–45. [Accessed 23 July 2018]. Available from: http://www.ncbi.nlm.nih.gov/pubmed/12692206.

Gardner, S.D., Field, A.M., Coleman, D. V and Hulme, B. 1971. New human papovavirus (B.K.) isolated from urine after renal transplantation. *Lancet (London, England)*. [Online]. **1**(7712), pp.1253–7. [Accessed 17 July 2018]. Available from: http://www.ncbi.nlm.nih.gov/pubmed/4104714.

Garlid, K.D. and Halestrap, A.P. 2012. The mitochondrial KATP channel—Fact or fiction? *Journal of Molecular and Cellular Cardiology*. [Online]. **52**(3), pp.578–583. [Accessed 22 July 2018]. Available from: http://www.ncbi.nlm.nih.gov/pubmed/22240339.

Gasparovic, M.L., Gee, G. V and Atwood, W.J. 2006. JC virus minor capsid proteins Vp2 and Vp3 are essential for virus propagation. *Journal of virology*. [Online]. **80**(21), pp.10858–61. [Accessed 18 July 2018]. Available from: http://www.ncbi.nlm.nih.gov/pubmed/17041227.

Gasteiger, E., Gattiker, A., Hoogland, C., Ivanyi, I., Appel, R.D. and Bairoch, A. 2003. ExPASy: The proteomics server for in-depth protein knowledge and analysis. *Nucleic acids research*. [Online]. **31**(13), pp.3784–8. [Accessed 12 November 2018]. Available from: http://www.ncbi.nlm.nih.gov/pubmed/12824418.

Gaynor, A.M., Nissen, M.D., Whiley, D.M., Mackay, I.M., Lambert, S.B., Wu, G., Brennan, D.C., Storch, G.A., Sloots, T.P. and Wang, D. 2007. Identification of a novel polyomavirus from patients with acute respiratory tract infections. *PLoS pathogens*. [Online]. **3**(5), p.e64. [Accessed 17 July 2018]. Available from: http://www.ncbi.nlm.nih.gov/pubmed/17480120.

Gee, G. V., Tsomaia, N., Mierke, D.F. and Atwood, W.J. 2004. Modeling a Sialic Acid Binding Pocket in the External Loops of JC Virus VP1. *Journal of Biological Chemistry*. [Online]. **279**(47), pp.49172–49176. [Accessed 23 July 2018]. Available from: http://www.ncbi.nlm.nih.gov/pubmed/15347668.

Gehring, G., Rohrmann, K., Atenchong, N., Mittler, E., Becker, S., Dahlmann, F., Pöhlmann, S., Vondran, F.W.R., David, S., Manns, M.P., Ciesek, S. and von Hahn, T. 2014. The clinically approved drugs amiodarone, dronedarone and verapamil inhibit filovirus cell entry. *Journal of Antimicrobial Chemotherapy*. [Online]. **69**(8), pp.2123–2131. [Accessed 20 July 2018]. Available from: http://www.ncbi.nlm.nih.gov/pubmed/24710028.

Geisow, M.J. and Evans, W.H. 1984. pH in the endosome. Measurements during pinocytosis and receptor-mediated endocytosis. *Experimental cell research*. [Online]. **150**(1), pp.36–46. [Accessed 20 July 2018]. Available from: http://www.ncbi.nlm.nih.gov/pubmed/6198190.

Gerits, N., Johannessen, M., Tümmler, C., Walquist, M., Kostenko, S., Snapkov, I., van

Loon, B., Ferrari, E., Hübscher, U. and Moens, U. 2015. Agnoprotein of polyomavirus BK interacts with proliferating cell nuclear antigen and inhibits DNA replication. *Virology Journal*. [Online]. **12**(1), p.7. [Accessed 18 July 2018]. Available from: http://www.virologyj.com/content/12/1/7.

Gerits, N. and Moens, U. 2012. Agnoprotein of mammalian polyomaviruses. *Virology*. [Online]. **432**(2), pp.316–326. [Accessed 17 July 2018]. Available from: http://www.ncbi.nlm.nih.gov/pubmed/22726243.

Gheit, T., Dutta, S., Oliver, J., Robitaille, A., Hampras, S., Combes, J.-D., McKay-Chopin, S., Le Calvez-Kelm, F., Fenske, N., Cherpelis, B., Giuliano, A.R., Franceschi, S., McKay, J., Rollison, D.E. and Tommasino, M. 2017. Isolation and characterization of a novel putative human polyomavirus. *Virology*. [Online]. **506**, pp.45–54. [Accessed 17 July 2018]. Available from: http://www.ncbi.nlm.nih.gov/pubmed/28342387.

Giebisch, G. 2001. Renal potassium channels: Function, regulation, and structure. *Kidney International*. [Online]. **60**(2), pp.436–445. [Accessed 20 July 2018]. Available from: http://www.ncbi.nlm.nih.gov/pubmed/11473623.

Giebisch, G. 1998. Renal potassium transport: mechanisms and regulation. *The American journal of physiology*. [Online]. **274**(5 Pt 2), pp.F817-33. [Accessed 20 July 2018]. Available from: http://www.ncbi.nlm.nih.gov/pubmed/9612319.

Gilbert, J. and Benjamin, T. 2004. Uptake pathway of polyomavirus via ganglioside GD1a. *Journal of virology*. [Online]. **78**(22), pp.12259–67. [Accessed 18 July 2018]. Available from: http://www.ncbi.nlm.nih.gov/pubmed/15507613.

Gilbert, J.M. and Benjamin, T.L. 2000. Early steps of polyomavirus entry into cells. *Journal of virology*. [Online]. **74**(18), pp.8582–8. [Accessed 23 July 2018]. Available from: http://www.ncbi.nlm.nih.gov/pubmed/10954560.

Gilbert, J.M., Goldberg, I.G. and Benjamin, T.L. 2003a. Cell penetration and trafficking of polyomavirus. *Journal of virology*. [Online]. **77**(4), pp.2615–22. [Accessed 18 July 2018]. Available from: http://www.ncbi.nlm.nih.gov/pubmed/12552000.

Gilbert, J.M., Goldberg, I.G. and Benjamin, T.L. 2003b. Cell penetration and trafficking of polyomavirus. *Journal of virology*. [Online]. **77**(4), pp.2615–22. [Accessed 23 July 2018]. Available from: http://www.ncbi.nlm.nih.gov/pubmed/12552000.

Gillingham, A.K., Sinka, R., Torres, I.L., Lilley, K.S. and Munro, S. 2014. Toward a Comprehensive Map of the Effectors of Rab GTPases. *Developmental Cell*. [Online]. **31**(3), pp.358–373. [Accessed 18 July 2018]. Available from: http://www.ncbi.nlm.nih.gov/pubmed/25453831.

Ginevri, F., Azzi, A., Hirsch, H.H., Basso, S., Fontana, I., Cioni, M., Bodaghi, S., Salotti, V., Rinieri, A., Botti, G., Perfumo, F., Locatelli, F. and Comoli, P. 2007. Prospective Monitoring of Polyomavirus BK Replication and Impact of Pre-Emptive Intervention in Pediatric Kidney Recipients. *American Journal of Transplantation*. [Online]. **7**(12), pp.2727–2735. [Accessed 17 July 2018]. Available from: http://www.ncbi.nlm.nih.gov/pubmed/17908275.

Giorda, K.M., Raghava, S. and Hebert, D.N. 2012. The Simian virus 40 late viral protein VP4 disrupts the nuclear envelope for viral release. *Journal of virology*. [Online]. **86**(6), pp.3180–92. [Accessed 17 July 2018]. Available from: http://www.ncbi.nlm.nih.gov/pubmed/22238309.

Glebov, O.O., Bright, N.A. and Nichols, B.J. 2006. Flotillin-1 defines a clathrin-independent endocytic pathway in mammalian cells. *Nature Cell Biology*. [Online]. **8**(1), pp.46–54. [Accessed 18 July 2018]. Available from: http://www.ncbi.nlm.nih.gov/pubmed/16341206.

Glotzer, J.B., Michou, A.I., Baker, A., Saltik, M. and Cotten, M. 2001. Microtubule-

independent motility and nuclear targeting of adenoviruses with fluorescently labeled genomes. *Journal of virology*. [Online]. **75**(5), pp.2421–34. [Accessed 23 July 2018]. Available from: http://www.ncbi.nlm.nih.gov/pubmed/11160745.

Gollasch, M., Bychkov, R., Ried, C., Behrendt, F., Scholze, S., Luft, F.C. and Haller, H. 1995. Pinacidil relaxes porcine and human coronary arteries by activating ATP-dependent potassium channels in smooth muscle cells. *The Journal of pharmacology and experimental therapeutics*. [Online]. **275**(2), pp.681–92. [Accessed 21 July 2018]. Available from: http://www.ncbi.nlm.nih.gov/pubmed/7473155.

González, Oades, Leychkis, Harootunian and Negulescu 1999. Cell-based assays and instrumentation for screening ion-channel targets. *Drug discovery today*. [Online]. **4**(9), pp.431–439. [Accessed 23 July 2018]. Available from: http://www.ncbi.nlm.nih.gov/pubmed/10461154.

Goodwin, E.C., Lipovsky, A., Inoue, T., Magaldi, T.G., Edwards, A.P.B., Van Goor, K.E.Y., Paton, A.W., Paton, J.C., Atwood, W.J., Tsai, B. and DiMaio, D. 2011. BiP and Multiple DNAJ Molecular Chaperones in the Endoplasmic Reticulum Are Required for Efficient Simian Virus 40 Infection. *mBio*. [Online]. **2**(3), pp.e00101-11. [Accessed 20 July 2018]. Available from: http://www.ncbi.nlm.nih.gov/pubmed/21673190.

Gorrill, T.S. and Khalili, K. 2005. Cooperative interaction of p65 and C/EBPβ modulates transcription of BKV early promoter. *Virology*. [Online]. **335**(1), pp.1–9. [Accessed 18 July 2018]. Available from: http://www.ncbi.nlm.nih.gov/pubmed/15823601.

Gosert, R., Rinaldo, C.H., Funk, G.A., Egli, A., Ramos, E., Drachenberg, C.B. and Hirsch, H.H. 2008. Polyomavirus BK with rearranged noncoding control region emerge in vivo in renal transplant patients and increase viral replication and cytopathology. *The Journal of Experimental Medicine*. [Online]. **205**(4), pp.841–852. [Accessed 18 July 2018]. Available from: http://www.ncbi.nlm.nih.gov/pubmed/18347101.

Goudsmit, J., Wertheim-van Dillen, P., van Strien, A. and van der Noordaa, J. 1982. The role of BK virus in acute respiratory tract disease and the presence of BKV DNA in tonsils. *Journal of medical virology*. [Online]. **10**(2), pp.91–9. [Accessed 17 July 2018]. Available from: http://www.ncbi.nlm.nih.gov/pubmed/6292361.

Greber, U.F. and Way, M. 2006. A Superhighway to Virus Infection. *Cell*. [Online]. **124**(4), pp.741–754. [Accessed 18 July 2018]. Available from: http://www.ncbi.nlm.nih.gov/pubmed/16497585.

Greger, R. 1985. Ion transport mechanisms in thick ascending limb of Henle's loop of mammalian nephron. *Physiological Reviews*. [Online]. **65**(3), pp.760–797. [Accessed 20 July 2018]. Available from: http://www.ncbi.nlm.nih.gov/pubmed/2409564.

Gribble, F.M., Tucker, S.J., Seino, S. and Ashcroft, F.M. 1998. Tissue specificity of sulfonylureas: studies on cloned cardiac and beta-cell K(ATP) channels. *Diabetes*. [Online]. **47**(9), pp.1412–8. [Accessed 22 July 2018]. Available from: http://www.ncbi.nlm.nih.gov/pubmed/9726229.

Grinde, B., Gayorfar, M. and Rinaldo, C.H. 2007. Impact of a polyomavirus (BKV) infection on mRNA expression in human endothelial cells. *Virus Research*. [Online]. **123**(1), pp.86–94. [Accessed 20 July 2018]. Available from: http://www.ncbi.nlm.nih.gov/pubmed/16996634.

Groux-Degroote, S., Guérardel, Y. and Delannoy, P. 2017. Gangliosides: Structures, Biosynthesis, Analysis, and Roles in Cancer. *ChemBioChem*. [Online]. **18**(13), pp.1146–1154. [Accessed 18 July 2018]. Available from: http://www.ncbi.nlm.nih.gov/pubmed/28295942.

Haggerty, S., Walker, D.L. and Frisque, R.J. 1989. JC virus-simian virus 40 genomes containing heterologous regulatory signals and chimeric early regions: identification of regions restricting transformation by JC virus. *Journal of virology*. [Online]. **63**(5),

pp.2180–90. [Accessed 23 July 2018]. Available from: http://www.ncbi.nlm.nih.gov/pubmed/2539511.

Haggie, P.M. and Verkman, A.S. 2009. Defective organellar acidification as a cause of cystic fibrosis lung disease: reexamination of a recurring hypothesis. *American Journal of Physiology-Lung Cellular and Molecular Physiology*. [Online]. **296**(6), pp.L859–L867. [Accessed 20 July 2018]. Available from: http://www.physiology.org/doi/10.1152/ajplung.00018.2009.

Halloran, P.F. 2004. Immunosuppressive Drugs for Kidney Transplantation. *New England Journal of Medicine*. [Online]. **351**(26), pp.2715–2729. [Accessed 17 July 2018]. Available from: http://www.nejm.org/doi/abs/10.1056/NEJMra033540.

Hallows, K.R., Raghuram, V., Kemp, B.E., Witters, L.A. and Foskett, J.K. 2000. Inhibition of cystic fibrosis transmembrane conductance regulator by novel interaction with the metabolic sensor AMP-activated protein kinase. *Journal of Clinical Investigation*. [Online]. **105**(12), pp.1711–1721. [Accessed 23 July 2018]. Available from: http://www.ncbi.nlm.nih.gov/pubmed/10862786.

Hamill, O.P., Marty, A., Neher, E., Sakmann, B. and Sigworth, F.J. 1981. Improved patch-clamp techniques for high-resolution current recording from cells and cell-free membrane patches. *Pflügers Archiv - European Journal of Physiology*. [Online]. **391**(2), pp.85–100. [Accessed 23 July 2018]. Available from: http://link.springer.com/10.1007/BF00656997.

Hanley, P.J., Dröse, S., Brandt, U., Lareau, R.A., Banerjee, A.L., Srivastava, D.K., Banaszak, L.J., Barycki, J.J., Van Veldhoven, P.P. and Daut, J. 2005. 5-Hydroxydecanoate is metabolised in mitochondria and creates a rate-limiting bottleneck for beta-oxidation of fatty acids. *The Journal of physiology*. [Online]. **562**(Pt 2), pp.307–18. [Accessed 22 July 2018]. Available from: http://www.ncbi.nlm.nih.gov/pubmed/15513944.

Hariharan, S. 2006. BK virus nephritis after renal transplantation. *Kidney International*. [Online]. **69**(4), pp.655–662. [Accessed 17 July 2018]. Available from: http://www.ncbi.nlm.nih.gov/pubmed/16395271.

Harikumar, P. and Reeves, J.P. 1983. The lysosomal proton pump is electrogenic. *The Journal of biological chemistry*. [Online]. **258**(17), pp.10403–10. [Accessed 20 July 2018]. Available from: http://www.ncbi.nlm.nih.gov/pubmed/6224789.

Harris, K.F., Christensen, J.B. and Imperiale, M.J. 1996. BK virus large T antigen: interactions with the retinoblastoma family of tumor suppressor proteins and effects on cellular growth control. *Journal of virology*. [Online]. **70**(4), pp.2378–86. [Accessed 18 July 2018]. Available from: http://www.ncbi.nlm.nih.gov/pubmed/8642665.

Harris, K.F., Christensen, J.B., Radany, E.H. and Imperiale, M.J. 1998. Novel mechanisms of E2F induction by BK virus large-T antigen: requirement of both the pRb-binding and the J domains. *Molecular and cellular biology*. [Online]. **18**(3), pp.1746–56. [Accessed 18 July 2018]. Available from: http://www.ncbi.nlm.nih.gov/pubmed/9488491.

Hayashi, K., Wakino, S., Sugano, N., Ozawa, Y., Homma, K. and Saruta, T. 2007. Ca2+ Channel Subtypes and Pharmacology in the Kidney. *Circulation Research*. [Online]. **100**(3), pp.342–353. [Accessed 20 July 2018]. Available from: http://www.ncbi.nlm.nih.gov/pubmed/17307972.

Haycox, C.L., Kim, S., Fleckman, P., Smith, L.T., Piepkorn, M., Sundberg, J.P., Howell, D.N. and Miller, S.E. 1999. Trichodysplasia spinulosa--a newly described folliculocentric viral infection in an immunocompromised host. *The journal of investigative dermatology. Symposium proceedings*. [Online]. **4**(3), pp.268–71. [Accessed 17 July 2018]. Available from: http://www.ncbi.nlm.nih.gov/pubmed/10674379.

Hebert, S.C. and Andreoli, T.E. 1984. Control of NaCl transport in the thick ascending limb.

American Journal of Physiology-Renal Physiology. [Online]. **246**(6), pp.F745–F756. [Accessed 20 July 2018]. Available from: http://www.ncbi.nlm.nih.gov/pubmed/6377912.

Hegedűs, T., Aleksandrov, A., Mengos, A., Cui, L., Jensen, T.J. and Riordan, J.R. 2009. Role of individual R domain phosphorylation sites in CFTR regulation by protein kinase A. *Biochimica et Biophysica Acta (BBA) - Biomembranes*. [Online]. **1788**(6), pp.1341–1349. [Accessed 12 November 2018]. Available from: http://www.ncbi.nlm.nih.gov/pubmed/19328185.

Heider, S. and Metzner, C. 2014. Quantitative real-time single particle analysis of virions. *Virology*. [Online]. **462**–**463**, pp.199–206. [Accessed 21 July 2018]. Available from: http://www.ncbi.nlm.nih.gov/pubmed/24999044.

Helle, F., Brochot, E., Handala, L., Martin, E., Castelain, S., Francois, C. and Duverlie, G. 2017. Biology of the BKPyV: An Update. *Viruses*. [Online]. **9**(11), p.327. [Accessed 18 July 2018]. Available from: http://www.ncbi.nlm.nih.gov/pubmed/29099746.

Henriksen, S., Hansen, T., Bruun, J.-A. and Rinaldo, C.H. 2016. The Presumed Polyomavirus Viroporin VP4 of Simian Virus 40 or Human BK Polyomavirus Is Not Required for Viral Progeny Release. *Journal of virology*. [Online]. **90**(22), pp.10398–10413. [Accessed 17 July 2018]. Available from: http://www.ncbi.nlm.nih.gov/pubmed/27630227.

Heritage, J., Chesters, P.M. and McCance, D.J. 1981. The persistence of papovavirus BK DNA sequences in normal human renal tissue. *Journal of medical virology*. [Online]. **8**(2), pp.143–50. [Accessed 17 July 2018]. Available from: http://www.ncbi.nlm.nih.gov/pubmed/6271922.

Herrmann, M., Ruprecht, K., Sauter, M., Martinez, J., van Heteren, P., Glas, M., Best, B., Meyerhans, A., Roemer, K. and Mueller-Lantzsch, N. 2010. Interaction of human immunodeficiency virus gp120 with the voltage-gated potassium channel BEC1. *FEBS Letters*. [Online]. **584**(16), pp.3513–3518. [Accessed 21 July 2018]. Available from: http://www.ncbi.nlm.nih.gov/pubmed/20638388.

Hille, B. 1978. Ionic channels in excitable membranes. Current problems and biophysical approaches. *Biophysical journal*. [Online]. **22**(2), pp.283–94. [Accessed 23 July 2018]. Available from: http://www.ncbi.nlm.nih.gov/pubmed/656545.

Hinrichsen, L., Harborth, J., Andrees, L., Weber, K. and Ungewickell, E.J. 2003. Effect of Clathrin Heavy Chain- and α-Adaptin-specific Small Inhibitory RNAs on Endocytic Accessory Proteins and Receptor Trafficking in HeLa Cells. *Journal of Biological Chemistry*. [Online]. **278**(46), pp.45160–45170. [Accessed 18 July 2018]. Available from: http://www.ncbi.nlm.nih.gov/pubmed/12960147.

Hirose, H., Arasaki, K., Dohmae, N., Takio, K., Hatsuzawa, K., Nagahama, M., Tani, K., Yamamoto, A., Tohyama, M. and Tagaya, M. 2004. Implication of ZW10 in membrane trafficking between the endoplasmic reticulum and Golgi. *The EMBO journal*. [Online]. **23**(6), pp.1267–78. [Accessed 18 July 2018]. Available from: http://www.ncbi.nlm.nih.gov/pubmed/15029241.

Hirsch, H.H., Brennan, D.C., Drachenberg, C.B., Ginevri, F., Gordon, J., Limaye, A.P., Mihatsch, M.J., Nickeleit, V., Ramos, E., Randhawa, P., Shapiro, R., Steiger, J., Suthanthiran, M. and Trofe, J. 2005. Polyomavirus-associated nephropathy in renal transplantation: interdisciplinary analyses and recommendations. *Transplantation*. [Online]. **79**(10), pp.1277–86. [Accessed 17 July 2018]. Available from: http://www.ncbi.nlm.nih.gov/pubmed/15912088.

Hirsch, H.H., Drachenberg, C.B., Steiger, J. and Ramos, E. 2006. Polyomavirus-Associated Nephropathy in Renal Transplantation *In*: *Polyomaviruses and Human Diseases* [Online]. New York, NY: Springer New York, pp.160–173. [Accessed 17 July 2018].

Available from: http://www.ncbi.nlm.nih.gov/pubmed/16626034.

Hirsch, H.H., Knowles, W., Dickenmann, M., Passweg, J., Klimkait, T., Mihatsch, M.J. and Steiger, J. 2002. Prospective Study of Polyomavirus Type BK Replication and Nephropathy in Renal-Transplant Recipients. *New England Journal of Medicine*. [Online]. **347**(7), pp.488–496. [Accessed 17 July 2018]. Available from: http://www.ncbi.nlm.nih.gov/pubmed/12181403.

Hirsch, H.H., Randhawa, P. and AST Infectious Diseases Community of Practice 2013. BK Polyomavirus in Solid Organ Transplantation. *American Journal of Transplantation*. [Online]. **13**(s4), pp.179–188. [Accessed 17 July 2018]. Available from: http://www.ncbi.nlm.nih.gov/pubmed/23465010.

Hirsch, H.H. and Steiger, J. 2003. Polyomavirus BK. *The Lancet. Infectious diseases*. [Online]. **3**(10), pp.611–23. [Accessed 20 July 2018]. Available from: http://www.ncbi.nlm.nih.gov/pubmed/14522260.

Ho, K., Nichols, C.G., Lederer, W.J., Lytton, J., Vassilev, P.M., Kanazirska, M. V. and Hebert, S.C. 1993. Cloning and expression of an inwardly rectifying ATP-regulated potassium channel. *Nature*. [Online]. **362**(6415), pp.31–38. [Accessed 23 July 2018]. Available from: http://www.ncbi.nlm.nih.gov/pubmed/7680431.

Hover, S., Foster, B., Barr, J.N. and Mankouri, J. 2017. Viral dependence on cellular ion channels – an emerging anti-viral target? *Journal of General Virology*. [Online]. **98**(3), pp.345–351. [Accessed 20 July 2018]. Available from: http://www.ncbi.nlm.nih.gov/pubmed/28113044.

Hover, S., Foster, B., Fontana, J., Kohl, A., Goldstein, S.A.N., Barr, J.N. and Mankouri, J. 2018. Bunyavirus requirement for endosomal K+ reveals new roles of cellular ion channels during infection S. P. J. Whelan, ed. *PLOS Pathogens*. [Online]. **14**(1), p.e1006845. [Accessed 20 July 2018]. Available from: http://dx.plos.org/10.1371/journal.ppat.1006845.

Hover, S., King, B., Hall, B., Loundras, E.-A., Taqi, H., Daly, J., Dallas, M., Peers, C., Schnettler, E., McKimmie, C., Kohl, A., Barr, J.N. and Mankouri, J. 2016. Modulation of Potassium Channels Inhibits Bunyavirus Infection. *The Journal of biological chemistry*. [Online]. **291**(7), pp.3411–22. [Accessed 20 July 2018]. Available from: http://www.ncbi.nlm.nih.gov/pubmed/26677217.

Howell, D.N., Smith, S.R., Butterly, D.W., Klassen, P.S., Krigman, H.R., Burchette, J.L. and Miller, S.E. 1999. Diagnosis and management of BK polyomavirus interstitial nephritis in renal transplant recipients. *Transplantation*. [Online]. **68**(9), pp.1279–88. [Accessed 17 July 2018]. Available from: http://www.ncbi.nlm.nih.gov/pubmed/10573064.

Hsu, K., Han, J., Shinlapawittayatorn, K., Deschenes, I. and Marbán, E. 2010. Membrane potential depolarization as a triggering mechanism for Vpu-mediated HIV-1 release. *Biophysical journal*. [Online]. **99**(6), pp.1718–25. [Accessed 21 July 2018]. Available from: http://www.ncbi.nlm.nih.gov/pubmed/20858415.

Hsu, K., Seharaseyon, J., Dong, P., Bour, S. and Marbán, E. 2004. Mutual functional destruction of HIV-1 Vpu and host TASK-1 channel. *Molecular cell*. [Online]. **14**(2), pp.259–67. [Accessed 21 July 2018]. Available from: http://www.ncbi.nlm.nih.gov/pubmed/15099524.

Humes, H.D., Fissell, W.H., Weitzel, W.F., Buffington, D.A., Westover, A.J., MacKay, S.M. and Gutierrez, J.M. 2002. Metabolic replacement of kidney function in uremic animals with a bioartificial kidney containing human cells. *American Journal of Kidney Diseases*. [Online]. **39**(5), pp.1078–1087. [Accessed 21 July 2018]. Available from: http://www.ncbi.nlm.nih.gov/pubmed/11979353.

Hunter, T. 2007. The Age of Crosstalk: Phosphorylation, Ubiquitination, and Beyond. *Molecular Cell*. [Online]. **28**(5), pp.730–738. [Accessed 18 July 2018]. Available from:

http://www.ncbi.nlm.nih.gov/pubmed/18082598.

Hurdiss, D.L., Frank, M., Snowden, J.S., Macdonald, A. and Ranson, N.A. 2018. The Structure of an Infectious Human Polyomavirus and Its Interactions with Cellular Receptors. *Structure (London, England : 1993)*. [Online]. **26**(6), p.839–847.e3. [Accessed 17 July 2018]. Available from: http://www.ncbi.nlm.nih.gov/pubmed/29706532.

Hurdiss, D.L., Morgan, E.L., Thompson, R.F., Prescott, E.L., Panou, M.M., Macdonald, A. and Ranson, N.A. 2016. New Structural Insights into the Genome and Minor Capsid Proteins of BK Polyomavirus using Cryo-Electron Microscopy. *Structure (London, England : 1993)*. [Online]. **24**(4), pp.528–536. [Accessed 17 July 2018]. Available from: http://www.ncbi.nlm.nih.gov/pubmed/26996963.

Hurdiss, D.L., Morgan, E.L., Thompson, R.F., Prescott, E.L., Panou, M.M., Macdonald, A. and Ranson, N.A. 2016. New Structural Insights into the Genome and Minor Capsid Proteins of BK Polyomavirus using Cryo-Electron Microscopy. *Structure*. **24**(4).

Hwang, T.-C. and Kirk, K.L. 2013a. The CFTR ion channel: gating, regulation, and anion permeation. *Cold Spring Harbor perspectives in medicine*. [Online]. **3**(1), p.a009498. [Accessed 12 November 2018]. Available from: http://www.ncbi.nlm.nih.gov/pubmed/23284076.

Hwang, T.-C. and Kirk, K.L. 2013b. The CFTR ion channel: gating, regulation, and anion permeation. *Cold Spring Harbor perspectives in medicine*. [Online]. **3**(1), p.a009498. [Accessed 22 July 2018]. Available from: http://www.ncbi.nlm.nih.gov/pubmed/23284076.

Hwang, T.C. and Sheppard, D.N. 1999. Molecular pharmacology of the CFTR Cl- channel. *Trends in pharmacological sciences*. [Online]. **20**(11), pp.448–53. [Accessed 20 July 2018]. Available from: http://www.ncbi.nlm.nih.gov/pubmed/10542444.

IARC Working Group on the Evaluation of Carcinogenic Risks to Humans 2014. MALARIA AND SOME POLYOMAVIRUSES (SV40, BK, JC, AND MERKEL CELL VIRUSES). *IARC monographs on the evaluation of carcinogenic risks to humans*. [Online]. **104**, pp.9–350. [Accessed 21 July 2018]. Available from: http://www.ncbi.nlm.nih.gov/pubmed/26173303.

Ichikawa, S., Nakajo, N., Sakiyama, H. and Hirabayashi, Y. 1994. A mouse B16 melanoma mutant deficient in glycolipids. *Proceedings of the National Academy of Sciences of the United States of America*. [Online]. **91**(7), pp.2703–7. [Accessed 18 July 2018]. Available from: http://www.ncbi.nlm.nih.gov/pubmed/8146177.

Igloi, Z., Mohl, B.-P., Lippiat, J.D., Harris, M. and Mankouri, J. 2015. Requirement for Chloride Channel Function during the Hepatitis C Virus Life Cycle M. S. Diamond, ed. *Journal of Virology*. [Online]. **89**(7), pp.4023–4029. [Accessed 21 July 2018]. Available from: http://www.ncbi.nlm.nih.gov/pubmed/25609806.

Inagaki, N., Gonoi, T., Clement, J.P., Namba, N., Inazawa, J., Gonzalez, G., Aguilar-Bryan, L., Seino, S. and Bryan, J. 1995. Reconstitution of IKATP: an inward rectifier subunit plus the sulfonylurea receptor. *Science (New York, N.Y.)*. [Online]. **270**(5239), pp.1166–70. [Accessed 20 July 2018]. Available from: http://www.ncbi.nlm.nih.gov/pubmed/7502040.

Inagaki, N., Gonoi, T., Clement, J.P., Wang, C.Z., Aguilar-Bryan, L., Bryan, J. and Seino, S. 1996. A family of sulfonylurea receptors determines the pharmacological properties of ATP-sensitive K+ channels. *Neuron*. [Online]. **16**(5), pp.1011–7. [Accessed 22 July 2018]. Available from: http://www.ncbi.nlm.nih.gov/pubmed/8630239.

Inoue, T., Dosey, A., Herbstman, J.F., Ravindran, M.S., Skiniotis, G. and Tsai, B. 2015. ERdj5 Reductase Cooperates with Protein Disulfide Isomerase To Promote Simian Virus 40 Endoplasmic Reticulum Membrane Translocation T. S. Dermody, ed. *Journal*

of Virology. [Online]. **89**(17), pp.8897–8908. [Accessed 19 July 2018]. Available from: http://www.ncbi.nlm.nih.gov/pubmed/26085143.

Inoue, T. and Tsai, B. 2011. A Large and Intact Viral Particle Penetrates the Endoplasmic Reticulum Membrane to Reach the Cytosol D. Galloway, ed. *PLoS Pathogens*. [Online]. **7**(5), p.e1002037. [Accessed 18 July 2018]. Available from: http://www.ncbi.nlm.nih.gov/pubmed/21589906.

Inoue, T. and Tsai, B. 2015. A nucleotide exchange factor promotes endoplasmic reticulum-to-cytosol membrane penetration of the nonenveloped virus simian virus 40. *Journal of virology*. [Online]. **89**(8), pp.4069–79. [Accessed 20 July 2018]. Available from: http://www.ncbi.nlm.nih.gov/pubmed/25653441.

Ishii, N., Minami, N., Chen, E.Y., Medina, A.L., Chico, M.M. and Kasamatsu, H. 1996. Analysis of a nuclear localization signal of simian virus 40 major capsid protein Vp1. *Journal of virology*. [Online]. **70**(2), pp.1317–22. [Accessed 20 July 2018]. Available from: http://www.ncbi.nlm.nih.gov/pubmed/8551602.

Isomoto, S., Kondo, C., Yamada, M., Matsumoto, S., Higashiguchi, O., Horio, Y., Matsuzawa, Y. and Kurachi, Y. 1996. A novel sulfonylurea receptor forms with BIR (Kir6.2) a smooth muscle type ATP-sensitive K+ channel. *The Journal of biological chemistry*. [Online]. **271**(40), pp.24321–4. [Accessed 22 July 2018]. Available from: http://www.ncbi.nlm.nih.gov/pubmed/8798681.

Iwata, M., Komori, S., Unno, T., Minamoto, N. and Ohashi, H. 1999. Modification of membrane currents in mouse neuroblastoma cells following infection with rabies virus. *British Journal of Pharmacology*. [Online]. **126**(8), pp.1691–1698. [Accessed 21 July 2018]. Available from: http://www.ncbi.nlm.nih.gov/pubmed/10372810.

Jeffers, L.K., Madden, V. and Webster-Cyriaque, J. 2009. BK virus has tropism for human salivary gland cells in vitro: Implications for transmission. *Virology*. [Online]. **394**(2), pp.183–193. [Accessed 18 July 2018]. Available from: http://www.ncbi.nlm.nih.gov/pubmed/19782382.

Jentsch, T.J. 1994. Structure and function of ClC chloride channels. *The Japanese journal of physiology*. [Online]. **44 Suppl 2**, pp.S1-2. [Accessed 20 July 2018]. Available from: http://www.ncbi.nlm.nih.gov/pubmed/7752510.

Jentsch, T.J., Hübner, C.A. and Fuhrmann, J.C. 2004. Ion channels: Function unravelled by dysfunction. *Nature Cell Biology*. [Online]. **6**(11), pp.1039–1047. [Accessed 20 July 2018]. Available from: http://www.ncbi.nlm.nih.gov/pubmed/15516997.

Jiang, M., Abend, J.R., Johnson, S.F. and Imperiale, M.J. 2009. The role of polyomaviruses in human disease. *Virology*.

Jiang, M., Abend, J.R., Tsai, B. and Imperiale, M.J. 2009. Early events during BK virus entry and disassembly. *Journal of virology*. [Online]. **83**(3), pp.1350–8. [Accessed 18 July 2018]. Available from: http://www.ncbi.nlm.nih.gov/pubmed/19036822.

Jiang, M., Entezami, P., Gamez, M., Stamminger, T. and Imperiale, M.J. 2011. Functional Reorganization of Promyelocytic Leukemia Nuclear Bodies during BK Virus Infection. *mBio*. [Online]. **2**(1), pp.e00281-10. [Accessed 20 July 2018]. Available from: http://www.ncbi.nlm.nih.gov/pubmed/21304169.

Jiang, M., Zhao, L., Gamez, M. and Imperiale, M.J. 2012. Roles of ATM and ATR-Mediated DNA Damage Responses during Lytic BK Polyomavirus Infection J. Pipas, ed. *PLoS Pathogens*. [Online]. **8**(8), p.e1002898. [Accessed 20 July 2018]. Available from: http://dx.plos.org/10.1371/journal.ppat.1002898.

Jin, L., Gibson, P.E., Booth, J.C. and Clewley, J.P. 1993. Genomic typing of BK virus in clinical specimens by direct sequencing of polymerase chain reaction products. *Journal of medical virology*. [Online]. **41**(1), pp.11–7. [Accessed 17 July 2018]. Available from:

http://www.ncbi.nlm.nih.gov/pubmed/8228931.

Johannessen, M., Myhre, M.R., Dragset, M., Tümmler, C. and Moens, U. 2008. Phosphorylation of human polyomavirus BK agnoprotein at Ser-11 is mediated by PKC and has an important regulative function. *Virology*. [Online]. **379**(1), pp.97–109. [Accessed 18 July 2018]. Available from: http://www.ncbi.nlm.nih.gov/pubmed/18635245.

Johannessen, M., Walquist, M., Gerits, N., Dragset, M., Spang, A. and Moens, U. 2011. BKV Agnoprotein Interacts with α-Soluble N-Ethylmaleimide-Sensitive Fusion Attachment Protein, and Negatively Influences Transport of VSVG-EGFP R. J. Geraghty, ed. *PLoS ONE*. [Online]. **6**(9), p.e24489. [Accessed 18 July 2018]. Available from: http://dx.plos.org/10.1371/journal.pone.0024489.

Johne, R., Buck, C.B., Allander, T., Atwood, W.J., Garcea, R.L., Imperiale, M.J., Major, E.O., Ramqvist, T. and Norkin, L.C. 2011. Taxonomical developments in the family Polyomaviridae. *Archives of Virology*. [Online]. **156**(9), pp.1627–1634. [Accessed 17 July 2018]. Available from: http://www.ncbi.nlm.nih.gov/pubmed/21562881.

Johnsen, J.I., Seternes, O.M., Johansen, T., Moens, U., Mantyjarvi, R. and Traavik, T. 1995. Subpopulations of non-coding control region variants within a cell culture-passaged stock of BK virus: sequence comparisons and biological characteristics. *Journal of General Virology*. [Online]. **76**(7), pp.1571–1581. [Accessed 18 July 2018]. Available from: http://www.ncbi.nlm.nih.gov/pubmed/9049364.

Johnston, O., Jaswal, D., Gill, J.S., Doucette, S., Fergusson, D.A. and Knoll, G.A. 2010. Treatment of Polyomavirus Infection in Kidney Transplant Recipients: A Systematic Review. *Transplantation*. [Online]. **89**(9), pp.1057–1070. [Accessed 17 July 2018]. Available from: http://www.ncbi.nlm.nih.gov/pubmed/20090569.

Jönsson, A., Rydberg, T., Ekberg, G., Hallengren, B. and Melander, A. 1994. Slow elimination of glyburide in NIDDM subjects. *Diabetes care*. [Online]. **17**(2), pp.142–5. [Accessed 23 July 2018]. Available from: http://www.ncbi.nlm.nih.gov/pubmed/8137685.

Jönsson, A., Rydberg, T., Sterner, G. and Melander, A. 1998. Pharmacokinetics of glibenclamide and its metabolites in diabetic patients with impaired renal function. *European journal of clinical pharmacology*. [Online]. **53**(6), pp.429–35. [Accessed 23 July 2018]. Available from: http://www.ncbi.nlm.nih.gov/pubmed/9551701.

Josephson, M.A., Gillen, D., Javaid, B., Kadambi, P., Meehan, S., Foster, P., Harland, R., Thistlethwaite, R.J., Garfinkel, M., Atwood, W., Jordan, J., Sadhu, M., Millis, M.J. and Williams, J. 2006. Treatment of Renal Allograft Polyoma BK Virus Infection with Leflunomide. *Transplantation*. [Online]. **81**(5), pp.704–710. [Accessed 17 July 2018]. Available from: http://www.ncbi.nlm.nih.gov/pubmed/16534472.

Jouret, F., Bernard, A., Hermans, C., Dom, G., Terryn, S., Leal, T., Lebecque, P., Cassiman, J.-J., Scholte, B.J., de Jonge, H.R., Courtoy, P.J. and Devuyst, O. 2007. Cystic Fibrosis Is Associated with a Defect in Apical Receptor-Mediated Endocytosis in Mouse and Human Kidney. *Journal of the American Society of Nephrology*. [Online]. **18**(3), pp.707–718. [Accessed 20 July 2018]. Available from: http://www.ncbi.nlm.nih.gov/pubmed/17287432.

Kartenbeck, J., Stukenbrok, H. and Helenius, A. 1989. Endocytosis of simian virus 40 into the endoplasmic reticulum. *The Journal of cell biology*. [Online]. **109**(6 Pt 1), pp.2721–9. [Accessed 23 July 2018]. Available from: http://www.ncbi.nlm.nih.gov/pubmed/2556405.

Kasamatsu, H. and Nakanishi, A. 1998. HOW DO ANIMAL DNA VIRUSES GET TO THE NUCLEUS? *Annual Review of Microbiology*. [Online]. **52**(1), pp.627–686. [Accessed 23 July 2018]. Available from: http://www.ncbi.nlm.nih.gov/pubmed/9891810.

Kavanaugh, M.P., Hurst, R.S., Yakel, J., Varnum, M.D., Adelman, J.P. and North, R.A. 1992. Multiple subunits of a voltage-dependent potassium channel contribute to the binding site for tetraethylammonium. *Neuron*. [Online]. **8**(3), pp.493–7. [Accessed 21 July 2018]. Available from: http://www.ncbi.nlm.nih.gov/pubmed/1550674.

Kazory, A., Ducloux, D., Chalopin, J.-M., Angonin, R., Fontani??re, B. and Moret, H. 2003. THE FIRST CASE OF JC VIRUS ALLOGRAFT NEPHROPATHY. *Transplantation*. [Online]. **76**(11), pp.1653–1655. [Accessed 17 July 2018]. Available from: http://www.ncbi.nlm.nih.gov/pubmed/14702550.

Kean, J.M., Rao, S., Wang, M. and Garcea, R.L. 2009. Seroepidemiology of Human Polyomaviruses W. J. Atwood, ed. *PLoS Pathogens*. [Online]. **5**(3), p.e1000363. [Accessed 17 July 2018]. Available from: http://dx.plos.org/10.1371/journal.ppat.1000363.

Kelley, W.L. and Georgopoulos, C. 1997. The T/t common exon of simian virus 40, JC, and BK polyomavirus T antigens can functionally replace the J-domain of the Escherichia coli DnaJ molecular chaperone. *Proceedings of the National Academy of Sciences of the United States of America*. [Online]. **94**(8), pp.3679–84. [Accessed 18 July 2018]. Available from: http://www.ncbi.nlm.nih.gov/pubmed/9108037.

Kenan, D.J., Mieczkowski, P.A., Burger-Calderon, R., Singh, H.K. and Nickeleit, V. 2015. The oncogenic potential of BK-polyomavirus is linked to viral integration into the human genome. *The Journal of Pathology*. [Online]. **237**(3), pp.379–389. [Accessed 18 July 2018]. Available from: http://www.ncbi.nlm.nih.gov/pubmed/26172456.

Kennedy, P.G.E., Montague, P., Scott, F., Grinfeld, E., Ashrafi, G.H., Breuer, J. and Rowan, E.G. 2013. Varicella-Zoster Viruses Associated with Post-Herpetic Neuralgia Induce Sodium Current Density Increases in the ND7-23 Nav-1.8 Neuroblastoma Cell Line J. C. Glorioso, ed. *PLoS ONE*. [Online]. **8**(1), p.e51570. [Accessed 21 July 2018]. Available from: http://dx.plos.org/10.1371/journal.pone.0051570.

Kielian, M. 2014. Mechanisms of Virus Membrane Fusion Proteins. *Annual Review of Virology*. [Online]. **1**(1), pp.171–189. [Accessed 21 July 2018]. Available from: http://www.ncbi.nlm.nih.gov/pubmed/26958720.

Kim, J.-B. 2014. Channelopathies. *Korean journal of pediatrics*. [Online]. **57**(1), pp.1–18. [Accessed 21 July 2018]. Available from: http://www.ncbi.nlm.nih.gov/pubmed/24578711.

Kim, M.H., Lee, Y.H., Seo, J.-W., Moon, H., Kim, J.S., Kim, Y.G., Jeong, K.-H., Moon, J.-Y., Lee, T.W., Ihm, C.-G., Kim, C.-D., Park, J.B., Chung, B.H., Kim, Y.-H. and Lee, S.-H. 2017. Urinary exosomal viral microRNA as a marker of BK virus nephropathy in kidney transplant recipients. *PloS one*. [Online]. **12**(12), p.e0190068. [Accessed 9 November 2018]. Available from: http://www.ncbi.nlm.nih.gov/pubmed/29267352.

King, J.D., Fitch, A.C., Lee, J.K., McCane, J.E., Mak, D.-O.D., Foskett, J.K. and Hallows, K.R. 2009. AMP-activated protein kinase phosphorylation of the R domain inhibits PKA stimulation of CFTR. *American Journal of Physiology-Cell Physiology*. [Online]. **297**(1), pp.C94–C101. [Accessed 12 November 2018]. Available from: http://www.physiology.org/doi/10.1152/ajpcell.00677.2008.

Kirsch, G.E., Taglialatela, M. and Brown, A.M. 1991. Internal and external TEA block in single cloned K+ channels. *American Journal of Physiology-Cell Physiology*. [Online]. **261**(4), pp.C583–C590. [Accessed 21 July 2018]. Available from: http://www.ncbi.nlm.nih.gov/pubmed/1928322.

Kizhatil, K. and Albritton, L.M. 1997. Requirements for different components of the host cell cytoskeleton distinguish ecotropic murine leukemia virus entry via endocytosis from entry via surface fusion. *Journal of virology*. [Online]. **71**(10), pp.7145–56. [Accessed 23 July 2018]. Available from: http://www.ncbi.nlm.nih.gov/pubmed/9311787.

Knoll, G.A., Humar, A., Fergusson, D., Johnston, O., House, A.A., Kim, S.J., Ramsay, T., Chassé, M., Pang, X., Zaltzman, J., Cockfield, S., Cantarovich, M., Karpinski, M., Lebel, L. and Gill, J.S. 2014. Levofloxacin for BK Virus Prophylaxis Following Kidney Transplantation. *JAMA*. [Online]. **312**(20), p.2106. [Accessed 17 July 2018]. Available from: http://www.ncbi.nlm.nih.gov/pubmed/25399012.

Knowles, W.A. 2006. Discovery and Epidemiology of the Human Polyomaviruses BK Virus (BKV) and JC Virus (JCV) *In*: *Polyomaviruses and Human Diseases* [Online]. New York, NY: Springer New York, pp.19–45. [Accessed 17 July 2018]. Available from: http://www.ncbi.nlm.nih.gov/pubmed/16626025.

Knowles, W.A. 2001. The Epidemiology of BK Virus and the Occurrence of Antigenic and Genomic Subtypes *In*: *Human Polyomaviruses* [Online]. New York, USA: John Wiley & Sons, Inc., pp.527–559. [Accessed 17 July 2018]. Available from: http://doi.wiley.com/10.1002/0471221945.ch19.

Knowles, W.A., Gibson, P.E. and Gardner, S.D. 1989. Serological typing scheme for BK-like isolates of human polyomavirus. *Journal of medical virology*. [Online]. **28**(2), pp.118–23. [Accessed 17 July 2018]. Available from: http://www.ncbi.nlm.nih.gov/pubmed/2544676.

Knowlton, R.G., Cohen-Haguenauer, O., Van Cong, N., Frézal, J., Brown, V.A., Barker, D., Braman, J.C., Schumm, J.W., Tsui, L.C. and Buchwald, M. 1985. A polymorphic DNA marker linked to cystic fibrosis is located on chromosome 7. *Nature*. [Online]. **318**(6044), pp.380–2. [Accessed 20 July 2018]. Available from: http://www.ncbi.nlm.nih.gov/pubmed/2999611.

Kopeikin, Z., Sohma, Y., Li, M. and Hwang, T.-C. 2010. On the mechanism of CFTR inhibition by a thiazolidinone derivative. *The Journal of General Physiology*. [Online]. **136**(6), pp.659–671. [Accessed 20 July 2018]. Available from: http://www.ncbi.nlm.nih.gov/pubmed/21078867.

Kort, J.J. and Jalonen, T.O. 1998. The nef protein of the human immunodeficiency virus type 1 (HIV-1) inhibits a large-conductance potassium channel in human glial cells. *Neuroscience letters*. [Online]. **251**(1), pp.1–4. [Accessed 21 July 2018]. Available from: http://www.ncbi.nlm.nih.gov/pubmed/9714450.

Korup, S., Rietscher, J., Calvignac-Spencer, S., Trusch, F., Hofmann, J., Moens, U., Sauer, I., Voigt, S., Schmuck, R. and Ehlers, B. 2013. Identification of a Novel Human Polyomavirus in Organs of the Gastrointestinal Tract J. Qiu, ed. *PLoS ONE*. [Online]. **8**(3), p.e58021. [Accessed 17 July 2018]. Available from: http://dx.plos.org/10.1371/journal.pone.0058021.

Krishna, A. and Prasad, N. 2011. BK virus nephropathy in renal transplantation. *Indian Journal of Transplantation*. [Online]. **5**(4), pp.182–190. [Accessed 17 July 2018]. Available from: https://www.sciencedirect.com/science/article/pii/S2212001712600069.

Kunz, S. 2009. Receptor binding and cell entry of Old World arenaviruses reveal novel aspects of virus–host interaction. *Virology*. [Online]. **387**(2), pp.245–249. [Accessed 21 July 2018]. Available from: http://www.ncbi.nlm.nih.gov/pubmed/19324387.

Kunzelmann, K. 2005. Ion Channels and Cancer. *Journal of Membrane Biology*. [Online]. **205**(3), pp.159–173. [Accessed 23 July 2018]. Available from: http://www.ncbi.nlm.nih.gov/pubmed/16362504.

Kunzelmann, K., Schreiber, R. and Boucherot, A. 2001. Mechanisms of the inhibition of epithelial Na+ channels by CFTR and purinergic stimulation. *Kidney International*. [Online]. **60**(2), pp.455–461. [Accessed 20 July 2018]. Available from: http://www.ncbi.nlm.nih.gov/pubmed/11473626.

Kuppachi, S., Thomas, B. and Kokko, K.E. 2013. BK Virus in the Kidney Transplant Patient. *The American Journal of the Medical Sciences*. [Online]. **345**(6), pp.482–488.

[Accessed 17 July 2018]. Available from: http://www.ncbi.nlm.nih.gov/pubmed/23698093.

Kuypers, D.R.J. 2012. Management of polyomavirus-associated nephropathy in renal transplant recipients. *Nature Reviews Nephrology*. [Online]. **8**(7), pp.390–402. [Accessed 17 July 2018]. Available from: http://www.ncbi.nlm.nih.gov/pubmed/22508181.

Kuypers, D.R.J., Bammens, B., Claes, K., Evenepoel, P., Lerut, E. and Vanrenterghem, Y. 2008. A single-centre study of adjuvant cidofovir therapy for BK virus interstitial nephritis (BKVIN) in renal allograft recipients. *Journal of Antimicrobial Chemotherapy*. [Online]. **63**(2), pp.417–419. [Accessed 17 July 2018]. Available from: https://academic.oup.com/jac/article-lookup/doi/10.1093/jac/dkn495.

L Cubitt, Xiaohong Cui, Hansjürgen, C., Cui, X., Agostini, H.T., Nerurkar, V.R., Scheirich, I., Yanagihara, R., Ryschkewitsch, C.F. and Stoner, G.L. 2001. Predicted amino acid sequences for 100 JCV strains. *Journal of Neurovirology*. [Online]. **7**(4), pp.339–344. [Accessed 23 July 2018]. Available from: http://www.ncbi.nlm.nih.gov/pubmed/11517413.

Lamarche, C., Orio, J., Collette, S., Senécal, L., Hébert, M.-J., Renoult, É., Tibbles, L.A. and Delisle, J.-S. 2016. BK Polyomavirus and the Transplanted Kidney. *Transplantation*. [Online]. **100**(11), pp.2276–2287. [Accessed 17 July 2018]. Available from: http://www.ncbi.nlm.nih.gov/pubmed/27391196.

Lamaze, C., Dujeancourt, A., Baba, T., Lo, C.G., Benmerah, A. and Dautry-Varsat, A. 2001. Interleukin 2 receptors and detergent-resistant membrane domains define a clathrin-independent endocytic pathway. *Molecular cell*. [Online]. **7**(3), pp.661–71. [Accessed 18 July 2018]. Available from: http://www.ncbi.nlm.nih.gov/pubmed/11463390.

Lange, A., Mills, R.E., Lange, C.J., Stewart, M., Devine, S.E. and Corbett, A.H. 2007. Classical Nuclear Localization Signals: Definition, Function, and Interaction with Importin α. *Journal of Biological Chemistry*. [Online]. **282**(8), pp.5101–5105. [Accessed 18 July 2018]. Available from: http://www.ncbi.nlm.nih.gov/pubmed/17170104.

Lashgari, M.S., Tada, H., Amini, S. and Khalili, K. 1989. Regulation of JCVL promoter function: transactivation of JCVL promoter by JCV and SV40 early proteins. *Virology*. [Online]. **170**(1), pp.292–5. [Accessed 23 July 2018]. Available from: http://www.ncbi.nlm.nih.gov/pubmed/2541545.

Lauber, C., Kazem, S., Kravchenko, A.A., Feltkamp, M.C.W. and Gorbalenya, A.E. 2015. Interspecific adaptation by binary choice at de novo polyomavirus T antigen site through accelerated codon-constrained Val-Ala toggling within an intrinsically disordered region. *Nucleic Acids Research*. [Online]. **43**(10), pp.4800–4813. [Accessed 17 July 2018]. Available from: http://www.ncbi.nlm.nih.gov/pubmed/25904630.

Lavoie, J.N., L'Allemain, G., Brunet, A., Müller, R. and Pouysségur, J. 1996. Cyclin D1 expression is regulated positively by the p42/p44MAPK and negatively by the p38/HOGMAPK pathway. *The Journal of biological chemistry*. [Online]. **271**(34), pp.20608–16. [Accessed 20 July 2018]. Available from: http://www.ncbi.nlm.nih.gov/pubmed/8702807.

Lee, B.T., Gabardi, S., Grafals, M., Hofmann, R.M., Akalin, E., Aljanabi, A., Mandelbrot, D.A., Adey, D.B., Heher, E., Fan, P.-Y., Conte, S., Dyer-Ward, C. and Chandraker, A. 2014. Efficacy of Levofloxacin in the Treatment of BK Viremia: A Multicenter, Double-Blinded, Randomized, Placebo-Controlled Trial. *Clinical Journal of the American Society of Nephrology*. [Online]. **9**(3), pp.583–589. [Accessed 17 July 2018]. Available from: http://www.ncbi.nlm.nih.gov/pubmed/24482066.

Lee, M.G., Wigley, W.C., Zeng, W., Noel, L.E., Marino, C.R., Thomas, P.J. and Muallem, S. 1999. Regulation of Cl-/ HCO3- exchange by cystic fibrosis transmembrane

conductance regulator expressed in NIH 3T3 and HEK 293 cells. *The Journal of biological chemistry*. [Online]. **274**(6), pp.3414–21. [Accessed 23 July 2018]. Available from: http://www.ncbi.nlm.nih.gov/pubmed/9920885.

Lee, T.-Y., Chen, S.-A., Hung, H.-Y. and Ou, Y.-Y. 2011. Incorporating Distant Sequence Features and Radial Basis Function Networks to Identify Ubiquitin Conjugation Sites V. Uversky, ed. *PLoS ONE*. [Online]. **6**(3), p.e17331. [Accessed 18 July 2018]. Available from: http://dx.plos.org/10.1371/journal.pone.0017331.

Lehmann-Horn, F. and Jurkat-Rott, K. 1999. Voltage-Gated Ion Channels and Hereditary Disease. *Physiological Reviews*. [Online]. **79**(4), pp.1317–1372. [Accessed 20 July 2018]. Available from: http://www.ncbi.nlm.nih.gov/pubmed/10508236.

Leopold, P.L. and Pfister, K.K. 2006. Viral Strategies for Intracellular Trafficking: Motors and Microtubules. *Traffic*. [Online]. **7**(5), pp.516–523. [Accessed 18 July 2018]. Available from: http://www.ncbi.nlm.nih.gov/pubmed/16643275.

Leuenberger, D., Andresen, P.A., Gosert, R., Binggeli, S., Ström, E.H., Bodaghi, S., Rinaldo, C.H. and Hirsch, H.H. 2007. Human polyomavirus type 1 (BK virus) agnoprotein is abundantly expressed but immunologically ignored. *Clinical and vaccine immunology : CVI*. [Online]. **14**(8), pp.959–68. [Accessed 18 July 2018]. Available from: http://www.ncbi.nlm.nih.gov/pubmed/17538118.

Li, C. and Naren, A.P. 2010. CFTR chloride channel in the apical compartments: spatiotemporal coupling to its interacting partners. *Integrative biology : quantitative biosciences from nano to macro*. [Online]. **2**(4), pp.161–77. [Accessed 23 July 2018]. Available from: http://www.ncbi.nlm.nih.gov/pubmed/20473396.

Li, M. and Garcea, R.L. 1994. Identification of the threonine phosphorylation sites on the polyomavirus major capsid protein VP1: relationship to the activity of middle T antigen. *Journal of virology*. [Online]. **68**(1), pp.320–7. [Accessed 18 July 2018]. Available from: http://www.ncbi.nlm.nih.gov/pubmed/8254743.

Li, M., Lyon, M.K. and Garcea, R.L. 1995. In vitro phosphorylation of the polyomavirus major capsid protein VP1 on serine 66 by casein kinase II. *The Journal of biological chemistry*. [Online]. **270**(43), pp.26006–11. [Accessed 18 July 2018]. Available from: http://www.ncbi.nlm.nih.gov/pubmed/7592792.

Li, R.-M., Mannon, R.B., Kleiner, D., Tsokos, M., Bynum, M., Kirk, A.D. and Kopp, J.B. 2002. BK virus and SV40 co-infection in polyomavirus nephropathy. *Transplantation*. [Online]. **74**(11), pp.1497–504. [Accessed 17 July 2018]. Available from: http://www.ncbi.nlm.nih.gov/pubmed/12490781.

Li, T.-C., Iwasaki, K., Katano, H., Kataoka, M., Nagata, N., Kobayashi, K., Mizutani, T., Takeda, N., Wakita, T. and Suzuki, T. 2015. Characterization of Self-Assembled Virus-Like Particles of Merkel Cell Polyomavirus H. Hotta, ed. *PLOS ONE*. [Online]. **10**(2), p.e0115646. [Accessed 18 July 2018]. Available from: http://www.ncbi.nlm.nih.gov/pubmed/25671590.

Li, T.-C., Takeda, N., Kato, K., Nilsson, J., Xing, L., Haag, L., Cheng, R.H. and Miyamura, T. 2003. Characterization of self-assembled virus-like particles of human polyomavirus BK generated by recombinant baculoviruses. *Virology*. [Online]. **311**(1), pp.115–24. [Accessed 18 July 2018]. Available from: http://www.ncbi.nlm.nih.gov/pubmed/12832209.

Liacini, A., Seamone, M.E., Muruve, D.A. and Tibbles, L.A. 2010a. Anti-BK Virus Mechanisms of Sirolimus and Leflunomide Alone and in Combination: Toward a New Therapy for BK Virus Infection. *Transplantation*. [Online]. **90**(12), pp.1450–1457. [Accessed 17 July 2018]. Available from: http://www.ncbi.nlm.nih.gov/pubmed/21079551.

Liacini, A., Seamone, M.E., Muruve, D.A. and Tibbles, L.A. 2010b. Anti-BK Virus

Mechanisms of Sirolimus and Leflunomide Alone and in Combination: Toward a New Therapy for BK Virus Infection. *Transplantation*. [Online]. **90**(12), pp.1450–1457. [Accessed 15 November 2018]. Available from: https://insights.ovid.com/crossref?an=00007890-201012270-00033.

Liebl, D., Difato, F., Horníková, L., Mannová, P., Stokrová, J. and Forstová, J. 2006. Mouse polyomavirus enters early endosomes, requires their acidic pH for productive infection, and meets transferrin cargo in Rab11-positive endosomes. *Journal of virology*. [Online]. **80**(9), pp.4610–22. [Accessed 23 July 2018]. Available from: http://www.ncbi.nlm.nih.gov/pubmed/16611921.

Lim, E.S., Reyes, A., Antonio, M., Saha, D., Ikumapayi, U.N., Adeyemi, M., Stine, O.C., Skelton, R., Brennan, D.C., Mkakosya, R.S., Manary, M.J., Gordon, J.I. and Wang, D. 2013. Discovery of STL polyomavirus, a polyomavirus of ancestral recombinant origin that encodes a unique T antigen by alternative splicing. *Virology*. [Online]. **436**(2), pp.295–303. [Accessed 17 July 2018]. Available from: http://www.ncbi.nlm.nih.gov/pubmed/23276405.

Linsdell, P. 2014. Cystic fibrosis transmembrane conductance regulator chloride channel blockers: Pharmacological, biophysical and physiological relevance. *World Journal of Biological Chemistry*. [Online]. **5**(1), p.26. [Accessed 20 July 2018]. Available from: http://www.ncbi.nlm.nih.gov/pubmed/24600512.

Linsdell, P. and Hanrahan, J.W. 1996. Disulphonic stilbene block of cystic fibrosis transmembrane conductance regulator Cl- channels expressed in a mammalian cell line and its regulation by a critical pore residue. *The Journal of physiology*. [Online]. **496 (Pt 3**, pp.687–93. [Accessed 20 July 2018]. Available from: http://www.ncbi.nlm.nih.gov/pubmed/8930836.

Liu, F., Zhang, Z., Csanády, L., Gadsby, D.C. and Chen, J. 2017. Molecular Structure of the Human CFTR Ion Channel. *Cell*. [Online]. **169**(1), p.85–95.e8. [Accessed 20 July 2018]. Available from: http://www.ncbi.nlm.nih.gov/pubmed/28340353.

Liu, P., Bartz, R., Zehmer, J.K., Ying, Y., Zhu, M., Serrero, G. and Anderson, R.G.W. 2007. Rab-regulated interaction of early endosomes with lipid droplets. *Biochimica et Biophysica Acta (BBA) - Molecular Cell Research*. [Online]. **1773**(6), pp.784–793. [Accessed 18 July 2018]. Available from: http://www.ncbi.nlm.nih.gov/pubmed/17395284.

Liu, S. and Storrie, B. 2012. Are Rab proteins the link between Golgi organization and membrane trafficking? *Cellular and Molecular Life Sciences*. [Online]. **69**(24), pp.4093–4106. [Accessed 18 July 2018]. Available from: http://www.ncbi.nlm.nih.gov/pubmed/22581368.

Liu, W., Yang, R., Payne, A.S., Schowalter, R.M., Spurgeon, M.E., Lambert, P.F., Xu, X., Buck, C.B. and You, J. 2016. Identifying the Target Cells and Mechanisms of Merkel Cell Polyomavirus Infection. *Cell host & microbe*. [Online]. **19**(6), pp.775–87. [Accessed 15 November 2018]. Available from: http://www.ncbi.nlm.nih.gov/pubmed/27212661.

Liu, X., Yan, S., Zhou, T., Terada, Y. and Erikson, R.L. 2004. The MAP kinase pathway is required for entry into mitosis and cell survival. *Oncogene*. [Online]. **23**(3), pp.763–776. [Accessed 20 July 2018]. Available from: http://www.ncbi.nlm.nih.gov/pubmed/14737111.

Lo, Y.-C., Lee, C.-F. and Powell, J.D. 2014. Insight into the role of mTOR and metabolism in T cells reveals new potential approaches to preventing graft rejection. *Current Opinion in Organ Transplantation*. [Online]. **19**(4), pp.363–371. [Accessed 17 July 2018]. Available from: http://www.ncbi.nlm.nih.gov/pubmed/24991977.

Low, J., Humes, H.D., Szczypka, M. and Imperiale, M. 2004. BKV and SV40 infection of human kidney tubular epithelial cells in vitro. *Virology*. [Online]. **323**(2), pp.182–188.

[Accessed 20 July 2018]. Available from: http://www.ncbi.nlm.nih.gov/pubmed/15193914.

Low, J.A., Magnuson, B., Tsai, B. and Imperiale, M.J. 2006. Identification of gangliosides GD1b and GT1b as receptors for BK virus. *Journal of virology*. [Online]. **80**(3), pp.1361–6. [Accessed 18 July 2018]. Available from: http://www.ncbi.nlm.nih.gov/pubmed/16415013.

Lukács, G.L. and Moczydlowski, E. 1990. A chloride channel from lobster walking leg nerves. Characterization of single-channel properties in planar bilayers. *The Journal of general physiology*. [Online]. **96**(4), pp.707–33. [Accessed 23 July 2018]. Available from: http://www.ncbi.nlm.nih.gov/pubmed/2175346.

Lynch, K.J. and Frisque, R.J. 1990. Identification of critical elements within the JC virus DNA replication origin. *Journal of virology*. [Online]. **64**(12), pp.5812–22. [Accessed 23 July 2018]. Available from: http://www.ncbi.nlm.nih.gov/pubmed/2173768.

Ma, T., Thiagarajah, J.R., Yang, H., Sonawane, N.D., Folli, C., Galietta, L.J. V and Verkman, A.S. 2002. Thiazolidinone CFTR inhibitor identified by high-throughput screening blocks cholera toxin-induced intestinal fluid secretion. *The Journal of clinical investigation*. [Online]. **110**(11), pp.1651–8. [Accessed 20 July 2018]. Available from: http://www.ncbi.nlm.nih.gov/pubmed/12464670.

Mackenzie, E.F., Poulding, J.M., Harrison, P.R. and Amer, B. 1978. Human polyoma virus (HPV)--a significant pathogen in renal transplantation. *Proceedings of the European Dialysis and Transplant Association. European Dialysis and Transplant Association*. [Online]. **15**, pp.352–60. [Accessed 17 July 2018]. Available from: http://www.ncbi.nlm.nih.gov/pubmed/216990.

Maitra, R., Sivashanmugam, P. and Warner, K. 2013. A rapid membrane potential assay to monitor CFTR function and inhibition. *Journal of Biomolecular Screening*. **18**(9), pp.1132–7.

MAJOR, E.O. 2011. History and current concepts in the pathogenesis of PML. *Cleveland Clinic Journal of Medicine*. [Online]. **78**(Suppl_2), pp.S3–S7. [Accessed 23 July 2018]. Available from: http://www.ncbi.nlm.nih.gov/pubmed/22123932.

Mankouri, J., Dallas, M.L., Hughes, M.E., Griffin, S.D.C., Macdonald, A., Peers, C. and Harris, M. 2009. Suppression of a pro-apoptotic K+ channel as a mechanism for hepatitis C virus persistence. *Proceedings of the National Academy of Sciences*. [Online]. **106**(37), pp.15903–15908. [Accessed 21 July 2018]. Available from: http://www.ncbi.nlm.nih.gov/pubmed/19717445.

Mannová, P., Liebl, D., Krauzewicz, N., Fejtová, A., Štokrová, J., Palková, Z., Griffin, B.E. and Forstová, J. 2002. Analysis of mouse polyomavirus mutants with lesions in the minor capsid proteins. *Journal of General Virology*. [Online]. **83**(9), pp.2309–2319. [Accessed 18 July 2018]. Available from: http://www.ncbi.nlm.nih.gov/pubmed/12185287.

Mansour, S.J., Matten, W.T., Hermann, A.S., Candia, J.M., Rong, S., Fukasawa, K., Vande Woude, G.F. and Ahn, N.G. 1994. Transformation of mammalian cells by constitutively active MAP kinase kinase. *Science (New York, N.Y.)*. [Online]. **265**(5174), pp.966–70. [Accessed 20 July 2018]. Available from: http://www.ncbi.nlm.nih.gov/pubmed/8052857.

Maraldi, N.M., Barbanti-Brodano, G., Portolani, M. and La Placa, M. 1975. Ultrastructural Aspects of BK Virus Uptake and Replication in Human Fibroblasts. *Journal of General Virology*. [Online]. **27**(1), pp.71–80. [Accessed 21 July 2018]. Available from: http://www.ncbi.nlm.nih.gov/pubmed/167108.

Marble, A. 1971. Glibenclamide, a new sulphonylurea: whither oral hypoglycaemic agents? *Drugs*. [Online]. **1**(2), pp.109–15. [Accessed 21 July 2018]. Available from:

http://www.ncbi.nlm.nih.gov/pubmed/4999930.

Markowitz, R.B., Tolbert, S. and Dynan, W.S. 1990. Promoter evolution in BK virus: functional elements are created at sequence junctions. *Journal of virology*. [Online]. **64**(5), pp.2411–5. [Accessed 18 July 2018]. Available from: http://www.ncbi.nlm.nih.gov/pubmed/2157897.

Marsh, M. and Helenius, A. 2006. Virus Entry: Open Sesame. *Cell*. [Online]. **124**(4), pp.729–740. [Accessed 21 July 2018]. Available from: http://www.ncbi.nlm.nih.gov/pubmed/16497584.

Marsh, M. and Helenius, A. 1989. Virus entry into animal cells. *Advances in virus research*. [Online]. **36**, pp.107–51. [Accessed 23 July 2018]. Available from: http://www.ncbi.nlm.nih.gov/pubmed/2500008.

Marty, F.M., Winston, D.J., Rowley, S.D., Vance, E., Papanicolaou, G.A., Mullane, K.M., Brundage, T.M., Robertson, A.T., Godkin, S., Momméja-Marin, H., Boeckh, M. and CMX001-201 Clinical Study Group 2013. CMX001 to Prevent Cytomegalovirus Disease in Hematopoietic-Cell Transplantation. *New England Journal of Medicine*. [Online]. **369**(13), pp.1227–1236. [Accessed 17 July 2018]. Available from: http://www.ncbi.nlm.nih.gov/pubmed/24066743.

Masutani, K., Ninomiya, T. and Randhawa, P. 2013. HLA-A2, HLA-B44 and HLA-DR15 are associated with lower risk of BK viremia. *Nephrology, dialysis, transplantation : official publication of the European Dialysis and Transplant Association - European Renal Association*. [Online]. **28**(12), pp.3119–26. [Accessed 17 July 2018]. Available from: http://www.ncbi.nlm.nih.gov/pubmed/24084328.

Masutani, K., Shapiro, R., Basu, A., Tan, H., Wijkstrom, M. and Randhawa, P. 2012. The Banff 2009 Working Proposal for Polyomavirus Nephropathy: A Critical Evaluation of Its Utility as a Determinant of Clinical Outcome. *American Journal of Transplantation*. [Online]. **12**(4), pp.907–918. [Accessed 17 July 2018]. Available from: http://www.ncbi.nlm.nih.gov/pubmed/22390378.

Mathews, C.J., Tabcharani, J.A., Chang, X.-B., Jensen, T.J., Riordan, J.R. and Hanrahan, J.W. 1998. Dibasic protein kinase A sites regulate bursting rate and nucleotide sensitivity of the cystic fibrosis transmembrane conductance regulator chloride channel. *The Journal of Physiology*. [Online]. **508**(2), pp.365–377. [Accessed 12 November 2018]. Available from: http://doi.wiley.com/10.1111/j.1469-7793.1998.365bq.x.

Maxfield, F.R. 1982. Weak bases and ionophores rapidly and reversibly raise the pH of endocytic vesicles in cultured mouse fibroblasts. *The Journal of cell biology*. [Online]. **95**(2 Pt 1), pp.676–81. [Accessed 20 July 2018]. Available from: http://www.ncbi.nlm.nih.gov/pubmed/6183281.

Mayor, S. and Pagano, R.E. 2007. Pathways of clathrin-independent endocytosis. *Nature Reviews Molecular Cell Biology*. [Online]. **8**(8), pp.603–612. [Accessed 18 July 2018]. Available from: http://www.ncbi.nlm.nih.gov/pubmed/17609668.

Mazalrey, S., Mcilroy, D. and Bressollette-Bodin, C. 2015. BK polyomavirus: virus-cell interactions, host immune response, and viral pathogenesis. *Virologie*. [Online]. **19**(5), pp.8–24. [Accessed 17 July 2018]. Available from: http://www.jle.com/download/vir-305808-bk_polyomavirus_virus_cell_interactions_host_immune_response_and_viral_pathogenesis--W031@X8AAQEAACa0Jh8AAAAR-a.pdf.

McNicholas, C.M., Nason, M.W., Guggino, W.B., Schwiebert, E.M., Hebert, S.C., Giebisch, G. and Egan, M.E. 1997. A functional CFTR-NBF1 is required for ROMK2-CFTR interaction. *The American journal of physiology*. [Online]. **273**(5 Pt 2), pp.F843-8. [Accessed 20 July 2018]. Available from: http://www.ncbi.nlm.nih.gov/pubmed/9374850.

van der Meijden, E., Kazem, S., Dargel, C.A., van Vuren, N., Hensbergen, P.J. and Feltkamp, M.C.W. 2015. Characterization of T Antigens, Including Middle T and Alternative T, Expressed by the Human Polyomavirus Associated with Trichodysplasia Spinulosa. *Journal of virology*. [Online]. **89**(18), pp.9427–39. [Accessed 17 July 2018]. Available from: http://www.ncbi.nlm.nih.gov/pubmed/26136575.

Melin, P., Hosy, E., Vivaudou, M. and Becq, F. 2007. CFTR inhibition by glibenclamide requires a positive charge in cytoplasmic loop three. *Biochimica et Biophysica Acta (BBA) - Biomembranes*. [Online]. **1768**(10), pp.2438–2446. [Accessed 22 July 2018]. Available from: http://www.ncbi.nlm.nih.gov/pubmed/17582383.

Mellman, I., Fuchs, R. and Helenius, A. 1986. Acidification of the Endocytic and Exocytic Pathways. *Annual Review of Biochemistry*. [Online]. **55**(1), pp.663–700. [Accessed 20 July 2018]. Available from: http://www.ncbi.nlm.nih.gov/pubmed/2874766.

Meng, L., Mohan, R., Kwok, B.H., Elofsson, M., Sin, N. and Crews, C.M. 1999. Epoxomicin, a potent and selective proteasome inhibitor, exhibits in vivo antiinflammatory activity. *Proceedings of the National Academy of Sciences of the United States of America*. [Online]. **96**(18), pp.10403–8. [Accessed 20 July 2018]. Available from: http://www.ncbi.nlm.nih.gov/pubmed/10468620.

Mengel, M., Marwedel, M., Radermacher, J., Eden, G., Schwarz, A., Haller, H. and Kreipe, H. 2003. Incidence of polyomavirus-nephropathy in renal allografts: influence of modern immunosuppressive drugs. *Nephrology, dialysis, transplantation : official publication of the European Dialysis and Transplant Association - European Renal Association*. [Online]. **18**(6), pp.1190–6. [Accessed 17 July 2018]. Available from: http://www.ncbi.nlm.nih.gov/pubmed/12748354.

Mercer, J. and Helenius, A. 2012. Gulping rather than sipping: macropinocytosis as a way of virus entry. *Current Opinion in Microbiology*. [Online]. **15**(4), pp.490–499. [Accessed 21 July 2018]. Available from: http://www.ncbi.nlm.nih.gov/pubmed/22749376.

Miles, B.D., Luftig, R.B., Weatherbee, J.A., Weihing, R.R. and Weber, J. 1980. Quantitation of the interaction between adenovirus types 2 and 5 and microtubules inside infected cells. *Virology*. [Online]. **105**(1), pp.265–269. [Accessed 23 July 2018]. Available from: https://www.sciencedirect.com/science/article/pii/0042682280901774.

Miller, C. 2000. An overview of the potassium channel family. *Genome Biology*. [Online]. **1**(4), reviews0004.1. [Accessed 20 July 2018]. Available from: http://www.ncbi.nlm.nih.gov/pubmed/11178249.

Mishra, N., Pereira, M., Rhodes, R.H., An, P., Pipas, J.M., Jain, K., Kapoor, A., Briese, T., Faust, P.L. and Lipkin, W.I. 2014. Identification of a Novel Polyomavirus in a Pancreatic Transplant Recipient With Retinal Blindness and Vasculitic Myopathy. *Journal of Infectious Diseases*. [Online]. **210**(10), pp.1595–1599. [Accessed 17 July 2018]. Available from: http://www.ncbi.nlm.nih.gov/pubmed/24795478.

Moens, U., Calvignac-Spencer, S., Lauber, C., Ramqvist, T., Feltkamp, M.C.W., Daugherty, M.D., Verschoor, E.J., Ehlers, B. and Ictv Report Consortium 2017. ICTV Virus Taxonomy Profile: Polyomaviridae. *Journal of General Virology*. [Online]. **98**(6), pp.1159–1160. [Accessed 17 July 2018]. Available from: http://www.ncbi.nlm.nih.gov/pubmed/28640744.

Moens, U. and Van Ghelue, M. 2005. Polymorphism in the genome of non-passaged human polyomavirus BK: implications for cell tropism and the pathological role of the virus. *Virology*. [Online]. **331**(2), pp.209–231. [Accessed 18 July 2018]. Available from: http://www.ncbi.nlm.nih.gov/pubmed/15629766.

Moens, U., Johansen, T., Johnsen, J.I., Seternes, O.M. and Traavik, T. 1995. Noncoding control region of naturally occurring BK virus variants: sequence comparison and functional analysis. *Virus genes*. [Online]. **10**(3), pp.261–75. [Accessed 18 July 2018].

Available from: http://www.ncbi.nlm.nih.gov/pubmed/8560788.

Moens, U., Subramaniam, N., Johansen, B., Johansen, T. and Traavik, T. 1994. A steroid hormone response unit in the late leader of the noncoding control region of the human polyomavirus BK confers enhanced host cell permissivity. *Journal of virology*. [Online]. **68**(4), pp.2398–408. [Accessed 18 July 2018]. Available from: http://www.ncbi.nlm.nih.gov/pubmed/8139026.

Moens, U., Sundsfjord, A., Flaegstad, T. and Traavik, T. 1990. BK virus early RNA transcripts in stably transformed cells: enhanced levels induced by dibutyryl cyclic AMP, forskolin and 12-O-tetradecanoylphorbol-13-acetate treatment. *Journal of General Virology*. [Online]. **71**(7), pp.1461–1471. [Accessed 18 July 2018]. Available from: http://www.ncbi.nlm.nih.gov/pubmed/2165132.

Morales, M.M., Capella, M.A. and Lopes, A.G. 1999. Structure and function of the cystic fibrosis transmembrane conductance regulator. *Brazilian journal of medical and biological research = Revista brasileira de pesquisas medicas e biologicas*. [Online]. **32**(8), pp.1021–8. [Accessed 20 July 2018]. Available from: http://www.ncbi.nlm.nih.gov/pubmed/10454765.

Morales, M.M., Carroll, T.P., Morita, T., Schwiebert, E.M., Devuyst, O., Wilson, P.D., Lopes, A.G., Stanton, B.A., Dietz, H.C., Cutting, G.R. and Guggino, W.B. 1996. Both the wild type and a functional isoform of CFTR are expressed in kidney. *American Journal of Physiology-Renal Physiology*. [Online]. **270**(6), pp.F1038–F1048. [Accessed 20 July 2018]. Available from: http://www.ncbi.nlm.nih.gov/pubmed/8764323.

Morales, M.M., Falkenstein, D. and Lopes, A.G. 2000. The cystic fibrosis transmembrane regulator (CFTR) in the kidney. *Anais da Academia Brasileira de Ciencias*. [Online]. **72**(3), pp.399–406. [Accessed 20 July 2018]. Available from: http://www.ncbi.nlm.nih.gov/pubmed/11028104.

Morel, V., Martin, E., François, C., Helle, F., Faucher, J., Mourez, T., Choukroun, G., Duverlie, G., Castelain, S. and Brochot, E. 2017. A Simple and Reliable Strategy for BK Virus Subtyping and Subgrouping Y.-W. Tang, ed. *Journal of Clinical Microbiology*. [Online]. **55**(4), pp.1177–1185. [Accessed 18 July 2018]. Available from: http://www.ncbi.nlm.nih.gov/pubmed/28151406.

Moreland, R.B. and Garcea, R.L. 1991. Characterization of a nuclear localization sequence in the polyomavirus capsid protein VP1. *Virology*. [Online]. **185**(1), pp.513–8. [Accessed 20 July 2018]. Available from: http://www.ncbi.nlm.nih.gov/pubmed/1656604.

Moriyama, T., Marquez, J.P., Wakatsuki, T. and Sorokin, A. 2007. Caveolar Endocytosis Is Critical for BK Virus Infection of Human Renal Proximal Tubular Epithelial Cells. *Journal of Virology*. [Online]. **81**(16), pp.8552–8562. [Accessed 18 July 2018]. Available from: http://www.ncbi.nlm.nih.gov/pubmed/17553887.

Moriyama, T. and Sorokin, A. 2009. BK Virus (BKV): Infection, Propagation, Quantitation, Purification, Labeling, and Analysis of Cell Entry. *Current Protocols in Cell Biology*. [Online]. **42**(1), 26.2.1-26.2.13. [Accessed 21 July 2018]. Available from: http://www.ncbi.nlm.nih.gov/pubmed/19283732.

Moriyama, T. and Sorokin, A. 2008a. Intracellular trafficking pathway of BK Virus in human renal proximal tubular epithelial cells. *Virology*. [Online]. **371**(2), pp.336–349. [Accessed 18 July 2018]. Available from: http://www.ncbi.nlm.nih.gov/pubmed/17976677.

Moriyama, T. and Sorokin, A. 2008b. Repression of BK Virus Infection of Human Renal Proximal Tubular Epithelial Cells by Pravastatin. *Transplantation*. [Online]. **85**(9), pp.1311–1317. [Accessed 18 July 2018]. Available from: http://www.ncbi.nlm.nih.gov/pubmed/18475189.

Muanprasat, C., Sonawane, N.D., Salinas, D., Taddei, A., Galietta, L.J.V. and Verkman, A.S. 2004. Discovery of Glycine Hydrazide Pore-occluding CFTR Inhibitors. *The Journal of General Physiology*. [Online]. **124**(2), pp.125–137. [Accessed 20 July 2018]. Available from: http://www.jgp.org/lookup/doi/10.1085/jgp.200409059.

Mudhakir, D. and Harashima, H. 2009. Learning from the Viral Journey: How to Enter Cells and How to Overcome Intracellular Barriers to Reach the Nucleus. *The AAPS Journal*. [Online]. **11**(1), pp.65–77. [Accessed 21 July 2018]. Available from: http://www.ncbi.nlm.nih.gov/pubmed/19194803.

Müller, H. and Johne, R. 2001. Avian polyomavirus agnoprotein 1a is incorporated into the virus particle as a fourth structural protein, VP4. *Journal of General Virology*. [Online]. **82**(4), pp.909–918. [Accessed 17 July 2018]. Available from: http://www.ncbi.nlm.nih.gov/pubmed/11257197.

Murata, M., Peränen, J., Schreiner, R., Wieland, F., Kurzchalia, T. V and Simons, K. 1995. VIP21/caveolin is a cholesterol-binding protein. *Proceedings of the National Academy of Sciences of the United States of America*. [Online]. **92**(22), pp.10339–43. [Accessed 18 July 2018]. Available from: http://www.ncbi.nlm.nih.gov/pubmed/7479780.

Myhre, M.R., Olsen, G.-H., Gosert, R., Hirsch, H.H. and Rinaldo, C.H. 2010. Clinical polyomavirus BK variants with agnogene deletion are non-functional but rescued by trans-complementation. *Virology*. [Online]. **398**(1), pp.12–20. [Accessed 18 July 2018]. Available from: http://www.ncbi.nlm.nih.gov/pubmed/20005552.

Nakanishi, A., Itoh, N., Li, P.P., Handa, H., Liddington, R.C. and Kasamatsu, H. 2007. Minor capsid proteins of simian virus 40 are dispensable for nucleocapsid assembly and cell entry but are required for nuclear entry of the viral genome. *Journal of virology*. [Online]. **81**(8), pp.3778–85. [Accessed 18 July 2018]. Available from: http://www.ncbi.nlm.nih.gov/pubmed/17267496.

Nakanishi, A., Shum, D., Morioka, H., Otsuka, E. and Kasamatsu, H. 2002. Interaction of the Vp3 nuclear localization signal with the importin alpha 2/beta heterodimer directs nuclear entry of infecting simian virus 40. *Journal of virology*. [Online]. **76**(18), pp.9368–77. [Accessed 20 July 2018]. Available from: http://www.ncbi.nlm.nih.gov/pubmed/12186919.

Nakshatri, H., Pater, M.M. and Pater, A. 1988. Functional role of BK virus tumor antigens in transformation. *Journal of virology*. [Online]. **62**(12), pp.4613–21. [Accessed 18 July 2018]. Available from: http://www.ncbi.nlm.nih.gov/pubmed/2846874.

Nelson, C.D.S., Carney, D.W., Derdowski, A., Lipovsky, A., Gee, G. V, O'Hara, B., Williard, P., DiMaio, D., Sello, J.K. and Atwood, W.J. 2013. A retrograde trafficking inhibitor of ricin and Shiga-like toxins inhibits infection of cells by human and monkey polyomaviruses. *mBio*. [Online]. **4**(6), pp.e00729-13. [Accessed 18 July 2018]. Available from: http://www.ncbi.nlm.nih.gov/pubmed/24222489.

Neu, U., Allen, S.A., Blaum, B.S., Liu, Y., Frank, M., Palma, A.S., Ströh, L.J., Feizi, T., Peters, T., Atwood, W.J. and Stehle, T. 2013. A Structure-Guided Mutation in the Major Capsid Protein Retargets BK Polyomavirus D. A. Galloway, ed. *PLoS Pathogens*. [Online]. **9**(10), p.e1003688. [Accessed 18 July 2018]. Available from: http://dx.plos.org/10.1371/journal.ppat.1003688.

Neyton, J. and Miller, C. 1988. Potassium blocks barium permeation through a calcium-activated potassium channel. *The Journal of general physiology*. [Online]. **92**(5), pp.549–67. [Accessed 22 July 2018]. Available from: http://www.ncbi.nlm.nih.gov/pubmed/3235973.

Nguyen, K.D., Lee, E.E., Yue, Y., Stork, J., Pock, L., North, J.P., Vandergriff, T., Cockerell, C., Hosler, G.A., Pastrana, D. V., Buck, C.B. and Wang, R.C. 2017. Human polyomavirus 6 and 7 are associated with pruritic and dyskeratotic dermatoses. *Journal*

of the American Academy of Dermatology. [Online]. **76**(5), p.932–940.e3. [Accessed 17 July 2018]. Available from: http://www.ncbi.nlm.nih.gov/pubmed/28040372.

Nickeleit, V., Hirsch, H.H., Binet, I.F., Gudat, F., Prince, O., Dalquen, P., Thiel, G. and Mihatsch, M.J. 1999. Polyomavirus infection of renal allograft recipients: from latent infection to manifest disease. *Journal of the American Society of Nephrology : JASN*. [Online]. **10**(5), pp.1080–9. [Accessed 17 July 2018]. Available from: http://www.ncbi.nlm.nih.gov/pubmed/10232695.

Nickeleit, V., Klimkait, T., Binet, I.F., Dalquen, P., Del Zenero, V., Thiel, G., Mihatsch, M.J. and Hirsch, H.H. 2000. Testing for Polyomavirus Type BK DNA in Plasma to Identify Renal-Allograft Recipients with Viral Nephropathy. *New England Journal of Medicine*. [Online]. **342**(18), pp.1309–1315. [Accessed 17 July 2018]. Available from: http://www.ncbi.nlm.nih.gov/pubmed/10793163.

Nilius, B. and Droogmans, G. 2003. Amazing chloride channels: an overview. *Acta Physiologica Scandinavica*. [Online]. **177**(2), pp.119–147. [Accessed 20 July 2018]. Available from: http://www.ncbi.nlm.nih.gov/pubmed/12558550.

Nilsson, J., Miyazaki, N., Xing, L., Wu, B., Hammar, L., Li, T.C., Takeda, N., Miyamura, T. and Cheng, R.H. 2005. Structure and Assembly of a T=1 Virus-Like Particle in BK Polyomavirus. *Journal of Virology*. [Online]. **79**(9), pp.5337–5345. [Accessed 18 July 2018]. Available from: http://www.ncbi.nlm.nih.gov/pubmed/15827148.

Norimatsu, Y., Ivetac, A., Alexander, C., O'Donnell, N., Frye, L., Sansom, M.S.P. and Dawson, D.C. 2012. Locating a Plausible Binding Site for an Open-Channel Blocker, GlyH-101, in the Pore of the Cystic Fibrosis Transmembrane Conductance Regulator. *Molecular Pharmacology*. [Online]. **82**(6), pp.1042–1055. [Accessed 20 July 2018]. Available from: http://www.ncbi.nlm.nih.gov/pubmed/22923500.

Norkin, L.C., Anderson, H.A., Wolfrom, S.A. and Oppenheim, A. 2002. Caveolar endocytosis of simian virus 40 is followed by brefeldin A-sensitive transport to the endoplasmic reticulum, where the virus disassembles. *Journal of virology*. [Online]. **76**(10), pp.5156–66. [Accessed 18 July 2018]. Available from: http://www.ncbi.nlm.nih.gov/pubmed/11967331.

Norris, C.A., He, K., Springer, M.G., Hartnett, K.A., Horn, J.P. and Aizenman, E. 2012. Regulation of Neuronal Proapoptotic Potassium Currents by the Hepatitis C Virus Nonstructural Protein 5A. *Journal of Neuroscience*. [Online]. **32**(26), pp.8865–8870. [Accessed 21 July 2018]. Available from: http://www.ncbi.nlm.nih.gov/pubmed/22745487.

Okada, Shuichi Endo, Hidehiro Takah, Y., Endo, S., Takahashi, H., Sawa, H., Umemura, T. and Nagashima, K. 2001. Distribution and function of JCV agnoprotein. *Journal of Neurovirology*. [Online]. **7**(4), pp.302–306. [Accessed 18 July 2018]. Available from: http://www.ncbi.nlm.nih.gov/pubmed/11517407.

Okada, Y., Maeno, E., Shimizu, T., Manabe, K., Mori, S. and Nabekura, T. 2004. Dual roles of plasmalemmal chloride channels in induction of cell death. *Pfl[illegible]gers Archiv European Journal of Physiology*. [Online]. **448**(3), pp.287–295. [Accessed 23 July 2018]. Available from: http://www.ncbi.nlm.nih.gov/pubmed/15103464.

Okada, Y., Suzuki, T., Sunden, Y., Orba, Y., Kose, S., Imamoto, N., Takahashi, H., Tanaka, S., Hall, W.W., Nagashima, K. and Sawa, H. 2005. Dissociation of heterochromatin protein 1 from lamin B receptor induced by human polyomavirus agnoprotein: role in nuclear egress of viral particles. *EMBO reports*. [Online]. **6**(5), pp.452–457. [Accessed 18 July 2018]. Available from: http://www.ncbi.nlm.nih.gov/pubmed/15864296.

Padgett, B.L., Walker, D.L., ZuRhein, G.M., Eckroade, R.J. and Dessel, B.H. 1971. Cultivation of papova-like virus from human brain with progressive multifocal leucoencephalopathy. *Lancet (London, England)*. [Online]. **1**(7712), pp.1257–60.

[Accessed 17 July 2018]. Available from: http://www.ncbi.nlm.nih.gov/pubmed/4104715.

Pagano, J.S. 1984. DNA tumor viruses. *Transplantation proceedings*. [Online]. **16**(2), pp.419–27. [Accessed 17 July 2018]. Available from: http://www.ncbi.nlm.nih.gov/pubmed/6326351.

Palmer, L.G. and Sackin, H. 1988. Regulation of renal ion channels. *FASEB journal : official publication of the Federation of American Societies for Experimental Biology*. [Online]. **2**(15), pp.3061–5. [Accessed 20 July 2018]. Available from: http://www.ncbi.nlm.nih.gov/pubmed/2461326.

Panou, M.-M., Prescott, E.L., Hurdiss, D.L., Swinscoe, G., Hollinshead, M., Caller, L.G., Morgan, E.L., Carlisle, L., Müller, M., Antoni, M., Kealy, D., Ranson, N.A., Crump, C.M. and Macdonald, A. 2018. Agnoprotein is an essential egress factor during BK Polyomavirus infection. *International Journal of Molecular Sciences*. **19**(3).

Panté, N. and Kann, M. 2002. Nuclear pore complex is able to transport macromolecules with diameters of about 39 nm. *Molecular biology of the cell*. [Online]. **13**(2), pp.425–34. [Accessed 20 July 2018]. Available from: http://www.ncbi.nlm.nih.gov/pubmed/11854401.

Pastrana, D. V., Ray, U., Magaldi, T.G., Schowalter, R.M., Cuburu, N. and Buck, C.B. 2013. BK Polyomavirus Genotypes Represent Distinct Serotypes with Distinct Entry Tropism. *Journal of Virology*. [Online]. **87**(18), pp.10105–10113. [Accessed 17 July 2018]. Available from: http://www.ncbi.nlm.nih.gov/pubmed/23843634.

Pelkmans, L., Kartenbeck, J. and Helenius, A. 2001. Caveolar endocytosis of simian virus 40 reveals a new two-step vesicular-transport pathway to the ER. *Nature Cell Biology*. [Online]. **3**(5), pp.473–483. [Accessed 18 July 2018]. Available from: http://www.ncbi.nlm.nih.gov/pubmed/11331875.

Pelkmans, L., Püntener, D. and Helenius, A. 2002. Local Actin Polymerization and Dynamin Recruitment in SV40-Induced Internalization of Caveolae. *Science*. [Online]. **296**(5567), pp.535–539. [Accessed 23 July 2018]. Available from: http://www.ncbi.nlm.nih.gov/pubmed/11964480.

Pepper, C., Jasani, B., Navabi, H., Wynford-Thomas, D. and Gibbs, A.R. 1996. Simian virus 40 large T antigen (SV40LTAg) primer specific DNA amplification in human pleural mesothelioma tissue. *Thorax*. [Online]. **51**(11), pp.1074–6. [Accessed 23 July 2018]. Available from: http://www.ncbi.nlm.nih.gov/pubmed/8958887.

Peretti, A., FitzGerald, P.C., Bliskovsky, V., Pastrana, D. V and Buck, C.B. 2015. Genome Sequence of a Fish-Associated Polyomavirus, Black Sea Bass (Centropristis striata) Polyomavirus 1. *Genome announcements*. [Online]. **3**(1). [Accessed 17 July 2018]. Available from: http://www.ncbi.nlm.nih.gov/pubmed/25635011.

Pho, M.T., Ashok, A. and Atwood, W.J. 2000. JC virus enters human glial cells by clathrin-dependent receptor-mediated endocytosis. *Journal of virology*. [Online]. **74**(5), pp.2288–92. [Accessed 18 July 2018]. Available from: http://www.ncbi.nlm.nih.gov/pubmed/10666259.

Piasta, K.N., Theobald, D.L. and Miller, C. 2011. Potassium-selective block of barium permeation through single KcsA channels. *The Journal of general physiology*. [Online]. **138**(4), pp.421–36. [Accessed 22 July 2018]. Available from: http://www.ncbi.nlm.nih.gov/pubmed/21911483.

Pietrement, C., Da Silva, N., Silberstein, C., James, M., Marsolais, M., Van Hoek, A., Brown, D., Pastor-Soler, N., Ameen, N., Laprade, R., Ramesh, V. and Breton, S. 2008. Role of NHERF1, Cystic Fibrosis Transmembrane Conductance Regulator, and cAMP in the Regulation of Aquaporin 9. *Journal of Biological Chemistry*. [Online]. **283**(5), pp.2986–2996. [Accessed 23 July 2018]. Available from:

http://www.ncbi.nlm.nih.gov/pubmed/18055461.

Pocock, G. and Richards, C.D. 2006. *Human physiology : the basis of medicine*. Oxford University Press.

Ponder, B.A.J., Robbins, A.K. and Crawford, L. V. 1977. Phosphorylation of Polyoma and SV40 Virus Proteins. *Journal of General Virology*. [Online]. **37**(1), pp.75–83. [Accessed 18 July 2018]. Available from: http://www.ncbi.nlm.nih.gov/pubmed/199707.

Possati, L., Rubini, C., Portolani, M., Gazzanelli, G., Piani, M. and Borgatti, M. 1983. Receptors for the human papovavirus BK on human lymphocytes. *Archives of virology*. [Online]. **75**(1–2), pp.131–6. [Accessed 18 July 2018]. Available from: http://www.ncbi.nlm.nih.gov/pubmed/6600921.

Purighalla, R., Shapiro, R., McCauley, J. and Randhawa, P. 1995. BK virus infection in a kidney allograft diagnosed by needle biopsy. *American journal of kidney diseases : the official journal of the National Kidney Foundation*. [Online]. **26**(4), pp.671–3. [Accessed 17 July 2018]. Available from: http://www.ncbi.nlm.nih.gov/pubmed/7573026.

Qian, M., Cai, D., Verhey, K.J. and Tsai, B. 2009. A Lipid Receptor Sorts Polyomavirus from the Endolysosome to the Endoplasmic Reticulum to Cause Infection D. Galloway, ed. *PLoS Pathogens*. [Online]. **5**(6), p.e1000465. [Accessed 23 July 2018]. Available from: http://dx.plos.org/10.1371/journal.ppat.1000465.

Quayle, J.M., Standen, N.B. and Stanfield, P.R. 1988. The voltage-dependent block of ATP-sensitive potassium channels of frog skeletal muscle by caesium and barium ions. *The Journal of physiology*. [Online]. **405**, pp.677–97. [Accessed 22 July 2018]. Available from: http://www.ncbi.nlm.nih.gov/pubmed/3267155.

Querbes, W., O'Hara, B.A., Williams, G. and Atwood, W.J. 2006. Invasion of Host Cells by JC Virus Identifies a Novel Role for Caveolae in Endosomal Sorting of Noncaveolar Ligands. *Journal of Virology*. [Online]. **80**(19), pp.9402–9413. [Accessed 23 July 2018]. Available from: http://www.ncbi.nlm.nih.gov/pubmed/16973546.

Radhakrishna, H. and Donaldson, J.G. 1997. ADP-ribosylation factor 6 regulates a novel plasma membrane recycling pathway. *The Journal of cell biology*. [Online]. **139**(1), pp.49–61. [Accessed 18 July 2018]. Available from: http://www.ncbi.nlm.nih.gov/pubmed/9314528.

Radtke, K., Dohner, K. and Sodeik, B. 2006. Viral interactions with the cytoskeleton: a hitchhiker's guide to the cell. *Cellular Microbiology*. [Online]. **8**(3), pp.387–400. [Accessed 18 July 2018]. Available from: http://www.ncbi.nlm.nih.gov/pubmed/16469052.

Raghava, S., Giorda, K.M., Romano, F.B., Heuck, A.P. and Hebert, D.N. 2013. SV40 Late Protein VP4 Forms Toroidal Pores To Disrupt Membranes for Viral Release. *Biochemistry*. [Online]. **52**(22), pp.3939–3948. [Accessed 17 July 2018]. Available from: http://www.ncbi.nlm.nih.gov/pubmed/23651212.

Raghava, S., Giorda, K.M., Romano, F.B., Heuck, A.P. and Hebert, D.N. 2011. The SV40 Late Protein VP4 Is a Viroporin that Forms Pores to Disrupt Membranes for Viral Release C. Parrish, ed. *PLoS Pathogens*. [Online]. **7**(6), p.e1002116. [Accessed 17 July 2018]. Available from: http://www.ncbi.nlm.nih.gov/pubmed/21738474.

Ramos, E., Drachenberg, C.B., Wali, R. and Hirsch, H.H. 2009. The Decade of Polyomavirus BK-Associated Nephropathy: State of Affairs. *Transplantation*. [Online]. **87**(5), pp.621–630. [Accessed 17 July 2018]. Available from: http://www.ncbi.nlm.nih.gov/pubmed/19295303.

Randhawa, P., Pastrana, D. V., Zeng, G., Huang, Y., Shapiro, R., Sood, P., Puttarajappa, C., Berger, M., Hariharan, S. and Buck, C.B. 2015. Commercially Available Immunoglobulins Contain Virus Neutralizing Antibodies Against All Major Genotypes of

Polyomavirus BK. *American Journal of Transplantation*. [Online]. **15**(4), pp.1014–1020. [Accessed 17 July 2018]. Available from: http://www.ncbi.nlm.nih.gov/pubmed/25736704.

Randhawa, P.S., Finkelstein, S., Scantlebury, V., Shapiro, R., Vivas, C., Jordan, M., Picken, M.M. and Demetris, A.J. 1999. Human polyoma virus-associated interstitial nephritis in the allograft kidney. *Transplantation*. [Online]. **67**(1), pp.103–9. [Accessed 21 July 2018]. Available from: http://www.ncbi.nlm.nih.gov/pubmed/9921805.

Randhawa, P.S., Schonder, K., Shapiro, R., Farasati, N. and Huang, Y. 2010. Polyomavirus BK neutralizing activity in human immunoglobulin preparations. *Transplantation*. [Online]. **89**(12), pp.1462–5. [Accessed 17 July 2018]. Available from: http://www.ncbi.nlm.nih.gov/pubmed/20568674.

Rang, H.P. 2003. *Pharmacology* [Online]. Churchill Livingstone. [Accessed 14 November 2018]. Available from: https://trove.nla.gov.au/work/25740167?q&versionId=45535332.

Ravindran, M.S., Bagchi, P., Inoue, T. and Tsai, B. 2015. A Non-enveloped Virus Hijacks Host Disaggregation Machinery to Translocate across the Endoplasmic Reticulum Membrane J. T. Schiller, ed. *PLOS Pathogens*. [Online]. **11**(8), p.e1005086. [Accessed 20 July 2018]. Available from: http://dx.plos.org/10.1371/journal.ppat.1005086.

Razani, B., Wang, X.B., Engelman, J.A., Battista, M., Lagaud, G., Zhang, X.L., Kneitz, B., Hou, H., Christ, G.J., Edelmann, W. and Lisanti, M.P. 2002. Caveolin-2-deficient mice show evidence of severe pulmonary dysfunction without disruption of caveolae. *Molecular and cellular biology*. [Online]. **22**(7), pp.2329–44. [Accessed 18 July 2018]. Available from: http://www.ncbi.nlm.nih.gov/pubmed/11884617.

Redman, P.T., He, K., Hartnett, K.A., Jefferson, B.S., Hu, L., Rosenberg, P.A., Levitan, E.S. and Aizenman, E. 2007. Apoptotic surge of potassium currents is mediated by p38 phosphorylation of Kv2.1. *Proceedings of the National Academy of Sciences of the United States of America*. [Online]. **104**(9), pp.3568–73. [Accessed 21 July 2018]. Available from: http://www.ncbi.nlm.nih.gov/pubmed/17360683.

Reenstra, W.W., Sabolic, I., Bae, H.R. and Verkman, A.S. 1992. Protein kinase A dependent membrane protein phosphorylation and chloride conductance in endosomal vesicles from kidney cortex. *Biochemistry*. [Online]. **31**(1), pp.175–81. [Accessed 20 July 2018]. Available from: http://www.ncbi.nlm.nih.gov/pubmed/1310027.

Reiss, K. and Khalili, K. 2003. Viruses and cancer: lessons from the human polyomavirus, JCV. *Oncogene*. [Online]. **22**(42), pp.6517–6523. [Accessed 15 November 2018]. Available from: http://www.nature.com/articles/1206959.

Richterova, Z., Liebl, D., Horak, M., Palkova, Z., Stokrova, J., Hozak, P., Korb, J. and Forstova, J. 2001. Caveolae Are Involved in the Trafficking of Mouse Polyomavirus Virions and Artificial VP1 Pseudocapsids toward Cell Nuclei. *Journal of Virology*. [Online]. **75**(22), pp.10880–10891. [Accessed 18 July 2018]. Available from: http://www.ncbi.nlm.nih.gov/pubmed/11602728.

Rinaldo, C.H., Gosert, R., Bernhoff, E., Finstad, S. and Hirsch, H.H. 2010. 1-O-Hexadecyloxypropyl Cidofovir (CMX001) Effectively Inhibits Polyomavirus BK Replication in Primary Human Renal Tubular Epithelial Cells. *Antimicrobial Agents and Chemotherapy*. [Online]. **54**(11), pp.4714–4722. [Accessed 17 July 2018]. Available from: http://www.ncbi.nlm.nih.gov/pubmed/20713664.

Rinaldo, C.H., Traavik, T. and Hey, A. 1998. The agnogene of the human polyomavirus BK is expressed. *Journal of virology*. [Online]. **72**(7), pp.6233–6. [Accessed 18 July 2018]. Available from: http://www.ncbi.nlm.nih.gov/pubmed/9621096.

Riordan, J.R. 1993. The Cystic Fibrosis Transmembrane Conductance Regulator. *Annual Review of Physiology*. [Online]. **55**(1), pp.609–630. [Accessed 20 July 2018]. Available from: http://www.ncbi.nlm.nih.gov/pubmed/7682047.

Riordan, J.R., Rommens, J.M., Kerem, B., Alon, N., Rozmahel, R., Grzelczak, Z., Zielenski, J., Lok, S., Plavsic, N. and Chou, J.L. 1989. Identification of the cystic fibrosis gene: cloning and characterization of complementary DNA. *Science (New York, N.Y.)*. [Online]. **245**(4922), pp.1066–73. [Accessed 21 July 2018]. Available from: http://www.ncbi.nlm.nih.gov/pubmed/2475911.

Riss, T.L., Moravec, R.A., Niles, A.L., Duellman, S., Benink, H.A., Worzella, T.J. and Minor, L. 2004. *Cell Viability Assays* [Online]. Eli Lilly & Company and the National Center for Advancing Translational Sciences. [Accessed 12 November 2018]. Available from: http://www.ncbi.nlm.nih.gov/pubmed/23805433.

Rosenblum, L.A., Coplan, J.D., Friedman, S. and Bassoff, T. 1991. Dose-response effects of oral yohimbine in unrestrained primates. *Biological Psychiatry*. [Online]. **29**(7), pp.647–657. [Accessed 21 July 2018]. Available from: http://linkinghub.elsevier.com/retrieve/pii/0006322391901348.

Royle, J., Dobson, S., Müller, M. and Macdonald, A. 2015. Emerging Roles of Viroporins Encoded by DNA Viruses: Novel Targets for Antivirals? *Viruses*. [Online]. **7**(10), pp.5375–5387. [Accessed 20 July 2018]. Available from: http://www.ncbi.nlm.nih.gov/pubmed/26501313.

Rozenblatt-Rosen, O., Deo, R.C., Padi, M., Adelmant, G., Calderwood, M.A., Rolland, T., Grace, M., Dricot, A., Askenazi, M., Tavares, M., Pevzner, S.J., Abderazzaq, F., Byrdsong, D., Carvunis, A.-R., Chen, A.A., Cheng, J., Correll, M., Duarte, M., Fan, C., Feltkamp, M.C., Ficarro, S.B., Franchi, R., Garg, B.K., Gulbahce, N., Hao, T., Holthaus, A.M., James, R., Korkhin, A., Litovchick, L., Mar, J.C., Pak, T.R., Rabello, S., Rubio, R., Shen, Y., Singh, S., Spangle, J.M., Tasan, M., Wanamaker, S., Webber, J.T., Roecklein-Canfield, J., Johannsen, E., Barabási, A.-L., Beroukhim, R., Kieff, E., Cusick, M.E., Hill, D.E., Münger, K., Marto, J.A., Quackenbush, J., Roth, F.P., DeCaprio, J.A. and Vidal, M. 2012. Interpreting cancer genomes using systematic host network perturbations by tumour virus proteins. *Nature*. [Online]. **487**(7408), pp.491–495. [Accessed 17 July 2018]. Available from: http://www.ncbi.nlm.nih.gov/pubmed/22810586.

Rubinstein, R., Pare, N. and Harley, E.H. 1987. Structure and function of the transcriptional control region of nonpassaged BK virus. *Journal of virology*. [Online]. **61**(5), pp.1747–50. [Accessed 18 July 2018]. Available from: http://www.ncbi.nlm.nih.gov/pubmed/3033304.

Ruknudin, A., Schulze, D.H., Sullivan, S.K., Lederer, W.J. and Welling, P.A. 1998. Novel subunit composition of a renal epithelial KATP channel. *The Journal of biological chemistry*. [Online]. **273**(23), pp.14165–71. [Accessed 20 July 2018]. Available from: http://www.ncbi.nlm.nih.gov/pubmed/9603917.

Russell, W.C., Graham, F.L., Smiley, J. and Nairn, R. 1977. Characteristics of a Human Cell Line Transformed by DNA from Human Adenovirus Type 5. *Journal of General Virology*. [Online]. **36**(1), pp.59–72. [Accessed 12 November 2018]. Available from: http://www.ncbi.nlm.nih.gov/pubmed/886304.

Saad, E.R., Bresnahan, B.A., Cohen, E.P., Lu, N., Orentas, R.J., Vasudev, B. and Hariharan, S. 2008. Successful Treatment of BK Viremia Using Reduction in Immunosuppression Without Antiviral Therapy. *Transplantation*. [Online]. **85**(6), pp.850–854. [Accessed 17 July 2018]. Available from: http://www.ncbi.nlm.nih.gov/pubmed/18360267.

Sagnella, G. and Swift, P. 2006. The Renal Epithelial Sodium Channel: Genetic Heterogeneity and Implications for the Treatment of High Blood Pressure. *Current Pharmaceutical Design*. [Online]. **12**(18), pp.2221–2234. [Accessed 20 July 2018]. Available from: http://www.eurekaselect.com/openurl/content.php?genre=article&issn=1381-

6128&volume=12&issue=18&spage=2221.

Sakura, H., Ammälä, C., Smith, P.A., Gribble, F.M. and Ashcroft, F.M. 1995. Cloning and functional expression of the cDNA encoding a novel ATP-sensitive potassium channel subunit expressed in pancreatic β-cells, brain, heart and skeletal muscle. *FEBS Letters*. [Online]. **377**(3), pp.338–344. [Accessed 22 July 2018]. Available from: http://www.ncbi.nlm.nih.gov/pubmed/8549751.

Sakurai, Y., Kolokoltsov, A.A., Chen, C.-C., Tidwell, M.W., Bauta, W.E., Klugbauer, N., Grimm, C., Wahl-Schott, C., Biel, M. and Davey, R.A. 2015. Ebola virus. Two-pore channels control Ebola virus host cell entry and are drug targets for disease treatment. *Science (New York, N.Y.)*. [Online]. **347**(6225), pp.995–8. [Accessed 20 July 2018]. Available from: http://www.ncbi.nlm.nih.gov/pubmed/25722412.

Sanchez, D.Y. and Blatz, A.L. 1994. Block of neuronal fast chloride channels by internal tetraethylammonium ions. *The Journal of general physiology*. [Online]. **104**(1), pp.173–90. [Accessed 23 July 2018]. Available from: http://www.ncbi.nlm.nih.gov/pubmed/7964594.

Sanchez, D.Y. and Blatz, A.L. 1992. Voltage-dependent block of fast chloride channels from rat cortical neurons by external tetraethylammonium ion. *The Journal of general physiology*. [Online]. **100**(2), pp.217–31. [Accessed 23 July 2018]. Available from: http://www.ncbi.nlm.nih.gov/pubmed/1383391.

Saribas, A.S., Abou-Gharbia, M., Childers, W., Sariyer, I.K., White, M.K. and Safak, M. 2013. Essential roles of Leu/Ile/Phe-rich domain of JC virus agnoprotein in dimer/oligomer formation, protein stability and splicing of viral transcripts. *Virology*. [Online]. **443**(1), pp.161–176. [Accessed 18 July 2018]. Available from: http://www.ncbi.nlm.nih.gov/pubmed/23747198.

Saribas, A.S., Arachea, B.T., White, M.K., Viola, R.E. and Safak, M. 2011. Human polyomavirus JC small regulatory agnoprotein forms highly stable dimers and oligomers: Implications for their roles in agnoprotein function. *Virology*. [Online]. **420**(1), pp.51–65. [Accessed 18 July 2018]. Available from: http://www.ncbi.nlm.nih.gov/pubmed/21920573.

Saribas, A.S., Coric, P., Hamazaspyan, A., Davis, W., Axman, R., White, M.K., Abou-Gharbia, M., Childers, W., Condra, J.H., Bouaziz, S. and Safak, M. 2016. Emerging From the Unknown: Structural and Functional Features of Agnoprotein of Polyomaviruses. *Journal of Cellular Physiology*. [Online]. **231**(10), pp.2115–2127. [Accessed 17 July 2018]. Available from: http://www.ncbi.nlm.nih.gov/pubmed/26831433.

Sariyer, I.K., Akan, I., Palermo, V., Gordon, J., Khalili, K. and Safak, M. 2006. Phosphorylation mutants of JC virus agnoprotein are unable to sustain the viral infection cycle. *Journal of virology*. [Online]. **80**(8), pp.3893–903. [Accessed 18 July 2018]. Available from: http://www.ncbi.nlm.nih.gov/pubmed/16571806.

Sasaki, S., Uchida, S., Kawasaki, M., Adachi, S. and Marumo, F. 1994. ClC family in the kidney. *The Japanese journal of physiology*. [Online]. **44 Suppl 2**, pp.S3-8. [Accessed 20 July 2018]. Available from: http://www.ncbi.nlm.nih.gov/pubmed/7752544.

Sawinski, D. and Goral, S. 2015. BK virus infection: an update on diagnosis and treatment. *Nephrology Dialysis Transplantation*. [Online]. **30**(2), pp.209–217. [Accessed 17 July 2018]. Available from: http://www.ncbi.nlm.nih.gov/pubmed/24574543.

Sawinski, D. and Goral, S. 2015. BK virus infection: An update on diagnosis and treatment. *Nephrology Dialysis Transplantation*.

Scadden, J.R., Sharif, A., Skordilis, K. and Borrows, R. 2017. Polyoma virus nephropathy in kidney transplantation. *World journal of transplantation*. [Online]. **7**(6), pp.329–338. [Accessed 17 July 2018]. Available from:

http://www.ncbi.nlm.nih.gov/pubmed/29312862.

Schowalter, R.M. and Buck, C.B. 2013. The Merkel Cell Polyomavirus Minor Capsid Protein M. J. Imperiale, ed. *PLoS Pathogens*. [Online]. **9**(8), p.e1003558. [Accessed 18 July 2018]. Available from: http://dx.plos.org/10.1371/journal.ppat.1003558.

Schowalter, R.M., Pastrana, D. V. and Buck, C.B. 2011. Glycosaminoglycans and Sialylated Glycans Sequentially Facilitate Merkel Cell Polyomavirus Infectious Entry M. Imperiale, ed. *PLoS Pathogens*. [Online]. **7**(7), p.e1002161. [Accessed 23 July 2018]. Available from: http://dx.plos.org/10.1371/journal.ppat.1002161.

Schowalter, R.M., Pastrana, D. V., Pumphrey, K.A., Moyer, A.L. and Buck, C.B. 2010. Merkel Cell Polyomavirus and Two Previously Unknown Polyomaviruses Are Chronically Shed from Human Skin. *Cell Host & Microbe*. [Online]. **7**(6), pp.509–515. [Accessed 17 July 2018]. Available from: http://www.ncbi.nlm.nih.gov/pubmed/20542254.

Schowalter, R.M., Reinhold, W.C. and Buck, C.B. 2012. Entry Tropism of BK and Merkel Cell Polyomaviruses in Cell Culture J. M. Brandner, ed. *PLoS ONE*. [Online]. **7**(7), p.e42181. [Accessed 18 July 2018]. Available from: http://www.ncbi.nlm.nih.gov/pubmed/22860078.

SCHULTZ, B.D., SINGH, A.K., DEVOR, D.C. and BRIDGES, R.J. 1999. Pharmacology of CFTR Chloride Channel Activity. *Physiological Reviews*. [Online]. **79**(1), pp.S109–S144. [Accessed 20 July 2018]. Available from: http://www.ncbi.nlm.nih.gov/pubmed/9922378.

Schwiebert, E.M., Morales, M.M., Devidas, S., Egan, M.E. and Guggino, W.B. 1998. Chloride channel and chloride conductance regulator domains of CFTR, the cystic fibrosis transmembrane conductance regulator. *Proceedings of the National Academy of Sciences of the United States of America*. [Online]. **95**(5), pp.2674–9. [Accessed 20 July 2018]. Available from: http://www.ncbi.nlm.nih.gov/pubmed/9482946.

Scott, C.C. and Gruenberg, J. 2011. Ion flux and the function of endosomes and lysosomes: pH is just the start. *BioEssays*. [Online]. **33**(2), pp.103–110. [Accessed 23 July 2018]. Available from: http://www.ncbi.nlm.nih.gov/pubmed/21140470.

Scuda, N., Hofmann, J., Calvignac-Spencer, S., Ruprecht, K., Liman, P., Kuhn, J., Hengel, H. and Ehlers, B. 2011. A Novel Human Polyomavirus Closely Related to the African Green Monkey-Derived Lymphotropic Polyomavirus. *Journal of Virology*. [Online]. **85**(9), pp.4586–4590. [Accessed 17 July 2018]. Available from: http://www.ncbi.nlm.nih.gov/pubmed/21307194.

Seamone, M.E., Wang, W., Acott, P., Beck, P.L., Tibbles, L.A. and Muruve, D.A. 2010. MAP kinase activation increases BK polyomavirus replication and facilitates viral propagation in vitro. *Journal of Virological Methods*. [Online]. **170**(1–2), pp.21–29. [Accessed 20 July 2018]. Available from: http://www.ncbi.nlm.nih.gov/pubmed/20813136.

Seehafer, J., Salmi, A., Scraba, D.G. and Colter, J.S. 1975. A comparative study of BK and polyoma viruses. *Virology*. [Online]. **66**(1), pp.192–205. [Accessed 18 July 2018]. Available from: http://www.ncbi.nlm.nih.gov/pubmed/166499.

Seehafer, J., Salmi, A., Scraba, D.G. and Colter, J.S. 1975. A comparative study of BK and polyoma viruses. *Virology*. [Online]. **66**(1), pp.192–205. [Accessed 21 July 2018]. Available from: https://www.sciencedirect.com/science/article/pii/0042682275901907.

Seo, G.J., Fink, L.H.L., O'Hara, B., Atwood, W.J. and Sullivan, C.S. 2008. Evolutionarily Conserved Function of a Viral MicroRNA. *Journal of Virology*. [Online]. **82**(20), pp.9823–9828. [Accessed 18 July 2018]. Available from: http://www.ncbi.nlm.nih.gov/pubmed/18684810.

Serrano-Martín, X., Payares, G. and Mendoza-León, A. 2006. Glibenclamide, a blocker of

K+(ATP) channels, shows antileishmanial activity in experimental murine cutaneous leishmaniasis. *Antimicrobial agents and chemotherapy*. [Online]. **50**(12), pp.4214–6. [Accessed 21 July 2018]. Available from: http://www.ncbi.nlm.nih.gov/pubmed/17015627.

Seth, P., Diaz, F., Tao-Cheng, J.-H. and Major, E.O. 2004. JC virus induces nonapoptotic cell death of human central nervous system progenitor cell-derived astrocytes. *Journal of virology*. [Online]. **78**(9), pp.4884–91. [Accessed 23 July 2018]. Available from: http://www.ncbi.nlm.nih.gov/pubmed/15078969.

Shah, K. and Nathanson, N. 1976. Human exposure to SV40: review and comment. *American journal of epidemiology*. [Online]. **103**(1), pp.1–12. [Accessed 23 July 2018]. Available from: http://www.ncbi.nlm.nih.gov/pubmed/174424.

Shah, K. V., Daniel, R.W. and Warszawski, R.M. 1973. High Prevalence of Antibodies to BK Virus, an SV40-Related Papovavirus, in Residents of Maryland. *The Journal of Infectious Diseases*. [Online]. **128**, pp.784–787. [Accessed 17 July 2018]. Available from: https://www.jstor.org/stable/30061652.

Sharma, B.N., Li, R., Bernhoff, E., Gutteberg, T.J. and Rinaldo, C.H. 2011. Fluoroquinolones inhibit human polyomavirus BK (BKV) replication in primary human kidney cells. *Antiviral Research*. [Online]. **92**(1), pp.115–123. [Accessed 17 July 2018]. Available from: http://www.ncbi.nlm.nih.gov/pubmed/21798289.

Shen, P.S., Enderlein, D., Nelson, C.D.S., Carter, W.S., Kawano, M., Xing, L., Swenson, R.D., Olson, N.H., Baker, T.S., Cheng, R.H., Atwood, W.J., Johne, R. and Belnap, D.M. 2011. The structure of avian polyomavirus reveals variably sized capsids, non-conserved inter-capsomere interactions, and a possible location of the minor capsid protein VP4. *Virology*. [Online]. **411**(1), pp.142–152. [Accessed 17 July 2018]. Available from: http://www.ncbi.nlm.nih.gov/pubmed/21239031.

Sheppard, D.N. and Robinson, K.A. 1997. Mechanism of glibenclamide inhibition of cystic fibrosis transmembrane conductance regulator Cl- channels expressed in a murine cell line. *The Journal of physiology*. [Online]. **503 (Pt 2**, pp.333–46. [Accessed 22 July 2018]. Available from: http://www.ncbi.nlm.nih.gov/pubmed/9306276.

Sheppard, D.N. and Welsh, M.J. 1992. Effect of ATP-sensitive K+ channel regulators on cystic fibrosis transmembrane conductance regulator chloride currents. *The Journal of general physiology*. [Online]. **100**(4), pp.573–91. [Accessed 22 July 2018]. Available from: http://www.ncbi.nlm.nih.gov/pubmed/1281220.

SHEPPARD, D.N. and WELSH, M.J. 1999. Structure and Function of the CFTR Chloride Channel. *Physiological Reviews*. [Online]. **79**(1), pp.S23–S45. [Accessed 12 November 2018]. Available from: http://www.ncbi.nlm.nih.gov/pubmed/9922375.

Shuda, M., Feng, H., Kwun, H.J., Rosen, S.T., Gjoerup, O., Moore, P.S. and Chang, Y. 2008. T antigen mutations are a human tumor-specific signature for Merkel cell polyomavirus. *Proceedings of the National Academy of Sciences*. [Online]. **105**(42), pp.16272–16277. [Accessed 23 July 2018]. Available from: http://www.ncbi.nlm.nih.gov/pubmed/18812503.

Siebrasse, E.A., Reyes, A., Lim, E.S., Zhao, G., Mkakosya, R.S., Manary, M.J., Gordon, J.I. and Wang, D. 2012. Identification of MW polyomavirus, a novel polyomavirus in human stool. *Journal of virology*. [Online]. **86**(19), pp.10321–6. [Accessed 17 July 2018]. Available from: http://www.ncbi.nlm.nih.gov/pubmed/22740408.

Sieczkarski, S.B. and Whittaker, G.R. 2002. Influenza virus can enter and infect cells in the absence of clathrin-mediated endocytosis. *Journal of virology*. [Online]. **76**(20), pp.10455–64. [Accessed 23 July 2018]. Available from: http://www.ncbi.nlm.nih.gov/pubmed/12239322.

Singh, H.K., Andreoni, K.A., Madden, V., True, K., Detwiler, R., Weck, K. and Nickeleit, V.

2009. Presence of Urinary Haufen Accurately Predicts Polyomavirus Nephropathy. *Journal of the American Society of Nephrology*. [Online]. **20**(2), pp.416–427. [Accessed 17 July 2018]. Available from: http://www.ncbi.nlm.nih.gov/pubmed/19158358.

Sinibaldi, L., Goldoni, P., Pietropaolo, V., Longhi, C. and Orsi, N. 1990. Involvement of gangliosides in the interaction between BK virus and Vero cells. *Archives of virology*. [Online]. **113**(3–4), pp.291–6. [Accessed 18 July 2018]. Available from: http://www.ncbi.nlm.nih.gov/pubmed/2171462.

Sodeik, B. 2000. Mechanisms of viral transport in the cytoplasm. *Trends in microbiology*. [Online]. **8**(10), pp.465–72. [Accessed 23 July 2018]. Available from: http://www.ncbi.nlm.nih.gov/pubmed/11044681.

Souza-Menezes, J. and Morales, M.M. 2009. CFTR structure and function: is there a role in the kidney? *Biophysical Reviews*. [Online]. **1**(1), pp.3–12. [Accessed 20 July 2018]. Available from: http://www.ncbi.nlm.nih.gov/pubmed/28510151.

Spurgeon, M.E. and Lambert, P.F. 2013. Merkel cell polyomavirus: A newly discovered human virus with oncogenic potential. *Virology*. [Online]. **435**(1), pp.118–130. [Accessed 23 July 2018]. Available from: http://www.ncbi.nlm.nih.gov/pubmed/23217622.

Stanfield, P.R. 1983. Tetraethylammonium ions and the potassium permeability of excitable cells. *Reviews of physiology, biochemistry and pharmacology*. [Online]. **97**, pp.1–67. [Accessed 23 July 2018]. Available from: http://www.ncbi.nlm.nih.gov/pubmed/6306751.

Stang, E., Kartenbeck, J. and Parton, R.G. 1997. Major histocompatibility complex class I molecules mediate association of SV40 with caveolae. *Molecular biology of the cell*. [Online]. **8**(1), pp.47–57. [Accessed 23 July 2018]. Available from: http://www.ncbi.nlm.nih.gov/pubmed/9017594.

Stauffer, E.K. and Ziegler, R.J. 1989. Loss of Functional Voltage-gated Sodium Channels in Persistent Mumps Virus-infected PC12 Cells. *Journal of General Virology*. [Online]. **70**(3), pp.749–754. [Accessed 21 July 2018]. Available from: http://www.ncbi.nlm.nih.gov/pubmed/2543758.

Stauffer, S., Feng, Y., Nebioglu, F., Heilig, R., Picotti, P. and Helenius, A. 2014. Stepwise Priming by Acidic pH and a High K+ Concentration Is Required for Efficient Uncoating of Influenza A Virus Cores after Penetration. *Journal of Virology*. [Online]. **88**(22), pp.13029–13046. [Accessed 23 July 2018]. Available from: http://www.ncbi.nlm.nih.gov/pubmed/25165113.

Stehle, T., Gamblin, S.J., Yan, Y. and Harrison, S.C. 1996. The structure of simian virus 40 refined at 3.1 A resolution. *Structure (London, England : 1993)*. [Online]. **4**(2), pp.165–82. [Accessed 18 July 2018]. Available from: http://www.ncbi.nlm.nih.gov/pubmed/8805523.

Stehle, T. and Harrison, S.C. 1996. Crystal structures of murine polyomavirus in complex with straight-chain and branched-chain sialyloligosaccharide receptor fragments. *Structure (London, England : 1993)*. [Online]. **4**(2), pp.183–94. [Accessed 18 July 2018]. Available from: http://www.ncbi.nlm.nih.gov/pubmed/8805524.

Steinke, K., Sachse, F., Ettischer, N., Strutz-Seebohm, N., Henrion, U., Rohrbeck, M., Klosowski, R., Wolters, D., Brunner, S., Franz, W.-M., Pott, L., Munoz, C., Kandolf, R., Schulze-Bahr, E., Lang, F., Klingel, K. and Seebohm, G. 2013. Coxsackievirus B3 modulates cardiac ion channels. *The FASEB Journal*. [Online]. **27**(10), pp.4108–4121. [Accessed 21 July 2018]. Available from: http://www.ncbi.nlm.nih.gov/pubmed/23825229.

Stephan, D., Winkler, M., Kühner, P., Russ, U. and Quast, U. 2006. Selectivity of repaglinide and glibenclamide for the pancreatic over the cardiovascular KATP channels.

Diabetologia. [Online]. **49**(9), pp.2039–2048. [Accessed 21 July 2018]. Available from: http://www.ncbi.nlm.nih.gov/pubmed/16865362.

Stewart, H., Bartlett, C., Ross-Thriepland, D., Shaw, J., Griffin, S. and Harris, M. 2015. A novel method for the measurement of hepatitis C virus infectious titres using the IncuCyte ZOOM and its application to antiviral screening. *Journal of Virological Methods*. [Online]. **218**, pp.59–65. [Accessed 21 July 2018]. Available from: http://www.ncbi.nlm.nih.gov/pubmed/25796989.

Stolt, A., Sasnauskas, K., Koskela, P., Lehtinen, M. and Dillner, J. 2003. Seroepidemiology of the human polyomaviruses. *Journal of General Virology*. [Online]. **84**(6), pp.1499–1504. [Accessed 17 July 2018]. Available from: http://www.ncbi.nlm.nih.gov/pubmed/12771419.

Strebel, K. 2004. HIV-1 Vpu: putting a channel to the TASK. *Molecular cell*. [Online]. **14**(2), pp.150–2. [Accessed 21 July 2018]. Available from: http://www.ncbi.nlm.nih.gov/pubmed/15099514.

Strickler, H.D., Rosenberg, P.S., Devesa, S.S., Hertel, J., Fraumeni, J.F. and Goedert, J.J. 1998. Contamination of poliovirus vaccines with simian virus 40 (1955-1963) and subsequent cancer rates. *JAMA*. [Online]. **279**(4), pp.292–5. [Accessed 23 July 2018]. Available from: http://www.ncbi.nlm.nih.gov/pubmed/9450713.

Stutts, M.J., Rossier, B.C. and Boucher, R.C. 1997. Cystic fibrosis transmembrane conductance regulator inverts protein kinase A-mediated regulation of epithelial sodium channel single channel kinetics. *The Journal of biological chemistry*. [Online]. **272**(22), pp.14037–40. [Accessed 23 July 2018]. Available from: http://www.ncbi.nlm.nih.gov/pubmed/9162024.

Sullivan, C.S., Grundhoff, A.T., Tevethia, S., Pipas, J.M. and Ganem, D. 2005. SV40-encoded microRNAs regulate viral gene expression and reduce susceptibility to cytotoxic T cells. *Nature*. [Online]. **435**(7042), pp.682–686. [Accessed 18 July 2018]. Available from: http://www.ncbi.nlm.nih.gov/pubmed/15931223.

Suomalainen, M., Nakano, M.Y., Keller, S., Boucke, K., Stidwill, R.P. and Greber, U.F. 1999. Microtubule-dependent plus- and minus end-directed motilities are competing processes for nuclear targeting of adenovirus. *The Journal of cell biology*. [Online]. **144**(4), pp.657–72. [Accessed 23 July 2018]. Available from: http://www.ncbi.nlm.nih.gov/pubmed/10037788.

Suzuki, T., Yamaya, M., Sekizawa, K., Hosoda, M., Yamada, N., Ishizuka, S., Nakayama, K., Yanai, M., Numazaki, Y. and Sasaki, H. 2001. Bafilomycin A(1) inhibits rhinovirus infection in human airway epithelium: effects on endosome ICAM-1. *American Journal of Physiology-Renal Physiology*. [Online]. **280**(6), pp.F1115–F1115. [Accessed 23 July 2018]. Available from: http://www.ncbi.nlm.nih.gov/pubmed/11350790.

Swale, D.R., Sheehan, J.H., Banerjee, S., Husni, A.S., Nguyen, T.T., Meiler, J. and Denton, J.S. 2015. Computational and Functional Analyses of a Small-Molecule Binding Site in ROMK. *Biophysical Journal*. [Online]. **108**(5), pp.1094–1103. [Accessed 21 July 2018]. Available from: http://www.ncbi.nlm.nih.gov/pubmed/25762321.

Sweet, B.H. and Hilleman, M.R. 1960. The Vacuolating Virus, S.V.40. *Experimental Biology and Medicine*. [Online]. **105**(2), pp.420–427. [Accessed 23 July 2018]. Available from: http://ebm.sagepub.com/lookup/doi/10.3181/00379727-105-26128.

Sze, C. and Tan, Y.-J. 2015. Viral Membrane Channels: Role and Function in the Virus Life Cycle. *Viruses*. [Online]. **7**(6), pp.3261–3284. [Accessed 20 July 2018]. Available from: http://www.ncbi.nlm.nih.gov/pubmed/26110585.

Taddei, A., Folli, C., Zegarra-Moran, O., Fanen, P., Verkman, A.. and Galietta, L.J.. 2004. Altered channel gating mechanism for CFTR inhibition by a high-affinity thiazolidinone blocker. *FEBS Letters*. [Online]. **558**(1–3), pp.52–56. [Accessed 20 July 2018].

Available from: http://www.ncbi.nlm.nih.gov/pubmed/14759515.

Tagawa, A., Mezzacasa, A., Hayer, A., Longatti, A., Pelkmans, L. and Helenius, A. 2005. Assembly and trafficking of caveolar domains in the cell. *The Journal of Cell Biology*. [Online]. **170**(5), pp.769–779. [Accessed 18 July 2018]. Available from: http://www.ncbi.nlm.nih.gov/pubmed/16129785.

Tagaya, M., Arasaki, K., Inoue, H. and Kimura, H. 2014. Moonlighting functions of the NRZ (mammalian Dsl1) complex. *Frontiers in Cell and Developmental Biology*. [Online]. **2**, p.25. [Accessed 18 July 2018]. Available from: http://www.ncbi.nlm.nih.gov/pubmed/25364732.

Tamir, H., Piscopo, I., Liu, K.P., Hsiung, S.C., Adlersberg, M., Nicolaides, M., al-Awqati, Q., Nunez, E.A. and Gershon, M.D. 1994. Secretogogue-induced gating of chloride channels in the secretory vesicles of parafollicular cells. *Endocrinology*. [Online]. **135**(5), pp.2045–2057. [Accessed 20 July 2018]. Available from: http://www.ncbi.nlm.nih.gov/pubmed/7525261.

Tang, L., Fatehi, M. and Linsdell, P. 2009. Mechanism of direct bicarbonate transport by the CFTR anion channel. *Journal of Cystic Fibrosis*. [Online]. **8**(2), pp.115–121. [Accessed 23 July 2018]. Available from: http://www.ncbi.nlm.nih.gov/pubmed/19019741.

Taub, M. 1997. Primary kidney cells. *Methods in molecular biology (Clifton, N.J.)*. [Online]. **75**, pp.153–61. [Accessed 12 November 2018]. Available from: http://www.ncbi.nlm.nih.gov/pubmed/9276267.

Taylor, M.P., Burgon, T.B., Kirkegaard, K. and Jackson, W.T. 2009. Role of Microtubules in Extracellular Release of Poliovirus. *Journal of Virology*. [Online]. **83**(13), pp.6599–6609. [Accessed 20 July 2018]. Available from: http://www.ncbi.nlm.nih.gov/pubmed/19369338.

Teramoto, N. 2006. Pharmacological Profile of U-37883A, a Channel Blocker of Smooth Muscle-Type ATP-Sensitive K+ Channels. *Cardiovascular Drug Reviews*. [Online]. **24**(1), pp.25–32. [Accessed 21 July 2018]. Available from: http://www.ncbi.nlm.nih.gov/pubmed/16939631.

Teunissen, E.A., de Raad, M. and Mastrobattista, E. 2013. Production and biomedical applications of virus-like particles derived from polyomaviruses. *Journal of Controlled Release*. [Online]. **172**(1), pp.305–321. [Accessed 18 July 2018]. Available from: http://www.ncbi.nlm.nih.gov/pubmed/23999392.

Thangaraju, S., Gill, J., Wright, A., Dong, J., Rose, C. and Gill, J. 2016. Risk Factors for BK Polyoma Virus Treatment and Association of Treatment With Kidney Transplant Failure. *Transplantation*. [Online]. **100**(4), pp.854–861. [Accessed 23 July 2018]. Available from: http://www.ncbi.nlm.nih.gov/pubmed/27003098.

Thiagarajah, J.R., Broadbent, T., Hsieh, E. and Verkman, A.S. 2004. Prevention of toxin-induced intestinal ion and fluid secretion by a small-molecule CFTR inhibitor. *Gastroenterology*. [Online]. **126**(2), pp.511–9. [Accessed 23 July 2018]. Available from: http://www.ncbi.nlm.nih.gov/pubmed/14762788.

Thoma, F., Koller, T. and Klug, A. 1979. Involvement of histone H1 in the organization of the nucleosome and of the salt-dependent superstructures of chromatin. *The Journal of cell biology*. [Online]. **83**(2 Pt 1), pp.403–27. [Accessed 17 July 2018]. Available from: http://www.ncbi.nlm.nih.gov/pubmed/387806.

Tikhanovich, I., Liang, B., Seoighe, C., Folk, W.R. and Nasheuer, H.P. 2011. Inhibition of human BK polyomavirus replication by small noncoding RNAs. *Journal of virology*. [Online]. **85**(14), pp.6930–40. [Accessed 20 July 2018]. Available from: http://www.ncbi.nlm.nih.gov/pubmed/21543481.

Tikhanovich, I. and Nasheuer, H.P. 2010. Host-Specific Replication of BK Virus DNA in

Mouse Cell Extracts Is Independently Controlled by DNA Polymerase -Primase and Inhibitory Activities. *Journal of Virology*. [Online]. **84**(13), pp.6636–6644. [Accessed 20 July 2018]. Available from: http://www.ncbi.nlm.nih.gov/pubmed/20392840.

Tognon, M. and Provenzano, M. 2015. New insights on the association between the prostate cancer and the small DNA tumour virus, BK polyomavirus. *Journal of Translational Medicine*. [Online]. **13**(1), p.387. [Accessed 18 July 2018]. Available from: http://www.ncbi.nlm.nih.gov/pubmed/26699530.

Torres, V.E., Harris, P.C. and Pirson, Y. 2007. Autosomal dominant polycystic kidney disease. *The Lancet*. [Online]. **369**(9569), pp.1287–1301. [Accessed 23 July 2018]. Available from: http://www.ncbi.nlm.nih.gov/pubmed/17434405.

Trofe, J., Gordon, J., Roy-Chaudhury, P., Koralnik, I.J., Atwood, W.J., Alloway, R.R., Khalili, K. and Woodle, E.S. 2004. Polyomavirus Nephropathy in Kidney Transplantation. *Progress in Transplantation*. [Online]. **14**(2), pp.130–142. [Accessed 17 July 2018]. Available from: http://journals.sagepub.com/doi/10.1177/152692480401400207.

Tusnády, G.E., Bakos, E., Váradi, A. and Sarkadi, B. 1997. Membrane topology distinguishes a subfamily of the ATP-binding cassette (ABC) transporters. *FEBS letters*. [Online]. **402**(1), pp.1–3. [Accessed 22 July 2018]. Available from: http://www.ncbi.nlm.nih.gov/pubmed/9013845.

Tycko, B. and Maxfield, F.R. 1982. Rapid acidification of endocytic vesicles containing alpha 2-macroglobulin. *Cell*. [Online]. **28**(3), pp.643–51. [Accessed 20 July 2018]. Available from: http://www.ncbi.nlm.nih.gov/pubmed/6176331.

Tylden, G.D., Hirsch, H.H. and Rinaldo, C.H. 2015. Brincidofovir (CMX001) Inhibits BK Polyomavirus Replication in Primary Human Urothelial Cells. *Antimicrobial Agents and Chemotherapy*. [Online]. **59**(6), pp.3306–3316. [Accessed 17 July 2018]. Available from: http://www.ncbi.nlm.nih.gov/pubmed/25801568.

Unterstab, G., Gosert, R., Leuenberger, D., Lorentz, P., Rinaldo, C.H. and Hirsch, H.H. 2010. The polyomavirus BK agnoprotein co-localizes with lipid droplets. *Virology*. [Online]. **399**(2), pp.322–331. [Accessed 18 July 2018]. Available from: http://www.ncbi.nlm.nih.gov/pubmed/20138326.

Vadzyuk, O.B. and Kosterin, S.O. 2018. Mitochondria from rat uterine smooth muscle possess ATP-sensitive potassium channel. *Saudi Journal of Biological Sciences*. [Online]. **25**(3), pp.551–557. [Accessed 22 July 2018]. Available from: https://www.sciencedirect.com/science/article/pii/S1319562X16000474.

Vasudev, B., Hariharan, S., Hussain, S.A., Zhu, Y.-R., Bresnahan, B.A. and Cohen, E.P. 2005. BK virus nephritis: Risk factors, timing, and outcome in renal transplant recipients. *Kidney International*. [Online]. **68**(4), pp.1834–1839. [Accessed 17 July 2018]. Available from: http://www.ncbi.nlm.nih.gov/pubmed/16164661.

Venkatasubramanian, J., Ao, M. and Rao, M.C. 2010. Ion transport in the small intestine. *Current Opinion in Gastroenterology*. [Online]. **26**(2), pp.123–128. [Accessed 23 July 2018]. Available from: http://www.ncbi.nlm.nih.gov/pubmed/20010100.

Vergani, P., Lockless, S.W., Nairn, A.C. and Gadsby, D.C. 2005. CFTR channel opening by ATP-driven tight dimerization of its nucleotide-binding domains. *Nature*. [Online]. **433**(7028), pp.876–880. [Accessed 20 July 2018]. Available from: http://www.ncbi.nlm.nih.gov/pubmed/15729345.

Verhalen, B., Justice, J.L., Imperiale, M.J. and Jiang, M. 2015. Viral DNA replication-dependent DNA damage response activation during BK polyomavirus infection. *Journal of virology*. [Online]. **89**(9), pp.5032–9. [Accessed 20 July 2018]. Available from: http://www.ncbi.nlm.nih.gov/pubmed/25694603.

Verkman, A.S. and Galietta, L.J. V. 2009. Chloride channels as drug targets. *Nature*

Reviews Drug Discovery. [Online]. **8**(2), pp.153–171. [Accessed 20 July 2018]. Available from: http://www.ncbi.nlm.nih.gov/pubmed/19153558.

Verkman, A.S., Synder, D., Tradtrantip, L., Thiagarajah, J.R. and Anderson, M.O. 2013. CFTR inhibitors. *Current pharmaceutical design*. [Online]. **19**(19), pp.3529–41. [Accessed 20 July 2018]. Available from: http://www.ncbi.nlm.nih.gov/pubmed/23331030.

Viscount, H.B., Eid, A.J., Espy, M.J., Griffin, M.D., Thomsen, K.M., Harmsen, W.S., Razonable, R.R. and Smith, T.F. 2007. Polyomavirus Polymerase Chain Reaction as a Surrogate Marker of Polyomavirus-Associated Nephropathy. *Transplantation*. [Online]. **84**(3), pp.340–345. [Accessed 17 July 2018]. Available from: http://www.ncbi.nlm.nih.gov/pubmed/17700158.

Wagstaff, K.M., Sivakumaran, H., Heaton, S.M., Harrich, D. and Jans, D.A. 2012. Ivermectin is a specific inhibitor of importin α/β-mediated nuclear import able to inhibit replication of HIV-1 and dengue virus. *Biochemical Journal*. [Online]. **443**(3), pp.851–856. [Accessed 20 July 2018]. Available from: http://www.ncbi.nlm.nih.gov/pubmed/22417684.

Walczak, C.P., Ravindran, M.S., Inoue, T. and Tsai, B. 2014. A Cytosolic Chaperone Complexes with Dynamic Membrane J-Proteins and Mobilizes a Nonenveloped Virus out of the Endoplasmic Reticulum C. B. Buck, ed. *PLoS Pathogens*. [Online]. **10**(3), p.e1004007. [Accessed 19 July 2018]. Available from: http://www.ncbi.nlm.nih.gov/pubmed/24675744.

Walczak, C.P. and Tsai, B. 2011. A PDI Family Network Acts Distinctly and Coordinately with ERp29 To Facilitate Polyomavirus Infection. *Journal of Virology*. [Online]. **85**(5), pp.2386–2396. [Accessed 19 July 2018]. Available from: http://www.ncbi.nlm.nih.gov/pubmed/21159867.

Walker, S.R. and Parrish, J.A. 1988. Innovation and New Drug Development *In*: *Trends and Changes in Drug Research and Development* [Online]. Dordrecht: Springer Netherlands, pp.1–28. [Accessed 21 July 2018]. Available from: http://www.springerlink.com/index/10.1007/978-94-009-2659-2_1.

Wang, F., Zeltwanger, S., Hu, S. and Hwang, T.-C. 2000. Deletion of phenylalanine 508 causes attenuated phosphorylation-dependent activation of CFTR chloride channels. *The Journal of Physiology*. [Online]. **524**(3), pp.637–648. [Accessed 12 November 2018]. Available from: http://doi.wiley.com/10.1111/j.1469-7793.2000.00637.x.

Wang, Q., Li, L. and Ye, Y. 2008. Inhibition of p97-dependent Protein Degradation by Eeyarestatin I. *Journal of Biological Chemistry*. [Online]. **283**(12), pp.7445–7454. [Accessed 20 July 2018]. Available from: http://www.ncbi.nlm.nih.gov/pubmed/18199748.

Wang, W. 1999. Regulation of the ROMK channel: interaction of the ROMK with associate proteins. *The American journal of physiology*. [Online]. **277**(6 Pt 2), pp.F826-31. [Accessed 20 July 2018]. Available from: http://www.ncbi.nlm.nih.gov/pubmed/10600928.

Wang, W., Hebert, S.C. and Giebisch, G. 1997. RENAL K $^{+}$ CHANNELS: Structure and Function. *Annual Review of Physiology*. [Online]. **59**(1), pp.413–436. [Accessed 20 July 2018]. Available from: http://www.ncbi.nlm.nih.gov/pubmed/9074771.

Warnock, D.G. and Rossier, B.C. 2005. Renal sodium handling: the role of the epithelial sodium channel. *Journal of the American Society of Nephrology : JASN*. [Online]. **16**(11), pp.3151–3. [Accessed 20 July 2018]. Available from: http://www.ncbi.nlm.nih.gov/pubmed/16192426.

Wei, L., Vankeerberghen, A., Cuppens, H., Cassiman, J.J., Droogmans, G. and Nilius, B. 2001. The C-terminal part of the R-domain, but not the PDZ binding motif, of CFTR is

involved in interaction with Ca(2+)-activated Cl- channels. *Pflugers Archiv : European journal of physiology*. [Online]. **442**(2), pp.280–5. [Accessed 23 July 2018]. Available from: http://www.ncbi.nlm.nih.gov/pubmed/11417226.

Welling, P.A. and Ho, K. 2009. A comprehensive guide to the ROMK potassium channel: form and function in health and disease. *American Journal of Physiology-Renal Physiology*. [Online]. **297**(4), pp.F849–F863. [Accessed 20 July 2018]. Available from: http://www.ncbi.nlm.nih.gov/pubmed/19458126.

Wen, M.-C., Wang, C.-L., Wang, M., Cheng, C.-H., Wu, M.-J., Chen, C.-H., Shu, K.-H. and Chang, D. 2004. Association of JC virus with tubulointerstitial nephritis in a renal allograft recipient. *Journal of Medical Virology*. [Online]. **72**(4), pp.675–678. [Accessed 17 July 2018]. Available from: http://www.ncbi.nlm.nih.gov/pubmed/14981772.

Whitmarsh, A.J. and Davis*, R.J. 2000. Regulation of transcription factor function by phosphorylation. *Cellular and Molecular Life Sciences*. [Online]. **57**(8), pp.1172–1183. [Accessed 18 July 2018]. Available from: http://link.springer.com/10.1007/PL00000757.

Wiethoff, C.M., Wodrich, H., Gerace, L. and Nemerow, G.R. 2005. Adenovirus Protein VI Mediates Membrane Disruption following Capsid Disassembly. *Journal of Virology*. [Online]. **79**(4), pp.1992–2000. [Accessed 23 July 2018]. Available from: http://www.ncbi.nlm.nih.gov/pubmed/15681401.

Williams, J.W., Javaid, B., Kadambi, P. V., Gillen, D., Harland, R., Thistlewaite, J.R., Garfinkel, M., Foster, P., Atwood, W., Millis, J.M., Meehan, S.M. and Josephson, M.A. 2005. Leflunomide for Polyomavirus Type BK Nephropathy. *New England Journal of Medicine*. [Online]. **352**(11), pp.1157–1158. [Accessed 17 July 2018]. Available from: http://www.nejm.org/doi/abs/10.1056/NEJM200503173521125.

Wiseman, A.C. 2009. Polyomavirus Nephropathy: A Current Perspective and Clinical Considerations. *American Journal of Kidney Diseases*. [Online]. **54**(1), pp.131–142. [Accessed 17 July 2018]. Available from: http://www.ncbi.nlm.nih.gov/pubmed/19394729.

Wojciechowski, D. and Chandran, S. 2016. BK Virus Infection After Kidney Transplantation. *Transplantation*. [Online]. **100**(4), pp.703–704. [Accessed 23 July 2018]. Available from: http://www.ncbi.nlm.nih.gov/pubmed/26760573.

Wolf, D.H. and Stolz, A. 2012. The Cdc48 machine in endoplasmic reticulum associated protein degradation. *Biochimica et Biophysica Acta (BBA) - Molecular Cell Research*. [Online]. **1823**(1), pp.117–124. [Accessed 20 July 2018]. Available from: http://www.ncbi.nlm.nih.gov/pubmed/21945179.

Wong, M., Pagano, J.S., Schiller, J.T., Tevethia, S.S., Raab-Traub, N. and Gruber, J. 2002. New associations of human papillomavirus, Simian virus 40, and Epstein-Barr virus with human cancer. *Journal of the National Cancer Institute*. [Online]. **94**(24), pp.1832–6. [Accessed 23 July 2018]. Available from: http://www.ncbi.nlm.nih.gov/pubmed/12488476.

Wright, P.J. and Di Mayorca, G. 1975. Virion polypeptide composition of the human papovavirus BK: comparison with simian virus 40 and polyoma virus. *Journal of virology*. [Online]. **15**(4), pp.828–35. [Accessed 18 July 2018]. Available from: http://www.ncbi.nlm.nih.gov/pubmed/163921.

Yang, B., Sonawane, N.D., Zhao, D., Somlo, S. and Verkman, A.S. 2008. Small-Molecule CFTR Inhibitors Slow Cyst Growth in Polycystic Kidney Disease. *Journal of the American Society of Nephrology*. [Online]. **19**(7), pp.1300–1310. [Accessed 23 July 2018]. Available from: http://www.ncbi.nlm.nih.gov/pubmed/18385427.

Yogo, Y., Zhong, S., Xu, Y., Zhu, M., Chao, Y., Sugimoto, C., Ikegaya, H., Shibuya, A. and Kitamura, T. 2008. Conserved archetypal configuration of the transcriptional control region during the course of BK polyomavirus evolution. *Journal of General Virology*.

[Online]. **89**(8), pp.1849–1856. [Accessed 18 July 2018]. Available from: http://www.ncbi.nlm.nih.gov/pubmed/18632955.

Yoneda, Y., Hieda, M., Nagoshi, E. and Miyamoto, Y. 1999. Nucleocytoplasmic protein transport and recycling of Ran. *Cell structure and function*. [Online]. **24**(6), pp.425–33. [Accessed 20 July 2018]. Available from: http://www.ncbi.nlm.nih.gov/pubmed/10698256.

Yu, F.H., Yarov-Yarovoy, V., Gutman, G.A. and Catterall, W.A. 2005. Overview of Molecular Relationships in the Voltage-Gated Ion Channel Superfamily. *Pharmacological Reviews*. [Online]. **57**(4), pp.387–395. [Accessed 21 July 2018]. Available from: http://www.ncbi.nlm.nih.gov/pubmed/16382097.

Zaman, R.A., Ettenger, R.B., Cheam, H., Malekzadeh, M.H. and Tsai, E.W. 2014. A Novel Treatment Regimen for BK Viremia. *Transplantation*. [Online]. **97**(11), pp.1166–1171. [Accessed 17 July 2018]. Available from: http://www.ncbi.nlm.nih.gov/pubmed/24531848.

Zehmer, J.K., Huang, Y., Peng, G., Pu, J., Anderson, R.G.W. and Liu, P. 2009. A role for lipid droplets in inter-membrane lipid traffic. *PROTEOMICS*. [Online]. **9**(4), pp.914–921. [Accessed 18 July 2018]. Available from: http://www.ncbi.nlm.nih.gov/pubmed/19160396.

Zhang, J., Chang, D., Yang, Y., Zhang, X., Tao, W., Jiang, L., Liang, X., Tsai, H., Huang, L. and Mei, L. 2017. Systematic investigation on the intracellular trafficking network of polymeric nanoparticles. *Nanoscale*. [Online]. **9**(9), pp.3269–3282. [Accessed 18 July 2018]. Available from: http://www.ncbi.nlm.nih.gov/pubmed/28225130.

Zhang, J., Zhang, X., Liu, G., Chang, D., Liang, X., Zhu, X., Tao, W. and Mei, L. 2016. Intracellular Trafficking Network of Protein Nanocapsules: Endocytosis, Exocytosis and Autophagy. *Theranostics*. [Online]. **6**(12), pp.2099–2113. [Accessed 18 July 2018]. Available from: http://www.ncbi.nlm.nih.gov/pubmed/27698943.

Zhao, L. and Imperiale, M.J. 2017. Identification of Rab18 as an Essential Host Factor for BK Polyomavirus Infection Using a Whole-Genome RNA Interference Screen W. P. Duprex, ed. *mSphere*. [Online]. **2**(4), pp.e00291-17. [Accessed 18 July 2018]. Available from: http://www.ncbi.nlm.nih.gov/pubmed/28815213.

Zhao, L., Marciano, A.T., Rivet, C.R. and Imperiale, M.J. 2016. Caveolin- and clathrin-independent entry of BKPyV into primary human proximal tubule epithelial cells. *Virology*. [Online]. **492**, pp.66–72. [Accessed 18 July 2018]. Available from: http://www.ncbi.nlm.nih.gov/pubmed/26901486.

Zheng, K., Chen, M., Xiang, Y., Ma, K., Jin, F., Wang, X., Wang, X., Wang, S. and Wang, Y. 2014. Inhibition of herpes simplex virus type 1 entry by chloride channel inhibitors tamoxifen and NPPB. *Biochemical and Biophysical Research Communications*. [Online]. **446**(4), pp.990–996. [Accessed 21 July 2018]. Available from: http://www.ncbi.nlm.nih.gov/pubmed/24657267.

Zhong, S., Randhawa, P.S., Ikegaya, H., Chen, Q., Zheng, H.-Y., Suzuki, M., Takeuchi, T., Shibuya, A., Kitamura, T. and Yogo, Y. 2009. Distribution patterns of BK polyomavirus (BKV) subtypes and subgroups in American, European and Asian populations suggest co-migration of BKV and the human race. *Journal of General Virology*. [Online]. **90**(1), pp.144–152. [Accessed 17 July 2018]. Available from: http://www.ncbi.nlm.nih.gov/pubmed/19088283.

Zhu, L., Yu, X., Xing, S., Jin, F. and Yang, W.-J. 2018. Involvement of AMP-activated Protein Kinase (AMPK) in Regulation of Cell Membrane Potential in a Gastric Cancer Cell Line. *Scientific Reports*. [Online]. **8**(1), p.6028. [Accessed 23 July 2018]. Available from: http://www.nature.com/articles/s41598-018-24460-6.